THE ESTABLISHMENT OF A FLOW CYTOMETRY SYSTEM TO STUDY *HTT* REGULATION AND EXPRESSION

by

Natalia Athina Kosior

B.Sc., University of British Columbia, 2014

A THESIS SUBMITTED IN PARTIAL FULFILLMENT OF THE REQUIREMENTS FOR THE DEGREE OF

MASTER OF SCIENCE

in

The Faculty of Graduate and Postdoctoral Studies

(Neuroscience)

THE UNIVERSITY OF BRITISH COLUMBIA

(Vancouver)

August 2017

Abstract

Huntington's disease (HD) is a late-onset neurodegenerative disorder characterized by motor deficits, behavioral abnormalities and psychiatric symptoms. HD is caused by a CAG trinucleotide repeat expansion in the *HTT* gene resulting in expression of a mutant polyglutamine stretch in the huntingtin protein. HD affects up to 14 per 100,000 people in British Columbia. This devastating disorder is characterized by relatively selective neuronal loss in the caudate and putamen, regions of the brain referred to collectively as the striatum. Numerous mechanisms leading to this selective neurodegeneration have been proposed but the pathways involved are still not well understood. The huntingtin protein (HTT) is ubiquitously expressed, meaning that it is present in all cell types in the central nervous system, prompting investigations into potential pathogenic mechanisms outside of the characteristic neuronal loss. The brain is composed of microglia and astrocyte cell populations that together, make up the central immune system. Immune system activation has been implicated in the disease pathogenesis of various neurodegenerative diseases, including HD. The purpose of this thesis was to establish a flow cytometry system to investigate potential *HTT* regulatory mechanisms as well as increase knowledge of immune cell dysfunction in HD. Following the establishment of the flow cytometry system I found that *HTT* expression does not vary across the cell cycle. Using an adapted technique, I identified robust but not absolute genetic knock-down in two microglia-specicfic conditional knock out mouse models. Adding to the neuroinflammation focus, I identified mutant-huntingtin specific changes in protein phosphorylation expression in microglia as a means of identifying potential signaling cascades involved in exaggerated cytokine release. Lastly, I investigated transcriptional dysregulation in HD microglia and astrocyte populations and the effect of a candidate therapeutic on gene expression in these cell types. My research provides additional insight into potential protein phosphorylation and genetic pathways involved in immune dysfunction in HD and will focus future experiments aimed at understanding the role of central inflammation in HD.

Lay Summary

Huntington's Disease (HD) is a relatively rare genetic brain disease affecting more than 1 in 10,000 Canadians. In HD, specific brain cells (neurons) expressing an abnormal protein called mutant huntingtin (mHTT) die, resulting in various symptoms. Most HD research focuses on the effects of mHTT exclusively in neurons. My research examined the effects of mHTT on microglia and astrocytes, two types of immune cells in the brain. These immune cells support neurons, regulate brain immune responses and remove dying cells. I established a technique to isolate pure microglia and astrocyte cells from adult mouse brain to look at potential dysfunction in these cells. I also used this technique to look at the effects of a current drug on these specific cell types. My research provides a basis on which future work assessing the role of brain inflammation in HD can be understood.

Preface

All of the work presented henceforth was conducted at the Center for Molecular Medicine and Therapeutics, part of the BC Children's Hospital Research Institute (BCHRI) at the University of British Columbia. All projects and associated methods were approved by the University of British Columbia Animal Care Committee (Certificate #A09-0673)

Chapter 1: Introduction was an updated and reworked version of published material from my book chapter. Kosior N., Leavitt BR. Murine Models of Huntington's disease for Evaluating Therapeutics. Methods in Molecular Biology: Huntington's Disease.

Chapter 2: I conducted all aspects of experimental design, with the assistance of T. Petkau, and conducted all experiments. Glial isolations were conducted at the BCHRI Flow core with the help of Lisa Xu and cell cycle experiments were conducted at the UBC Flow core with the technical assistance of Justin Wong and Andy Johnson. HeLa FUCCI cells were generously donated by the Maxwell lab (located in the BCHRI). Immunocytochemical analysis of HTT expression in the HeLa FUCCI cells was visualized using the Maxwell lab confocal microscope with the assistance of Helen Chen.

Chapter 3: I conducted all aspects of experimental design for this chapter and conducted all experiments with the technical assistance of T. Petkau. Ge Lu performed all Western blots. Figure 3.5 was quantified by C. Connolly.

Chapter 4: I conducted all experiments with the assistance of T. Petkau. Both BR Leavitt and T.Petkau had significant input into aspects of experimental design and subsequent analysis. Protein phosphorylation arrays and subsequent validation of the priority leads I identified was conducted at Kinexus Bioinformatics Corporation (UBC). I conducted the additional STRING analysis and pathway analysis.

Chapter 5: I conducted all experiments with the assistance of T. Petkau. Ge Lu

performed all therapeutic treatments. Figure 5 was generated by C. Connolly. Both BR Leavitt and T.Petkau had significant input into aspects of experimental design. RNA isolation and RNA-sequencing was conducted at the BRC-Seq Core at UBC with the assistance of Ryan van der Werff. RNA-seq analysis was completed by E. Graham and F. Farhadi under the supervision of S. Mostafavi.

Table of Contents

List of Tables

List of Figures

List of Abbreviations

Astrocyte cell surface antigen-2 (ACSA-2)
Alzheimers disease (AD)
Adenosine tri-phosphate (ATP)
Analysis of variance (ANOVA)
Anti-sense oligonucleotide (ASO)
Blood-brain-barrier (BBB)
Brain-derived neurotropic factor (BDNF)
Bovine serum albumin (BSA)
Calcium/calmodulin-dependent protein kinase II (Camk2a)
Cannabinoid receptor (CB)
Cluster of Differentiation (CD11b, CD45)
Percent change from control (%CFC)
Central nervous system (CNS)
Control standard endotoxin (CSE)
Cerebrospinal fluid (CSF)
Control standard endotoxin (CSE)
4',6-diamidino-2-phenylindole (DAPI)
Differentially expressed genes (DEGs)
Dulbeco's Modified Eagle's Medium (DMEM)
Ethylene Diamine Triacetic Acid (EDTA)
Extracellular-signal related kinases (ERKs)
Flourescence activated cell sorting (FACS)
Fetal bovine serum (FBS)
False Discovery rate (FDR)
Family-wise error rate (FWER)
Forward scatter (FSC)
L-glutamate/L-aspartate (GLAST)
Gene Set Enrichment Analysis (GSEA)
Hanks Buffered Saline Solution (HBSS)
Huntington's Disease (HD)
Human embryonic kidney 293 (HEK293)
Huntingtin protein (HTT)
Huntingtin gene (*HTT*)
Mutant huntingtin protein (mHTT)
Endogenous mouse huntingtin (*hdh*)
Ionized calcium adaptor molecule (Iba-1)
Interferon-gamma (IFN-γ)
C-jun amino-terminal kinases (JNKs)
Knockout (KO)
Laquinimod (LAQ)
Log-fold change (LogFC)
Lipopolysaccharide (LPS)
Magenetic activated cell sorting (MACS)

Mitogen-activated protein kinases (MAPKs)
Metalloproteinases (MMPs)
Medium spiny neurons (MSNs)
Nuclear-factor-κB (NF-κB)
Normalization factor 2 (NF2)
N-methyl D-aspartate (NMDA)
Phosphate buffer saline (PBS)
Phosphate buffer saline triton (PBS-Tx)
Side scatter (SSC)
Striatal rat neuronal progenitor 14 (ST14)
Tumor necrosis factor-α (TNF- α)
Wild-type (WT)
7-Aminoactinomycin D (7-AAD)

Acknowledgements

First of all, I would like to thank my supervisor, Dr. Blair Leavitt for his guidance and mentorship throughout the course of my graduate degree and for teaching me to critically examine the scientific literature as well as my own results. I would also like to thank my supervisory committee—Sara Mostafavi, Brian MacVicar, and Lynn Raymond—for their insight along the way.

Second, I would like to thank my colleagues in the Leavitt lab. To Austin Hill, Ge Lu, Colum Connolly, Kathleen de Asis, Pamela Wagner and Jasmine Yang for their technical and theoretical contributions to my research and to Angela Gurney for her help in all things non-science related. I would also like to thank our collaborators Emma Graham, Farnush Farhadi and Sara Mostafavi for their contributions to my work. To Rebecca de Souza and Terri Petkau for being amazing mentors and for teaching me the basics in both bench skills and scientific inquiry.

Lastly to my incredible family and friends for their support and encouragement throughout this process. I would especially like to thank my parents, Leszek and Irena. This would not have been possible without them. To my sisters, Karolina and Kasia for keeping things interesting and entertaining. Kocham cie.

1 Introduction

1.1 Thesis Introduction

Huntington's disease (HD) is a late onset neurodegenerative disease caused by a CAG trinucleotide repeat expansion in exon 1 of the huntingtin (*HTT*) gene, resulting in the expression of a polyglutamine expansion on the resulting HTT protein. The discovery of the causative HD mutation occurred in 1993 and has since instigated 24 years of investigation into the cellular mechanisms involved in disease pathogenesis. Although a disease primarily associated with the medium spiny neurons, dysfunction in other central nervous system cell types also occurs in HD, adding to the complexity involved in establishing successful therapeutic strategies. Neuroinflammation has become increasingly implicated in a variety of neurodegenerative diseases, including HD. Whether the neuroinflammation identified in HD is a consequence of neuronal death or a direct result of intrinsic dysfunction in HD immune cells, however, is not well understood. As a result, the aim of my thesis was to identify potential downstream signaling pathways involved in glial cell dysfunction in HD in order to focus future work involved in understanding the role of central inflammation in the progression of HD.

1.2 Huntington's Disease

1.2.1 History and Prevalence

Huntington's Disease (HD) is an autosomal dominant neurodegenerative disorder characterized by progressive motor, cognitive and psychiatric symptoms. HD is found in populations worldwide with an estimated prevalence of 2.71 per 100,000 individuals (Pringsheim et al. 2012). Differences in prevalence rates exist with higher frequencies seen in populations of European descent compared to those of Asian and African ancestry (Rawlins *et al.* 2016). The most comprehensive prevalence study performed to date determined a prevalence rate of over 14 per 100,000 for an ethnically mixed population in British Columbia (Fisher and Hayden, 2014).

The first widely accepted account of the disease has been attributed to physician George Huntington who correctly detailed both the physical nature of the disease as well as the hereditary component in an article titled "On Chorea" published in *The Medical and Surgical Reporter of Philadelphia* in 1872. More than a century later, in 1983, the genetic defect was mapped to chromosome 4p16.3 (Gusella *et al.* 1983). A decade following this discovery, linkage analysis uncovered a CAG repeat expansion in the huntingtin gene (*HTT*), originally termed *IT15* (interesting transcript 15) and found to be the genetic mutation responsible for HD (Anon *et al.* 1993). This introductory chapter will outline the main clinical, genetic and neurological features of HD along with current mouse models of HD aimed at evaluating therapeutics. In addition, we will explore the evidence suggesting a role for microglial-mediated inflammation in HD pathogenesis.

1.2.2 Clinical Features

HD clinical features can be grouped into three main categories: motor, cognitive and psychiatric, with deficits usually appearing in the fourth or fifth decade of life. Motor abnormalities include involuntary movements such as chorea and dystonia as well as disturbances in voluntary movements comprising of bradykinesia (slowed voluntary movement), rigidity, dysphagia, dysarthria and gait irregularities (Harper, 2005). Chorea,

considered a clinical hallmark of the disease, is described as swift, irregular jerking, dancing or writhing movements of the face, limbs or trunk (Harper, 2005). Early in the disease, involuntary movements often predominate with rigidity, bradykinesia (slowness in the execution of movement) and voluntary movement deficits appearing as the disease progresses (Young *et al.* 1986). Juvenile HD cases, defined as those with age of onsets under the age of 20, account for 5-10% of HD patients and present with distinct motor abnormalities. Rapid manifestation of bradykinesia, dystonia, and seizures have been described in Juvenile HD cases but interestingly, chorea is often less prominent than in adult-onset HD cases (Nance and Myers, 2001).

Cognitive defects in HD typically begin with subtle deficits in intellectual processes, personality changes, disinhibition and reduced mental flexibility (Butters *et al.* 1985). Similar to motor disturbances, when they occur, cognitive impairments generally worsen as the disease progresses and eventually develop into a "subcortical dementia" (learning and memory disturbances primarily in recall versus storage) (Zakzanis, 1998).

Neuropsychiatric symptoms present in HD include depression, apathy, suicidal ideation and anxiety (Anderson and Marder, 2001). In contrast to motor and cognitive defects that worsen with time, psychiatric abnormalities are highly variable and are often absent or can occur at any time during disease progression and the onset or severity of these symptoms do not readily correlate with disease stage or motor impairment (Anderson and Marder, 2001). Symptoms of psychosis and obsessive-compulsive tendencies also manifest in HD but are usually hereditary in nature suggesting that certain psychiatric features may be influenced by environmental and genetic factors outside the HD mutation (Lovestone *et al.* 1996). Other common systemic features of HD include weight loss due to changes in metabolism (Sanberg *et al.* 1981), sleep and circadian rhythm disturbances (Morton *et al.* 2005) and testicular degeneration (Van Raamsdonk *et al.* 2007).

The formal diagnosis of HD is clinical in nature and depends on the presence of a defined (but otherwise unexplained) extrapyramidal movement disorder in a patient at risk for HD. Once clinically diagnosed, testing for the gene mutation that causes HD is generally conducted as confirmation in individuals who have not previously undergone predictive genetic testing.

1.2.3 Neuropathology

The most striking neuropathological hallmark of HD is the relatively selective and early progressive degeneration of the caudate and putamen (collectively referred to as the striatum) (Vonsattel and DiFiglia, 1998). Neurodegeneration in this brain region correlates with disease progression and severity and is relatively cell-type specific. The striatum is composed of two major neuronal subtypes: medium spiny neurons (MSNs) and aspiny interneurons.

Medium-spiny neurons (MSNs) are the neuronal subtype most severely affected in HD with aspiny interneurons largely unaffected. Although the majority of cell loss occurs in the striatum, as the disease progresses, degeneration occurs in the cortex as well as the hippocampus, global pallidus, subthalamic nucleus, substantia nigra, cerebellum and thalamus (Vonsattel *et al.* 1985).

Nuclear and cytoplasmic intracellular inclusions are another pathogenic feature of HD and other polyglutamine diseases. These inclusions are composed of insoluble, ubquinated protein aggregates that contain both full-length and fragmented forms of huntingtin. The presence of these huntingtin inclusions was initially discovered in HD mice (Davies *et al.* 1997) and was later confirmed in HD patient tissue (DiFiglia *et al.* 1997). The impact of these aggregates on disease pathogenesis is unknown but differences in inclusion properties in juvenile and adult HD cases exist with earlier, more widespread inclusions identified in juvenile cases (DiFiglia *et al.* 1997).

1.2.4 Genetics

HD is caused by a CAG trinucleotide repeat expansion in exon 1 of the *HTT* gene that encodes for an expanded polyglutamine stretch near the N-terminus of the huntingtin protein. Translation of the *HTT* gene results in the formation of a 350-kDa protein, which is ubiquitously expressed throughout the body with higher expression in the brain and testis (Sharp *et al.* 1995). Expanded CAG repeat sizes of greater than 35 are considered pathogenic, with repeat sizes of 36-39 having reduced penetrance or delayed age of onset (Andrew *et al.* 1993).

HD displays an autosomal dominant pattern of inheritance and a unique non-Mendelian trait of anticipation. The CAG repeat expansion is a dynamic mutation with larger repeat sizes exhibiting greater instability. This instability leads to a phenomenon called anticipation, which is defined as decreasing age of onset or increasing severity of disease in successive generations (Mahadevan *et al.* 1992). Intermediate alleles with 27-35 CAG repeats are not associated with HD diagnosis but can rarely expand into the pathogenic range during intergenerational transmission to cause HD in subsequent generations (Semaka *et al.* 2006). Paternal transmission of the CAG repeat is more likely to result in expansion with most juvenile HD cases resulting from paternal transmission of a large expanded allele (CAG repeat sizes greater than 60) (Telenius *et al.* 1993).

There is an inverse relationship between CAG repeat size and age of onset meaning that individuals with longer CAG expansions demonstrate earlier and more severe symptoms. This inverse correlation between length and age of onset accounts for 60-70% of the variance in age of onset (Andrew *et al.* 1993) with other putative causative modifiers recently identified.

One of these modifiers includes a SNP in the *HTT* promoter found to alter NF-κB binding. The non-coding SNP, rs13102260: G>A was found to impair NF-κB binding, resulting in reduced *HTT* transcriptional expression ad subsequent protein production (Becanovic *et al.* 2015). Interestingly, the presence of the same SNP on the wild-type *HTT* allele was correlated with earlier age of onset (Becanovic *et al.* 2015). This work identified the first bidirectional genetic modifier of a human disease and was instrumental in describing previously unknown allele-specific SNP effects on HD age of onset.

Other genetic modifiers identified using genome-wide association (GWA) analysis found genetic loci in two independent chromosomes involved in accelerating and delaying disease onset (Genetic Modifiers of Huntington's Disease (GeM-HD) Consortium, 2015). Subsequent pathway analysis implicated the DNA handling and repair pathway as a potential mediator of HD onset. Similar to the work of Becanovic *et al.,* the GWA analysis demonstrated that HD age of onset is modified by genetic factors outside the causative HTT CAG repeat expansion.

1.2.5 Mouse Models of Huntington's Disease

Since the identification of the disease-causing gene in 1993, numerous mouse models have been generated to recapitulate disease pathogenesis and progression (Table 1.1). Mouse (*Mus musculus*) models are widely used for modeling human neurodegenerative disease for several reasons. The first rests on the close genetic relationship between rodents and humans and the similar developmental progression of both species. The availability of inbred mouse strains is also advantageous in studying the contribution of discrete genetic manipulations on homogenous backgrounds. Other more general benefits of mouse models include low cost, rapid generation (18.5-21 days), and reliable methods of genetic manipulation (Gama Sosa *et al.* 2012). Specific behavioral, molecular and *in vivo* assays in mouse models are also well established to allow for careful consideration of therapeutic interventions.

In the case of HD mouse models, four general categories exits: 1) chemical models created using neurotoxin administration 2) fragment transgenic models established following insertion of N-terminal human *HTT* containing the expanded CAG repeat into the mouse genome 3) full-length transgenic models produced by the insertion of full-length mutated human *HTT* into the mouse genome 4) knock-in transgenic models generated by the specific introduction of a CAG repeat expansion into the endogenous mouse *hdh* gene (Wagner *et al.* 2008). Different genetic HD mice recapitulate specific features of the cognitive dysfunction, motor impairment and striatal neurodegeneration seen in human HD patients (detailed above) and may served as adequate models for target validation and drug discovery in the case of pre-clinical therapeutic trials.

The numerous genetic manipulations underlying HD mouse models all seek to recapitulate the human disease, but do so to various degrees of success. All established models demonstrate different levels of behavioral changes, motor dysfunction and neurodegeneration as a result of the introduction of either fragment or full-length huntingtin. Still, the human condition differs from current HD mouse models in the duration of disease, severity of symptoms and robust striatal specificity of neuropathology, which ultimately calls into question the effectiveness of using mouse models to mimic human disease.

N-terminal fragment models demonstrate the most robust and rapid disease phenotype and as a result serve as attractive initial models for preclinical testing. Although these benefits exit, fragment models fail to demonstrate the striatal-specific atrophy and cell loss present in human HD patients. The early onset of severe phenotypes and rapid death also preclude fragment models from being used to study early disease pathogenesis as well as potentially preventative therapeutics.

Full-length models improve upon the limitations of the fragment models and exhibit more slowly progressive abnormalities and relatively normal lifespans. The robust and striatum-specific neuropathological changes identified at 12 months of age in the YAC and BAC models mimic those seen in the human condition and provide reasonable neuropatholgic outcome measures for preclinical trials. More importantly, the full-length huntingtin protein and lower onset of disease phenotypes allows for the study of early disease events and drug targets.

Knock-in models generally display the weakest and most variable phenotypes, and as a result are generally considered to be less effective preclinical models. Instead, similar to full-length HD mice, knock-in models are generally considered to be more useful for investigating early steps in HD pathogenesis. An exception to this may be the new higher expressing forms of Q175 mice (Southwell *et al.* 2016). More importantly, due to the differences in HD gene mouse models, it is now common to use multiple mouse models to screen drug targets and measure their accuracy and efficacy prior to progression to human clinical trials.

With the discovery of the HD mutation in 1993, thousands of studies have sought to investigate the molecular mechanisms underlying the disease. The various established HD mouse models have furthered our understanding of pathogenic mechanisms and have also been used to develop and screen potential therapeutics. Unfortunately, as no effective therapy that alters disease progression in HD patients currently exists, there is no "gold standard" agent that can be used to assess the predictive value of the various HD mouse models in preclinical trials of therapeutics. A main challenge in the HD field in the future is the effective selection of therapeutic agents for progression from preclinical testing to human clinical trials. With the variety of HD mouse models available and the different phenotypes, advantages and disadvantages that each possess, prioritizing

potential therapeutics on the basis of one model is difficult. New therapeutic agents should be proven efficacious in several animal models prior to clinical testing. Considerable progress has been made in understanding HD pathogenesis, partly due to the development of genetic mouse models. As new approaches and therapeutic interventions are identified, these models will continue to play a prominent role in developing effective treatments for HD.

Common Name	**Repeat Length**	**Model Type**	**Gene Characteristics**	**Comments**
R6/2	150	Fragment	HTT promoter, exon 1 of human huntingtin gene	Most commonly used fragment HD mouse model; neuronal intranuclear inclusions (Davies *et al.* 1997)
Q175FDN	200	Knock-in	Human huntingin exon 1 introduced into endogenous mouse *hdh* (zQ175); Deletion of neo cassette from zQ175 restores mHTT levels to generate Q175FND strain	Display early and progressive HD pathology (motor deficits, neurodegeneration) unlike previous knock-in models (Southwell *et al.* 2016)
YAC128	128	Full-length	Full length human huntingtin	Most commonly used full-length HD mouse model; motor deficits at 2months & striatal-specific neuronal loss at 12 months (Slow *et al.* 2003)
BACHD	97	Full-length	Human mutant huntingtin (exon 1); floxed	Similar phenotype to YAC128 (Gray *et al.* 2008)

Hu97/18	97	Humanized	Two full-length human HTT alleles in absence of endogenous mouse *hdh*; heterogeneous HD mutation	First humanized model (no endogenous *hdh*) motor deficits at 2 months & neurodegeneration at 12months (Southwell *et al.* 2013)

Table 1.1 Overview of HD mouse models. Presented the most commonly used mouse models in the HD literature along with the most recent knock-in (Q175FDN) and humanized (Hu97/18) models.

1.2.5.1 Using Mouse Models for Evaluating Therapeutics

In order for a drug candidate to be approved for human clinical trials it must be proven effective in more than one HD mouse model. Rigorous standardization of operating procedures across different labs and trial design must be in place in order to successfully reproduce drug efficacy studies. Trial design considerations can generally be divided into two categories 1) Animal husbandry 2) Experimental Design and Primary Endpoints.

Animal husbandry is an important means of controlling for genetic or environmental factors that may influence phenotype and/or response to the drug candidate. Standardized breeding, housing and testing procedures along with animal strain, sex and sample size reduce potential variability between subjects and across preclinical trials. Because HD mouse models are currently available on multiple congenic backgrounds, each with their own distinct set of benefits and limitations, choosing the correct strain is of particular importance. One example is in therapeutics targeting excitotoxicity where a FVB/N background is more robust (Schauwecker, 2005).

Standardized experimental design measures also contribute to preclinical study utility and interlab reproducibility. Animal assignment into treatment groups, behavioral tests, and molecular and histological endpoints should be closely related to the domains expected to be altered by the treatment. Along with behavioral tests of motor control and function, including accelerating rotarod and open field activity, molecular and

histological measures are commonly used in assessing treatment efficacy in HD mouse models. This is due to the fact that neuropathological abnormalities such as striatal loss (Vonsattel and DiFigilia 1998) and protein inclusions (Davies *et al.* 1997, DiFigilia *et al.* 1997) have been widely described in both HD mouse models and human patients, allowing for standard assessments of therapeutic effects are possible.

Since the presence of mutant HTT (mHTT) protein is a component of HD pathogenesis, therapies have been developed aimed at reducing mutant protein levels in an effort to halt disease progression. Several HTT protein assays have been designed to quantify mHTT protein levels in tissue in response to various therapeutics including TR-FRET (Baldo *et al.* 2012), Seprion (Sathasivam *et al.* 2010), and AGERA (Weiss *et al.* 2007). Western blot analysis is also commonly used to assess protein levels, however, in the case of HTT, specifically mutant HTT, several caveats exist. A recent paper compared the sensitivity of five widely used mHTT antibodies (S830, MW8, EM48, 1C2, ubiquitin) in five standard HD mouse models (R6/1, YAC128, HdhQ92, B6 HdhQ150, B6 x 129/Ola HdhQ150) at 18 months of age (with the exception of R6/1 mice which had a reduced lifespan and have comparable disease burdens at 4 and 7 months of age). Unique antibody binding profiles were identified even in instances where only the background strain varied (as in the case of HdhQ150), demonstrating the importance of avoiding generalization both between studies using different antibodies as well as across mouse lines using the same antibody (Bayram-Weston *et al.* 2016).

Gene expression analysis, through the use of standard qPCR methods and global Affymetrix microarrays and RNA-Seq, is another therapeutic endpoint measure. In the case of microarrays and RNA-Seq, the effect of a therapeutic on gene networks and biological pathways can be identified. Recent RNA-Seq analyses have focused on gene expression profiles in HD patient brain (Labadorf *et al.* 2015) and peripheral immune cells (Miller *et al.* 2016) but there is the possibility of applying these technologies to HD mouse models to better understand gene expression changes resulting from therapeutic intervention. This idea will be discussed in greater detail in subsequent chapters.

Histopathological measures, including brain regional volume and neuronal cell counts, are also used to evaluate therapeutic endpoints in HD mouse models. Histological methods have been used to measure brain region volumes (striatal, cortical, hippocampal

and whole brain) and have demonstrated regional reductions in HD mouse models (Carroll *et al.* 2011). Neuronal cell counts in these same regions have also reported reductions in HD mouse models, particularly in zQ175 and YAC128 mice (Heikkinen *et al.* 2012, Hickey *et al.* 2008, Slow *et al.* 2003). The use of unbiased stereoscopic methods to quantify regional volume loss and neuronal cell counts allow for reliable measures of therapeutic interventions.

1.2.5.2 Current Preclinical Therapeutic Strategies

Numerous preclinical trials have been conducted in HD mouse models and can be generally divided into: energy metabolism, antioxidants, protease inhibitors, transglutaminase inhibitors, general enrichment of environment and nutrition, aggregate formation inhibitors, specific gene-targeted transcription (using viral vectors, drugs, transgenic over-expressors or mouse knock-outs), excitotoxicity and tissue transplants. New approaches have also been recently highlighted as targets for future clinical trials in HD. These including reducing HTT expression using RNAi, ASO, Zinc Finger and CRISPR/Cas9 technology, along with proteosomal degradation, autophagy enhancement, aggregate prevention, dopamine stabilization, neurotropic support, immunomodulation and astrocytic glutamate uptake (Reviewed in Wild and Tabrizi, 2014).

1.2.7 Normal Huntingtin Function

Although the causative mutation in the *HTT* gene was identified in 1993, the wild-type function of the huntingtin protein (HTT) is not yet fully understood. HTT is ubiquitously expressed throughout the body, yet displays increased expression in the brain and testes compared to other peripheral tissues (Sharp *et al.* 1995). Even though the exact function of HTT remains unclear, it has been implicated in a wide range of cellular processes including vesicular trafficking, cell division and survival, ciliogenesis, endocytosis, as well as embryogenesis and development (Reviewed in Saudou and Humbert, 2016).

The *HTT* gene plays an important role in development both within the CNS as

well as the periphery. Mouse HTT knockout models (termed *hdh null* mice) are embryonic lethal at embryonic day 7.5 (E7.5) (Nasir *et al.* 1995; Duyao *et al.* 1995; Zeitlin *et al.* 1995), demonstrating the essential role of the *HTT* gene in embryonic development. This deficit in embryogenesis, however, can be rescued if HTT is expressed in extra-embryonic tissues (Nasir *et al.* 1995). In cortical neurogenesis, HTT depletion in radial glial progenitor populations in the ventricular zone promotes neuronal differentiation but reduces the levels or progenitors (Godin *et al.* 2010). The involvement of HTT in the regulation of the dynein complex during mitosis influences the rate of cell division in these cortical progenitors (Godin et al. 2010). In the post-embryonic stage, HTT has also been shown to play a role in forebrain formation, particularly the cortex and striatum, as well as neuronal survival (Reiner *et al.* 2001).

Several studies have also identified a pro-survival role for normal huntingtin. The stable over-expression of wild-type human HTT in cell lines and primary striatal neuronal cultures showed a protective effect against various toxic stimuli including mutant HTT (Ho et al. 2001; Leavitt et al. 2006; Rigamonti *et al.* 2001). The depletion of HTT *in vitro* produces the converse results with increased vulnerability to cell death (Zhang *et al.* 2006). Similar pro-survival effects were also replicated *in vivo* where overexpression of wild-type HTT protected against ischemic and excitotoxic injury (Zhang *et al.* 2003; Leavitt *et al.* 2006). The antiapoptotic/prosurvival properties of wild-type HTT is of particular importance in HD. This is due to the massive neuronal atrophy seen in both human postmortem brain (Vonsattel and DiFiglia, 1998) as well as cellular and mouse HD models (Gray et al. 2008, Saudou et al. 1998). One of the mechanisms by which wild-type HTT mediates its prosurvival effects has been suggested to include inactivation of caspase-3 and 9 (Rigamonti *et al.* 2001; Zhang *et al.* 2003).

1.2.8 Mutant Huntingtin Toxicity

The expression of an expanded CAG repeat in the *HTT* gene results in the translation of a polyglutamine expansion in the HTT protein. This mutation is thought to primarily result in a toxic gain of function, although loss of wild-type huntingtin function may also impact disease pathogenesis (Cattaneo *et al.* 2001). Specifically, loss of wild-

type huntingtin results in more severe motor deficits and hyperkinesia along with testicular degeneration and reduced lifespan (van Raaamsdonk *et al.* 2005). In instances where wild-type huntingtin is overexpressed, neuronal vulnerability to excitotoxicty (Leavitt *et al.* 2006) and striatal neuronal atrophy is improved (van Raamsdonk *et al.* 2006). Similar pro-survival results were also identified in cell models of HD *in vitro* following transfection with full-length wild-type huntingtin (Ho *et al.* 2001), suggesting that loss of wild-type huntingtin may play a role in HD pathology. Various toxic gain-of-function mechanisms underlying mHTT expression have also been identified. These include: protein aggregation, cleavage of mHTT leading to toxic fragments, transcriptional dysregulation, mitochondrial dysfunction and RNA toxicity, among others.

1.2.8.1 Protein Aggregation

The presence of mHTT protein aggregates, termed inclusion bodies (IBs) (Arrasate and Finkbeiner, 2012) has long been considered a hallmark of HD (DiFiglia *et al.* 1997). The subsequent identification of mHTT aggregates in the R6/2 HD mouse model (Davies *et al.* 1997) generated the idea that protein aggregates were involved in disease pathogenesis. This idea, however, has been debated in the literature, whereby the presence of neuronal huntingtin inclusions does not correspond with neuropathological abnormalities (including neuronal dysfunction and degeneration) (Slow *et al.* 2005). Despite this, mutant huntingtin aggregates have been shown to affect axonal transport and degeneration (Li *et al.* 2001), sequestration of transcriptional activators (Cha, 2007), mitochondrial import (Yano *et al.* 2014), and nuclear integrity and nucleocytoplasmic transport (Gasset-Rosa *et al.* 2017). Mutant huntingtin inclusions also correlate with disease progression in HD mouse models (Yamamoto *et al.* 2000), and may result from failures in the ability of the ubiquitin-proteasome system (UPS) to degrade mutant huntingtin (Martin-Aparicio *et al.* 2001; Ortega and Lucas, 2014). UPS dysfunction is more pronounced in neurons as compared to glial cells (Tydlacka *et al.* 2008), and may be an important contributor to the increased neuronal vulnerability seen in HD. Recent work has investigated the effect of activating proteosomal function in HD mouse models.

PA28γ, a proteasome activator, increases proteasome activity and modulates cellular surivival in HD patient skin fibroblasts and HD mouse model striatal neurons *in vitro* (Seo *et al.* 2007). Lenti-viral mediated injection of PA28γ into the striatum of 14-18 month old YAC128 mice resulted in reductions in the number of ubiquitin positive inclusion bodies, increased BDNF levels and improved rotarod motor performance (Jeon *et al.* 2016). As a result, proteasome activity may underlie an important pathological mechanism in HD.

1.2.8.1 Mutant Huntingtin Cleavage

Another potential toxic gain-of-function mechanism in HD pathogenesis is the proteolysis of the mHTT protein to produce a toxic fragment. The wild-type huntingtin protein is cleaved by caspases (Goldberg *et al.* 1996, Wellington *et al.* 1998) and calpains (Gafni and Ellerby, 2002), producing smaller protein fragments. Similar to wild-type HTT, mHTT is also cleaved by caspases, yielding smaller, toxic N-terminal fragments containing expanded PolyQ tails. These fragments form insoluble nuclear and cytoplasmic aggregates in affected cells, resulting in various forms of cellular dysfunction. Caspase 6, one of the caspases responsible for huntingtin cleavage, has been implicated as an important mediator of HD behavioral and neuropathological abnormalities in the YAC128 HD mouse model. Inhibition of caspase 6, not caspase-3, was shown to improve striatal atrophy and motor deficits and protect against neurotoxicity in response to various stressors including NMDA, quinolinic acid and staurosporine (Graham *et al.* 2006), suggesting that caspase-6 mediated mHTT proteolysis is an important contributor to HD pathogenesis. Recent work using continuous subcutaneous administration of a caspase-6 inhibitor specific for huntingtin, protected against motor and behavioral deficits in presymptomatic BACHD mice and partially ameliorated dysfunction in later disease stage BACHD mice (Aharony *et al.* 2015). Caspase-6 activity is not restricted to the CNS but is also found in the muscle tissue derived from HD patients and HD mouse models (Ehrnhoefer *et al.* 2014), suggesting that caspase-6 mediated cleavage of mHTT may be involved in both central as well as peripheral dysfunction in HD.

1.2.8.2 Transcriptional Dysregulation

Numerous studies have investigated changes in transcript expression in the context of HD. Early work identified reductions in neuropeptides and neurotransmitter receptors mRNA levels in striatal neurons (Arzberger *et al.* 1997; Augood *et al.* 2006) in postmortem HD brain, which was replicated in R6/2 dopamine receptor levels (Cha *et al.* 1999). With the advent of DNA microarray and RNA-seq transcriptomic technology, unbiased assessment of transcriptional dysregulation has become increasingly simple. Coordinated efforts in the HD field also conducted whole-genome analyses on a variety of HD disease models to identify genes differentially expressed at different disease stages. The differentially expressed genes identified overlapped with HD-related cellular dysfunction, including transcriptional processes, neurotransmitter receptors, synaptic transmission, cytoskeletal and structural proteins, intracellular signaling and calcium homeostasis. The majority of genes were down regulated in HD models and changes were more pronounced in N-terminal fragment (i.e. R6/2) HD mouse models as compared to full length (i.e. YAC128). This may imply that mHTT cleavage fragments affect transcription more significantly than full-length huntingtin (Chan *et al.* 2002; reviewed in Zuccato *et al.* 2010). Additional work investigating transcriptional dysregulation has been completed in human HD brain and peripheral immune cells and will be discussed in greater detail in subsequent sections.

1.2.8.3 Mitochondrial Dysfunction

As discussed in the clinical features section of the chapter, HD patients exhibit metabolic abnormalities (Sanberg *et al.* 1981) and energetic deficits, as exhibited by profound weight loss despite sustained caloric intake. In early patient studies, altered mitochondrial morphology was identified in ultrastrucutral studies of cortical biopsies (Tellez-Nagel *et al.* 1974). Prior to the onset of symptoms, significant reductions in glucose utilization in the striatum were also discovered even before characteristic striatal atrophy (Kuhl *et al.* 1984). This was identified in concordance with elevated glycolytic rate in the cortex and basal ganglia of HD patients, as evidenced by increased production

of lactate (283, 314). Functional mitochondrial studies in HD patients have also been conducted. In these investigations, mitochondrial enzymes involved in oxidative phosphorylation including complex II, III, and IV, demonstrated reduced activity in the brains regions implicated in HD (Brown *et al.* 1997), suggesting that energy deficits may a consequence of alterations in mitochondrial function.

Similar mitochondrial abnormalities have also been identified in HD cell and animal models. Mutant huntingtin binds directly to mitochondria (Choo *et al.* 2004), mediating changes in energy metabolism, calcium handling (De Mario *et al.* 2016), mitochondrial function (Quintanilla *et al.* 2013) and ultimately contributing to oxidative stress. Mitochondrial dysfunction is also present in several well-established HD mouse models, including R6/2 (Aidt *et al.* 2013; Braubach *et al.* 2014) and YAC128 mouse models. Mitochondria isolated from YAC128 HD mice also show dysregulated mitochondrial calcium handling, resulting in elevated mitochondrial oxidative stress (Wang *et al.* 2013).

Oxidative stress is defined as an imbalance between oxidants and anti-oxidants, where elevated levels of oxidants result in cellular damage, dysfunction or death. Cells produce oxidants in various forms, including reactive oxygen species (ROS), reactive nitrogen species (RNS), or reactive lipid species (RLS). Mitochondria are considered major sources of ROS production, whereby a small percentage of electrons transferred down the electron transport chain to produce ATP inappropriately interact with oxygen molecules to produce free radicals. These free radicals then interact with other surrounding biomolecules to produce reactive species (reviewed in Kumar and Ratan, 2016). Mutant huntingtin mediates mitochondrial dysfunction and may play a role in the elevated oxidative stress seen in in the basal ganglia of HD patients (Browne *et al.* 1999) and in HD mouse models (Gray *et al.* 2008). Several investigations have been aimed at reducing oxidative stress, including various PPAR activators. The peroxisome proliferator-activated receptor γ (PPARγ) controls mitochondrial biogenesis and oxidative stress. Previous studies have demonstrated that mutant huntingtin disrupts these transcriptional functions (Cui *et al.* 2006). Induction of PPARγ in HD N171-82Q mice prevented mHTT aggregation formation and improved rotarod deficits (Tsunemi *et al.* 2012; Jin *et al.* 2013). Other pan-PPAR agonists, including bezafibrate, restore motor and

neuropathological deficits in BACHD mouse models (Chandra *et al.* 2016), suggesting that mitochondrial function is a strong therapeutic target for treatment of HD.

1.3 Inflammation in Huntington's Disease

The brain is composed of four major cell types: neurons, microglia, astrocytes and oligodendrocytes. Microglia, accounting for less than 10% of the total brain cells (Lawson *et al.* 1990) are monocyte lineage cells and represent the main immune cell population in the brain. Ubiquitously expressed throughout the grey matter, microglia alternate between resting and activated states (Kaur *et al.* 2007). Under normal physiological conditions, these cells are characterized by a small cell body and ramified processes. In this quiescent state, these processes protrude and retract to survey the environment and maintain brain homeostasis through phagocytosis, scavenging activity, secretion of homeostatic factors such as TGFβ and synaptic pruning (Nimmerjahn *et al.* 2005). In instances of insult or injury, these cells become activated leading to changes in morphology, increased expression of various antigens, secretion of proteases and proinflammatory cytokines (Bonifati and Kishore, 2007) as well as increased cell numbers or "gliosis." These cytokine and protease signals, in turn, activate signaling cascades in the remaining cell types in the brain, namely neurons and astrocytes, to induce neuronal cell death. Although not typically viewed as initiators of neurodegenerative disease, inflammatory events have been shown to contribute to disease progression in various HD mouse models, but the role of neuroinflammation in HD is currently unknown.

1.3.1 Microglia Biology and Function

1.3.1.2 Microglial Origin

Microglial cells are the resident macrophages in the central nervous system and fulfill numerous functions both during brain development as well as in neurodegeneration and aging. Although microglia account for only 10% of total brain cells, they are the

most abundant mononuclear phagocytes in the CNS. Microglia are a unique cell population for several reasons. First, in terms of ontogeny, microglia arise from erythromyeloid precursors in the yolk sac and populate the brain early in development. Second, unlike peripheral immune cells that are constantly replaced by bone marrow derived hematopoietic stem cells, resident microglia repopulate in the adult brain via constant self-renewal. The combination of their ontogeny, rigid self-renewal and contained environment in the CNS make microglia distinct from other brain populations as well as peripheral immune cells. Macrophages, located in the meninges, choroid plexus and perivascular space, are another distinct set of CNS mononuclear phagocytes. The long-standing consensus was that these macrophages were bone marrow derived, subject to rapid turnover, and precluded from CNS entry by the blood-brain barrier (BBB) (Aguzzi *et al.* 2013). Recent work using parabiosis and fate mapping approaches in mice, however, has suggested that only macrophages of the choroid plexus arise from the bone marrow and are rapidly turned over. In contrast, perivascular and meningeal macrophages are derived from primitive hematopoietic progenitors during development and are stable CNS macrophages (Goldmann *et al.* 2016). In a normal brain, microglia and CNS macrophages exist and function cohesively as two genetically distinct myeloid populations. In the event of inflammation, however, the brain is infiltrated with blood-derived monocytes of the peripheral immune system (reviewed in Colonna and Butovsky, 2016). This concept of peripheral immune cell infiltration is a component of neuroinflammation. HD, however, is not characterized by immune cell infiltration from the blood stream (Silvestroni *et al.* 2009) and as a result, immune activation may be a consequence of cell-intrinsic dysfunction of CNS microglia with increased pro-inflammatory cytokine production.

1.3.1.2 Microglial Morphology and Function

Under normal conditions, microglia are characterized by small cell bodies and ramified processes. The projection and retraction of these ramified processes allows for inspection of the environment (Cartier *et al.* 2014) and the secretion of anti-inflammatory

and neurotropic actors (Streit, 2002) necessary for maintenance of brain homeostasis. Microglia express a wide-range of immune receptors including chemokine receptors such as CX3CR1 and CXCR4 and integrins such as CD11b and CD11c. The chemokine receptor CX3CR1 is present on all microglia and is responsible for controlling microglial localization and migration (Jung *et al.* 2000). CX3CR1 is the microglial receptor for the neuronal chemokine fractalkine (CX2CL1), suggesting that this pathway is involved in neuron-glial crosstalk (Sheridan and Murphy, 2013) as a result of complementary expression of ligand and receptor on neurons and microglia, respectively. The integrin CD11b is constitutively expressed while CD11c is up regulated in activated microglia. Both, however, promote microglial migration, adhesion and phagocytosis (Akiyama and McGeer, 1990). Microglia also express receptors for various pro-inflammatory and anti-inflammatory cytokines, both produced in the CNS and secreted from the periphery. In addition to immune receptors, microglia also express receptors for various neurotransmitters and neuropeptides in order to facilitate neuronal-microglial interactions (Pocock and Kettenmann, 2007). These include: glutamate ionotropic receptors including AMPA and *N*-methyl-D-aspartate (NMDA) receptors (Kaindl *et al.* 2012), purinergic receptors for ATP such as P2X7 (Monif *et al.* 2009) as well as the receptors for GABA (Kuhn *et al.* 2004), and dopamine (Huck *et al.* 2015). The expression of these various neurotransmitters affects microglial activation and interleukin release (Pocock and Kettenmann, 2007) and guides microglia to areas of neuronal activity to affect synaptic plasticity, sculpt dendritic spine density, eliminate damaged neurons and secrete neurotropic factors for neuronal growth (reviewed in Colonna and Butovsky, 2016).

Functionally, microglia play roles in neurogenesis, synaptic pruning and plasticity, and neuronal activity in the healthy brain. In terms of neurogenesis, microglia regulate the proliferation and differentiation of neural progenitor and neural stem cells as well as control the number of neurons through phagocytosis (reviewed in Sato, 2015). During development, excess synaptic connections are formed between neurons, which are subsequently removed by a process called synaptic pruning. Microglia shape neural circuitry by pruning and sculpting neuronal synapses, through the engulfment of pre and post-synaptic elements (Paolicelli *et al.* 2011) to ensure correct CNS circuitry is established. The chemokine CX3CR1 receptor, along with the complement system, has

been directly implicated in this process of synaptic pruning. The classical complement cascade is an innate immune pathway involved in removal of pathogens and apoptotic cells from the periphery (Dunkelberger and Song, 2010). Several components of the pathway, including C1q and C3, localize to immature synapses (Stephan *et al.* 2012), while complement receptor 3 (CR3) is expressed primarily in CNS microglia (Stevens *et al.* 2007). Experiments in Cx3cr1 and C3 and CR3 knockout mice have implicated the chemokine and complement system cascades in synapse pruning. Cx3crl KO mice demonstrate increased numbers of immature synapses (Paolicelli *et al.* 2011) while C3 and CR3 KO mice show decreased microglial elimination at synapses (Schafer *et al.* 2012) (reviewed in Wu *et al.* 2015).

Synaptic strength and plasticity is also controlled my microglia through the release of various proinflammatory cytokines and neurotopic factors (Vezzani and Viviani, 2015). Tumor necrosis factor- (TNF)-α is one cytokine that modifies synaptic strength through a process called synaptic scaling (Stellwagen and Malenka, 2006). In synaptic scaling, microglia secrete TNF-α, which activates astrocytes to release ATP and glutamate. The activation of astrocytes leads to the activation of presynaptic metabotropic receptors on neurons, leading to an increase in synaptic current (reviewed in Colonna and Butovsky, 2016). More specifically, the process of synaptic scaling directly influences both neuronal activity as well as subsequent synaptic strength. Functionally, microglia mediate changes in synaptic plasticity through proteolytic modification of the perisynaptic environment, dendritic spine morphology remodeling and phagocytic engulfment of dendritic spines and axon terminals (reviewed in Tremblay and Majewska, 2011). Inflammatory molecules secreted from microglia also affect synaptic activity. Treating cultured neurons or acute brain slices with conditioned media from cultured microglia result in increased NMDA amplitudes and currents (Moriguchi *et al.* 2003; Hayashi *et al.* 2006). In instances of increased neurotoxicity (i.e. excessive release of glutamate and subsequent activation of NMDA receptors on neurons), neurons release ATP, which activates the ATP receptor, P2X7 on microglia. The activation of P2X7, in turn, results in the secretion of TNF-α, which modulates NMDA-induced toxicity. The presence of ATP and glutamate receptors on microglia also induces microglial migration to neuronal axons, resulting in membrane repolarization and prevention of subsequent

excitotoxicity (Kato *et al.* 2016). Taken together, microglia fulfill numerous functions in the healthy CNS and are important for neuronal development, synaptic signaling and plasticity and neuronal activity.

1.3.1.3 Activated Microglia

In response to CNS injury or neurodegenerative, microglia are activated display a more "amoeboid" appearance (Ransohoff and Perry, 2009). This alteration from a "resting" to "activated" state is accompanied by an increase in secretion of pro-inflammatory molecules such as interleukin (IL-6) (Kraft *et al.* 2012) and TNF-α (Olmos and Llado, 2008). Activated microglia also demonstrate increased phagocytic activity, where microglia migrate along the chemokine gradient in response to brain injury or immunological distress to phagocytose apoptotic cells and debris (Cartier *et al.* 2005). Acute neuroinflammation is beneficial as it eliminates toxins and dead cells but instances of chronic inflammation are detrimental. Chronic activation and proliferation of microglia along with increased secretion of proinflammatory cytokines and increased production of superoxide and nitric oxide are consequences of prolonged neuroinflammation. This sustained response, more importantly, affects the blood-brain-barrier (BBB), allowing macrophages of the choroid plexus to rapidly infiltrate the brain and intensify the immune response (reviewed in Nayak *et al.* 2011). The activated microglia interact with neurons and other brain cell populations, including astrocytes and oligodendrocytes. In instances where the CNS insult or injury cannot be removed, the sustained secretion of inflammatory molecules impacts these other brain cell populations, leading to tissue damage and altered disease progression. The presence of an immune component has been identified in various neurodegenerative disease including Alzheimer's (Hensley, 2010) and Parkinson's disease (Samii *et al.* 2004). Immune activation is also implicated in HD pathogenesis, and will be discussed in greater detail below.

1.3.2 Clinical Features of Neuroinflammation in HD

Although HD is primarily considered as a neurodegenerative disease, immune activation has also been identified as a potential contributor to disease pathogenesis. In a healthy brain, the innate immune system is beneficial as it promotes the clearance of pathogens and other cellular debris. In instances of chronic inflammation, inflammatory molecules (i.e. cytokines and chemokines) that normally modulate immune cell function also act on neurons, contributing to neuronal death. Neuronal death then further activates inflammatory responses, resulting in a vicious cycle of inflammation and neurodegeneration (reviewed in Rocha *et al.* 2016).

Immune activation has been identified in both the CNS as well as the periphery of HD patients (Björkvist *et al.* 2008), demonstrating a link between inflammation and HD-related pathology. Various investigations in patient post-mortem tissue, PET scans and cerebrospinal fluid (CSF) have identified evidence of microglial activation. Increased numbers of activated microglia have been identified in the striatum of HD patients, with the number of activated microglia correlating with neuronal loss (Sapp *et al.* 2001). Immune activation has also been identified prior to onset of disease symptoms (Sapp *et al.* 2001), where microglial activation correlates with disease severity (Simmons *et al.* 2007). Functionally, microglial activation in the human HD brain also resulted in the increased production of various inflammatory molecules. Interleukin (IL-6), IL-8, IL-10, and tumor necrosis (TNF)-α transcript levels were significantly increased in the striatum of HD patients compared to controls (Björkvist *et al.* 2008; Silvestroni *et al.* 2009), along with the expression of various metalloproteinases (MMPs) including MMP-9 and MMP-3 (Connolly *et al.* 2016). Investigations of microglial activation *in vivo* using positron emission tomography (PET) scans, also demonstrate significant up regulation of microglia activation in HD striatum (Tai *et al.* 2007). Other brain regions also demonstrate increased microglial activation, including the hypothalamus (Politis *et al.* 2008) and the somatosensory cortex (Politis *et al.* 2015), suggesting that immune activation may play a role in other HD-related phenotypes, in addition to neurodegeneration, including alterations in metabolism, sleep and circadian rhythms (reviewed in Rocha *et al.* 2016). More importantly, increased activation in the

somatosensory cortex of HD patients was correlated with increased levels of proinflammatory molecules in the plasma (Politis *et al.* 2015), suggesting that an association between central and peripheral immune responses may exist.

Cerebrospinal fluid (CSF) analysis in HD patients has also provided evidence for the role of immune activation in HD. Various inflammatory molecules including complement factors (Fang *et al.* 2009) and metalloproteinases (MMPs) (Connolly *et al.* 2016) have demonstrated alterations in HD patient CSF. As a proximal measure of the brain, CSF has long been considered a relevant biomaterial for biomarker discovery (Fang *et al.* 2009), both to uncover relevant pathways implicated in disease pathogenesis and to monitor the effect of therapeutic intervention. YKL-40, a marker of microglial activation, was significantly increased in patient CSF and correlated with disease stage, as well as cognitive and motor outcomes (Rodrigues *et al.* 2016a). Other molecules including neurofilament light protein (NFL) and the axonal protein, Tau (Rodrigues *et al.* 2016b) have been implicated as potential CSF biomarkers (Niemelä *et al.* 2017; Vinther-Jensen *et al.* 2016), although NFL was shown to correlated more significantly to clinical outcomes than Tau in a small patient cohort (Niemelä *et al.* 2017). More importantly, the levels of tau and NfL were also significantly correlated to mutant huntingtin quantities in the CSF (Wild *et al.* 2015), suggesting a potential link between neuronal mHTT levels and the levels of these potential biomarkers.

1.3.2.1 Peripheral Immune System Dysfunction in HD

Although primarily a disease of the CNS, multiple systemic changes have also been identified in HD (reviewed in van der Burg *et al.* 2009). *HTT* is ubiquitously expressed and mHTT inclusions have been found a variety of non-CNS tissues including muscle (Sathasivam *et al.* 1999), liver, spleen, stomach wall, adrenal glands and pancreas (Moffit H *et al.* 2009). Peripheral immune dysfunction has also been previously identified in HD using flow cytometry (Gollin *et al.* 1985). Bidirectional cross talk between the CNS and the peripheral immune system through neuroimmune, neuroendocrinal and bioenergetic mechanisms may influence neuronal function and survival (reviewed in Zheng *et al.* 2015) and, more importantly, impact HD pathogenesis. In the peripheral

immune system, increased concentrations of proinflammatory molecules, including interleukin (IL)-6 and IL-8 (Björkvist *et al.* 2008, Dalrymple *et al.* 2007) have been identified in HD monocytes. Various peripheral myeloid immune cell populations also demonstrate dysfunction in numerous HD mouse models. Spleen and blood myeloid cells derived from R6/2, HdhQ150 and YAC128 mice demonstrate increased cytokine release following stimulation (Träger *et al.* 2015), similar to peripheral dysfunction identified in human HD patients.

Significant transcriptional differences, corresponding to increased inflammatory activation, have also been identified in basal, unstimulated HD myeloid cells compared to controls (Miller *et al.* 2016). Interestingly, transcriptional changes in HD peripheral immune cells involving macrophage phagocytosis and microglial synaptic pruning were identified recently using RNA-seq and overlap with immune signatures identified in Alzheimer's disease (Hensmann Moss *et al.* 2017). This implies that several pathogenic mechanisms may overlap between these two neurodegenerative diseases. Isolated monocytes, or peripheral immune cells, from both HD and premanifest HD patients also demonstrate an exaggerated inflammatory response to stimulation (Björkvist *et al.* 2008), suggesting that inflammatory changes result from immune cell dysfunction and are not a consequence of CNS phenotypes (reviewed in van der Burg *et al.* 2009).

Peripheral HD immune cells have demonstrated mitochondrial and metabolic deficits. Down regulation of various genes involved in metabolism and oxidative stress response were identified in HD peripheral leukocytes (Almeida *et al.* 2008; Chang *et al.* 2012) along with increased expression of apoptotic genes (Almeida *et al.* 2008). HD patient monocytes also demonstrate increased caspase (2, 3, 6, 8, 9) activity, decreased cell viability and significant morphological changes in mitochondria (Squitieri *et al.* 2011) compared to controls. The altered caspase activity may play a role in huntingin cleavage, as discussed previously, and impact peripheral immune function in HD. Taken together, mutant huntingtin expression in peripheral immune cells alters various cellular processes and may impact both peripheral immune system function as well as CNS activity. Similar to the CSF, peripheral blood from HD patients has also been used for biomarker discovery using transcriptomic analysis (Mastrokolias *et al.* 2015) and subsequent identification of potential candidate genes. Neurofilament (NFL), recently

implicated as a CSF biomarker, also demonstrates increased expression in HD patient plasma compared to controls, with the difference increasing with each subsequent stage. Clinical outcomes, including cognitive and motor function along with global and regional brain volume were also correlated with NfL levels, with increased levels corresponding to worse clinical measures (Byrne *et al.* 2017).

Various therapeutic strategies have been tested in the peripheral immune system as a means of ameliorating dysfunction and potentially impacting the CNS. Recent work has identified nuclear factor- (erythroid-derived 2) (NRF2) signaling as a potential mediator of peripheral immune function. Selective activation of NFR2 signaling in HD monocytes from both patients and mouse models resulted in decreased proinflammatory cytokine release (Quinti *et al.* 2017). Another major approach has centered on reducing huntingtin expression using various gene-silencing approaches. As discussed previously, HD peripheral immune cells demonstrate an exaggerated cytokine release following LPS stimulation (Björkvist *et al.* 2008). The use of small-interfering RNA to lower huntingtin expression resulted in the reversal of HD-related cytokine and transcriptional changes resulting from NFκB pathway dysregulation (Träger *et al.* 2014). The nuclear-factor-κB (NFκB) pathway has been implicated in HD peripheral immune cell function. More specifically, mutant huntingtin in HD peripheral immune cells interacts with the key kinase in the NFκB pathway, IKKγ, leading to increased NFκB activity (Khoshnan *et al.* 2004).

The interaction with mutant huntingtin and the NFκB pathway, more importantly, points to a potential mechanism by which mutant huntingtin is involved in peripheral immune dysfunction. Since HD is characterized by the presence one wild-type and one mutant allele in the *HTT* gene, the selective lowering of mutant *HTT* is an important consideration, as gene-silencing approaches become widely accepted therapeutics. The work completed by Träger and colleagues, discussed above, targeted both wild-type and mutant huntingtin levels. Recent work has built upon the specificity of this approach and assessed the effect of selective mutant huntingtin silencing in monocytes derived from HD patients. Similar to Träger and colleagues, mutant huntingtin silencing in HD peripheral immune cells ameliorated increased cytokine release in response to LPS stimulation (Miller *et al.* 2017), once again implicating mutant huntingtin expression as a

mediator of increased inflammatory responses in the peripheral immune system.

1.3.3 The Role of Microglia in HD

Although HD is a CNS disorder, the innate immune system in the brain has not been well investigated in terms of disease pathogenesis. This may be because neuroinflammation in HD is still a relatively new field and may also be a consequence of technical considerations. Peripheral immune cells are more easily isolated from HD patients compared to microglia and other CNS macrophages, allowing for direct investigation. Despite this, knowledge of microglial dysfunction is important in understanding the role of central inflammation in HD pathology.

Until recently, the brain was viewed as an immune-privileged organ, whereby inflammation occurred only as a result of direct infection or blood-brain barrier infiltration and subsequent peripheral immune cell entrance. Current knowledge, however, has identified microglia-mediated immune cell mechanisms as contributors to inflammation in the brain (Heneka *et al.* 2014). This process, termed neuroinflammation, is defined as inflammation, in which there is little to no infiltration of blood-derived immune cells into the brain (Crotti and Glass, 2015) but is a result of intrinsic dysfunction in the immune cells themselves. HD does not demonstrate peripheral immune system infiltration (Silvestroni *et al.* 2009), suggesting that inflammation identified in the brain is a consequence of immune cell dysregulation. Microglia, the brain resident immune cells, are altered in HD in terms of activation state, cytokine release (Connolly *et al.* 2016) and migration (Kwan *et al.* 2012), suggesting that mutant huntingtin expression may impact immune cell function.

As discussed previously, increased microglial activation has been identified in postmortem HD brain as well as various PET scan and CSF investigations in human patients. Similar evidence of microglial activation has also been recapitulated in HD mouse models, including the R6/2 (Simmons *et al.* 2007) and YAC128 (Björkvist *et al.* 2008) models. These instances of microglial activation also have similar functional consequences on inflammatory molecule release as identified in human HD patients. Previous work completed in the lab identified altered cytokine release in mutant

huntingtin containing microglia in response to proinflammatory stimuli (Connolly *et al.* 2016). Increased expression of proinflammatory cytokine release (IL-8, IL-1β) from microglia derived from HD minipigs has also been recently identified (Valekova *et al.* 2016).

The increase in microglial reactivity may be a consequence of increased expression and transcriptional activity of the myeloid lineage-determining factors, PU.1 and C/EBPs. These transcription factors are responsible for the development and function of various macrophage/microglia lineage cells and are acted upon by numerous transcription factors, including NFκB (Heinz *et al.* 2010). Mutant huntingin expressing microglia demonstrate increased PU.1 and C/EBPs activity. This in turn, enhances the toxic effects on wild-type neurons *ex vivo*, meaning that co-culturing wild-type neurons with mHTT microglia increases neuronal death as compared to wild-type microglia (Crotti *et al.* 2014). Recent work has built upon this idea and has transplanted human mHTT-containing microglia into normal mice. The presence of mHTT expressing microglia in normal mice resulted in motor deficits and hyperexcitable striatal neurons. The converse experiment was also conducted, whereby normal human microglia were transplanted into R6/2 HD mice. Normal microglia were able to restore motor dysfunction and electrophysiological abnormalities, as well as slow disease progression and extend survival (Benraiss *et al.* 2016). As a result, glial transplantation may suggest a potential cell-based therapy in HD and more importantly implicates central inflammation as a component of HD pathogenesis.

1.3.4 Altered Signaling Pathways in Microglia

Numerous signaling pathways have been implicated in microglial dysfunction in HD, including the endocannabinoid and kyrurenine pathways along with caspase activation and iron regulation (reviewed in Connolly *et al.* 2012). Endocannabinoid signaling has also been previously implicated as a potential pathway involved in neuroinflammation in HD (Dowie *et al.* 2009). There are two main cannabinoid receptors (CB1 and CB2) and two major endogenous cannabinoid molecules (Anadamide and 2-Archadonylglycerol) (Devane and Axelrod, 1994). CB1 receptors are expressed primarily

within the CNS in neurons and astrocytes while CB2 receptors are located in immune cells, including microglia (Nuñez *et al.* 2004). The endocannabinoid system is an attractive target in HD research for several reasons. The first is the CB1 receptors are highly expressed in the caudate and putamen, the regions mainly affected in HD (Mailleux *et al.* 1992). The second is that activation of CB2 in microglia results in decreased secretion of proinflammatory cytokines (Correa *et al.* 2011). The scarcity of CB2 receptors, specifically in the CNS, also means that any psychoactive effects of CB2 receptor agonist therapeutics would be minimal (reviewed in Cassano *et al.* 2017).

Genetic ablation of CB2 receptors in the R6/2 mouse model of HD exaggerated behavioral abnormalities, increased microglial activation and reduced life span (Palazuelos *et al.* 2009). Previous work completed in the lab expanded on the immune phenotype identified and examined the effect of CB2 deletion on microglial cytokine release. YAC128 mice were crossed with mice lacking the CB2 receptor (CB2KO) mice, resulting in CB2 deletion. The absence of CB2 receptors caused an increase in IL-6 release in YAC128-CB2KO microglia as compared to YAC128. Increasing CB2 activation using AA-5HT, a CB2 agonist, reversed this exaggerated cytokine release, implicating CB2 and endocannabinoid signaling as potential therapeutics targets for HD-related neuroinflammation. Similar work completed in the BACHD found similar results, whereby CB2KO, in the presence of mutant huntingtin, worsened HD progression.

Administration of CB2 agonist was able to reverse several HD-phenotypes including synaptic loss, motor deficits and ultimately extended lifespan (Bouchard *et al.* 2012). Both studies suggest that CB2 receptors may play a role in HD pathogenesis and serve as attractive therapeutic targets. As a result, various therapeutic investigations into endocannabinoid signaling have been conducted. Administration of CB2 agonists in HD lesion rat models of HD reduces the generation of proinflammatory molecules such as TNF-α (Sagredo *et al.* 2009). R6/2 HD mice treated with cannabigerol (CBG), an activator of CB1/CB2 receptors, significantly improved motor deficits and increased expression of BDNF and insulin-like growth factor 1 (IGF-1) (Valdeolivas *et al.* 2015). Other CGB derivatives have been assessed in QA and 3-NP induced HD mouse models, leading to reversal of striatal degeneration, motor impairment and microglial activation (Diaz-Alonso *et al.* 2016). Human trials have also been recently established to test the

safety of cannabinoid treatment in HD (Lopez-Sendon Moreno JL *et al.* 2016).

The kyrurenine pathway (KP) is the primary route of tryptophan degradation in mammalian cells (Tan *et al.* 2012). Various metabolites are produced in this pathway including quinolinic acid (QUIN), which is a selective NMDA receptor agonist involved in neurotoxicity (Szalardy *et al.* 2012) and has been used as an early mouse model of HD (Coyle and Schwarcz, 1976). As a result, the kyrurenine pathway may play a role in the excitototoxicity and selective degeneration of the striatum identified in HD. The primary enzyme responsible for producing QUIN, KMO, is predominately expressed in microglia (Heyes *et al.* 1992). QUIN levels have been have been found to be significantly increased in human HD patient brain (Guidetti *et al.* 2004) and in HD mouse models (Sathyasaikumar *et al.* 2010). These findings suggest that mutant huntingtin expression may alter tryptophan metabolism within the CNS and may contribute to neuronal excitotoxicity (reviewed in Vecsei *et al.* 2013). As a result, KMO inhibition may underlie a potential therapeutic target in HD. Treatment of R6/2 HD mice with JM6, a KMO inhibitor, for example, prevented striatal neurodegeneration and increased survival in the mice, through the reduction of microglial activation (Zwilling *et al.* 2011). Recent work has used a more selective KMO inhibitor, CHDI-340246, in HD mice leading to restoration of electrophysiological alterations characteristic of HD (Beaumont *et al.* 2016).

Iron is the most abundant transition metal in the brain and plays a role in various cellular processes, including neurotransmitter synthesis, neuronal myelination, and mitochondrial function. In terms of mitochondrial function, specifically, iron is an important cofactor in various mitochondrial enzymes needed to generate ATP by the electron transport chain. Iron deficiency alters mitochondrial morphology, damages mitochondrial DNA and alters function, leading to increased oxidative stress (reviewed in Hare *et al.* 2013). Increased iron deposition has been found in various neurodegenerative diseases including Parkinson's disease (Sofic *et al.* 1988) and amyotrophic lateral sclerosis (Kwan *et al.* 2012). In the case of HD, MRI studies in human patients found elevated levels of iron as compared to both controls and Alzheimer's and Parkinson's patients (Bartzokis *et al.* 1999). In the R6/2 HD mouse model, iron accumulates in striatal neurons. Administration of an intra-ventricular iron chelator reversed this accumulation

and improved the R6/2 motor phenotype (Chen *et al.* 2013). Recent work has also looked at the impact of amyloid precursor protein (APP) in brain iron accumulation in HD. APP promotes neuronal iron export and, as a result, may modulate elevated iron levels in HD. Suppression of APP levels in YAC128 HD mice results in increased cerebral and striatal iron levels and accompanying motor deficits (Berggren *et al.* 2017), suggesting that APP may be important in clearing excess iron in HD brain. In terms of microglia, similar iron elevations were also seen in the striatum, hippocampus and cortex of R6/2 HD mice and were predominately localized to microglia (Simmons *et al.* 2007). Microglia simulated with LPS in the presence of iron also demonstrate altered gene expression (Saleppico *et al.* 1996).

1.4 Conclusions

HD is a late onset-neurodegenerative disease characterized by motor, cognitive and psychiatric symptoms. Significant immune activation has also been identified in the CNS and periphery, implicating the immune system in disease pathogenesis. Although inflammation is beneficial in the CNS as it clears pathogens and cellular debris, sustained inflammation affects neuronal health and function. Both peripheral HD immune cells and microglia derived from HD mouse models demonstrate dysfunction in terms of activation state, release of inflammatory molecules and downstream signaling cascades. As a result, expression of mutant huntingtin in immune cells of the brain and periphery may mediate cell-intrinsic microglial dysfunction. These immune cell alterations may, ultimately, lead to a sustained inflammatory response and contribute to neuronal cell death in HD.

Numerous signaling pathways have been implicated in HD-related microglial dysfunction including endocannabinoid and kyrurenine pathway. It is safe to assume, however, that other relevant signaling pathways and potential mechanisms exist. One of the ways to uncover potential mechanisms of immune cell dysfunction in HD is through the use of unbiased microarray technology. Microarray and RNA-seq transcriptomic analysis of isolated microglia from HD mouse models may provide further insight into the mechanisms underlying microglial dysfunction in HD. Using an established *ex vivo* culture and flow cytometry system, microglia and astrocytes were isolated from HD

mouse brain and subject to protein phosphorylation and transcriptomic analysis, respectively. The data generated from these projects will further inform future work aimed at understanding microglial dysfunction in HD.

1.5 Objectives

The objectives of my thesis were to develop a flow cytometry system to isolate specific cell populations from culture and whole mouse brain and apply it to: 1) evaluate *HTT* expression in the cell cycle, 2) verify the efficacy of various microglia-specific conditional knockout mouse models, 3) investigate signaling transduction cascades in mutant-huntingtin expressing microglia and, 4) evaluate the glial transcriptome in response to *in vivo* LAQ treatment.

2 Establishment of a Flow Cytometry System and Application to *HTT* Expression in the Cell Cycle

2.1 Introduction

Previous assays aimed at studying the effect of mutant huntingtin expression in different cell types relied on the generation of primary cultures generated from embryonic or neonatal pups. Since Huntington's disease is a late-onset neurodegenerative disease, the use of primary cultures may not entirely reflect the cellular mechanisms and environment underlying disease pathogenesis in the aged brain. By isolating specific cell populations from adult murine brain, we gain important insights into the cell-intrinsic effect of mutant huntingtin expression as well as the response of different cell types to therapeutic intervention. Generating an assay that is both reproducible and quantifiable is a powerful tool as it allows researchers to compare potential gene expression changes in wild-type and transgenic brain in specific cell types. The validity of this assay, however, relies heavily on optimization steps to ensure that viable and enriched cellular populations are isolated. To investigate *HTT* expression in the cell cycle, cell-specificity of conditional knockout mouse models, and transcriptional changes in glial populations, I developed a flow cytometry system to isolate specific cells of interest from both cultured cells as well as intact adult murine brain. Assessing cell-specific transcript expression in isolated cell populations was used to validate this assay and ensure sorting purity.

2.1.1 Flow Cytometry Sorting

Flow Cytometry sorting is a technique whereby specific cell populations of interest can be physically isolated from cultured cells as well as intact mouse brain on the basis of specific antibody binding. In addition to phenotypic characterization, flow cytometry allows for the measurement of DNA and RNA content of cells (Ormerod, 2000; El Naggar, 2004), along with features such as ion flux or pH (Rabinovitch, 2000), and apoptosis or cell death (Darzynkiewicz *et al.* 1997). A typical flow cytometer is composed of fluidics, optics (excitation and collection), electronic network (detector) and a computer. The fluidics system focuses the sample to the light source, which then excites

the cells/particles and collects the information using the optics component of the machine. The electronic network detects the signals emitted from the sample and converts to the signals into digital data that is then analyzed by the computer system (reviewed in Adan *et al.* 2017). Generally there are two main analysis parameters in cell sorting: cell size/granularity and antibody labeling. The combination of both considerations allows for specific, live cells of interest to be isolated.

A single cell suspension is stained with conjugated fluorochrome antibodies and hydrodynamically focused through the flow cytometer so that cells can pass through one at a time. As each cell passes through the laser, the flurochrome attached to the cells absorbs light and emits a specific color of light (fluorescence) depending on the type of flurochrome. The fluorescence intensity data collected corresponds to the density of the fluorochrome on or within the cell. At the same time, the light scatter emitted from each cell is measured to identify live cells. The light scatter measured at 90° from incidence corresponds to side scatter (SSC) and at 180° reflects forward scatter (FSC). The side scatter (SSC) reflects the granularity or the complexity of the cell while the forward scatter (FSC) corresponds to cell size (reviewed in Davies, 2010). These two parameters alone are sufficient to distinguish different cell populations and to exclude dead cells and debris.

In order to identify specific cell populations, a single cell suspension is stained with multiple flurochrome antibodies. False signals resulting from spectral overlap between fluorescent dyes in these multicolor staining panels is a potential limitation of the flow cytometry system. In order to eliminate these false signals, compensation techniques are used to ensure that fluorescent intensities reflect the nature of the analyzed cells and are not false positive populations (Ormerod, 2009).

In cell sorting, different cell populations are physically sorted at the end of the run into separate tubes. An electronic system in the flow cytometer processes the fluorescent and scatter signals of each cell and determines an appropriate charge to give each cell. In the beginning, only two populations were sorted with one population given a negative charge signal and the other a positive one. Recent advances have allowed the separation of up to four populations simultaneously by varying the negative and positive signals.

2.1.2 Applications of Flow Cytometry System to Huntington's Disease

As described in the introductory chapter, HTT is ubiquitously expressed throughout the body and has been implicated in a wide range of cellular processes including vesicle transport, survival and development (reviewed in Sadou and Humbert, 2016). In the brain, HTT is present in both neurons as well as glial cell populations. Although the majority of research has focused on neuronal dysfunction in HD, the contribution of the innate immune system has become an area of increased interest. In the context of HD, previous work has demonstrated exaggerated cytokine release in mutant-huntingtin containing microglia in response to proinflammatory stimulation (Connolly *et al.* 2016). It is unclear, however, if the increased inflammatory response identified in HD is a result of a reaction to neuronal dysfunction/degeneration or is a consequence of intrinsic dysfunction in the immune cells themselves.

The flow cytometry system is one way to address this question, whereby pure glial populations can be isolated for adult murine brain for a variety of downstream applications including transcriptomic (RNA-seq) analysis. Comparing gene expression in wild-type and transgenic glial populations provides insight into the cellular and molecular mechanisms underlying mutant huntingtin expression in immune cells. This may provide a better understanding of any potential innate dysfunction in HD glial populations and can focus future therapeutic interventions centered on immune system modulation. It is also possible to isolate glial populations from distinct brain regions, including the cortex and striatum, to better understand the cellular mechanisms involved in the innate immune system in the areas most affected by HD.

System optimization is necessary to ensure that pure, viable populations are isolated. In establishing a system for isolation of glial populations from adult murine brain, numerous technical considerations were taken into account, namely rapid isolation, buffer composition, tissue homogenization, removal of debris and myelin (Percoll gradients, magnetic beads), antibody dilutions and sufficient cell number for downstream applications. Generally, cell populations are isolated from adult murine brain in four steps: 1) Enzymatic dissociation and mechanical homogenization 2) Myelin removal 3) Magnetic Bead Enrichment 4) Antibody labeling and cell sorting. Isolation of the main

glial populations for adult murine brain is outlined in Figure 1.

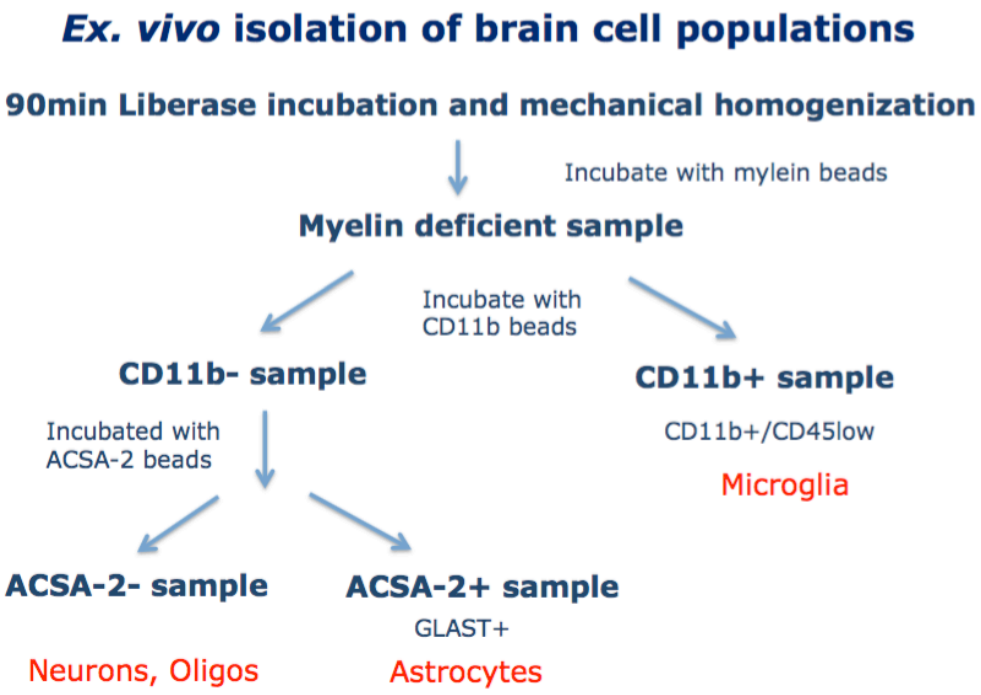

Figure 2. *Ex. vivo* Isolation of Murine Brain Cell Populations for Downstream Transcript and Protein Analysis. Following enzymatic dissociation and mechanical homogenization, single cell suspensions are incubated sequentially with magnetic bead solutions (myelin, CD11b, ACSA-2) and stained with microglia-specific (CD11b, CD45) and astrocyte (GLAST) antibodies. Microglia and astrocyte populations can be reliably isolated for quantification of transcript and protein expression.

2.1.3 Applications of Flow Cytometry System to Cell Cycle Analysis

As mentioned previously, there are numerous flow cytometry applications, one of which is the measurement of cell cycle progression. The cell cycle is the main process leading to cellular proliferation and, is composed of Interphase and Mitosis. Interphase is then divided into 4 sub-phases: G1, S, G2 and mitosis. In G1, cells integrate environmental and internal signals that are aimed at the “replicate” and “do not replicate” decision. S phase is defined as the ability to synthesize genomic DNA. G2 is a time of DNA damage repair and preparation for entering mitosis (or the M phase). The transition

from one cell cycle phase to the other is a tightly regulated process where key regulatory proteins called cyclin-dependent kinases (CDKs) ensure proper progression (reviewed in Vermeulen *et al.* 2003).

One simple way to evaluate the cell cycle in dividing cells is through microscopic visualization. Simple observation can be used to identify cells undergoing mitosis, or cell division, while more sensitive measures are necessary to visualize the specific phases of interphase, including S phase. In this case, bromo-deoxyuridine (BrdU) dyes are incorporated into newly synthesized DNA in the S phase and visualized using fluorescent microscopy (Alberts *et al.* 2002). Flow cytometry uses a similar technique, whereby cells are stained with intercalating fluorescent dyes and analyzed. In contrast to standard microscopy, flow cytometry allows large numbers of cells to be analyzed rapidly and automatically and ultimately physically isolated. Recent advances in flow cytometry technology allow live cells to be isolated in the different phases of the cell cycle. Previous methods using propidium iodine (PI) staining were limited in two respects, particularly for use in downstream applications. First, PI staining is confined to ethanol-fixed cells. PI also stains double-stranded RNA, meaning that RNase A is a required component of the staining solution and is needed to degrade RNA and prevent incorrect labeling (Pozarowski and Darzynkiewicz, 2002). The combination of both technical considerations prevents reliable transcript analysis of sorted populations. Newly manufactured fluorescent Hoechst DNA dyes, on the other hand, allow for the direct analysis of live cells and isolation of populations for downstream analysis.

2.1.4 *HTT* Transcriptional Regulation and the Cell Cycle

Although used primarily in cancer research to evaluate the effect of potential therapeutics on cellular proliferation (Vermeulen *et al.* 2003), the investigation of the cell cycle can also be used to evaluate *HTT* transcriptional regulation. As described in the introductory chapter, HD is a monogenic disorder caused by a CAG expansion of the *HTT* gene. There is an inverse relationship between CAG repeat length and age of onset, but this correlation only accounts for 60-70% of variance of age of onset (Andrew *et al.* 1993), meaning that other putative causative modifiers may be present that affect disease

pathogenesis. One of these modifying factors may by the differential expression of the *HTT* gene. Although numerous studies have investigated the function of wild-type and mutant *HTT,* how the gene itself is regulated has been largely overlooked. Previous work aimed at assessing *HTT* regulation focused primarily on relatively short regions proximal to the translational start site of the gene (Lin *et al.* 1995, Coles et al. 1997)**.** While these studies identified several transcription factors able to modify *HTT* expression (Becanovic *et al*. 2015, Ryan *et al*. 2006, Tanaka *et al.* 2004, R. Wang *et al.* 2012)**,** a greater understanding of the regulation of the gene is still needed. Knowledge of *HTT* regulation at the transcriptional level would provide insight into the gene's function and would help focus therapeutic strategies aimed at lowering mutant *HTT* expression.

Gene expression at the transcript level may vary through the progression of the cell cycle. With the regulation of *HTT* poorly understood, this aim investigated the cell cycle as a novel mechanism of *HTT* regulation in cultured cells. Various cell types, including human embryonic kidney HEK293, rat neuronal progenitor ST14 and human cervical HeLa cells, were isolated in different phases of the cell cycle using flow cytometry and *HTT* expression at the transcript and protein level was measured. The use of both cell types from the periphery (kidney and cervix) and CNS (brain) were used to evaluate potential *HTT* expression differences in the cell cycle between the brain and periphery.

2.1.5 Subcellular Huntingtin Localization

Another component of genetic regulation is the subcellular localization of the resulting protein product following translation. Understanding where a protein is localized is important to define its role within the cell both normally and, in the case of huntingtin, pathologically (Hughes and Jones, 2011). Within the cellular environment, huntingtin is predominately cytoplasmic, where it localizes to the endoplasmic reticulum (Atwal *et al.* 2007), vesicles (DiFiglia *et al.* 1995), along with endocytic, lysosomal and plasma membranes (Velier *et al*. 1998). Huntingtin has also been shown to localize to the mitotic spindle and play a role in mitosis, or cell division. Endogenous mouse huntingtin (*hdh*) localizes to the spindle to mediate proper orientation. The orientation of the mitotic

spindle is important in ensuring correct cell division, where disruptions can promote increased cell death. Transfection of siRNA-targeting *hdh* in mouse neuronal cells resulted in disrupted spindle orientations, and increased post-mitotic cell death with no changes in cell cycle progression (Godin *et al.* 2010). Similar effects are seen following *hdh* silencing *in vivo* with increased spindle misorientation seen in neuronal progenitor cells. Huntingtin depletion in this context did not alter the proportion of dividing cells in the different layers of the cortex, demonstrating that *hdh* silencing does not interfere with neuronal migration (Godin *et al.* 2010). Taken together, these data suggest that wild-type huntingtin is directly involved in mitosis and as a result, huntingtin expression may be regulated by cell-cycle dependent mechanisms.

In addition to a variety of localizations inside the cell, huntingtin has also been found to be present in the nuclear compartment. Fractionation and immunofluorescence studies in healthy neurons have identified nuclear huntingtin localization, although the levels are considerably lower than those seen in the cytoplasmic cellular compartment (De Rooij *et al.* 1996, Hoogeveen *et al.* 1993). Similar low levels of nuclear localization have also been previously identified in dividing glial cells (Martin-Aparicio *et al.* 2001), demonstrating a potential shuttling mechanism whereby HTT moves between the nucleus and cytoplasm (Truant *et al.* 2007). This localization to the nucleus can be affected by different stimuli including ER stress (Atwal *et al.* 2007) and reactive oxygen species (ROS) stress, which is a common symptom of aging. Recent work has demonstrated that induction of ROS using 3-NP treatment, a mitochondrial activator, results in increased levels of huntingtin phosphorylation and nuclear puncta formation. A highly conserved methionine residue at position 8 in the N17 domain of huntingtin senses reactive oxygen species and undergoes a structural change to enhance N17 phosphorylation and nuclear targeting of endogenous huntingtin (DiGiovanni *et al.* 2016). ROS stress, as a result, may be a critical mediator of huntingtin localization and may contribute to disease pathogenesis, particularly as nuclear localization of mHTT is thought to contribute to the selective vulnerability of neurons in HD.

The N17 amino acid domain of huntingtin also plays a role in modulating mutant huntingtin toxicity resulting from nuclear localization. Two serine residues, Ser13 and Ser16, within the N17 domain are hyperphosphorylated in mutant huntingtin containing

cells. This same phosphorylation can be induced in wild-type containing huntingtin cells, resulting in huntingtin localization to sub-regions of the nucleus, and the mitotic spindle. Kinase inhibitors, including casein kinase-2, can reduce N17 phosphorylation and decrease huntingtin nuclear and subnuclear localization. As a result, huntingtin phosphorylation at Ser13 and Ser16 may mediate nuclear huntingtin localization and contribute to the mutant huntingtin toxicity (Atwal *et al.* 2011). Another possible mechanism underlying selective neuronal vulnerability in neurons may be related to cell cycle re-entry. In a rat model of HD, increased expression of cell cycle markers of G1, specifically E2F-1, were detected in the striatum following neurotoxin administration (3-nitropropionic acid; 3-NP). Similar analysis in HD post-mortem brain demonstrated similar increases in E2F-1 and cyclin D1 protein expression compared to controls (Pelegri *et al.* 2008). The elevated levels of G1 proteins in HD rat and human brain indicate that cell cycle re-entry may be activated in HD and may influence apopotic cascades.

2.1.6 HeLa FUCCI Cells in Cell Cycle Localization Analysis

One way to evaluate huntingtin localization is through the use of a line of commercially available HeLa cells. As mentioned previously, huntingtin is primarily located in the cytoplasm, but there are instances of nuclear localization (Martin-Aparicio *et al.* 2001, DiGiovanni *et al.* 2016). The shuttling between these two cellular compartments may be cell cycle-dependent, meaning that as the cell progresses through the different phases of the cell cycle, huntingtin may move from the nucleus to the cytoplasm. More importantly, evaluating the localization of huntingtin in each cell cycle phase would provide greater insight into the gene's function and would identify potential pathways that could be targeted therapeutically.

HeLa FUCCI cells express a genetically encoded two-color indicator that allows for rapid identification of the cell cycle. A dual vector was transfected into the cells with an RFP-cdt1 tag and a GFP-geminin-tag. The cdt1 protein is preferentially expressed in G1 cells, while geminin is present in cells in the S/G2/M phases. As a result, cells in G1 will express RFP and cells in S/G2/M will be identified using GFP, allowing for

visualization of cell cycle using confocal microscopy. Previous iterations of this cell line were used to identify the role of huntingtin expression in mitosis. Similar to the effect of *hdh* depletion in mouse neuronal cells, RNA interference in dual-vector expressing HeLa cells resulted in spindle misorientation (Godin *et al.* 2010). The HeLa cell line used by Godin *et al.* expressed red nuclear and green cytoplasmic proteins, similar to the FUCCI cells, allowing for the direct visualization of the cell cycle using video microscopy. In this context, silencing of human *HTT* did not affect the duration of mitosis but the angle and amplitude of the mitotic spindle was more variable in depleted cells, underlying the role of huntingtin in spindle orientation (Godin *et al.* 2010). The same HeLa cells were also used to assess huntingtin localization in interphase (G1, S, and G2/M) and the various stages of mitosis (prophase, metaphase, anaphase, telophase/cytokinesis). Nuclear puncta were identified in interphase and in the stages of mitosis, hdh was localized to the mitotic spindle (Godin *et al.* 2010). The establishment of the HeLa FUCCI cell line improves upon localization studies and allows a protein of interest, in this case HTT, to be visualized in the three separate stages of interphase. The HeLa FUCCI cell line can also be used to identify potential localization differences between endogenous wild-type huntingtin and mutant huntingtin. Previously generated expression vectors in the lab contain wild-type and mutant huntingtin along with an HA tag. The HA tag is a surface glycoprotein that is used extensively as a general epitope tag in expression vectors (Schembri *et al.* 2007). More importantly, the presence of the HA tag in the expression tag allows for wild-type and mutant huntingtin to be visualized using immunofluorescence following transfection in HeLa FUCCI cells.

As discussed in the introduction, the flow cytometry system has various applications. I have established a system to isolate glial cells from the adult mouse brain to study the effect of mutant huntingtin expression in response to a current HD therapeutic. The relative ease of the system also allows for the evaluation of *HTT* regulation and localization in the cell cycle. Both applications, although different, provide greater insight into HD disease pathogenesis and the biology of HTT.

2.2 Methods

2.2.1 Isolation of Adult Microglia from Murine Brain

Adult microglia were isolated from murine brain using a combination of enrichment techniques followed by flow cytometry sorting. Cell populations obtained using the FACS system yield sufficient quality RNA and protein for downstream trancriptomics and protein analysis. For isolating adult murine brain cell populations, I used a general protocol of 1) Enzymatic and Mechanical Homogenization 2) Myelin depletion using the AutoMACS 3) Cell-specific enrichment using the AutoMACS 4) Antibody staining and Flow Cytometry Sorting. Each component of the system will be discussed in greater detail below.

The adult murine brain is composed of a large percentage of myelin. In order to isolate brain cell populations the brain tissue must be homogenized in such a way that a single cell suspension is achieved. Numerous techniques use a tissue homogenizer to dissociate adult brain tissue but the process is detrimental to cell survival. The combination of gentle enzymatic dissociation and mechanical homogenization using a pipette tip results in a single cell suspension while retaining adequate cell viability for subsequent flow cytometry sorting.

The Miltenyi® AutoMACS machine is a fully automated cell separator that uses magnetic separation to select for populations of interest. Samples incubated with specific magnetic solutions run through an AutoMACS column and are either magnetically retained in the column (positive selection) or flow through (negative selection). The magnetic bead enrichment steps, also termed immunomagnetic separation, are used for several reasons. Instead of staining a single cell suspension with the antibodies of choice, the sample is enriched for the population of interest. This ensures that large amounts of antibodies are not used to stain rare cells and that the population of interest is isolated quickly to ensure cell viability (Bedi *et al.* 2013).

2.2.2 Enzymatic and Mechanical Homogenization

Mice were sacrificed using CO_2 followed by cervical dislocation. Whole brains (minus the cerebellum and olfactory bulbs) were removed and briefly washed in 1mL of HBSS. Brains were quickly placed in 4mL of Liberase cocktail solution composed of 4mL of 0.1M HBSS and re-constituted Liberase at a concentration of 47.7uL/mL. Whole brains were rotated in the Liberase solution for 45min at 37°C. Brains were then mechanically homogenized in solution using a P1000 pipette tip until tissue was dissociated, then spun at 200g for 5min at 18°C. Supernatant was removed and homogenates were re-suspended in 2mL of Re-Suspension buffer (0.1M HBSS, 0.5uL/mL filtered $MgCl_2$) and filtered through a 70μm cell strainer. Sample tube was washed with another 2mL of Re-suspension buffer and put through the same 70μm cell strainer. The cell strainer was then washed with an additional 1mL of Re-suspension buffer. Homogenates were spun at 200g for 5min at 18°C.

2.2.3 Myelin Removal using AutoMACS

Following homogenization, supernatant was removed and samples were re-suspended in 4mL of FACS buffer (0.1M PBS, 1mM EDTA, 1% BSA). 500uL of Miltenyi® Myelin Removal Beads II were added to the solution and samples were incubated at 4°C for 15min. Samples were then washed with 10mL of FACS buffer to remove any unattached myelin beads and spun at 200g for 10min at 18°C. Sample supernatants were removed and re-suspended in 4mL of FACS buffer prior to AutoMACS use.

The Miltenyi® AutoMACS machine was used for myelin depletion. The samples were subject to the Deplete_S program, chosen because the frequency of myelin-positive cells is considered normal to high in the whole brain sample. In cases where the level of myelin is small, a different AutoMACS program would be chosen to complete the depletion. Following the automated magnetic separation, the negative fraction (Myelin-deficient sample) was collected and spun at 200g for 5min at 18°C.

2.2.4 Monocyte Selection using AutoMACS

Following myelin removal, samples were then incubated with 30uL of Miltenyi® CD11b magnetic beads in 270uL of FACS buffer for 15min at 4°C. Similar to the Myelin Beads, the samples were washed with 2mL of FACS buffer to remove any unattached CD11b beads and spun at 200g for 10min at 18°C. Sample supernatants were removed and re-suspended in 500uL of FACS buffer prior to AutoMACS selection (Nikodemova and Watters, 2012).

Unlike the myelin removal step, the Miltenyi® AutoMACS machine was used for CD11b positive monocyte cell selection. The Possel_S program was selected and the both the CD11b-positive was collected. Similar to the myelin depletion detailed above, the AutoMACS program chosen for positive selection was a consequence of antigen-expression but purity of selected populations was also taken into consideration. The Possel_S program allows for the selection of cell populations with low antigen-expression where the recovery is the highest priority. By using the Possel_S program, the recovery or selection of cell of interest increases at the expense of purity. For our purposes, the microglia populations required subsequent antibody labeling and flow cytometry sorting, which would help isolate pure populations, and as a result, purity was not the most important factor. Following AutoMACS positive selection, the samples were spun at 200g for 5min at 18°C and re-suspended in 100uL of FACS buffer for subsequent antibody staining.

2.2.5 Microglia Antibody Labeling and Flow Cytometry Sorting

The samples were incubated with Ebioscience® CD11b-PE and Ebioscience® CD45-APC antibodies at a dilution of 1:1000 for 15min at 4°C. An additional 150uL of FACS buffer was added to the sample along with Ebioscience® 7AAD Viability Dye at a dilution of 1:250. The sample was then subject to flow cytometry sorting.

The FACSAria machine, with an 85nozzle and 45psi setting, was used to isolate adult microglia. Briefly, first dead cells were excluded from analysis using 7AAD staining and then the microglia population was identified as CD11b positive and CD45

low. The small population of live cells with high CD45 staining, identified as 10^4 and above on the antibody plot, are characterized as activated microglia or infiltrating macrophages (Greter *et al.* 2015; Ford *et al.* 1995). For our purposes, the quiescent microglia present in the brain are of interest and as such a CD45 antibody is used to distinguish these microglia populations from activated or infiltrating monocyte populations.

2.2.6 Isolation of Adult Murine Astrocytes

Similar methods were used in isolating adult astrocyte populations as microglia, namely in terms of enzymatic/mechanical homogenization and myelin depletion. The positive selection of astrocytes was accomplished using Miltenyi® ACSA-2 beads. Myelin deficient samples were incubated with 30uL of ACSA-2 beads in 270uL of FACS buffer for 15min at 4°C (Feldmann *et al.* 2014). The samples were then washed with 2mL of FACS buffer and spun at 200g for 5min at 18°C. The supernatant was removed and the sample was incubated with an astrocyte-specific antibody. Briefly, the sample was incubated with Miltenyi® Anti-GLAST-APC antibody at a concentration of 1:11 in 100uL of FACS buffer for 15min at 4°C. Similar to isolating microglia populations, an additional 150uL of FACS buffer along with Ebioscience® 7AAD Viability Dye at a dilution of 1:250 was added to identify live cells. The sample was then subject to flow cytometry sorting.

The FACSAria machine, with an 85nozzle and 45psi setting, was used to identify live astrocyte populations. Similar to the isolation of microglia cells, dead cells were excluded using 7AAD staining and astrocyte populations were identified as GLAST-positive cells. We set a threshold for GLAST-positive cells at those with fluorescent intensities above 10^4 to ensure the specificity of both the antibody staining as well as the sorted population.

2.2.7 Sequential Isolation of Microglia and Astrocyte Populations from One Brain Sample

In instances where both microglia and astrocyte populations were sorted from a single brain, a modified protocol was used. Whole brains were subject to similar enzymatic/mechanical homogenization and myelin depletion protocols as described above. Once myelin-deficient samples were collected, the Miltenyi® CD11b bead protocol detailed above was followed. The modification occurred in this AutoMACS step when two specific cell populations were required. In each AutoMACS separation, the sample is divided between a positive fraction and a negative fraction. In the case of specific cell populations, microglia for example, the positive fraction consists of CD11b-positive monocyte cells and the CD11b-negative fraction is composed of the remaining cell populations present in the brain. Because simultaneous bead incubations are not possible, a sequential AutoMACS purification is necessary.

In most cases, microglia were selected first followed by astrocytes but the order of isolations can be completed interchangeably. Once the CD11b-AutoMACS selection is completed, the CD11b-positive sample is collected and stained with microglia-specific antibodies as detailed above. The CD11b-negative fraction is also collected, spun down and incubated with Miltenyi® Anti-GLAST beads similar to the protocol described previously. The CD11b-negative sample is put through the AutoMACS Possel_S program, resulting in an ACSA2-positive and ACSA2-negative sample. The ACSA2-positive sample is collected and incubated with the astrocyte specific antibody prior to flow cytometry sorting.

2.2.8 Isolation of Adult Microglia and Astrocytes from Cortex and Striatum

Mice were sacrificed using CO_2 followed by cervical dislocation. Striatum and cortex were microdissected and placed in 2mL of Liberase solution for 45min. Following mechanical homogenization, two striatal samples were combined and subject to subsequent isolation protocols as outlined in Section 2.2.2-2.2.7. Cortical samples were not combined but microglia and astrocyte populations were isolated separately.

2.2.9 Quantitative Real-Time PCR (RT-qPCR)

Microglia and astrocyte populations were sorted into empty Eppendorf tubes and were processed for cell-type specific transcript quantification. Samples were spun down at 140,000rpm for 5min at 4°C. Cell pellets were then processed for RNA extraction using the protocol detailed in the PureLink® RNA Mini Kit (Invitrogen) with the following modifications: 1) Homogenization was achieved using two freeze-thaw cycles in which samples incubated with 600uL of lysis buffer supplemented with β-mercaptoethanol were placed on dry ice 2) An additional DNase step was used to degrade any residual genomic DNA in the prep column in order to increase RNA yield and purity. The PureLink® DNase kit was used according to the manufacturers protocol. The concentration and purity of RNA was then assessed using a nanodrop spectrometer (Thermo Scientific). Reverse transcription was performed using the SuperScript® VILO™ cDNA synthesis kit (Invitrogen). Quantitative analysis of mRNA expression was performed using the FastSYBR® green mastermix according to the user's manual (Applied Biosystems). Amplification of cDNA was performed using the StepOne Plus Real-Time PCR System (Applied Biosystems). Primers used for cell-specific transcripts and normalization genes are provided below in Table 2.1 and 2.2. Quantification of mRNA levels was calculated using the standard curve method using 10-fold serial dilutions composed of primary cells as standard samples. Normalization of the quantified mRNA levels was completed using a normalization factor generated by the GeNorm program included in the qBase® software package. A normalization factor (NF2) was generated for each sample using two mouse normalization genes, Rpll13a and Usfi9.

Table 2.1 RT-qPCR Primers for Sorted Microglia

Transcript Target	Forward (5'-3')	Reverse (5'-3')
Iba-1	GTCCTTGAAGCGAATGCTGG	CATTCTCAAGATGGCAGATC
CD68	GTGCTCATCGCCTTCTGCATCA	GGCGCTCCTTGGTGGCTTAC
Rpll13a	GGAGGAGAAACGGAAGGAAAAG	CCGTAACCTCAAGATCTCGTTCTT
Usf1	CCTGTGGCGTGGCAGTCT	TGCACGCCCACACTGTTT

Table 2.2 RT-qPCR Primers for Sorted Astrocytes

Transcript Target	Forward (5'-3')	Reverse (5'-3')
GLAST	CTCCAGTCTCGTCACAGGAAT	TTATGCCAATCACCACAGCAA
S100-β	TCTAACTCAGGACCGAGAATCA	GGAGCAAGGAAGATACAACAACTAACT
Aquaporin	TCTGGCCACGCTTATCTTTGT	TTTCTGAGCCACCCCAGTTT

2.2.10 Isolation of HEK293 Cells in Different Phases of the Cell Cycle

Human Embryonic Kidney (HEK293) cells are a peripheral-derived cell line that expresses low levels of endogenous human *HTT* transcript. HEK293 cells were maintained in complete media, DMEM supplemented with 10%FBS, 2mM L-glutamine, 2mM Penicillin/Streptomycin, and 130 μg/mL of Hygromycin in a cell culture incubator at 37°C and 5% CO_2. Prior to flow cytometry sorting, HEK293 cells were subject a serum deprivation protocol. T75 flasks were seeded with 500,000 cells and allowed to grow for 24h. The next day, the media was exchanged for DMEM only (starvation) media for 48h. After 48h, the media was exchanged for complete media (detailed above) and allowed to grow for 72h. Flasks were collected and flow cytometry samples were prepared containing 1mL of cell suspension in complete media at a concentration of $1x10^6$ cells. To each tube, 1μL of Vybrant® DyeCycle™ Violet stain (Invitrogen) was added to a final concentration of 5μM. The samples were incubated at 37°C for 30min, protected from light. The samples were then sorted without washing or fixing on the FACSInflux flow cytometry using 405nm excitation and 488nm emission parameters.

Using the flow cytometer, live cells (P1) were identified on the basis of forward scatter (FSC) and side scatter (SSC) parameters with live cell density gated at larger FSC values, corresponding to larger, more complex cells. Next, doublets, or cells clumped together, were excluded from subsequent sorting using FSC-width and SSC-width parameters. The exclusion of doublet cells is imperative in cell cycle analysis where DNA content distinguishes the different phases of the cell cycle. The fluorescence intensity is then identified and represented in a histogram as DNA content. The DNA histogram and fluorescent intensity is then used to sort cells as G1, S and G2/M for subsequent RNA extraction and mRNA transcript quantification.

2.2.11 Isolation of ST14 Cells in Different Phases of the Cell Cycle

Striatal rat neuronal progenitor (ST14) cells, a central-derived cell line, were maintained in DMEM medium supplemented with 10%FBS, 2mM L-glutamine, 2mM Penicillin/Streptomycin, and 125 μg/mL of Hygromycin in a cell culture incubator at 34°C and 5% CO_2. Similar to HEK293 cells, T75 flasks with 250,000 cells were seeded and subject to a serum deprivation protocol. Briefly, flasks were seeded and allowed to grow for 24h in complete media (detailed above). The next day, media was exchanged for DMEM starvation media for 48h. Complete media was then replaced and flasks were incubated at 34°C for 5 days prior to flow cytometry sorting. Flasks were collected and flow cytometry samples were prepared containing 1mL of cell suspension in complete media at a concentration of $1x10^6$ cells. Vybrant® DyeCycle™ Violet stain (Invitrogen) was added to the samples at a final concentration of 5μM, similar to HEK293 cells. The samples were incubated at 37°C for 30min, protected from light and then sorted without washing or fixing on the FACSInflux flow cytometry using 405nm excitation and 488nm emission parameters**.** G1, S and G2/M samples were sorted according to similar parameters outlined in the HEK293 methods above. The samples were then subject to RNA extraction and mRNA transcript quantification to assess *HTT* expression across the cell cycle.

2.2.12 Isolation of HeLa FUCCI cells in the Different Phases of the Cell Cycle

Human cervical cancer (HeLa FUCCI) cells were maintained in DMEM media supplemented with 110mg/L sodium pyruvate, 2mM glutamine and 2mM Penicillin/Streptomycin in a cell culture incubator at 37°C and 5% CO_2. T75 flasks were seeded and collected when 80% confluent for flow cytometry sorting. Briefly, flasks were passaged in 10mL of media and pelleted. Pellets were re-suspended in 1mL FACS buffer (1% BSA, 2% EDTA) and sorted on the FACSAria using 85nozzle, 45psi parameters.

Live cells were identified using FSC and SSC parameters as described in the previous HEK293 methods section. Identification of G1, early S and late S/G2/M populations was completed using Aria parameters as described in Otani *et al.* 2016.

2.2.13 Quantitative Real-Time PCR (RT-qPCR)

G1, S and G2/M samples were sorted into empty Eppendorf tubes and processed for *HTT* transcript quantification. Following sorting, samples were spun down at 140,000 rpm for 5min at 4°C. Cell pellets were then processed for RNA extraction using the protocol detailed in the PureLink® RNA Mini Kit (Invitrogen) and the modifications outlined in Chapter 2 Methods. The concentration and purity of RNA was assessed using a nanodrop spectrometer (Thermo Scientific). Reverse transcription was performed using the SuperScript® VILO™ cDNA synthesis kit (Invitrogen). Quantitative analysis of mRNA expression was performed using the FastSYBR® green mastermix according to the user's manual (Applied Biosystems). Amplification of cDNA was performed using the StepOne Plus Real-Time PCR System (Applied Biosystems). Primers used for human (*HTT*) and mouse (*hdh*) huntingtin and normalization genes are provided below in Tables 2.2-2.4. Quantification of mRNA levels was calculated using the standard curve method using 10-fold serial dilutions composed of unsorted cells as standard samples. Normalization of the quantified mRNA levels was completed using a normalization factor generated by the GeNorm program included in the qBase® software package. A normalization factor was generated for each sample using two mouse normalization genes (Normalization Factor 2, NF2).

Table 2.3 RT-qPCR Primers for Sorted HEK293 cells

Transcript Target	Forward (5'-3')	Reverse (5'-3')
HTT	TCCACCATGCAAGACTCACTTAG	TGGGATTTGACAAGATGAACGT
ACTB	AGTACTCCGTGTGGATCGGC	GCTGATCCACATCTGCTGGA
HPRT1	TTATGGACAGGACTGAACGTCTTG	GCACACAGAGGGCTACAATGTG

Table 2.4 RT-qPCR Primers for Sorted ST14 cells

Transcript Target	Forward (5'-3')	Reverse (5'-3')
hdh	GGAGGAGAAACGGAAGGAAAA	CCGTAACCTCAAGATCTCGTTCTT
Rpll13a	ACAAGAAAAGCGGATGGTG	TTCCGGTAATGGATCTTTGC
CycA	ACAAGAAAAAGCGGATGGTG	TTCCGGTAATGGATCTTTGC

Table 2.5 RT-qPCR Primers for Sorted HeLa FUCCI cells

Transcript Target	Forward (5'-3')	Reverse (5'-3')
HTT	TCCACCATGCAAGACTCACTTAG	TGGGATTTGACAAGATGAACGT
PGK1	CAAATGGAACACGGAGGATAAAG	CTTTACCTTCCAGGAGCTCCAA
GAPDH	GAAGGTGAAGGTCGGAGTC	GAAGATGGTGATGGGATTTC

2.2.14 Immunocytochemistry in HeLa FUCCI Cells

HeLa FUCCI cells were seeded on PDL-coated glass coverslips in 24-well plates at a concentration of 75,000 cells per mL of media. Cells were allowed to recover for 24hr and were fixed with 3% paraformaldehyde for 15min at room temperature and stained for immunocytochemistry. Fixed cells were washed three times in PBSTx (0.1& Triton-x in PBS) and blocked in 10% donkey serum for 1hr. Wells were then incubated 2% donkey serum in PBS-Tx with N-terminal 2166-HTT (anti-mouse MAB 2166 Millipore, 1:1000), and C-term 2 (anti-rabbit CHDI 90000139, 1:500) overnight at 4°C. Cells were washed three times in PBS-Tx and treated with fluorescent secondary antibodies diluted in 2% goat serum and PBS-Tx. 2166-HTT stained wells were incubated with goat anti-mouse 647 secondary (Life Technologies, 1:1000) and C-term 2 cells were stained with goat anti-rabbit 647 (Alexa Fluor, Invitrogen, 1:1000) for 1hour at room temperature, protected from light. Cells were washed twice with PBS-Tx and counter-stained with 200nM 4', 6-diamidino-2-phenylindole (DAPI) solution for 5min. After a final 5min wash in PBS followed by deionized water, coverslips were air-dried, cleared in xylenes and mounted onto glass slides using DePeX Mounting medium (ElectronMicroscopySciences).

2.3 Results

2.3.1 Microglia Isolated from Intact Adult Murine Brain Express Microglia Specific Transcripts

Three-month old wild-type (B6 background) mice were subject to the flow cytometry protocol outlined in Sections 2.21- 2.2.5. Briefly, myelin was depleted from whole brain and monocyte populations were enriched using AutoMACS magnetic separation. Enriched monocyte populations were incubated with CD11b and CD45 antibodies to identify microglia and stained with 7AAD to select for live cells. As discussed in the introductory chapter, CD11b is an integrin constitutively expressed on quiescent and activated microglia (Sedgwick *et al.* 1991; Frank *et al.* 2006). The addition of a CD45 antibody is used to identify quiescent microglia (Greter *et al.* 2015) and to differentiate microglia from other CNS-associated macrophages (Ford *et al.* 1995). The combination of both antibodies allow for the identification of perivascular (resident) microglia (CD11b+/CD45+), parenchymal microglia (CD11b+/CD45 low), and macrophages (CD11b-/CD45+) (Volden *et al.* 2015). An average of 150,000-250,000 microglia cells were obtained per whole brain. RNA was extracted from isolated microglia populations according to Section 2.2.9 and microglia-specific transcripts were measured. Ionized calcium binding adaptor molecule (Iba1) is a microglia markers frequently used to population purity (Ito *et al.* 1998). The lysosomal marker, CD68 is another commonly used microglia marker, in addition to Iba1 (Kofler and Wiley, 2011). Isolated microglia populations highly express Iba1 (Figure 2.1 D) and CD68 (Figure 2.1 E), suggesting that the sorted populations demonstrate high purity for microglia cells. CD68 is also considered a marker of activated microglia and is expressed at higher levels in microglia derived for postnatal mice as compared to isolated microglia, suggesting that these primary microglia may be in a more activated state.

A

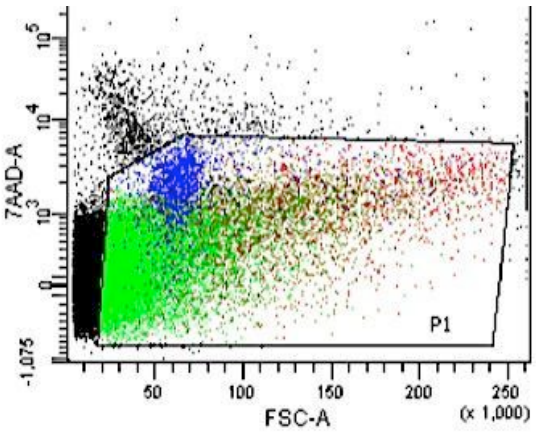

B

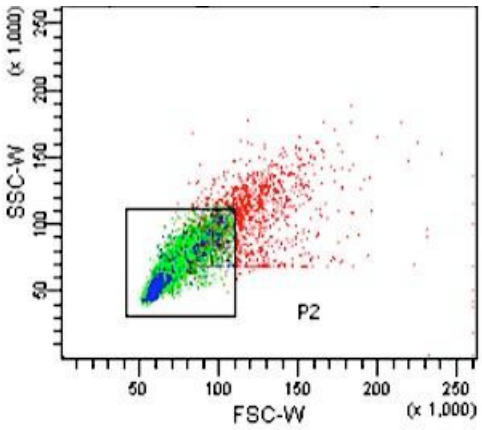

C

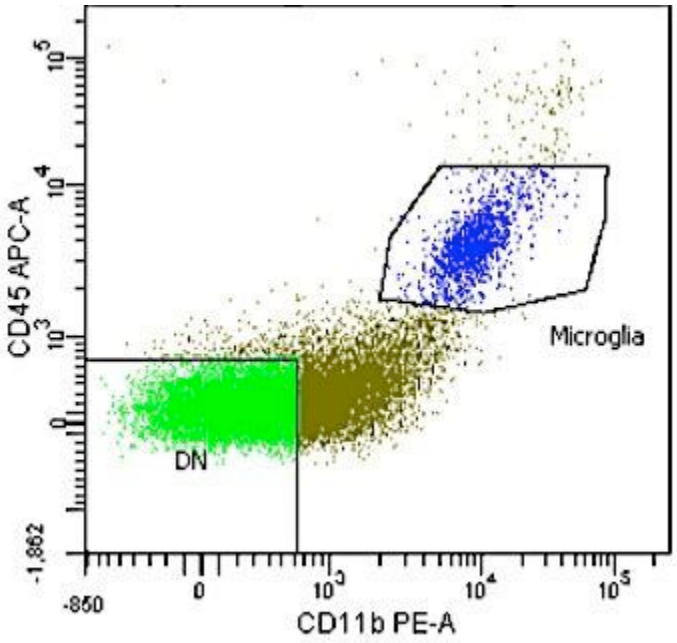

Population	#Events	%Parent	%Total
All Events	40,000	####	100.0
P1	19,040	47.6	47.6
P2	18,056	94.8	45.1
DN	9,548	52.9	23.9
Microglia	1,640	9.1	4.1

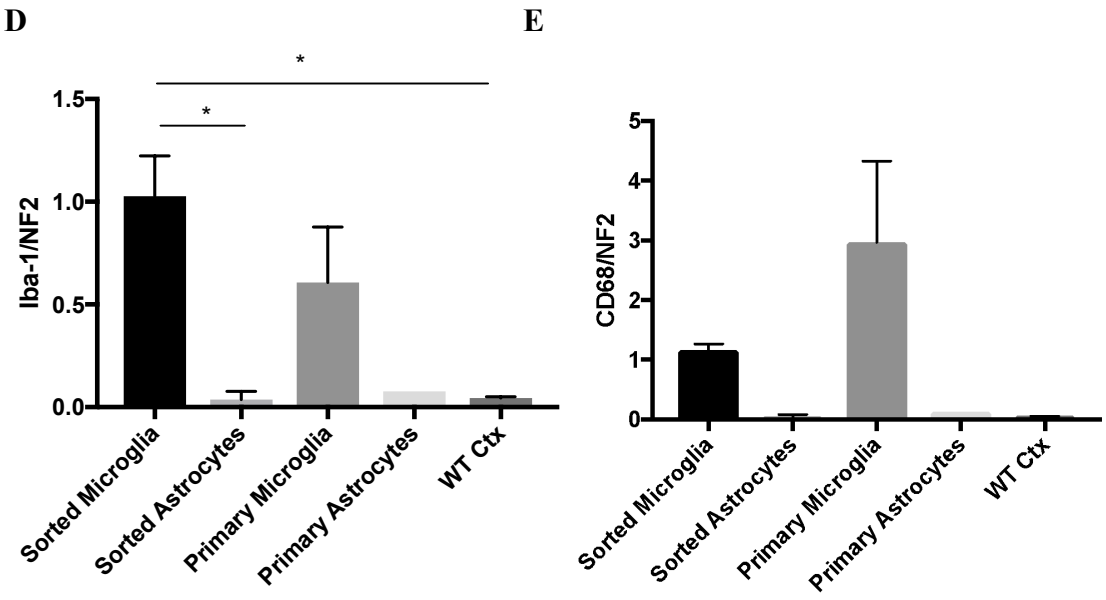

Figure 2.1 Isolated Microglia Populations Express Microglia-Specific Transcripts. Representative data acquired from microglia isolated from WT adult murine brain (3 months of age) (A-C). Primary microglia and primary astrocytes samples refer to populations isolated from postnatal WT pups using an established *ex vivo* co-culture system (McCarthy and de Vellis, 1980). A) Identification of live cells using 7AAD viability staining. Cells with negative 7AAD staining gated as P1 population, corresponding to live cells. B) Exclusion of doublets using forward scatter-width (FSC-W) and side scatter-width (SSC-W) settings. C) Microglia identified as CD11b-positive and CD45-low expressing cells. Double negative (DN) cells sorted as negative control. D) RT-qPCR quantification of isolated microglia populations demonstrate significant levels of Iba-1 mRNA compared to sorted astrocytes (* $p<0.0415$) and WT cortex (ctx) (p*<0.0427) (One-way ANOVA; * p-value<0.0142; Bonferroni correction for both) E) Isolated microglia populations also express CD68 transcript (n=2) (One-way ANOVA; * p-value<0.0484; Bonferroni correction), although to a lesser extent than primary microglia, which may be in a more activated state. NF2 corresponds to normalization factor 2 (normalization to two control genes; Rpll13a, Usf1).

2.3.2 Isolated Astrocytes from Intact Adult Murine Brain Express Astrocyte-Specific Transcripts

Three-month old wild-type (B6 background) mice were subject to the flow cytometry protocol outlined in Sections 2.21- 2.2.3; Sections 2.2.6, 2.27, 2.2.9. Briefly, myelin was depleted from whole brain and sequential microglia and astrocyte enrichments were completed using AutoMACS magnetic separation. Enriched astrocyte populations were incubated with GLAST antibodies to identify astrocytes and stained with 7AAD to select for live cells. L-glutamate/L-aspartate (GLAST) (EAAT1) is a glutamate transporter primarily expressed in astrocytes (Lehre *et al.* 1995), involved in maintaining extracellular glutamate levels (Rothstein *et al.* 1996; Perego *et al.* 2000). GLAST also co-expresses with other common astrocyte markers such as GFAP and S100β (Kantzer *et al.* 2013; Feldmann *et al.* 2014). An average of 300,000 astrocytes were isolated per whole brain. Similar to isolated microglia populations, RNA was extracted from sorted astrocytes and astrocyte-specific transcripts were measured. S100β is a Ca^{2+} binding protein highly expressed in astrocytes (Brozzi *et al.* 2009) and Aquaporin 4 is a bidirectional water channel that is found in astrocytes (Hubbard *et al.* 2015). Isolated astrocytes highly express both S100β (Figure 2.2 C) and Aquaporin (Figure 2.2 D), suggesting that the sorted populations demonstrate high purity for astrocyte cells.

A

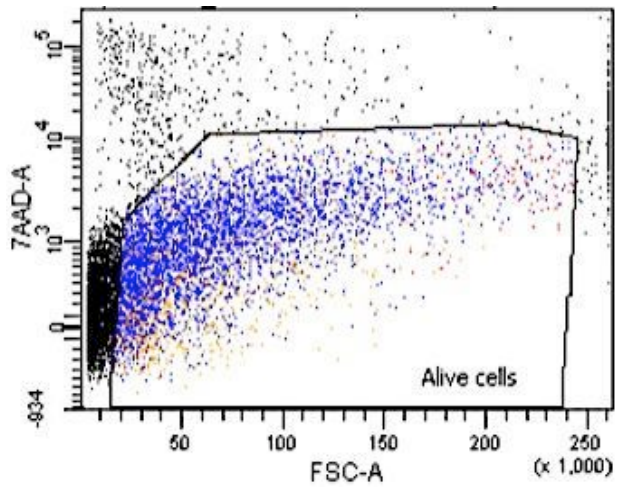

B

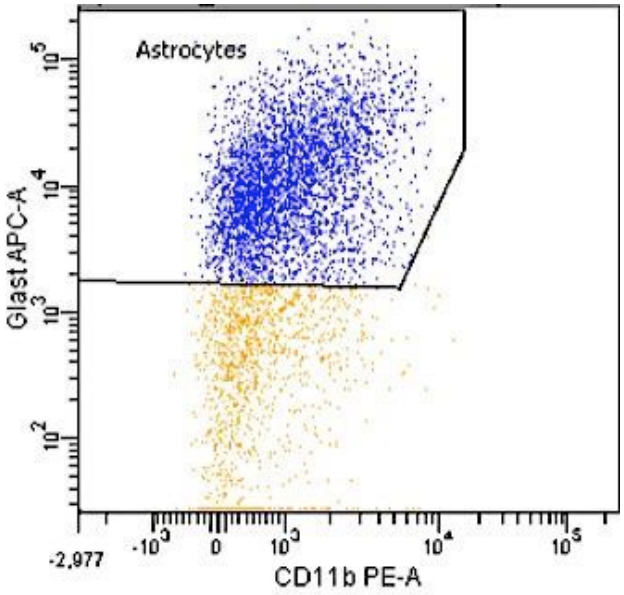

Population	#Events	%Parent	%Total
All Events	10,000	####	100.0
Alive cells	5,520	55.2	55.2
Singlets	5,396	97.8	54.0
Astrocytes	4,066	75.4	40.7

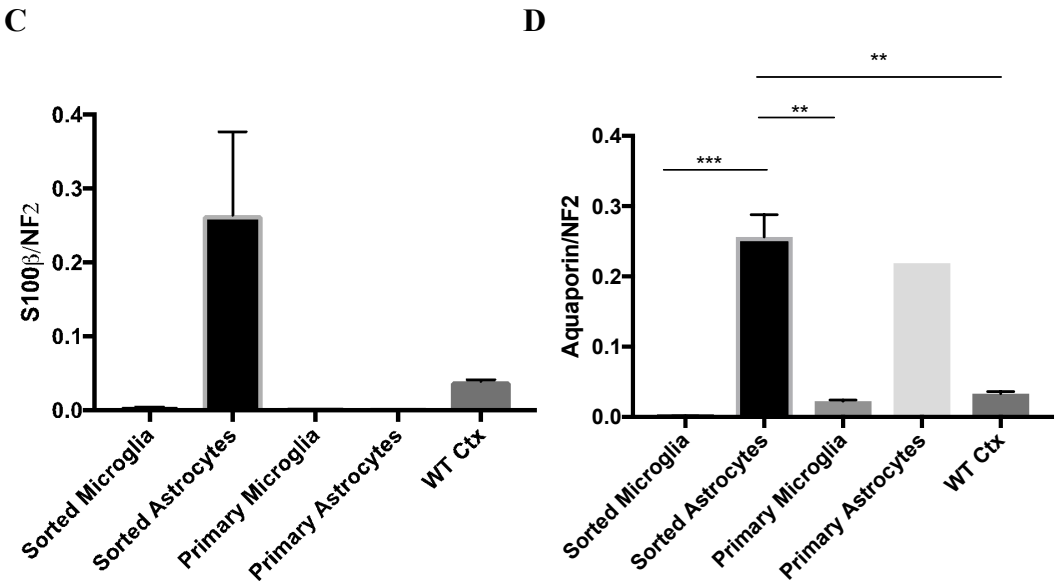

Figure 2.2 Isolated Astrocyte Populations Express Astrocyte-Specific Transcripts. Representative data acquired from microglia isolated from WT adult murine brain (3 months of age) (A-B). A) Identification of live cells using 7AAD viability staining. Cells with negative 7AAD staining gated as P1 population, corresponding to live cells. B) Astrocytes identified as GLAST-positive expressing cells. C) RT-qPCR quantification of isolated astrocyte populations demonstrate high levels of S100β mRNA (n=2) (One-way ANOVA; *p-value<0.0354; Bonferroni correction) D) RT-qPCR quantification of isolated astrocyte populations (n=2) demonstrate significant Aquaporin mRNA levels compared to sorted microglia (***p<0.0009), primary microglia (**p<0.013) and WT cortex (ctx) (**p<0.015) (One-way ANOVA; *** p-value< 0.0003; Bonferroni correction for all). NF2 corresponds to normalization factor 2 (normalization to two control genes; Rpll13a, Usf1).

2.3.3 Endogenous Mouse huntingtin Expression is Decreased in Isolated Microglia Populations compared to Astrocytes in both WT and YAC128 Whole Brain

Microglia and astrocyte populations were sequentially isolated from three-month old wild-type (FVB/N background) and YAC128 mice according to the protocol outlined in Sections 2.21- 2.2.7; 2.2.9. Briefly, myelin was depleted from whole brain and sequential microglia and astrocyte enrichments were completed using AutoMACS magnetic separation. YAC128 mice express both endogenous mouse huntingtin (*hdh*) along with full-length human huntingtin (*HTT*) containing 128 CAG repeats (Slow *et al.* 2003) while wild-type mice express only endogenous mouse huntingtin. *hdh* mRNA levels were decreased in isolated microglia populations in WT (Figure 2.3 A) and YAC128 (Figure 2.3 B) compared to astrocytes. Recent work has also measured endogenous *hdh* mRNA expression in isolated microglia and astrocyte populations from WT mice and found significant reductions in microglia compared to astrocytes at 6 weeks of age (Jansen *et al.* 2017). This work, however, did not evaluate *hdh* expression in YAC128 HD mice to identify any potential implications of human *HTT* transgene expression on the levels of endogenous huntingtin.

A

B

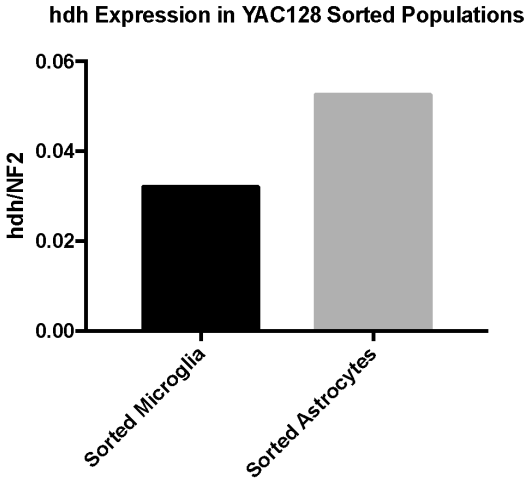

Figure 2.3 Decreased Endogenous Mouse huntingtin Expression in Microglia Isolated from WT and YAC128 Mice. Endogenous huntingtin (*hdh*) mRNA levels are lower in both WT (A) and YAC128 (B) isolated microglia populations compared to astrocytes. (n=1 for each sorted population). NF2 corresponds to normalization factor 2 (normalization to two control genes; Rpll13a, Usf1).

2.3.4 Brain Region Specific Endogenous Mouse huntingtin eExpression in Isolated WT and YAC128 Microglia and Astrocyte Populations

The next step was to evaluate potential brain region-specific differences in endogenous mouse huntingtin expression in isolated microglia and astrocyte populations. Striatum and cortex were microdissected from three-month old wild-type (FVB/N background) and YAC128 mice. Microglia and astrocyte populations were isolated and endogenous *hdh* mRNA levels were assessed. Similar to whole brain, *hdh* levels were decreased in both cortex and striatum compared to astrocytes isolated from both brain regions in WT mice (Figure 2.4 A). In YAC128 mice, *hdh* levels were decreased in microglia isolated from cortex similar to WT and whole brain (Figure 2.3 B) but *hdh* transcript was elevated in microglia sorted from striatum. Together, these results demonstrate potential brain-region specific differences in endogenous mouse huntingtin expression but additional populations will need to be sorted in order to verify these results.

A

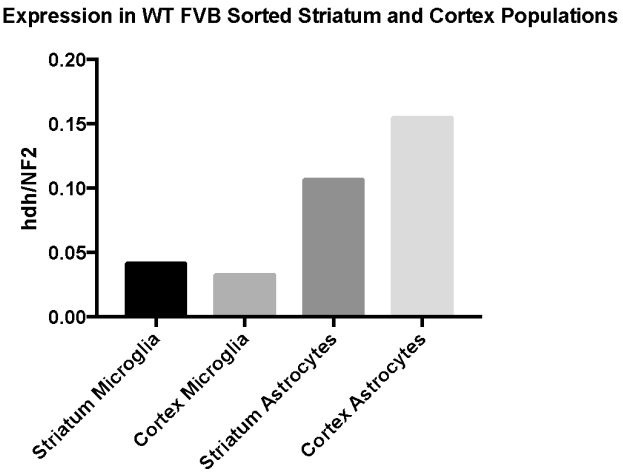

B

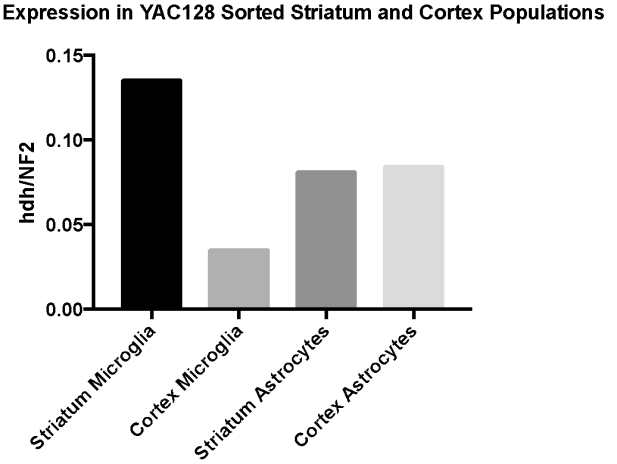

Figure 2.4 Microglia and Astrocyte Populations Isolated from WT and YAC128 Striatum and Cortex Demonstrate Region-Specific Endogenous Mouse huntingtin (*hdh*) Levels. Isolated WT astrocytes in both striatum and cortex show increased *hdh* expression (A). Elevated *hdh* transcript in microglia isolated from YAC128 striatum (B) (n=1 for each sorted population). NF2 corresponds to normalization factor 2 (normalization to two control genes; Rpll13a, Usf1).

2.3.5 Mutant Huntingtin Transgene Expression is Equivalent in Cell Populations Sorted from YAC128 Whole Brain and Striatum and Cortex

As discussed previously, YAC128 mice express the full-length human *HTT* transgene with 128 CAG repeats (Slow *et al.* 2003). The flow cytometry system allows for the investigation of transgene expression in specific cell types and in distinct brain regions. It is important to ensure that the human *HTT* transgene is equally expressed in diverse cell types and brain regions, particularly for investigations into the cell-intrinsic effect of mutant huntingtin expression. Microglia and astrocyte populations were isolated from YAC128 whole brain and microdissected striatum and cortex similar to previous experiments. RNA was extracted and human *HTT* expression was evaluated. Relative *HTT* expression is similar in sorted microglia and astrocyte populations in YAC128 whole brain (Figure 2.5 A) and striatum and cortex (Figure 2.5 B).

A

B

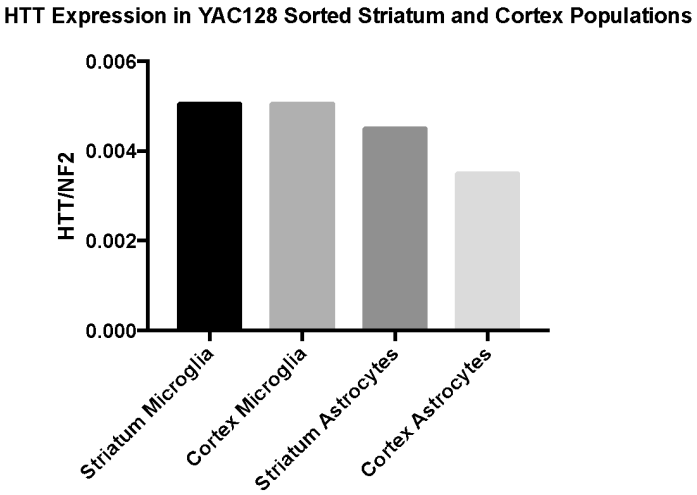

Figure 2.5 Equivalent Mutant huntingtin Transgene Expression in Sorted Microglia and Astrocyte Populations from YAC128 Cortex and Striatum. A) *HTT* expression is relatively similar in sorted microglia and astrocyte populations from whole brain (n=1 per sorted population). B) *HTT* expression is comparable in microglia and astrocyte populations from striatum and cortex (n=1 for each sorted population). NF2 corresponds to normalization factor 2 (normalization to two control genes; Rpll13a, Usf1).

2.3.6 *HTT* Expression Does Not Vary Across the Cell Cycle in Isolated HEK293 cells

Human embryonic kidney (HEK293) cells were isolated into G1, S and G2/M phases according to the protocol outlined in Section 2.4.1. RNA was extracted and human *HTT* transcript expression was measured. No significant differences in *HTT* mRNA levels were identified across the different phases of the cell cycle (n=4 per population) (Figure 2.6).

A

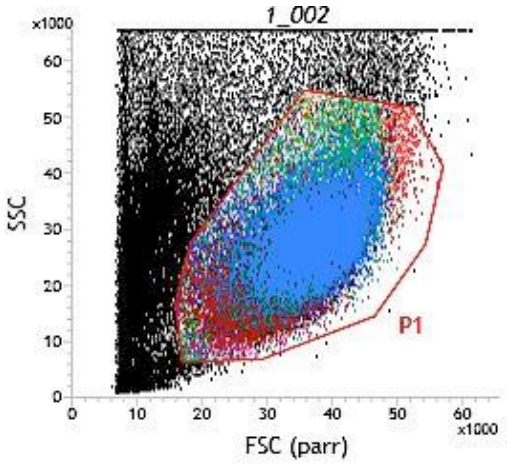

B

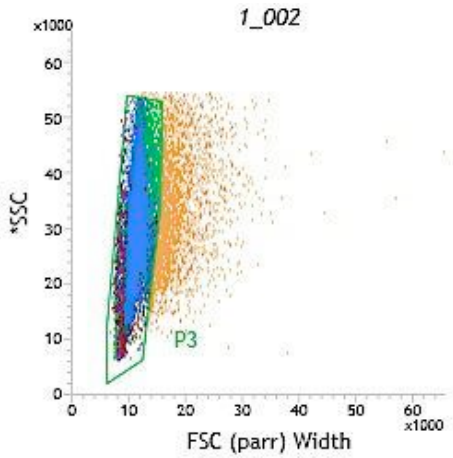

C

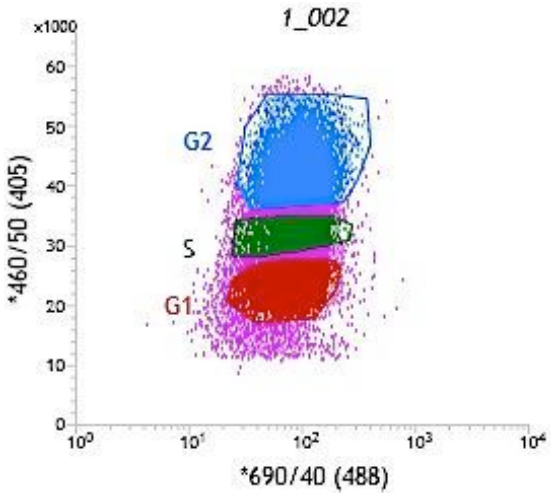

Statistics: *Cytometer*

Populations	Events	% Total	% Parent	*460/50... Mean
G1	27,991	27.99%	51.51%	22,857
S	5,196	5.20%	9.56%	31,803
G2	15,766	15.77%	29.01%	42,579

D

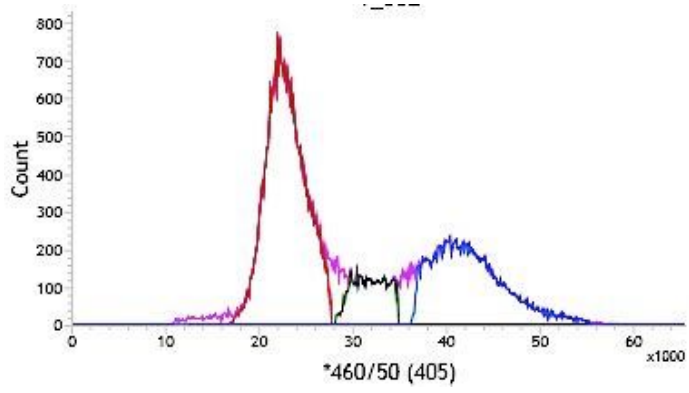

E

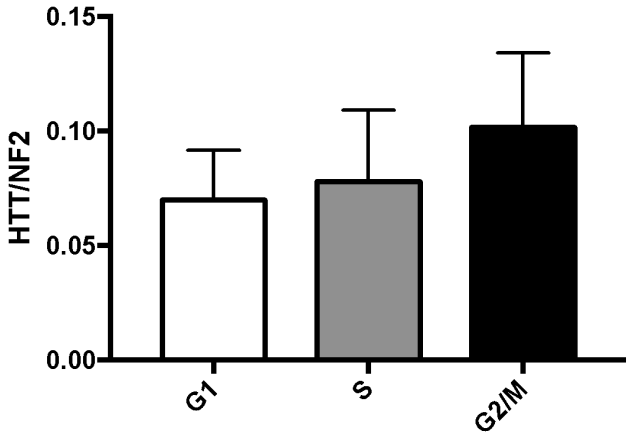

Figure 2.6 *HTT* Expression Does Not Vary Across the Cell Cycle in Isolated HEK 293 Cells. (A-D) Representative data acquired from cell cycle analysis of cultured HEK293 cells. A) Identification of live cells using forward scatter (FSC; cell size) and side scatter (SSC; cell granularity) parameters. B) Exclusion of doublets using forward scatter-width (FSC-W) and side scatter-width (SSC-W) settings. C) Antibody fluorescence of single, live cells and quantification of DNA content (D). E) *HTT* mRNA quantification in isolated G1, S and G2/M populations (n=4 per population). No significant difference in human huntingtin (*HTT*) transcript levels in sorted populations (One-way ANOVA; p value= 0.2082; Bonferroni multiple-comparisons correction). NF2 corresponds to normalization factor 2 (normalization to two control genes; ActB, HPRT).

2.3.7 Isolated ST14 Cells Do Not Demonstrate Significant Differences in *hdh* Transcript Expression Across the Different Phases of the Cell Cycle

Rat neuronal progenitor (ST14) cells were isolated into G1, S and G2/M phases according to the protocol outlined in Section 2.4.2. RNA was extracted and mouse *hdh* mRNA levels were measured. No significant differences in *hdh* transcript expression were identified across the different phases of the cell cycle (n=4 per population) (Figure 2.7).

A

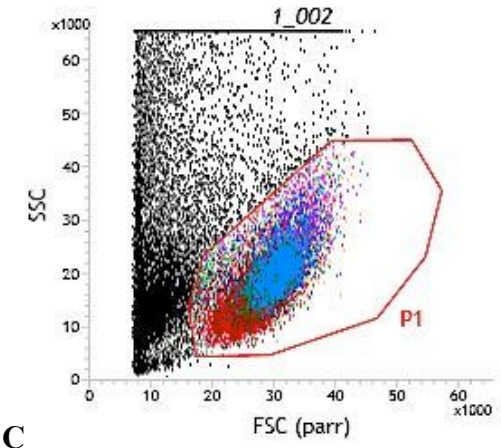

B

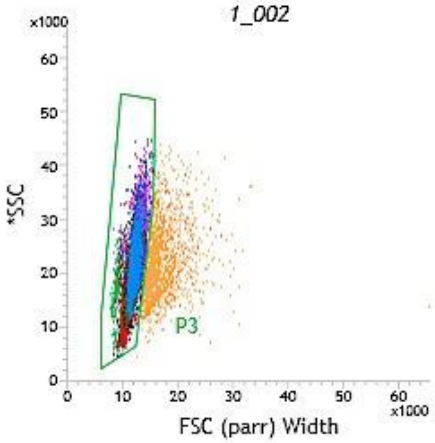

C

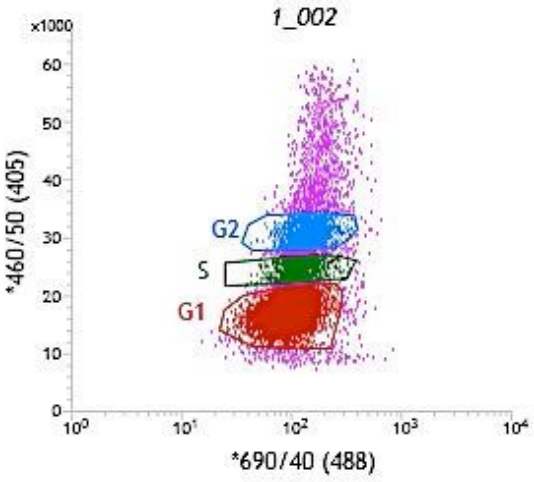

Statistics: *Cytometer*

Populations	Events	% Total	% Parent	*460/50... Mean
G1	10,709	33.36%	60.86%	16,934
S	1,933	6.02%	10.99%	24,390
G2	2,434	7.58%	13.83%	30,622

D

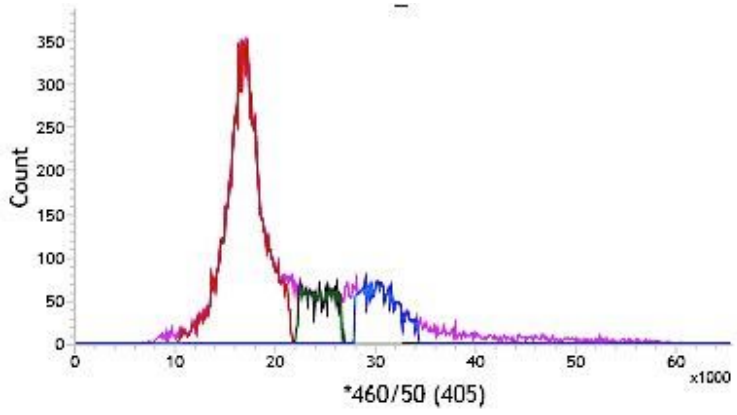

E

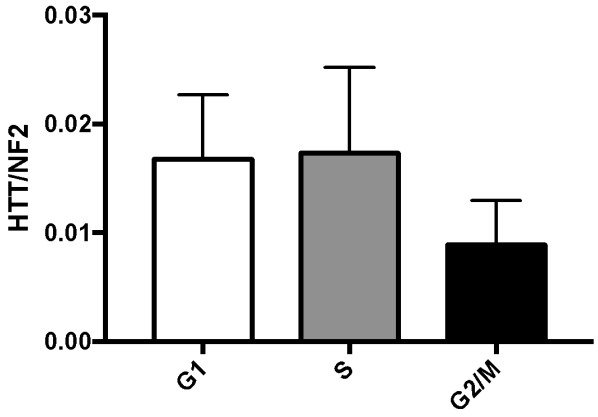

Figure 2.7 *hdh* Expression Does Not Vary Across the Cell Cycle in Isolated ST14 Cells.
(A-D) Representative data acquired from cell cycle analysis of cultured ST14 cells. A) Identification of live cells using forward scatter (FSC; cell size) and side scatter (SSC; cell granularity) B) Exclusion of doublets using forward scatter-width (FSC-W) and side scatter-width (SSC-W) settings. C) Antibody fluorescence of single, live cells and quantification of DNA content (D). *hdh* mRNA quantification in isolated G1, S and G2/M populations (n=4 per population). No significant difference in endogenous mouse huntingtin (*hdh*) transcript levels in sorted populations (One-way ANOVA; p-value= 0.0918; Bonferonni correction). NF2 corresponds to normalization factor 2 (normalization to two control genes; Rpll13a, CycA).

2.3.8 *HTT* Expression Does Not Vary Across the Cell Cycle in Isolated HeLa FUCCI Cells

Human cervical cancer (HeLa FUCCI) cells, encoded with a dual vector, were isolated into the three phases of the cell cycle using the parameters outlined in Otani *et al.* 2016. RNA was extracted and *HTT* mRNA levels were evaluated. (n=4 per population). Similar to both HEK293 and ST14 cells, no significant difference in *HTT* transcript expression was identified across the different phases of the cell cycle.

A

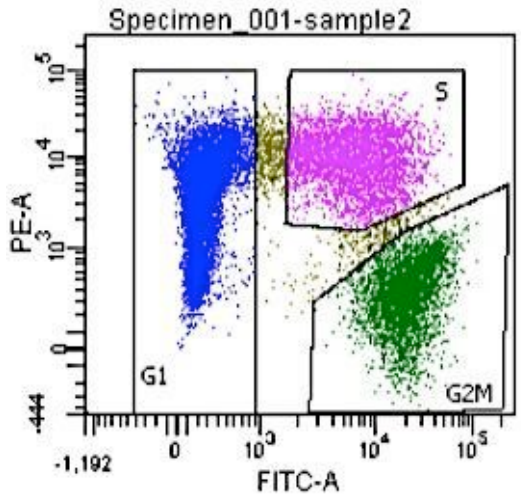

B

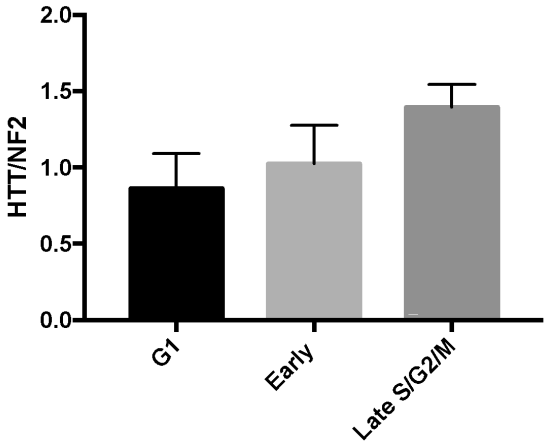

Figure 2.8 *HTT* Expression Does Not Significantly Vary Across the Cell Cycle in HeLa FUCCI Cells. A) Representative data acquired from cell cycle analysis of genetically encoded HeLa FUCCI cells. B) *HTT* mRNA quantification in isolated G1, S and G2/M populations (n=4 per population). No significant difference in human huntingtin (*HTT*) transcript levels in sorted populations (One-way ANOVA, p-value= 0.3571; Bonferroni multiple-comparisons correction). NF2 corresponds to normalization factor 2 (normalization to two control genes; PGK1, GAPDH).

2.3.9 Nuclear HTT Protein Localization Identified in G1 phase HeLa FUCCI cells

Immunocytochemical analysis of HTT protein expression in HeLa FUCCI cells demonstrated antibody-specific differences in HTT localization. N-terminal HTT was localized primarily in the cytoplasm in G1 cells (Figure 2.9 A) while C-terminal HTT demonstrated nuclear puncta in G1 cells (Figure 2.9 B). Previous work has identified technical considerations that may impact HTT localization, including fixation and permeabilization techniques (Hughes and Jones, 2011). As a result, additional antibodies would need to be assessed in order to definitively conclude that nuclear puncta are reliably identified in G1 cells.

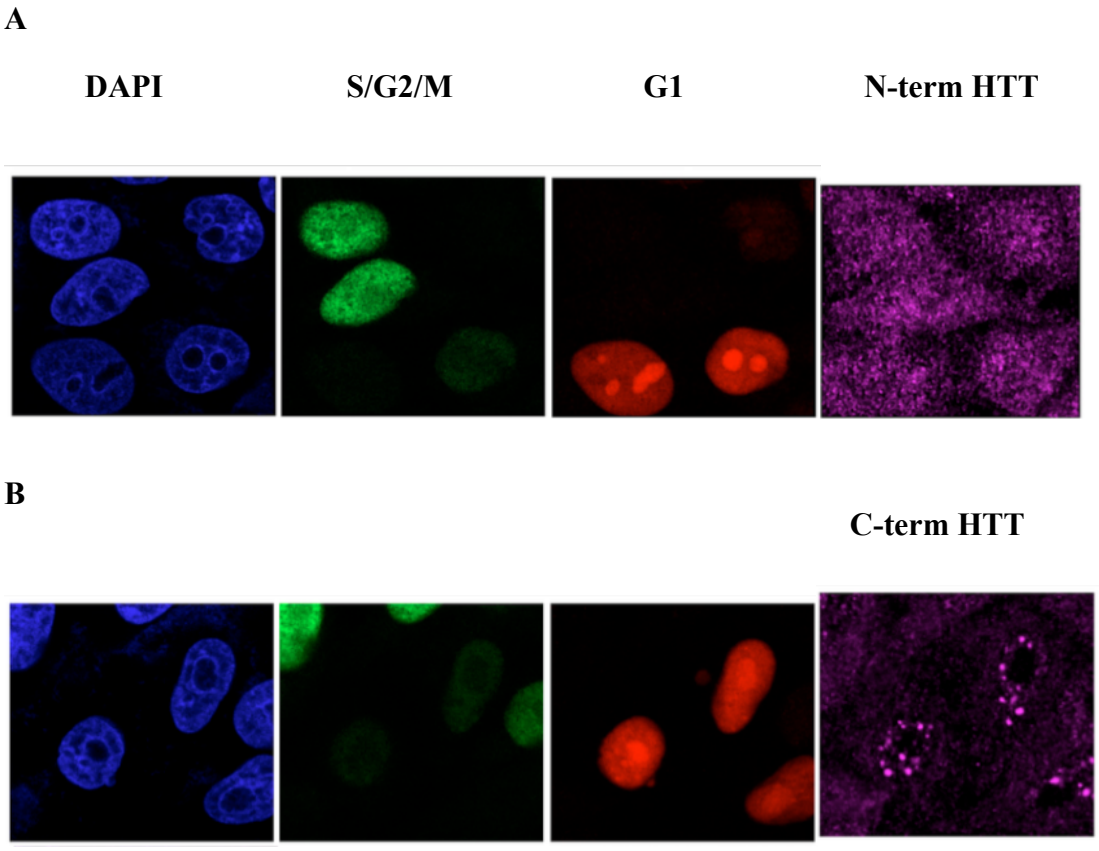

Figure 2.9 HTT Protein Demonstrates Nuclear Localization in G1 Phase in HeLa FUCCI Cells. N-terminal and C-terminal HTT expression in cultured HeLa FUCCI cells (A-B). A) G1 cells (red) demonstrated primarily cytoplasmic N-terminal HTT expression and do not show co-expression with S/G2/M cells (green) B) Nuclear C-terminal HTT puncta present in G1 cells (red). All images are counterstained with DAPI nuclear stain (blue). Pictures were taken with a 100x objective confocal lens.

2.3.10 HTT Protein is Predominately Cytoplasmic in S2/G2/M HeLa FUCCI cells

Immunocytochemical analysis of N and C-terminal HTT localization in S/G2/M cells demonstrated predominately cytoplasmic localization (Figure 2.10). This finding is similar to previous results that suggested that HTT localization is frequently cytoplasmic in primary murine neurons (DiFiglia *et al.* 1995) and glial cells (Martin-Aparicio *et al.* 2001).

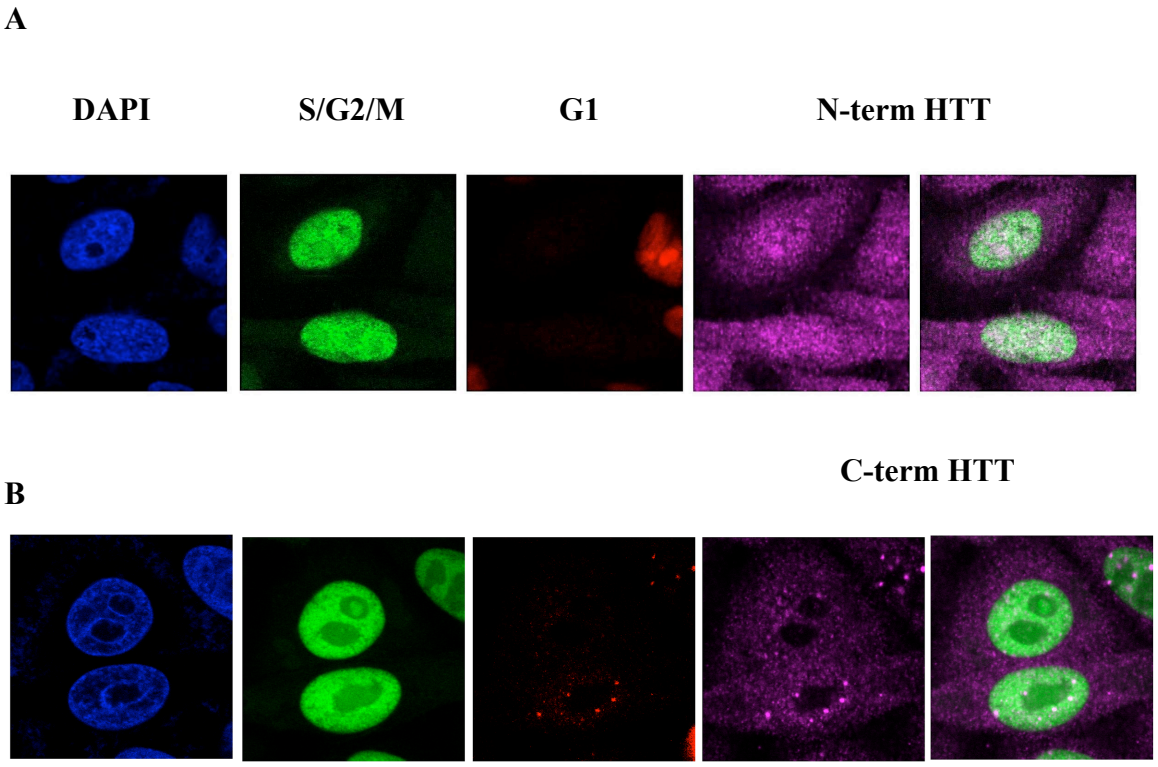

Figure 2.10 Cytoplasmic HTT Localization in S/G2/M HeLa FUCCI Cells. N-terminal and C-terminal HTT expression in cultured HeLa FUCCI cells (A-B). A) S/G2/M cells (green) demonstrate cytoplasmic N-terminal (A) and C-terminal (B) HTT expression. All images are counterstained with DAPI nuclear stain (blue). Pictures were taken with a 100x objective confocal lens.

2.3.11 HTT is Localized on the Mitotic Spindle in HeLa FUCCI cells

HTT has been previously implicated in cell division and plays an important role in mediating correct spindle orientation (Godin *et al.* 2010). Both N and C-terminal HTT is localized to the mitotic spindle in S/G2/M cells as demonstrated using immunocytochemical analysis (Figure 2.11).

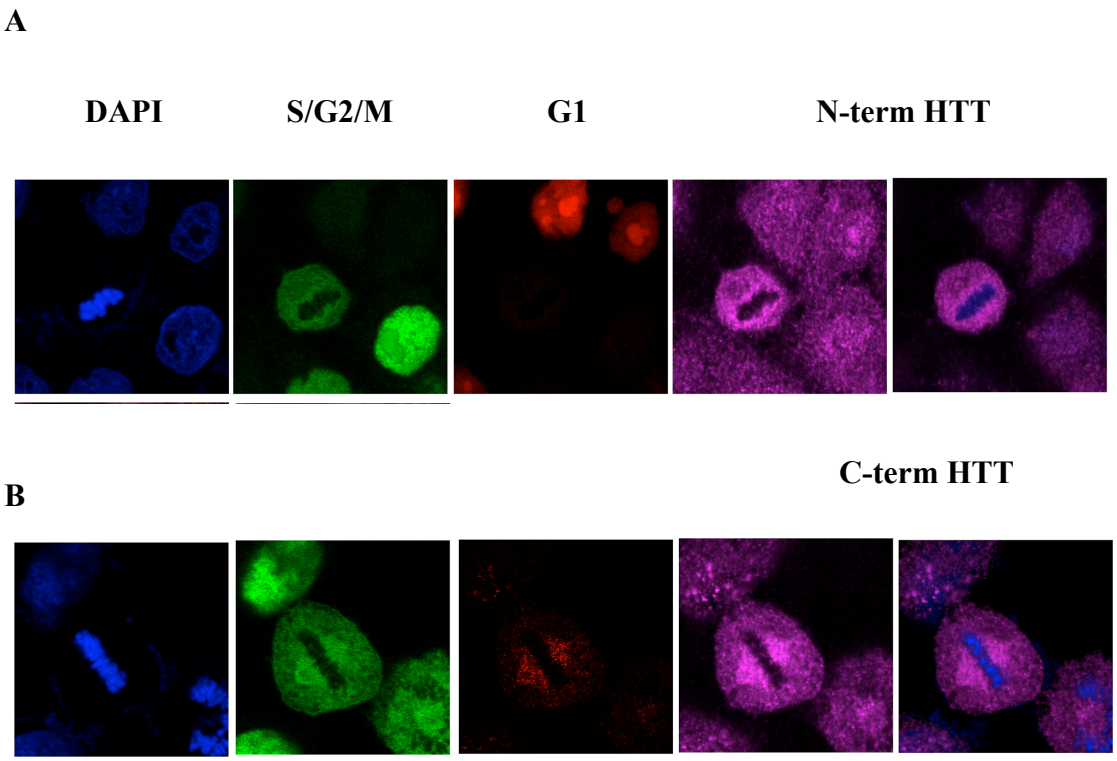

Figure 2.11 HTT Co-Localizes with the Mitotic Spindle in HeLa FUCCI Cells. N-terminal and C-terminal HTT expression in cultured S/G2/M HeLa FUCCI cells (A-B). A) Mitotic spindle identified using DAPI nuclear stain (blue). N-terminal HTT co-localizes with mitotic spindle. B) C-terminal HTT also co-localizes to mitotic spindle in S/G2/M cells (green). Pictures were taken with a 100x objective confocal lens.

2.4 Discussion

I have successfully established a flow cytometry system to isolate specific cell populations from both adult murine brain as well as cultured cells to study huntingtin expression and regulation. In the case of the adult murine brain, technical optimizations have allowed for the isolation of pure glial populations. These adult microglia and astrocyte populations express cell-type specific transcripts and can be used for downstream transcript analysis. The ability to separate pure brain cell populations builds upon previous *in vitro* methods that are constrained by age. In late-onset neurodegenerative diseases such as HD, the use of adult brain cells provides greater insight into the cell-intrinsic effect of mutant huntingtin expression and the effect of current therapeutics on specific cell types. The flow cytometry system can also be used to isolate glial populations from highly affected brain regions, including the striatum and cortex, for additional insight into the molecular mechanisms underlying disease pathogenesis specifically in these regions.

In this chapter, I measured endogenous mouse huntingtin expression in the striatum and cortex of WT and YAC128 mice as an application of the flow cytometry system. In the WT brain, huntingtin transcript levels were elevated in sorted astrocyte populations compared to microglia. In the YAC128 brain, elevated huntingin levels were seen in microglia isolated specifically from the striatum (Figure 2.4 B). The genotype and region-specific differences in huntingtin expression may be due to mutant human huntingtin overexpression in the YAC128 HD mouse model but further studies with additional samples would need to be conducted to safely conclude that endogenous huntingtin levels vary based on genotype and region.

The YAC128 HD mouse model expresses full-length human *HTT* from a genomic copy of the gene with 128 CAG repeats. The levels of mutant *HTT* transgene expression were also assessed with similar levels of expression seen in microglia and astrocyte populations obtained from YAC128 striatum and cortex. This implies that the YAC128 construct is equally expressed throughout the adult brain and that therapeutic strategies aimed as lowering mutant expression need to be equally effective in all brain cell types. As a result, another application of the flow cytometry system may be to assess the

relative mutant huntingtin reduction in specific brain cell populations following HTT-ASO (anti-sense oligonucleotide) administration.

I was also able to establish a system to evaluate the cell cycle as a novel *HTT* regulatory mechanism. *HTT* expression was not significantly different in the isolated cell cycle phases in the various cell types assessed. The reason for this may be that the *HTT* gene half-life is long and that transcript expression is fairly stable over time. HTT localization was also found to be predominately cytoplasmic each of the phases of the cell cycle. The presence of nuclear puncta was identified in G1 cells using a C-terminal HTT antibody. This contrasts the work of Godin *et al.* where the majority of huntingtin localization in interphase was identified in the nuclear compartment. The reason for this discrepancy may be due to technical differences. Previous work has demonstrated that immunostaining patterns are influenced by the antibody used and the fixation and permeabilization employed. The huntingtin protein may also adopt different confirmations according to cell type, thus presenting different epitopes under different conditions (Hughes and Jones, 2011). With these considerations in mind, future experiments are needed to finalize subcellular HTT localization.

The established flow cytometry system allows for the rapid isolation of pure viable cellular populations from both adult murine brain as well as cultured cells. Purified RNA of excellent quality can be obtained from these cells to measure huntingtin expression and cell-type specific transcripts. Future work will evaluate the efficacy of conditional genetic knockout models and the response of the glial transcriptome to a current HD therapeutic.

3 Verification of Microglia-Specific Conditional Genetic Knock-out Mouse Models

3.1 Introduction

With the advent of conditional genetic technology, numerous mouse models aimed at assessing the temporal and spatial importance of a gene of interest have been established. The *Cre/loxP* system is most widely used to directly investigate the function of a single gene in the nervous system. The Cre recombinase enzyme, isolated from bacteriophage P1, catalyzes the recombination between two 34-bp *loxP* sites located in a section of genomic DNA. The DNA segment present between the two *loxP* sites is irreversibly excised (Gaveriaux-Ruff and Kieffer, 2007). The expression of Cre under the control of a cell-type specific promoter allows the deletion of a gene of interest in a cell population of interest. Several conditional knockout models exist in the lab including GLyz and BACCre, where a specific gene is removed from monocyte-lineage cells using the *Cre/loxP* system. In the context of HD, conditional genetic mouse models are used to understand: 1) the contribution of mutant huntingtin expression and the effect of preventing expression on disease phenotypes and progression, and 2) the effect of cell-specific mutant huntingtin expression (Mazarei and Leavitt, 2014). Conditional HD mice have been generated using the *Cre/loxP* system to study the cell-intrinsic effect of mutant *HTT* expression. Despite the selective striatal loss present in HD, mutant *HTT* is expressed ubiquitously throughout the body. This implies that mutant *HTT* expression in cell types outside the striatum may play a role in HD pathogenesis. In order to better understand the cell-specific effect of mutant *HTT* expression on disease pathology and progression, various conditional models have been generated.

A glial-specific HD mouse model has been established following the introduction of N-terminal mutant *HTT* under the control of the human GFAP promoter (Bradford *et al.* 2009, Bradford *et al.* 2010, Faideau *et al.* 2010). The selective expression of mutant *HTT* in astrocytes resulted in age-dependent neurological symptoms and motor deficits along with premature death (Bradford *et al.* 2010). These phenotypes, particularly the neuronal dysfunction observed, were attributed to glutamate uptake deficits, as primary

astrocytes isolated from these mice demonstrated decreased expression of glutamate transport proteins (Bradford *et al.* 2009). The severity of symptoms observed in the glial-specific HD model also correlated with CAG repeat length, where longer expansions resulted in more severe phenotypes (Bradford *et al.* 2010). The selective expression of mutant *HTT* in neurons has also been evaluated. The BACHD model was used to delete mHTT in specific neuronal populations to evaluate the contribution of cortical and striatal mHTT expression in HD pathogenesis. BACHD mice express a floxed mutant huntingtin exon 1 construct containing a polyglutamine (Q97) expansion (Gray *et al.* 2008) that can be removed specifically in cells of interest. Reduction of mHTT expression in cortical and striatal neurons, separately, did not alter observed HD phenotypes. The decreased expression in both cortical and striatal neurons, simultaneously, however, did modify motor deficits, psychiatric-like behaviors and neurodegeneration (Wang *et al.* 2014).

Conditional deletion models have also been used to study the contribution of developmental alterations to HD pathogenesis. Developmental changes are a hallmark of HD but whether these impairments are due to a loss or gain of function mechanism is unknown. In order to distinguish between these two potential mechanisms, BACHD mice were modified to selectively express mHTT during development or develop in the absence of huntingtin. The presence of the loxP sites in the BACHD mouse allows for temporal regulation of mHTT expression. In the case of gain of function, these mice were crossed to Cre mice where the Cre recombinase was under the control of the tamoxifen promoter. The subsequent administration of tamoxifen at postnatal day 21 resulted in the removal of the floxed mHtt-exon 1 and the termination of mHtt expression, meaning that the mice developed in the presence of mHTT only until postnatal day 21. The resulting mice, identified as Q97CRE, demonstrated similar phenotypes to mice expressing mHtt throughout life including striatal loss, vulnerability to NMDA-mediated neurotoxicity, motor deficits, as well as synaptic dysfunction (Molero *et al.* 2016). The lack of phenotypic reversal following mHtt removal has been interpreted by some investigators to suggest that developmental alterations may play a role in HD pathogenesis and earlier interventions or multiple strategies may be required for therapeutic success, but this result needs to be confirmed and this hypothesis assessed by further studies.

The converse experiment was also completed to examine the role of selective loss

of endogenous huntingtin (*hdh*) during development on postnatal vulnerability to cell death. $Hdh^{d•hyp}$ mice expressing 15% of normal *hdh* levels early in development were generated. These mice demonstrated hyperkinetic behavior, increased gliosis and neurodegeneration, deficits in neurogenesis and white-matter abnormalities (Arteaga-Bracho *et al.* 2016). Together, this implies that loss of *hdh* function during neural development leads to HD-like neurological abnormalities. Previous work also used conditional Cre/loxP recombination technology to assess the effect of loss of function mechanisms on disease pathogenesis. Mice expressing endogenous mouse huntingtin (*hdh*) along with two *loxP* sites were crossed with mice expressing Cre under the control of the neuronal-specific *Camk2a* promoter, resulting in *hdh* inactivation in neurons of the forebrain. The Cre-mediated deletion also eliminated huntingtin expression in the adult testis, although this result was unexpected. More importantly, loss of *hdh* in forebrain and testis resulted in a progressive degenerative neuronal phenotype and sterility (Dragatsis *et al.* 2000), providing additional evidence of the impact of loss of huntingtin in neuronal function and survival in the brain. Taken together, the use of conditional knockout models has identified a role for developmental alterations in HD pathogenesis with both gain-of-function and loss-of-function mechanisms potentially contributing to disease pathology.

3.1.1 Generation of the BACCre Mouse

As detailed in Chapter 1, immune activation has been identified in both the CNS as well as the peripheral immune system in HD mouse models as well as human HD patients (Bjorkqvist *et al.* 2008). Despite the relative contribution to disease progression, the role of mutant huntingtin in inflammation is currently unknown. In order to study the cell intrinsic effect of mutant *HTT* in microglia, a conditional genetic mouse model was generated. By removing mutant *HTT* specifically from microglia, the involvement of the immune system in disease progression and neuropathology can be better understood.

The BAC-Cre mouse model is a microglia-specific mutant *HTT* conditional knockout model previously generated in the lab. BACHD mice expressing mutant *HTT* exon 1 along with 97 CAG repeats (Gray *et al.* 2008) flanked by two loxP sites were

crossed to mice carrying the Cre recombinase enzyme under the control of the endogenous lysozyme promoter (LysMcre; consists of nuclear Cre recombinase inserted into the first coding ATG of the lysozyme 2 gene (Lyz2) (Clausen *et al.* 1999). The LysMcre was obtained from the Jackson Lab (B6.129P2-Lyz2tm1(cre)Ifo/J) and maintained on the B6 background. This promoter will cause Cre to be expressed in all cells of the myeloid lineage including microglia, and will result in microglia-specific mutant *HTT* deletion. The crossing resulted in four genotypes: WT, WT-lys-CRE (WT mice expressing Cre driven by the lysozyme promoter), BACHD and BACCre (expressing both mHTT and Cre driven by the lysozyme promoter).

Previous work completed in the lab identified altered cytokine release in mutant huntingtin containing microglia in response to proinflammatory stimuli (Connolly *et al.* 2016). Microglia cultured from BACHD mice and stimulated for one hour with CSE and IFNγ, well-characterized microglia activators, demonstrate an increase in proinflammatory cytokine (IL-6) secretion compared to WT microglia. The reduction of mHTT in BAC-Cre primary microglia normalizes this exaggerated microglial cytokine release to those of WT microglia levels. No differences were seen in microglia counts in BAC-Cre mice but the presence of Cre did alter microglial morphology *in vivo*. More specifically, reductions in the number of processes per cell, cell area, and cell volume were detected in both WT-Cre and BAC-Cre striatal sections.

Motor deficits and neuropathology were also assessed in BACCre mice to assess the effect of mHTT deletion in microglia on well-characterized HD phenotypes. BACHD demonstrate significant impairments in rotarod performance (Gray *et al.* 2008). The microglia-specific reduction of mHTT resulted in a mild improvement in rotarod performance in BACCre mice compared to BACHD. BACHD mice also demonstrate hypoactivity in open field tasks (Menalled *et al.* 2009), which was not improved by mHTT knockdown in microglia cells. BACHD mice also display decreased whole brain and forebrain weight (Pouladi *et al.* 2012), however no reversals in brain weight reductions were identified in BACCre mice. Finally, striatal and cortical volumes were assessed with striatal, but not cortical volume, significantly reduced in BACHD mice. The striatal volume loss, however, was not reversed following microglial deletion of mHTT in BACCre mice. Taken together, mHTT reduction in microglia resulted in a mild

improvement in motor deficits but did not significantly alter brain atrophy.

3.1.2 Progranulin and the Generation of GLyz Mouse

Conditional knockout models have also been used to study progranulin expression and frontotemporal dementia (FTD) pathogenesis. Progranulin is a secreted growth factor expressed ubiquitously throughout the body. Previously linked to cancer and inflammation, its role in the brain is largely unknown. Loss-of-function mutations in the progranulin (*GRN*) gene are a common cause of familial Frontotemporal Dementia (FTD), a fatal neurodegenerative disorder. FTD is a characterized by the selective atrophy of the frontal and temporal lobes, resulting in behavioral and executive function deficits. The clinical presentation of FTD due to *GRN* mutations is highly heterogeneous with respect to age of onset, and disease duration even among individuals or families carrying the same mutation. Asymmetric brain atrophy is the most common neuroimaging feature of *GRN* mutations (reviewed in Petkau and Leavitt, 2014).

Progranulin is expressed in both neurons and microglia but not astrocytes in the brain (Petkau *et al.* 2010). Previous studies have demonstrated that proganulin-deficient mice have a greater response to inflammatory stimuli and exhibit increased release of cytokines from peripheral macrophages (Yin *et al.* 2010). The presence and altered phenotype of progranulin-expressing microglia point to a potential role of progranulin-deficiency in neuroinflammation and disease pathogenesis. Despite knowledge of the consequences of *Grn* deficiency on neuropathology, particularly in terms of exaggerated gliosis (Ghoshl *et al.* 2012, Filiano *et al.* 2013) and lipofuscin deposition (Ahmed *et al.* 2010), the relative contribution of specific *Grn* deficiency in microglia is currently unknown. In order to study this question, conditional knockout mice that lack progranulin in lysozyme-expressing cells (LyzKO) were generated. Briefly, the Cre-loxP recombinase system was used to specifically knockout *Grn* from microglia to yield GLyz mice. In this system, mice expressing *Grn* flanked by two loxP sites are crossed to mice carrying the Cre recombinase enzyme under the control of the endogenous lysozyme promoter. This promoter will cause Cre to be expressed in all cells of the myeloid lineage, including microglia and result in microglia-specific *Grn* deletion.

It is important to note that during the course of this work, Krabbe *et al.* developed a microglia-specific progranulin knockout model. In this model, *Grn* was removed from myeloid-lineage cells, including microglia, by crossing floxed Grn mice to mice expressing CreER recombinase under the control of the fractalkine receptor (Cx3Cr1) promoter (Cx3Cr1-CreER^{+}/Grn$^{F/F}$ mice). In contrast to the GLyz mice where Cre was driven under the lysozyme promoter, these mice were also inducible knockouts, meaning that Grn was deleted only in the presence of tamoxifen administration. The deletion of Grn specifically in microglia in the Cx3Cr1-CreER^{+}/Grn$^{F/F}$ mice induced excessive grooming and OCD-like behavior. The increased grooming behavior was prevented following NFκB pathway inactivation in microglia/myeloid cells, demonstrating a putative link between immune system activation and OCD-like behavior (Krabbe *et al.* 2017).

The GLyz mouse generated in the lab demonstrates no differences in neuropathology or behavior when compared to a full *Grn* knockout (Petkau *et al.,* manuscript in preparation). This contrasts the work of Krabbe *et al.* who observed NFκB-TNFα hyper-activation in microglia derived from Cx3Cr1-CreER^{+}/Grn$^{F/F}$ mice. The reason for this discrepancy may be due to the distinct promoters driving Cre expression as well as the temporal Cre induction in the Cx3Cr1-CreER^{+}/Grn$^{F/F}$ mice.

Knowledge of the efficiency of Cre-mediated deletion in these various microglia-specific conditional mouse models will help interpret neuropathologic and behavioral measures. As outlined in Chapter 2, adult microglia can be efficiently isolated from adult murine brain using the established flow cytometry system. The sorted microglia express multiple transcript markers characteristic of microglia, including Iba-1 and CD68, demonstrating high levels of sorting purity. In order to reasonably believe the lack of phenotypic effect seen in both the GLyz and BACCre mouse models, it is important to verify the efficacy of the conditional knockout. The flow cytometry system was used to assess the extent of microglia-specific knockout in both the GLyz and BACCre mouse models.

3.2 Methods

3.2.1 Isolation of Adult Microglia from GLyz and BACCre Brain

Microglia populations were isolated from two-month old GLyz and BAC-Cre adult murine brain according to the methods outlined in Chapter 2. In each experiment, microglia populations were isolated from genotype littermate controls in addition to GLyz and BAC-Cre conditional knockout mice. In the case of the GLyz experiment, microglia were sorted from WT, *Grn*-heterozygotes, GLyz and *Grn*-KO mice. Similarly, for BAC-Cre verification, microglia populations were isolated from WT, WT-Cre, BACHD and BAC-Cre mice. Transcript and protein expression of specific deleted genes were then assessed.

3.2.2 Isolation of Primary Microglia from BACCre Postnatal Brain using QuadroMACS™ separation

Microglia populations from BAC-Cre postnatal pups (P1-P3) and litter-matched controls were isolated according to an adjusted FACS protocol. Whole brains were dissected with the cerebellum and meninges removed and placed on ice for genotyping results. Tails from each pup were incubated with 89uL of deionized water and DNA was extracted using the prepGEM Tissue Fast Extraction kit according to the manufacturer's protocol. 1uL of extracted DNA was used for a standard PCR reaction using MyTaq™ DNA polymerase with primers for IL-2 (F: GAG CAG AGT GTT CAT GTT CCC AGT T; R: TCC TCT AGG CCA CAG AAT TGA AAG A) and BAC (F: AGC TAC GCT GCT CAC AGA AA; R: GAGCCATGATTGTGCTATCG). The PCR program used included an annealing temperature of 55°C with 30 cycles of 30 second extensions. The reactions were run on a 1.5% TBE gel at 100V for 25min. The presence of the BAC band at approximately 130bp was used to identify BACHD and BAC-Cre samples from WT and WT-Cre littermates.

Two to three brains per genotype were combined and incubated in 5mL of FACS buffer (PBS, 10% BSA, 2% EDTA) and homogenized using a 5mL pipette and a yellow

tip. Single cell suspensions were spun down at 1000rpm for 5min at 4°C. Supernatants were removed and samples were re-suspended in 270uL of FACS buffer and filtered through a 70μm cell strainer and transferred to a 15mL Falcon tube. Each sample was incubated with 30uL of Miltenyi® CD11b magnetic beads for 15min at 4°C. The samples were washed with 2mL of FACS buffer to remove any unattached CD11b beads and spun at 200g for 5min at 18°C. Sample supernatants were removed and re-suspended in 500uL of FACS buffer prior to QuadroMACS™ column selection.

During the wash step, MACS® LS columns were primed with 3mL of FACS buffer. The effluent was discarded and labeled 15mL Falcon collection tubes (CD11b-negative) were placed under the columns. The samples were applied to the columns and washed three times with 3mL of FACS buffer. The column was then removed and placed in a labeled 15mL Falcon collection tube (CD11b-positive). 5mL of FACS buffer was added to the column and the volume was plunged to remove CD11b positive cells retained in the magnetic column. The CD11b-positive samples were spun down at 1000rpm for 5min at 4°C and re-suspended in 100uL of FACS buffer for antibody labeling. The samples were incubated with Ebioscience® CD11b-PE and Ebioscience® CD45-APC antibodies at a dilution of 1:1000 for 15min at 4°C. An additional 150uL of FACS buffer was added to the sample along with Ebioscience® 7AAD Viability Dye at a dilution of 1:250. The sample was then subject to flow cytometry sorting as detailed in Chapter 2.

3.2.3 Quantitative Real-Time PCR (RT-qPCR)

Microglia samples were sorted into empty Eppendorf tubes and processed for specific transcript quantification. Following sorting, samples were spun down at 140,000 rpm for 5min at 4°C. Cell pellets were then processed for RNA extraction using the protocol detailed in the PureLink® RNA Mini Kit (Invitrogen) and the modifications outlined in Chapter 2 Methods. The concentration and purity of RNA was assessed using a nanodrop spectrometer (Thermo Scientific). Reverse transcription was performed using the SuperScript® VILO™ cDNA synthesis kit (Invitrogen). Quantitative analysis of mRNA expression was performed using the FastSYBR® green mastermix according to

the user's manual (Applied Biosystems). Amplification of cDNA was performed using the StepOne Plus Real-Time PCR System (Applied Biosystems). Primers used for *Grn,* and normalization genes are provided below in Table 3.1. Microglia specific transcript primers used were detailed in Chapter 2. Quantification of mRNA levels was calculated using the standard curve method using 10-fold serial dilutions composed of primary cells as standard samples. Normalization of the quantified mRNA levels was completed using a normalization factor generated by the GeNorm program included in the qBase® software package. A normalization factor was generated for each sample using two mouse normalization genes, Rpll13a and Usfi91.

Table 3.1 RT-qPCR Primers for Sorted GLyz Microglia Populations

Transcript Target	Forward (5'-3')	Reverse (5'-3')
Grn	CTGTAGTGCAGATGGGAAATCCTGCT	GTGGCAGAGTCAGGACATTCAAACT
Usf1	CCTGTGGCGTGGCAGTCT	TGCACGCCCACACTGTTT
Paklip1	CCCCAAGTGGAGGGAAGTACA	TGCCCAGCCGATAGACATC

Table 3.2 RT-qPCR Primers for Sorted BACCre Microglia Populations

Transcript Target	Forward (5'-3')	Reverse (5'-3')
Iba1	GTCCTTGAAGCGAATGCTGG	CATTCTCAAGATGGCAGATC
CD68	GTGCTCATCGCCTTCTGCATCA	GGCGCTCCTTGGTGGCTTAC
hdh	GGAGGAGAAACGGAAGGAAAA	CCGTAACCTCAAGATCTCGTTCTT
Cre	GCGGTCTGGCAGTAAAAACTATC	GTGAAACAGCATTGCTGTCACTT

3.2.4 HTT Western blots for BACCre verification

Adult microglia were sorted from four mice per genotype (WT, WT-Cre, BACHD and BACCre) and combined for HTT protein detection. Samples were spun down at 140,000 rpm for 5min at 4°C and cell pellets were subject to protein lysis. To each pellet, 5uL of lysate buffer was added with additional protein inhibitors and centrifuged at

15,000 rpm for 15min. Following lysis, 2µL of sample was combined with 798µL of deionized water and 200µL of Bradford reagent to quantify protein concentration at 598nm. For each sample, 50µg of protein was mixed with NuPAGE® LDS loading buffer and reducing agent and denatured by heating for 10min at 70°C. The samples were then loaded into the wells of a 3-8% Nu-PAGE® Novex® Tris-Acetate and run at 150V for 1h at room temperature. The protein gel was transferred to a PVDF membrane at 30V overnight at 4°C. The membranes were blocked with 5%-BSA-PBS_T and incubated overnight with primary antibodies at a 1:1000 dilution. These antibodies included: HTT (MAB2166 Millipore); IC2 (MAB1574 Millipore). Calnexin was used as a loading control (1:5000 from C4731 Sigma). The secondary antibodies were LiCor Goat-anti-mouse-800 (LiCor, Lincoln, NE) and Goat-anti-rabbit-680 (LiCor, Lincoln, NE). The membranes were imaged using a LiCor Odyssey scanner (LiCor, Lincoln, NE). Quantification of protein was performed using the accompanying Image Studio software (version 3.1.4).

Microglia were sorted from postnatal pups and combined across multiple sorts to generate one million cells from each genotype (WT, WT-Cre, BACHD, BAC-Cre) to run a HTT Western. A similar Western protocol (detailed above) was used to evaluate mHTT knockdown in sorted primary microglia.

3.3 Results

3.3.1 GLyz Mouse Model Demonstrates Significant Reduction in *Grn* Transcript Expression in Isolated Microglia

In order to evaluate the extent of *Grn* transcript knockdown in the GLyz mouse model, microglia populations were isolated from two-month old GLyz mice and additional genotypes (WT, *Grn*-heterozygotes, *Grn*-KO). WT mice contain two copies of the *Grn* gene, *Grn*-heterozygotes express one copy and *Grn*-KO express no *Grn*. With this in mind, *Grn*-heterozygotes are expected to express fifty-percent of *Grn* mRNA levels compared to WT and *Grn*-KO are anticipated to express no *Grn* mRNA in all cell populations. Microglia isolated from *Grn*-heterozygotes demonstrate half of the amount of *Grn* as expected and microglia sorted from *Grn*-KO do not express *Grn* transcript (Figure 3.1). The addition of both control samples demonstrates the utility of measuring *Grn* transcript. In contrast to the *Grn*-KO, microglia isolated from GLyz mice retain approximately 25% of *Grn* mRNA levels, compared to WT (Figure 3.1). This suggests that the Lysozyme-Cre-recombinase system significantly reduces the expression of the gene of interest in microglia but that this reduction is not absolute.

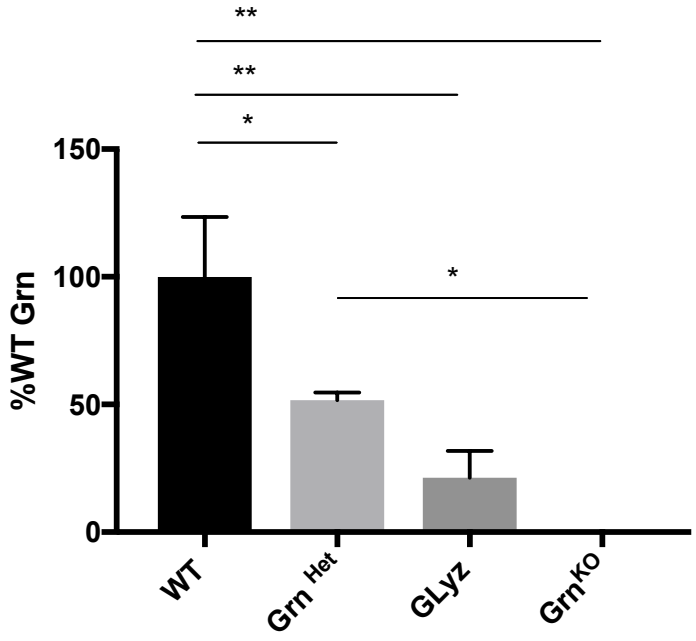

Figure 3.1 GLyz Mouse Model is not an Absolute Conditional Knockout model. Microglia isolated from adult GLyz mice and control littermates (2 months of age; n=4 per genotype) demonstrate decreased but not entirely absent *Grn* transcript expression. Cre-recombinase system used in GLyz mice significantly reduces *Grn* mRNA levels compared to WT but this knockout is not absolute. One-way ANOVA with Bonferroni correction; WT vs. Grn^{Het} *$p<0.0452$; WT vs. GLyz **$p<0.0026$; WT vs. Grn^{KO} **$p<0.0013$; Grn^{Het} vs. Grn^{KO} * $p< 0.046$. (Normalization Factor 2; normalized to two control genes, Usf1, Paklip1).

3.3.2 Microglia Isolated from BACCre Whole Brain Demonstrate Cell Specific and Cre Transcript Expression

Microglia were isolated from two-month old BACCre whole brain in addition to other corresponding genotypes (WT, WT-Cre and BACHD). Isolated populations highly express microglia-specific transcripts including Iba-1 and CD68 (Figure 3.2 A and B), demonstrating high sorting purity. BACHD and BACCre mice also demonstrate similar levels of endogenous mouse huntingtin (*hdh*) expression compared to WT and WT-Cre microglia. Normal expression of *hdh* in BACHD microglia suggests that the insertion of a human mHTT transgene does not alter endogenous huntingtin expression. Similar *hdh* levels in BACCre microglia also suggest that Cre-mediated removal of the human mHTT transgene does not affect endogenous huntingtin expression (Figure 3.2 C). In order to effectively evaluate the efficacy of Cre-mediated knockdown, it is important to assess if isolated microglia express the Cre recombinase enzyme. Both WT-Cre and BACCre microglia highly express *Cre* mRNA (Figure 3.2 D), suggesting that the enzyme needed to specifically remove the human mHTT transgene is expressed in the cell population of interest. Interestingly, BACCre microglia demonstrate increased levels of Cre transcript expression as compared to WT-Cre. This may contribute to Cre toxicity and will be discussed further in the discussion section.

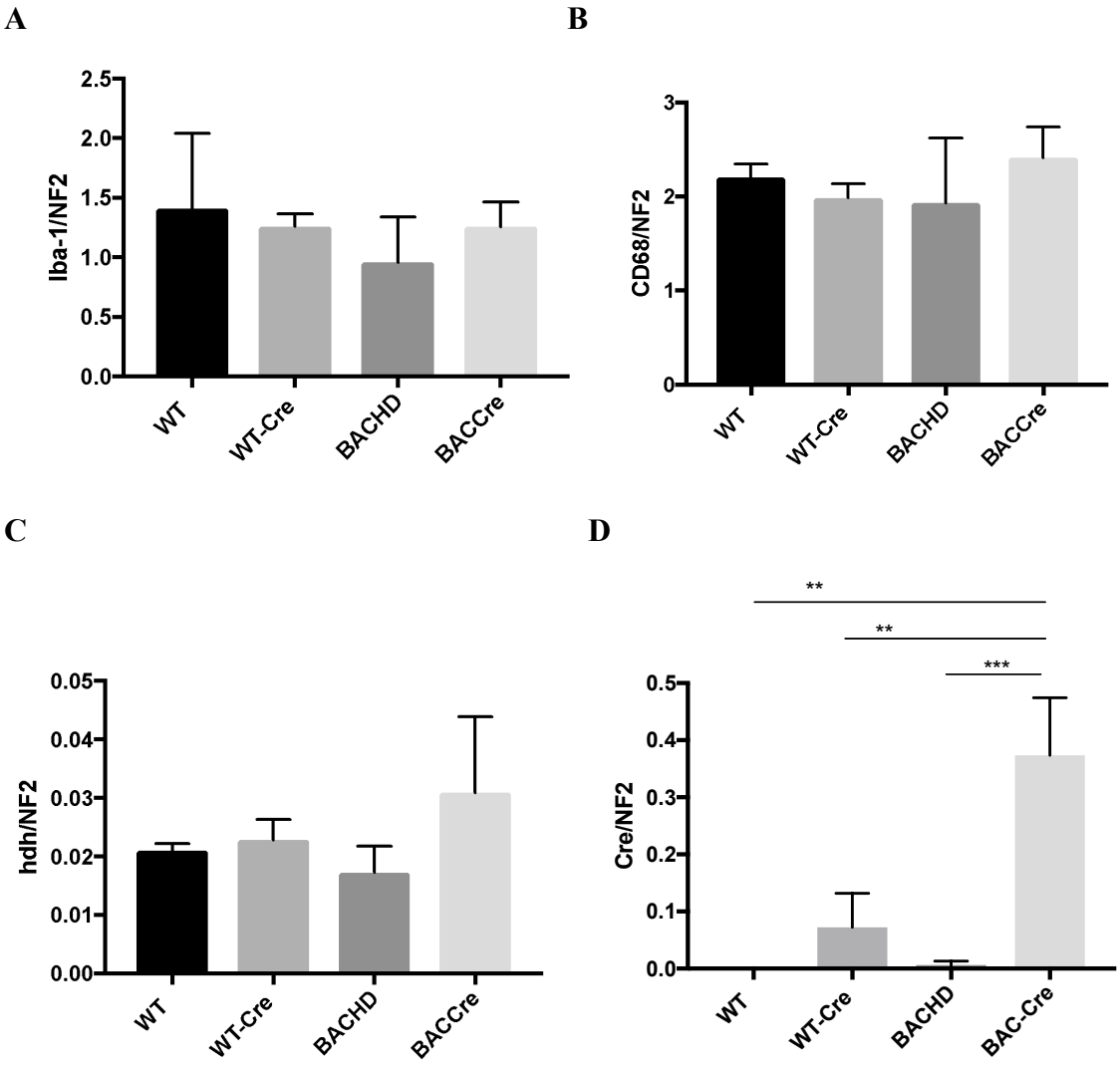

Figure 3.2 Sorted BACCre Microglia Express Cell-Specific Transcripts and Cre Expression. Isolated microglia from adult murine brain express high levels of microglia-specific transcripts including Iba-1 (A) and CD68 (B). C) Sorted microglia populations express endogenous mouse huntingtin (*hdh*) D) Microglia isolated from WT-Cre and BACCre brain express Cre mRNA. Significant increased Cre levels are seen in BACCre brain compared to WT (**p-value <0.0013), WT-Cre (**p-value<0.0048) and BACHD (***p-value<0.0005) (One-way ANOVA; ***p-value<0.0003; Bonferroni correction). NF2 corresponds to Normalization Factor 2; normalized to two control genes, Usf1, Paklip1.

3.3.3 Microglia Isolated from Cre-Expressing Mouse Whole Brain Demonstrate Reduced Cell Numbers

Previous work completed in the lab has demonstrated that Cre expression alters microglia morphology, specifically in terms of reductions in the number of reductions in the number of processes per cell, cell area, and cell volume. Cell survival may also be affected by Cre expression and can be evaluated by assessing the numbers of sorted microglia. Both GLyz and BACCre mice express the Cre recombinase enzyme. In both cases, Cre expression did affect the number of microglia isolated from whole brain. No significant reductions in isolated microglia were identified in GLyz mice but there were a decreased number of microglia isolated from both WT-Cre expressing and GLyz whole brain (Figure 3.3 A). Cre expression, however, significantly reduced the numbers of microglia isolated from BACCre and WT-Cre whole brain (Figure 3.3 B).

A

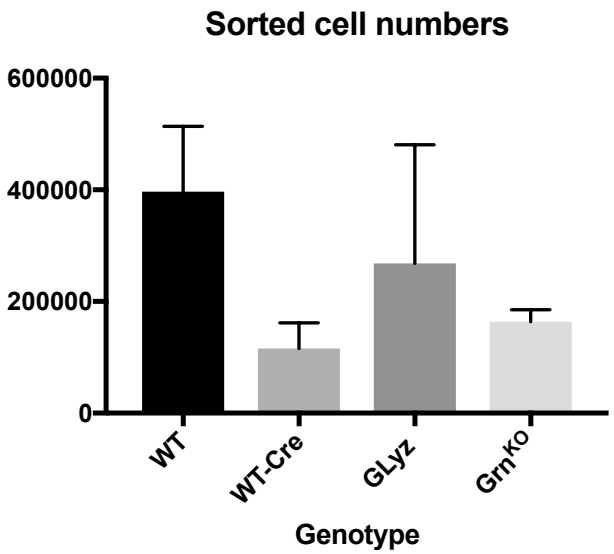

B

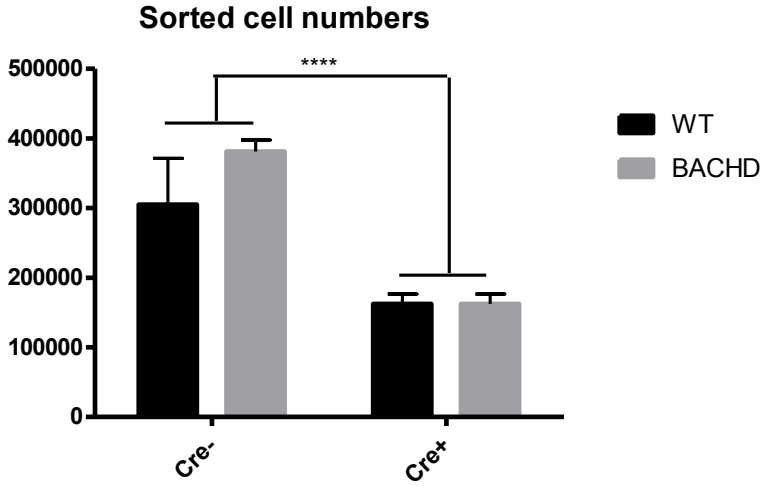

Figure 3.3 Reduced Number of Cells Sorted in Populations Expressing Cre. A) Microglia sorted from WT-Cre and Grn^{KO} mice demonstrate reductions in cell number compared to WT (not significant). GLyz microglia also demonstrate non-significant reductions in sorted cell numbers (n=4 per genotype) B) Isolated microglia (n=4 per genotype) show reductions in cell number in Cre-expressing WT-Cre and BACCre adult murine brains. (Cre interaction; Two-way ANOVA; $F(1,12)=102.2$; $P<0.001$).

3.3.4 Mutant huntingtin Protein Expression is Reduced in Sorted BACCre Microglia

To investigate the efficacy of Cre-mediated deletion, microglia were isolated from two-month old BACCre whole brain and additional genotypes (WT, WT-Cre and BACHD). Microglia populations were sorted from four mice per genotype and combined for immunoblot analysis. 1C2 is a commercial antibody that detects long stretches of glutamine residues and has been previously used to detect mHTT in human HD brain (Herndon *et al.* 2009) as well as astrocyte-specific HD mouse models (Bradford *et al.* 2009). 1C2 was also used in the initial generation of the BACHD mouse model (Gray *et al.* 2008) in order to identify founder mouse lines that expressed full-length mHTT. As a result, 1C2 is a relevant antibody to use in order to assess the efficiency of mHTT excision in BACCre microglia. mHTT protein levels were reduced in sorted BACCre microglia but an absolute reduction was not identified (Figure 3.4).

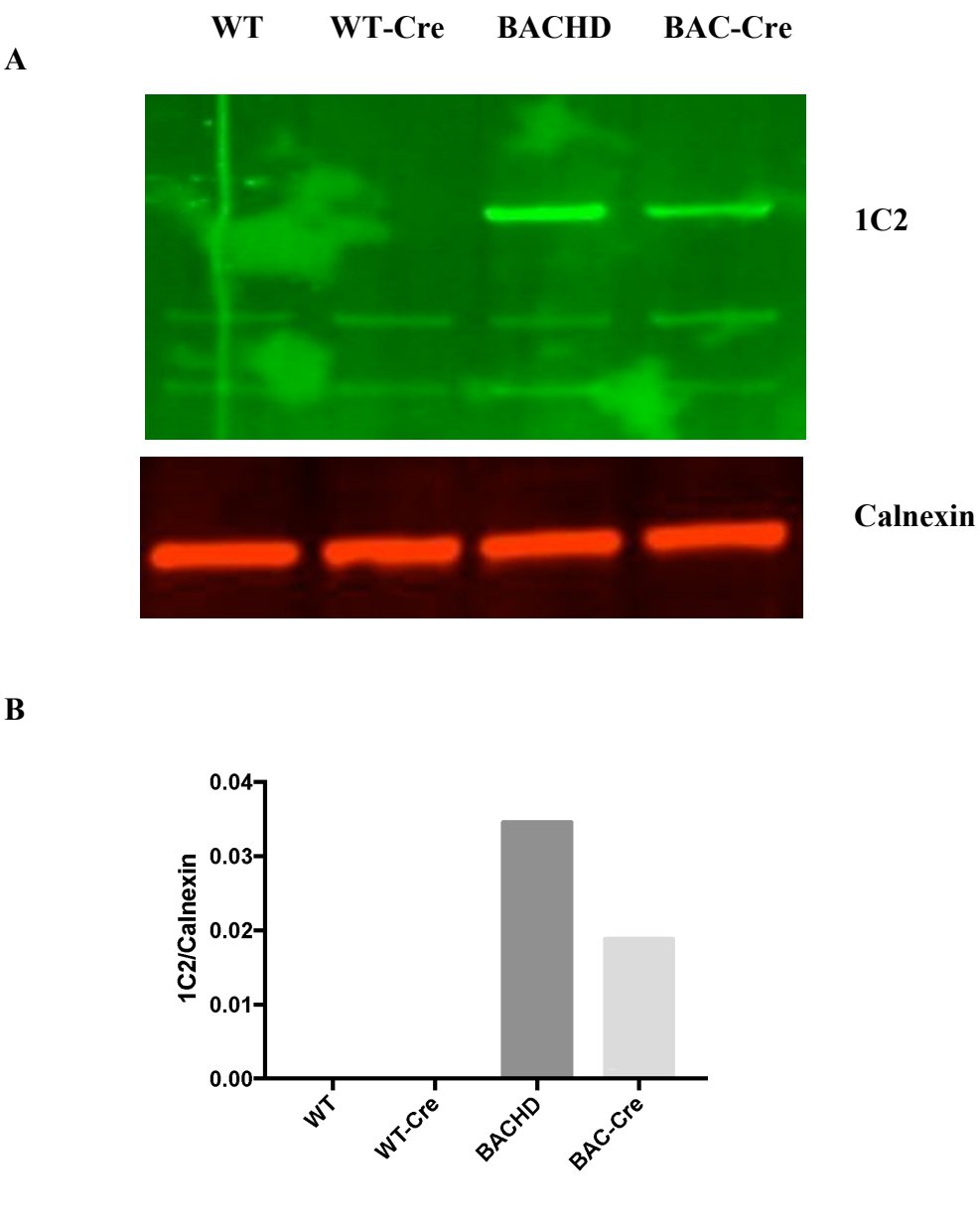

Figure 3.4 Mutant HTT Protein is Reduced in Isolated BACCre Microglia. A) Immunoblot of isolated microglia populations (n=4 per genotype) B) 1C2 levels were reduced in sorted BACCre microglia but not an absolute reduction was not measured. 1C2 protein signal was normalized to calnexin loading control.

3.3.5 Mutant huntingtin Protein Expression is Reduced in Primary Microglia Sorted from BACCre Whole Brain

In order to identify any potential age-related differences in Cre-mediated mHTT deletion efficiency, microglia were sorted from post-natal pups and mHTT protein was assessed. mHTT protein expression was reduced in microglia isolated from BACCre pups as compared to BACHD (Figure 3.5). A similar reduction of approximately fifty percent was identified in both microglia isolated from adult BACCre brain (Figure 3.4) as well as microglia sorted from postnatal brain (Figure 3.5), suggesting that age-related differences do not impact Cre-mediated deletion efficiency.

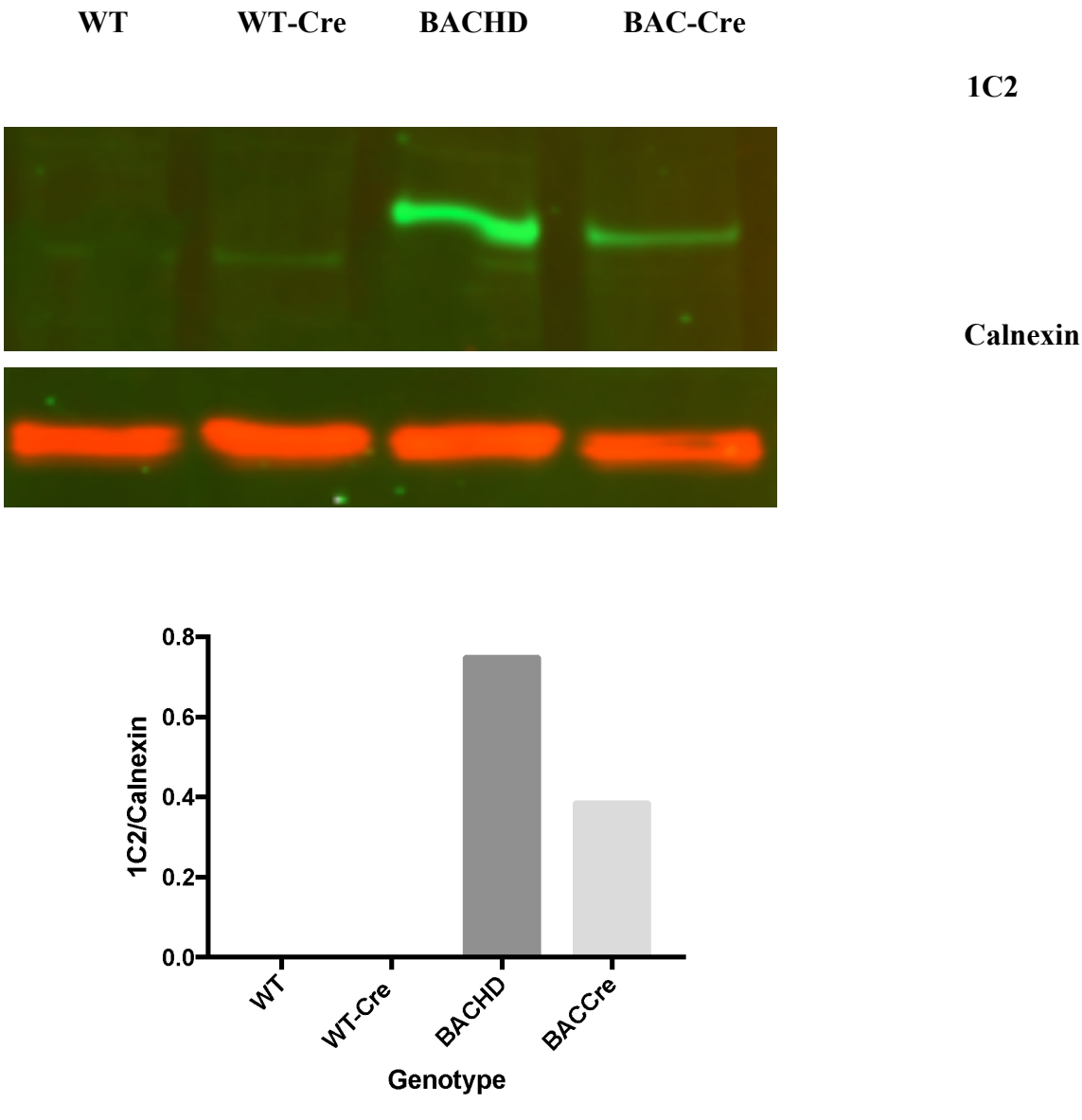

Figure 3.5 Microglia Isolated from Postnatal BACCre Mice show Significant Mutant HTT Protein Reduction. Immunoblot of isolated postnatal microglia populations (one million cells per genotype) A) 1C2 levels were reduced in sorted BACCre microglia compared to BACHD as quantified in B). Calnexin was used as the loading control.

3.3.6 Mutant huntingtin Protein Levels are Significantly Reduced in Primary Microglia Cultures derived from BACCre Whole Brain

In order to evaluate if the flow cytometry system impacts the interpretation of Cre-mediated deletion efficiency, microglia cultures from BACCre whole brain were generated as outlined in Chapter 4. 2.1. Immunoblot analysis demonstrated significant reduction in mHTT protein expression in BACCre primary microglia as compared to BACHD (Figure 3.5). As a result, different protocols do not impact the extent of mHTT reduction identified in BACCre microglia.

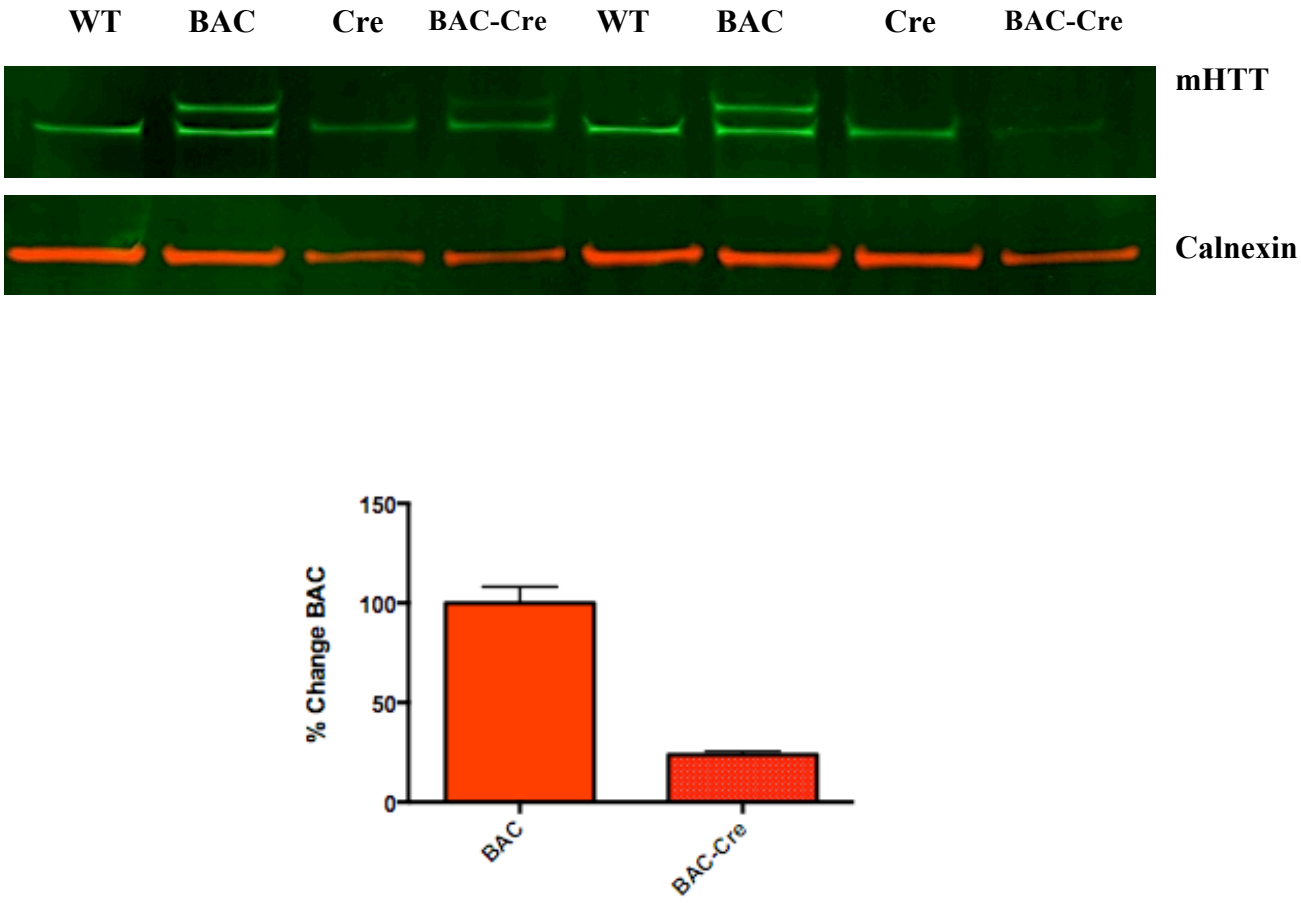

Figure 3.6 Microglial Huntingtin Protein Levels are Reduced in BACCre Cultures. A) Immunoblot of huntingtin demonstrates a decrease in mHTT levels (top band in green channel) in BACCre primary microglia compared to BACHD; calnexin was used as the loading control (Connolly *et al.*,). B) Quantification of mutant huntingtin levels show 75% reduction in BAC (BACHD) microglia compared to BACCre.

3.4 Discussion

The ability to isolate pure samples of distinct cellular populations from cell lines and from mouse tissue allows for the direct investigation of various biological questions. As detailed in Chapter 2, transcript expression can be evaluated across different phases of the cell cycle as a potential mechanism of genetic regulation. Glial populations can also be separated from intact adult murine brain for downstream analysis of endogenous dysfunction or response to current therapeutics. In this chapter, I applied the flow cytometry system to determine the efficiency of various microglia-specific conditional genetic knockout models. This is the first time that the efficacy of this genetic manipulation has been assessed in purified populations in the adult murine brain. It is interesting to note that although the gene of interest is significantly reduced in purified GLyz and BACCre microglia populations, the knockdown is not absolute. This finding is relevant to the lack of phenotypic reversal seen in both the mouse models, whereby the remaining 25-50% gene expression may contribute to retention of relevant disease phenotypes.

The sorting protocol may preferentially identify a specific microglial population that has escaped Cre-mediated recombination. One way to evaluate this concern is to measure Cre expression in the sorted populations. BACCre microglia highly express Cre transcript, as seen in Figure 3.2 (D) implying that the sorted microglia express the necessary genetic machinery for Cre-mediated deletion. Another way to ensure that the sorting protocol does not impact genetic knockdown is to measure the extent of reduction using a separate protocol. Primary microglia show a slightly more robust reduction of mHTT expression as compared to purified adult microglia as seen in Figure 3.5. The similar reduction seen using both *in vitro* and sorting protocols demonstrates that the incomplete genetic knockdown is not a consequence of technical differences.

The incomplete reduction of gene expression identified in microglia from GLyz and BACCre brains may be due to: 1) Cre toxicity 2) Nature of floxed gene 3) Function of floxed gene in cell proliferation/survival (reviewed in Sharma and Zhu, 2014). Cre has cell toxicity when expressed at high levels (Loonstra *et al.* 2001), leading to changes in cell morphology and survival. Previous work completed in the lab has shown that Cre expression impacts microglial morphology *in vivo* with reductions in the number of

processes per cell, cell area and cell volume identified (Connolly *et al.* manuscript in preparation). Cre toxicity may also result in DNA damage, which could affect the number of microglia present in the brain (Loonstra *et al.* 2001). Sorted microglia numbers obtained from both GLyz and BACCre whole brain are reduced (Figure 3.3), suggesting that Cre expression may affect cell survival. Differences in *Grn* and mutant *HTT* transgenes may account for the more robust cell survival effect seen in BACCre microglia, whereby *Grn* is less susceptible to Cre toxicity as compared to and mutant *HTT*. It is important to note, however, that technical considerations (brain homogenization, monocyte enrichment, antibody staining) may impact the number of microglia isolated. The use of replicates in each experiment, particularly in the BACCre experiment, provides preliminary insight into the effect of Cre expression on microglia survival. Additional sorts as well as immunocytochemical analysis of microglia numbers in brain sections will need to be conducted in order to definitively conclude that Cre expression impacts the number of microglia sorted from whole brain. Cre expression may also affect the process of constant self-renewal in the brain characteristic of microglia (Colonna and Butovsky, 2016). This may, in turn, contribute to the lack of genetic knockdown, meaning that *HTT* and *Grn* depleted microglia do not readily repopulate the brain. It would be interesting to measure this potential effect by assessing the extent of genetic knockdown in mice of increasing ages. Overall, additional experiments will need to be conducted to evaluate the impact of Cre expression in microglia before the extent of genetic knockdown is interpreted.

The nature of the floxed gene can also impact deletion efficiency. Although the BACHD mouse model was generated to contain two *loxP* sites flanking the mHTT transgene, there is the possibility that the BACHD model contains additional *loxP* sites, reducing the efficiency of Cre recombinase deletion. Further sequencing studies would need to be conducted in order to assess this possibility. Quantitative PCR analysis of BACHD mouse DNA has also revealed that the mice contain approximately 5 copies of the BAC transgene (Gray *et al.* 2008). Previous work has demonstrated that increased BAC transgene copy number correlates with increased BAC transgene expression (Chandler *et al.* 2007), suggesting that the Cre expression may not be sufficient to remove mHTT from all the transgenes expressed in the cells.

Finally, the function of the floxed gene in cell proliferation and survival may affect deletion efficiency. The floxed gene may be crucial for microglia development or play a role in cell proliferation and/or survival in mature microglia. In both cases, cells that escape deletion may preferentially expand (reviewed in Sharma and Zhu, 2014). *Grn* is expressed within the CNS in both neurons and microglia. In the developing brain, *Grn* expression in neurons increases as the cells mature while expression in microglia varies with cell activation state, whereby *Grn* expression is upregulated in microglia exposed to excitotoxic stimulation (Petkau *et al.* 2010). As a result, while *Grn* is expressed in microglia early in development, it may play a larger role in inflammatory processes as opposed to cell proliferation and survival. This means that reducing *Grn* expression in microglia does not impact cell survival and that *Grn*-depleted microglia can readily repopulate the brain. *HTT* also plays a role in cell division and survival (Godin *et al.* 2010) as well as embryogenesis (Nasir *et al.* 1995; Duyao *et al.* 1995; Zeitlin *et al.* 1995). Mouse HTT knockout models (termed *hdh null* mice) are embryonic lethal at embryonic day 7.5 (E7.5), demonstrating that *HTT* is necessary for cell survival. The BACHD mouse model contains the entire 170kb human *HTT* gene, with wild type *HTT*-exon 1 replaced with *mHTT*-exon 1-containing 97-mixed CAA-CAG repeats (Gray *et al.* 2008). The *loxP* sites flank *mHTT*-exon 1, meaning that Cre-mediated excision is focused on *mHTT*-exon 1, and should theoretically not influence wild type human *HTT* gene expression. There is the chance, however, that *mHTT*-exon 1 excision does impact normal *HTT* expression in the introduced transgene. If this were the case, then cells retaining *mHTT*-exon 1 would preferentially populate the brain as a result of the normal *HTT* role in cell survival. Further studies will need to be conducted in order to better understand the BACHD transgene and, more specifically, the impact of *mHTT*-exon 1 excision on normal *HTT* expression and cell survival.

Another technical consideration that may affect the interpretation of the Cre deletion efficiency is the HTT antibodies used. As discussed in the introductory chapter, mHTT antibodies vary in terms of sensitivity (Bayram-Weston *et al.* 2016) and recognize different epitopes of the HTT protein. 1C2 recognizes the expanded polyQ epitope and may not necessarily specifically recognize *mHTT*-exon 1, meaning that *mHTT*-exon1 may be excised while portions of the polyQ are retained, resulting in elevated 1C2 levels

in BACCre microglia. I also obtained the inserted *mHTT*-exon1 transgene sequence from the Wang lab at UCLA that generated the BACHD model in order to design quantitative-PCR primers to evaluate *mHTT*-exon1 transcript expression. Numerous iterations of primer design did not generate workable primers for assessment of *mHTT*-exon1 transcript expression. This may be because of the CAA-CAG repeat section of the sequence that prevents useable primers from being produced. I also attempted to use primers previously published (Molero *et al.* 2016) for assessment of the floxed *mHTT*-exon1 transcript expression. These primers also did not reliably assess *mHTT*-exon1 mRNA levels in according to the quantitative-PCR and normalization protocol used in the lab.

Finally, the tissue-specific promoter used to express Cre may also influence deletion efficiency. Both the GLyz and BACCre mouse models used a Lysozyme specific Cre promoter but other monocyte-specific promoters exist including the fractalkine receptor (Cx3Cr1) promoter. In order to uncover if the Cre effect in microglia is robust and not just an effect of the lysozyme promoter, the extent of genetic knockdown in microglia isolated from Cx3Cr1-expressing cells would need to be assessed. Taken together, the flow cytometry system can be used to verify the extent of genetic knockdown in microglia-specific conditional mouse models.

Taken together, numerous considerations, both technical and biological, may influence the extent of Cre-mediated deletion identified in this chapter. Further investigation into the effect of Cre expression in monocyte-lineage cells as well as antibody sensitivity is necessary in order to interpret both the extent of genetic knockdown as well as the ultimate role of the gene of interest in disease pathogenesis.

4 Signal Transduction Pathways in Microglia Expressing Mutant Huntingtin

4.1 Introduction

As discussed in my introductory chapter, neuroinflammation has been suggested to play a role in the progression of HD. Although the majority of HD research focuses on the effects of mHTT exclusively in neurons; the innate immune system of the CNS, consisting of microglia, has also been previously implicated in disease pathogenesis. Evidence for microglial morphological activation is evident prior to the onset of symptoms in HD patients and correlates with disease severity in both patients (Simmons *et al.* 2007) and HD mice (Francisoi *et al.* 2012). Elevated inflammatory cytokine levels (IL-6, IL-8 and TNF-α) in the plasma and cerebrospinal fluid (CSF) of HD patients have also been demonstrated to correlate with increased age and disease stage (Björkqvist *et al.* 2008). In terms of immune cells themselves, monocytes from human HD patients and primary macrophages from HD mice are hyperactive in response to inflammatory stimuli, resulting in exaggerated cytokine responses (Björkqvist *et al.* 2008).

Cytokines are inflammatory proteins secreted by cells of the monocyte lineage, including microglia, in response to various stimuli (Turnball and River, 1999). Up-regulation of cytokines induces cross talk with neighboring brain cells *in vivo* (Kim *et al.* 2005) and can lead to a variety of processes implicated in neurodegeneration including NMDA-mediated excitotoxicity, caspase activation and free radical production (Moller, 2010). There are numerous inflammatory-linked molecules that may induce cytokine release, including lipopolysaccharide (LPS) and matrix metalloproteinases (MMPs).

Bacterial endotoxin lipopolysaccharide (LPS) is a cell wall component of gram-negative bacteria used for pro-inflammatory activation. Stimulation of microglia and macrophages with LPS *in vitro* results in release of various proinflammatory cytokines including TNF-α, IL-1β and IL-6 (Nakamura *et al.* 1999). Cytokine release is mediated by numerous signaling molecules, including protein tyrosine kinases, mitogen-activated protein kinases (MAPKs) and transcription factors such as nuclear factor κB (NFκB) (Qin *et al.* 2005). The innate immune receptor Toll-like 4 (TLR4) is also highly expressed in

microglia in the brain and is activated by LPS. Blocking LPS-induced activation of TLR4 using interfering peptides reverses HD-related changes in microglial morphology and cytokine production, implicating TLR4 signaling in microglial activation and subsequent inflammation (Hines *et al.* 2013). In the context of HD, chronic peripheral challenge with LPS potentiates microglial activation in YAC128 mice as indicated by increases in microglial cell body size and retraction of processes (Francisoi *et al.* 2012). The peripheral inflammation induced by chronic LPS also induces changes in vascular remodeling including dilation, increased vessel wall thickness and increased blood-brain barrier (BBB) permeability. Stimulation of HD microglia with LPS *in vitro* also results in an increase in various pro-inflammatory cytokines including IL-12, IL-10, IL-1B, IL-2, IL-4 and IL-5, demonstrating a robust inflammatory phenotype in microglia cultured from YAC128 HD mice (Connolly *et al.* 2016).

The other proinflammatory stimuli I studied are the metalloproteinases (MMPs), a family of Zn (2+)-dependent endopeptidases. MMPs have been previously implicated in various biological processes including wound healing and metastatic cancer. In the CNS, MMPs have both beneficial as well as detrimental roles. They are involved in myelinogenesis, cell survival, axonal growth and repair processes. When their proteolytic function is not tightly regulated, they are implicated in tumorigenesis, disruption of the blood-brain barrier, demyelination, neuronal death and perpetuation of inflammatory responses (reviewed in Yong *et al.* 2001). Although most MMPs are expressed at low levels in the brain, up-regulation has been reported in several neurodegenerative diseases, including HD.

MMPs show increased activity in the striatum of HD mice compared to control mice (Sathasivam et al. 1999), and have been implicated as potential modifiers of huntingtin proteolysis and toxicity (Miller *et al.* 2010). MMP inhibition was found to reduce huntingtin proteolysis and have beneficial therapeutic effects (Johri and Beal, 2010). Other studies have also looked at MMPs in the peripheral immune system and blood-brain barrier (BBB) disruption in HD mouse models. In the peripheral immune system, R6/2 HD mice show increased levels of MMP-9 in the plasma compared to WT mice (Chang *et al.* 2015). In a 3-nitropropionic acid rat model of HD, MMP-9 is present in most of the degraded blood vessels in the injured striatum (Duran-Vilaregut *et al.*

2011). 3-nitropropionic (3-NPA) is a natural toxin that recapitulates the selective striatal neurodegeneration seen in HD. In addition to the neuronal loss, these lesions also cause alterations in the BBB, which causes increased permeability of foreign substances and degradation of BBB components. The presence of MMP-9 in these lesions suggests that matrix metalloproteinases play a prominent role in BBB disruption in the context of HD specific neurodegeneration.

In the case of HD patients, increased MMP-3 transcript expression has been identified in the cortex (Silvestroni *et al.* 2009). Elevated levels of MMP-3 and MMP-9 have also been identified in the plasma (Chang *et al.* 2015) and CSF of HD patients with higher levels correlated with advanced age and worsening of disease progression (Connolly *et al.* 2016). Matrix metalloproteinase-3 (MMP-3) is an important endogenous modulator of microglial function in the brain. It is released from damaged neurons to activate microglia (Yoon *et al.* 2006) and is of particular interest in HD, as a disease predominated by neuronal damage.

Previous work completed in the lab identified elevated levels of proinflammatory cytokines in YAC128 HD microglia in response to various stimuli including MMP-3 and CSE (an analogue of LPS). The elevated secretion profile seen in YAC128 microglia resulted from increased cytokine release from individual microglia and not increased production at the mRNA level. Cytokine transcript expression was not significantly different between WT and YAC128 microglia post-stimulation, implying that increased cytokine secretion, but not production, was induced by mHTT in microglia (Connolly *et al.* 2016). Modulating mHTT levels using anti-sense oligonucleotides (ASO's) targeting mHTT specifically reversed the elevated cytokine release seen in HD microglia, demonstrating that the immune phenotype is dependent on the presence of mHTT (Connolly *et al.* 2016).

4.1.1 Kinase Signaling Cascades in HD

Protein phosphorylation is a reversible posttranslational regulatory mechanism that controls signaling pathways underlying numerous cellular processes. In the CNS, numerous types of extracellular signals, including neurotransmitters, neurotropic factors

and cytokines exert their physiological effects by regulating phosphorylation proteins in their target cells. Protein phosphorylation refers to the process of adding a phosphate group to a substrate protein by a protein kinase enzyme (converting "dephospho-" to "phosphor-" form) and the removal of the phosphate group from the same protein by a phosphatase enzyme ("phosphor-" to "dephospho-" form). The addition of a highly negatively charged phosphate group to a protein alters the protein's charge, which can then alter both its conformation as well as its functional activity. Other alterations in stability, protein-protein interactions, transport and subcellular localization (Hong and Pelech, 2012) can also be a consequence of changes in protein phosphorylation status. In the CNS, complex temporal patterns of protein phosphorylation are achieved through increases or decreases of protein kinase or protein phosphatase activity (reviewed in Nestler and Greengard, 1999).

Protein kinase and protein phosphatase dysfunction has been associated with cancer, diabetes and neurodegenerative diseases such as Alzheimer's (Martin *et al.* 2013). Over two-thirds of the 23,000 proteins encoded by the human genome are phosphorylatable, making them robust biomarkers for disease diagnosis as well as potential targets for therapeutics (Hong and Pelech, 2012). In the context of HD, the majority of work assessing protein phosphorylation has focused on the mutant huntingtin protein, itself. HTT phosphorylation of serine 421 (S421) by the pro-survival protein kinase Akt (PKB) has been shown to reduce nuclear mHTT fragments (Warby *et al.* 2009) and NMDA-mediated excitotoxicity *in vitro* (Metzler *et al.* 2010). The polyQ expansion characteristic of HD decreases the proportion of serine 421 phosphorylation of HTT (Pardo *et al.* 2006), specifically in the striatum (Warby *et al.* 2005) with an inverse correlation seen in the levels of serine 421 phosphorylation and neurodegeneration in human HD brain tissue. S421 phosphorylation has also been shown to ameliorate mHTT-induced striatal neurodegeneration and behavioral dysfunction *in vivo* (Kratter *et al.* 2016), providing further evidence for the importance of post-translational phosphorylation modifications as potential HD therapeutics.

Other work in the context of HD has focused on phosphorylation signals mediated by MAPKs pathways. Mitogen activated protein kinases (MAPKs) control various cellular processes including gene expression, mitosis, movement, metabolism and

programmed death. These enzymes are a part of a phosphorelay system consisting of three sequentially activated kinases, ERKs, JNKs and p38, in which the protein kinases phosphorylate and activate one another. Extracellular-signal related kinases (ERKs) are involved in cell division with inhibitors of these enzymes designed as potential anti-cancer therapeutics. The other two members of the system, C-Jun amino-terminal kinases (JNKs) and p38 MAPKs, regulate transcription and are activated by inflammatory cytokines and environmental stressors (reviewed in Johnson and Lapadat, 2002). MEK/ERK signaling is generally pro-survival while p39 and JNK cascades are associated with pro-apoptosis signaling (reviewed in Bowles and Jones, 2014). More importantly, abnormal MAPK signaling is a feature of HD with increased activation of ERKs, JNKs and p38 kinases identified.

The expression of mHTT has been shown to activate MAPKs signaling pathways, specifically JNK, resulting in apoptotic cell death (Liu, 1998). This activation involves the mixed lineage kinase 2 (MLK2), a brain activator of JNK, and can be attenuated by blocking MLK2 activity (Liu *et al.* 2000). MAPKs can also be activated by various growth factors, including nerve growth factor (NGF) and epidermal growth factor (EGF). Wild-type huntingtin has been previously shown to associate with the epidermal growth factor receptor complex (Liu *et al.* 1997). Expression of mHTT disrupts EGF and NFG signaling *in vitro*, providing further evidence for altered signal transduction pathways resulting from the presence of mHTT (Song *et al.* 2002).

Mutant huntingtin has also been shown to activate ERK pathways, resulting in dysregulation of downstream signaling cascades. The activation of ERK pathways by wild-type huntingtin, on the other hand, has a beneficial effect on HD pathology (Apostol *et al.* 2006, Maher *et al.* 2011). This positive effect has primarily been associated with BDNF and glutamate signaling but other pathways may also play a role (reviewed in Bodai and Marsh, 2012). Brain-derived neurotropic factor (BDNF) is expressed in the cortex and hippocampus and promotes neuronal growth, survival and plasticity (Lu *et al.* 2013). In the context of HD, BDNF is of particular interest as it may protect against neuronal excitotoxicity in the striatum, the region most prominently affected in the disease. The presence of mutant huntingtin, however, suppresses BDNF expression in both HD mouse models (Zuccato *et al.* 2001) and human patients (Zuccato *et al.* 2008)

and inhibits downstream signaling events in the BDNF pathway (Gines *et al.* 2010), impairing the neuroprotective effect of BDNF expression. In the case of glutamate, mutant huntingtin impairs glutamate uptake from the synaptic cleft through ERK-dependent down-regulation of glutamate transporters on glial cells (Lievens *et al.* 2005). High levels of glutamate, the major excitatory neurotransmitter in the brain, as a result may contribute to neuronal exitotoxicity and selective neurodegeneration in the striatum. Although numerous signaling pathways have been investigated in HD, it is safe to assume that unidentified signal transduction cascades exist that also contribute to HD pathogenesis.

4.1.2 Signal Transduction Pathways in HD Immune Cells

Although HD microglia show exaggerated immune activation in response to both CSE and MMP3, the mechanism by which mutant HTT expression in these immune cells influences dysfunction is not well understood. Uncovering alterations in signaling cascades responsible for and activated by this increase in proinflammatory cytokine production is important for understanding immune dysfunction in HD. The NFκB pathway, and to a lesser extent JAK/STAT signaling, have been previously implicated in peripheral immune cell dysfunction in HD and serve as candidate pathways by which mHTT alters immune cell activity.

The JAK/STAT pathway is a common candidate pathway involved in cytokine signaling in immune cells. In this signaling cascade, cytokines, including IL-6, bind to specific receptors and activate JAK tyrosine kinases, which are bound to the intracellular domain of the cytokine receptor. The activation of JAK kinases allows for STAT signaling molecules (STAT1-6) to bind and translocate into the nucleus. The nuclear STAT molecules then act as transcription factors capable of inducing transcription of cytokine genes (Shuai and Liu, 2003; Levy and Darnell 2002). Different stimuli have been shown to activate different STATs. IFN-γ, for example, activates STAT1 (Heinrich *et al.* 2003), while IL-6 production in monocytes is activated by STAT5 transcription (Heinrich *et al.* 1998). Previous work completed in HD patient monocytes assessed the phosphorylation states of three transcription factors (STAT 1, STAT 3, and STAT5)

linked to IL-6 signaling. The phosphorylation level of STAT5 was slightly elevated at baseline in HD monocytes compared to controls with no changes in STAT1 and STAT3 (Träger *et al.* 2013a). Interestingly, STAT5 activation may enhance the DNA-binding activity of NFκB leading to IL-6 production (Kawashima *et al.* 2001). NFκB signaling has been shown to be abnormal in HD (Träger *et al.* 2013; Khoshnan *et al.* 2004), demonstrating the possibility of a small additive effect in JAK/STAT signaling in pathways altered in HD immune cells. As a result, changes in STAT5 activity, combined with NFκB dysfunction, could potentially contribute to the elevated IL-6 production identified in HD monocytes.

The NFκB pathway is another candidate pathway involved in immune dysfunction in HD. Mutant huntingtin in glial cells interacts with the IKK complex, the major kinase in the pathway, leading to increased NFκB activity (Khoshnan *et al.* 2004). In the context of HD, LPS-stimulated astrocytes isolated from R6/2 HD mice demonstrate increased NFκB activity that can be reversed following IKK blockade. The reversal of NFκB activation, following IKK blockage, also leads to a reduction in the neuronal toxicity caused by mutant-huntingtin expressing astrocytes and ameliorates HD-related symptoms including motor deficits and cognitive dysfunction (Hsiao *et al.* 2013). In the case of human HD myeloid cells, the NFκB pathway is similarly overactive, resulting in increased proinflammatory cytokine production upon LPS stimulation. The same direct interaction between mutant huntingtin and IKK as seen in the R6/2 HD mouse brain was also observed in isolated HD patient myeloid cells. Furthermore, the exaggerated cytokine release profile and transcriptional changes observed in HD myeloid cells were reversed using small-interfering RNA particles used to lower huntingtin levels. Taken together, NFκB signaling plays an important role in the exaggerated proinflammatory cytokine release seen in HD myeloid cells and may be an underlying pathway involved in immune cell dysfunction.

One of the ways to identify additional HD-dependent changes in phosphorylation and signaling cascades is through the use of commercially available antibody arrays. Recent advances have built upon previous mass-spectrometry (MS)-based phosphoproteomics technology to allow for the analysis of thousands of proteins and their phosphorylation sites simultaneously in protein lysates obtained from cells and

tissues (Zhang and Pelech, 2012). The commercially available Kinex™ KAM-900P Antibody Microarray features 613 phosphosite-specific antibodies (for phosphorylation) and 265 pan-specific antibodies (for expression levels of these phosphoproteins), allowing for the simultaneous analysis of protein expression and phosphorylation status.

Altered signaling pathways caused by mHTT in microglia can contribute to increased IL-6 cytokine release seen *in vitro* and influence HD pathogenesis. In this chapter, primary microglia were isolated from WT and YAC128 HD mice using an established *ex vivo* culture system and were stimulated with MMP-3 and CSE. The Kinex™ Protein Phosphorylation Array (KAM-900P) was then used to identify differences in protein expression, phosphorylation and protein-protein interactions in the collected microglia samples. Signal transduction pathway differences in three basic cellular conditions in primary microglia were assessed: Genotype (WT vs. HD), activation state (MMP-3 and CSE stimulated vs. resting) and modulator (MMP3 vs. CSE). Priority proteins and pathways in the activation state condition were identified and validated using Western blot analysis. Future experiments will decrease mHTT levels with a HTT-specific ASO to reverse critical signaling cascades identified using the unbiased signal transduction array screen. The intervention will be hypothesized to at least partially restore normal cell function and reverse the exaggerated cytokine release profile seen in HD microglia, underlining the importance of lowering mHTT levels as a therapy for HD.

4.2 Methods

Mixed gender YAC128 and non-transgenic littermates were maintained on the FVB/N (Charles River, Wilmington, MA) strain background and were used for these experiments. All experiments were carried out in accordance with protocols approved by the UBC Animal Care Committee.

4.2.1 Isolation of Primary Microglia from WT and YAC128 Mice

Whole brains were dissected from post-natal day 1 to 3 of WT and YAC128 mouse pups on the FVB/N background strain as previously detailed (Saura *et al.* 2003**)**. Briefly, following collection, meninges were carefully removed and the remaining brain tissue was incubated in growth medium (DMEM, 10% FBS, 1% L-glutamine, 1% penicillin/streptomycin) and homogenized using a 5mL pipette. Single cell suspensions from each animal were pelleted, re-suspended in 5mL of growth medium, transferred to a T150 flask and cultured at 37°C with 5% CO_2. Growth media was replaced after 24h and then every 7 days with no PBS washes. After 18 to 21 days in culture, loosely attached microglia were harvested and seeded in a 6-well plate at a density of 420,000 cells ($1.4x10^5$ cells/mL in 3mL total) for Kinexus protein array. The same set of cultures were also seeded in 96-well PRIMARIA™ tissue culture plates at a density of $1.4x10^5$ cells/mL to be used for confirmation of stimulation effect by IL-6 ELISA.

4.2.2 CSE and MMP3-Stimulation of Primary Microglia for Kinexus Array

Microglia were isolated from both WT and YAC128 mice and seeded in 6-well plates as described above. Media was changed to 1% growth media (DMEM, 1%FBS, 1% L-glutamine) on the pure microglia cultures 24-hours post isolation. 24-hours after this, microglia were separately stimulated with Control Standard Endotoxin (CSE) and Matrix Metalloproteinase-3 (MMP-3). For CSE stimulation, 1% growth medium was supplemented with CSE (O113:H10, Associates of Cape Cod) at a final concentration of 100ng/mL and Interferon-γ (INF- γ) at a final concentration of 10ng/mL for 30min.

Microglia were simultaneously stimulated with 400ng/mL of MMP3 (Active human MMP3 full length protein ab96555; AbCam, <0.10 EU endotoxin per 1ug of the protein) for 30min. Media was removed and wells were washed once with PBS and then cells were removed with cell-Scrapers in 500uL PBS. 4 six well plates were combined per condition (Unstimulated, CSE and MMP3) and cells were pelleted prior to protein lysis.

Kinexus™ signal transduction protein array (Kinexus Bioinformatics Corporation, UBC) was conducted for 6 samples total: WT Unstimulated, WT-CSE, WT-MMP3, YAC128 Unstimulated, YAC128-CSE and YAC128-MMP3. Unbiased analyses of the basic cellular conditions in primary microglia were assessed: Genotype (WT vs. HD) and activation state (MMP-3 or CSE stimulated vs. resting), activation stimulant (MMP-3 vs. CSE).

4.2.3 CSE and MMP3-Stimulation of Primary Microglia for IL-6 ELISA

Microglia isolated from WT and YAC128 mice for the Kinexus protein array were also seeded in 96-well PRIMARIA™ plates as described above for IL-6 protein quantification. CSE and MMP3-stimulation concentrations were identical to those used for the Kinexus protein array with stimulations extended for 24h. Supernatants from independent wells from each condition were collected and IL-6 concentrations were quantified using the mouse IL6 ELISA (eBioscience, Ready Set Go IL-6 ELISA). Cells were lysed and total protein levels were determined using the Micro BCA kit (Thermo Scientific) according to the manufacturer's protocol.

4.2.4 IL-6 ELISA

Five-independent wells per condition described above (Section 4.2.3) were used to quantify IL-6 cytokine concentrations following stimulation. Briefly, ELISA: Nunc 96-well plates were coated with capture antibody in 1X Coating Buffer for 24-hours prior to use and sealed at 4°C. Plates were washed 3 times with Wash Buffer (1xPBS, 0.05% Tween-20) and blocked in 1X ELISA/ELISPOT Diluent or 1hr at room temperature. Plates were washed once with Wash Buffer and 100uL of samples (diluted 6X to attain

values within readable range) and reconstituted standards (as per manufacturers protocol) were added to appropriate wells. The plates were sealed and incubated at room temperature for 2 hours. The wells were aspirated and washed 3 times with Wash Buffer and incubated with 100uL of detection antibody diluted in 1X ELISA/ELISPOT Diluent for 1hr at room temperature. Plates were washed 3 times with Wash Buffer and incubated with 100uL of Avidin-HRP for 30min at room temperature. Finally, plates were washed 5 times and 100uL of 1X TMB solution was added to each well for 15min at room temperature. Following the 15min incubation, 50uL of Stop solution (2N H_2SO_4) was added and plates were read at 450nm and 570nm using the MSD plate reader (Sector Imager 6000). 570nm values were subtracted from 450nm values (background subtraction) and the concentration of IL-6 cytokine (pg/mL) was determined and normalized to total cell protein.

4.2.5 Kinex^{TM} (KAM-900) Antibody Microarray

Primary microglia cultures from WT and YAC128 pups were generated according to methods outlined in Section 4.2.1 and stimulated with CSE and MMP3 as outlined in Section 4.2.2 for two separate phosphorylation microarrays. Samples were processed at Kinexus and protein concentrations for each sample are summarized in Table 4.1 and 4.2. In the first array, 17ug of protein was loaded for WT-Ctrl sample and 20ug of protein for the other samples. In the second array, 25ug of protein was loaded for all samples.

Lysate protein from each sample was covalently labeled with biotin. Free biotin molecules were removed from labeling reactions using gel filtration. One control and one matching treated sample were loaded side by side on the same array with an incubation chamber preventing mixing of samples. Following sample incubation, unbound proteins were washed away and the array was probed with an anti-biotin antibody labeled with a fluorescent dye combination. Each array produced a pair of 16-bit images, which were captured with a Perkin-Elmer ScanArray Reader laser array scanner (Waltham, MA).

Signal quantification was performed using ImaGene 9.0 from BioDiscovery (El Segundo, CA) using predetermined settings for sport segmentation and background correction. The strength of the signal refers to the expression level or phosphorylation

state of the target protein found in the sample. Changes in spot intensity between control and treatment samples were identified as the percent change from control (%CFC) using globally normalized data. Additional measures were also identified; including Z-scores (Cheadle *et al.* 2003) but for the purposes of both this thesis and future publications, %CFC will be used. The selection of antibodies for validation studies relied on %CFC values to ensure that the proteins of interest yielded higher signals in the experimental model system than in average microrarray experiments.

Table 4.1 Sample Details for First Microarray

Sample Name	Treatments	Protein Concentration (mg/mL)
WT-Ctrl	None	0.33
WT-MMP3	400ng/mL MMP3 for 30min	0.57
WT-CSE	100ng/mL CSE and 10ng/mL IFN-γ for 30min	0.53
YAC-Ctrl	None	0.70
YAC-MMP3	400ng/mL MMP3 for 30min	0.90
YAC-CSE	100ng/mL CSE and 10ng/mL IFN-γ for 30min	0.98

Table 4.2 Sample Details for Second Microarray

Sample Name	Treatments	Protein Concentration (mg/mL)
WT-Ctrl	None	0.58
WT-MMP3	400ng/mL MMP3 for 30min	0.42
WT-CSE	100ng/mL CSE and 10ng/mL IFN-γ for 30min	0.43
YAC-Ctrl	None	0.59
YAC-MMP3	400ng/mL MMP3 for 30min	0.30
YAC-CSE	100ng/mL CSE and 10ng/mL IFN-γ for 30min	0.35

4.2.6 Kinex™ Analysis Reports

Analysis reports generated by Kinexus^{TM} consisted of five separate comparisons corresponding to 1) WT Unstimulated vs. YAC Unstimulated 2) WT Unstimulated vs. WT CSE & WT MMP3 3) YAC Unstimulated vs. YAC CSE & YAC MMP3 4) WT CSE vs. YAC CSE 5) WT MMP3 vs. YAC MMP3. Priority leads were identified as differentially expressed proteins with i) %CFC ≥75 ii) SUM of %Error Ranges <0.75 x % CFC value iii) at least one globally normalized intensity value ≥ 1500. These selection criteria were used to prioritize large differential expression values between conditions for subsequent follow-up. Initial screens of generated reports focused on phosphorylation changes potentially involved in altered cytokine release seen in HD microglia in response to both CSE and MMP3 stimulation.

4.2.7 Identification of Priority Proteins following CSE stimulation

Priority leads were obtained from the analysis reports from WT CSE vs. YAC CSE comparisons. Stimulation effect was assessed in each of the priority leads. In this analysis, each of the priority leads were assessed in the WT Ctrl vs. WT CSE comparison to identify the priority leads that increased following stimulation (referred to as WT Stim effect in Figure 4.2). A similar separate comparison was also completed in the YAC Ctrl vs. YAC CSE analysis report (corresponding to YAC Stim effect in Figure 4.2). The addition of these separate comparisons was used to identify priority proteins that demonstrated increased expression following stimulation with an exaggerated response in HD microglia. The top nine-phosphorylation proteins were identified from both microarrays using the following criteria 1) robust globally normalized signal to ensure detectable protein expression 2) large % CFC (WT CSE vs. YAC CSE) 3) WT Stim effect and/or YAC Stim effect present in one or more of the microarrays. Prioritization of signal intensity and large %CFC changes omitted several proteins of interest with stimulation effects. This was completed to maximize the prospects of successful validation in subsequent Western blot analysis. The corresponding pan-specific proteins were also included in the priority list to assess the phosphorylation ratio of the protein of interest (phosphorylation: pan-specific expression). Three additional pan-specific proteins

were included in the validation list, as three of the top nine-phosphorylation proteins did not have corresponding pan-specific proteins available.

4.2.8 Identification of Priority Proteins following MMP3 Stimulation

A similar analysis was completed to identify priority proteins following MMP3 stimulation. Priority leads were obtained from the analysis reports from WT MMP3 vs. YAC MMP3 comparisons. Stimulation effect was assessed in each of the priority leads. In this analysis, each of the priority leads were assessed in the WT Ctrl vs. WT MMP3 comparison to identify the priority leads that increased following stimulation (referred to as WT Stim effect in Figure 4.5). A similar separate comparison was also completed in the YAC Ctrl vs. YAC MMP3 analysis report (corresponding to YAC Stim effect in Figure 4.5). The addition of these separate comparisons was used to identify priority proteins that demonstrated increased expression following stimulation with an exaggerated response in HD microglia. The top nine-phosphorylation proteins were identified from both microarrays using the following criteria 1) robust globally normalized signal to ensure detectable protein expression 2) large % CFC (WT CSE vs. YAC CSE) 3) WT Stim effect and/or YAC Stim effect present in one or more of the microarrays. Similar prioritization of signal intensity and large %CFC changes omitted several proteins of interest with stimulation effects. The corresponding pan-specific proteins were also included in the priority list to assess the phosphorylation ratio of the protein of interest (phosphorylation: pan-specific expression).

4.2.9 Western Blot Validation of Kinexus Array CSE Stimulation Leads

Primary microglia from WT and YAC128 post-natal day 1-3 pups were isolated as described in section 4.2.1. 6-well plates were seeded for CSE stimulation for both genotypes as described in section 4.2.2. Twelve to fifteen million cells per genotype were collected, corresponding to 229µg of protein, and were processed by Kinexus^{TM} for Western blot validation of the 18 candidate proteins identified in the initial analysis detailed in section 4.2.7 (Figure 4.2). The Kinetworks^{TM} Custom KCPS 1.0 Multi-

Antibody Protein Screen allows for one sample to be incubated with 18 antibodies simultaneously. The antibodies used in the Western blot analysis were the same ones used in the initial microarray screens.

4.2.10 Protein-Protein Interaction Network of Candidate Proteins using STRING

Proteins are often found to work in associating groups to affect signaling transduction pathways. To identify clusters of known protein interactors within the candidate proteins, I utilized an online protein-protein interaction network database, STRING (Franceschini *et al.* 2012). The following settings were used to create the protein interaction network: High confidence (required confidence score 0.700), co-occurrence, co-expression, experiments, and databases. This online database allowed the creation of an interaction network based on known and predicted interactions between the candidate proteins. The clustering feature of the database was used to identify clusters of associating proteins based on the defined interaction criteria (Markov Clustering algorithm with an inflation setting of 3).

4.2.11 Pathway Analyses of Candidate Proteins using STRING

The online STRING database (version 10.5) also allows for pathway analysis to be conducted in order to evaluate highly expressed potential biological mechanisms involved in the samples of interest. Biological Process (GO), Molecular Function (GO), KEGG pathways were identified in the candidate protein interactions for both CSE and MMP3 conditions.

4.3 Results

4.3.1 Mutant Huntingtin Expressing Microglia have an Increased IL-6 Cytokine Response when Stimulated with CSE and MMP3

Microglial cultures were isolated from WT and YAC128 postnatal pups and subject to CSE and MMP3 stimulation in order to confirm the exaggerated inflammatory response in HD microglia previously identified (Connolly *et al.* 2016). Previous work using the same microglia-astrocyte co-culture protocol characterized the microglia cultures as over 99% pure based on ionized calcium-binding adaptor molecule 1 (Iba-1) immunocytochemical staining. The remaining <1% of cultured cells were glial fibrilliary acid protein (GFAP) positive astrocytes (Connolly *et al.* 2009). These same cultures were also used for the Kinex^{TM} KAM-900P phosphorylation array to evaluate signal transduction cascades differing between WT and YAC128 HD microglia that may mediate the increased inflammatory response. Microglia secrete the proinflammatory cytokine, IL-6, when stimulated with CSE (Control Standard endotoxin, an analogue of LPS) by activating the Toll-like receptor (TLR4) (Hines *et al.* 2013). Similar secretion of IL-6 is also seen in microglia following MMP3 stimulation (Connolly *et al.* 2016), although the mechanism is poorly understood. YAC128 microglia expressing mHTT display significantly increased levels of IL-6 cytokine secretion following CSE stimulation (Figure 4.1 A) and MMP3 stimulation (Figure 4.1 B) compared to WT littermate cultures.

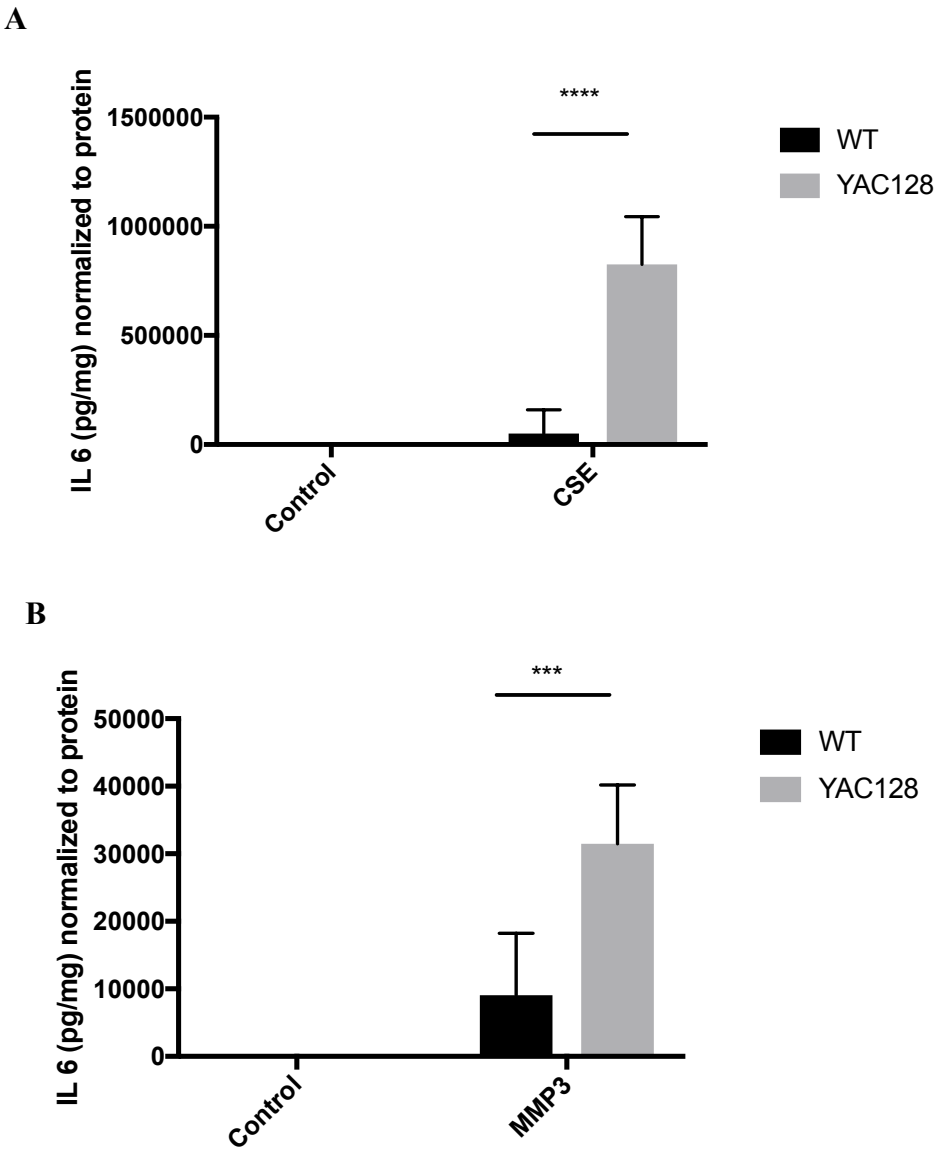

Figure 4.1 IL-6 Cytokine Levels are Increased in YAC128 Microglia compared to WT following CSE and MMP3 Stimulation. Supernatants from WT and YAC128 unstimulated and stimulated cultures were analyzed for IL-6 secretion (n=5 per condition). A) IL-6 levels were significantly increased following CSE stimulation in YAC128 microglia compared to WT (Stimulation interaction $F(1,16)= 63.82$; $p<0.001$; Two-way ANOVA; Bonferroni correction). B) Significant increase in IL-6 levels in YAC128 microglia compared to WT following MMP3 stimulation (Stimulation interaction $F(1,14)=53.56$; $P<0.001$; Two-way ANOVA; Bonferroni correction).

4.3.2 Proteins with Increased Phosphorylation Expression in YAC128 HD microglia compared to WT following CSE stimulation

Microglia cultures isolated from WT and YAC128 pups were stimulated with CSE for 30min and collected for Kinex^{TM} KAM-900P phosphorylation array. Protein lysis was conducted at Kinexus using established chemical cleavage, pre-homogenization and biotin labeling protocols. Two separate arrays were completed as technical replicates with separate microglia cultures generated and stimulated for each (WT CSE and YAC CSE). Kinexus generated analysis reports identified priority proteins in the WT CSE vs. YAC CSE comparison. These priority proteins demonstrated an increased %CFC (percent change from control) compared to WT meaning that these proteins demonstrated significantly increased phosphorylation in YAC CSE microglia versus WT CSE. Additional analysis was also conducted to identify candidate proteins for subsequent Western blot validation.

As discussed in Section 4.2.7, candidate proteins were also assessed for stimulation effect. This refers to increased phosphorylation following CSE stimulation but an exaggerated response in HD microglia compared to control. Using the combination of priority leads generated by Kinexus (based entirely on %CFC) and the additional stimulation effect, nine top phosphorylation proteins were identified. The Kinex^{TM} KAM-900P phosphorylation array also evaluates the expression of pan-specific proteins. The corresponding pan-specific proteins for the top nine-phosphorylation candidates were also included in the validation list. Four of the nine-phosphorylation proteins (PGK1, GluR1, NR1 and NBS1) did not have corresponding pan-specific proteins available on the array. As a result, three additional pan-specific proteins with large %CFC differences and stimulation effects were included in the candidate list (MEK2, MET, PTP1D) (Figure 4.2). PKCq (phosphorylation at serine 676; S676) was included as the last candidate protein as it met the required criteria outlined in Section 4.2.7 and also corresponded to a different phosphorylated residue on the previously identified PKCq candidate.

Protein Name	Phospho-site (human)	Full Target Protein Name	WT Stim effect		YAC Stim Effect	
EphA3	Y779	Ephrin type A receptor 3	✔		✔	✔
AKS1	S1046	Apoptosis signal regulating protein-serine			✔	✔
PGK1	Y196	Phosphoglycerate kinase 1	✔		✔	✔
PKCq	S676	Protein serine kinase C-theta			✔	✔
Ron	Y1238	Macrophage stimulating protein receptor	✔	✔	✔	✔
Rb	S780	Retinoblastoma-associated protein 1	✔		✔	✔
GluR1	S849	Glutamate receptor 1			✔	✔
NR1 (NMDAR1)	S896	N-methyl-D-aspartate (NMDA) glutamate receptor 1 subunit zeta			✔	✔
NBS1	S343	'Nijmegen breakage syndrome protein 1		✔	✔	✔
EphA1	Pan-specific	Ephrin type A receptor 1		✔		✔
AKS1	Pan-specific	Apoptosis signal regulating protein-serine kinase 1	✔	✔	✔	✔
PKCq	Pan-specific	Protein-serine kinase C theta		✔		✔
Ron	Pan-specific	Macrophage-stimulating protein receptor alpha chain	✔	✔	✔	
Rb	Pan-specific	Retinoblastoma-associated protein 1	✔			
MEK2	Pan-specific	MAPK/ERK protein-serine kinase 2	✔	✔	✔	✔
MET	Pan-specific	Hepatocyte growth factor (HGF) receptor-tyrosine kinase	✔	✔	✔	
PKCq	S676	Protein-serine kinase C theta	✔		✔	✔
PTP1D	S580	Protein-tyrosine phosphatase 1D	✔			

Figure 4.2 CSE Protein Candidate Validation List. Eighteen candidate proteins identified from WT CSE and YAC CSE comparison using both arrays. WT Stim and YAC Stim column divided into first and second array. Presence of checkmark corresponds to stimulation effect in the corresponding array.

4.3.3 Candidate Proteins Identified following CSE stimulation Cluster into Three Protein-Protein Interaction Groups

Next, I wanted to assess the potential interactions between the CSE candidate proteins to further focus potential signaling cascades involved in mHTT-dependent expression in microglia. The online STRING database can be used to identify known and predicted protein-protein interactions between candidates of interest. The top-nine phosphorylation proteins identified in Figure 4.2 along with the three unique pan-specific proteins (MEK2, MET, PTP1D) were inputted into the database and clustered using a Markov Clustering factor of 3 (refers to high associations). Within the twelve candidates, I identified three putative clusters, each highlighted by a different color in Figure 4.3. One of the proteins (PGK1) does not cluster in any of the groups. Each of the clusters contains interactions corresponding to known protein interactions identified from curated databases (blue edges) and experimentally determined (magenta). Putative interactions between the three clusters (corresponding to dashed edges) were also identified. The STRING analysis resulted in protein-protein interactions that can be investigated in the future as potential signaling cascades and not individual phosphorylated and differentially expressed proteins.

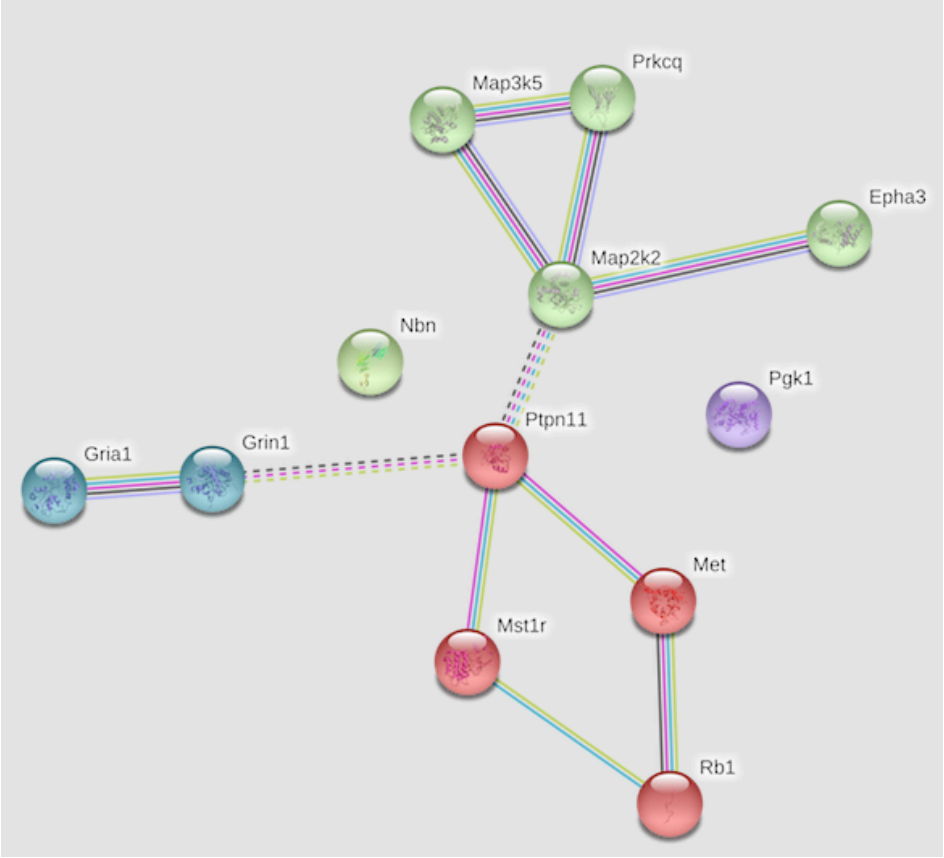

Figure 4.3 Protein-Protein Interactions between Candidate CSE Proteins. An online database (http://string-db.org/) was used to identify known protein-protein interactions between the top nine-phosphorylation proteins as well as three additional pan-specific proteins (MEK2, MET, PTP1D) (n=12 total) (Listed in Figure 5.2). Matching colors, as identified by Markov Cluster analysis, indicates clusters of interacting proteins. Figure adapted from http://string-db.org/. Equivalent names for several candidate proteins used in STRING analysis including (MAP3K5= ASK1; MAP2K2=MEK2; Ptpn11= PTP1D; Grin1= NR1; Gria1= GluR1; Nbn= NBS1; Mst1r= Ron). The first protein name is found in the STRING analysis and the corresponding name is identified in Figure 5.2. Edges (lines) represent protein-protein interactions, which jointly contribute to a shared function but no not necessarily physically bind together. Color of the edges corresponds to different levels of interactions. Blue and magenta correspond to known interactions from curated databases and experimentally determined, respectively. Yellow refers to interactions identified using text-mining, black corresponds to protein co-expression and purple indicates protein homology.

4.3.4 Pathway Analysis of CSE Candidate Proteins Result in Significant Enrichment in Cell Communication and Signal Transduction Pathways

In order to better understand the potential pathways involved in the effect of CSE stimulation on mutant-huntingtin expressing microglia, the online STRING database was used to identify enriched biological pathways. STRING allows for functional associations to be made between proteins allowing common biological purposes to be identified. These interactions are derived from multiple sources including: i) known experimental interactions identified in the literature, ii) pathways derived from manually curated databases and iii) text-mining of published literature iv) *de novo* interactions based on co-expression analysis v) interactions observed in different organisms. Several manual curated databases including Biological Processes, Molecular Functions and Kyoto Encyclopedia of Genes and Genomes (KEGG) are used to identify both protein-protein interactions as well as protein functions (reviewed in Szlarczyk *et al.* 2015). STRING pathway analysis using these three-curated databases identified 66 enriched protein sets in Biological Processes, 11 in Molecular function and 26 in KEGG. Numerous pathways potentially involved in CSE stimulation including various iterations of MAPK and other kinase pathways as expected (Figure 4.3 A). The Molecular Function and KEGG databases also identify additional pathways potentially involved in the increased response of YAC128 microglia to CSE stimulation including small molecule and anion binding (Figure 4.3 B) as well as Ras signaling (Figure 4.3 C). The identification of potential biological pathways involved in YAC-CSE stimulated microglia may provide further insight into the effect of mutant huntingtin in microglia exposed to pro-inflammatory stimuli.

A

Pathway ID	Description	Gene Count	FDR
GO.0007154	Cell communication	11	2.5E-05
GO.0007165	Signal transduction	11	2.5E-05
GO.0043549	Regulation of kinase activity	7	2.5E-05
GO.0044700	Signal organism signaling	11	2.5E-05
GO.0043406	Positive regulation of MAP kinase activity	5	2.4E-05
GO.0033674	Positive regulation of kinase activity	6	2.5E-05
GO.0051247	Positive regulation of protein metabolic process	8	2.5E-05
GO.0065009	Regulation of molecular function	9	1.0E-04
GO.0000187	Activation of MAPK activity	4	1.3E-04
GO.0010604	Positive regulation of marcromolecule metabolic process	9	1.6E-04

B

Pathway ID	Description	Gene Count	FDR
GO.0004672	Protein kinase activity	6	6.1E-04
GO.0004713	Protein tyrosine kinase activity	4	6.1E-04
GO.0004714	Transmembrane receptor protein tyrosine kinase activity	3	3.1E-03
GO.0004871	Signal transducer activity	6	4.1E-03
GO.0004888	Transmembrane signaling receptor activity	5	1.1E-02
GO.0004970	Ionotropic glutamate receptor activity	2	1.1E-02
GO.0005234	Extracellular-glutamate-gated ion channel activity	2	1.1E-02
GO.0005524	ATP binding	6	1.1E-02
GO.0036094	Small molecule binding	7	1.3E-02
GO.0043168	Anion binding	7	1.4E-02
GO.0019899	Enzyme binding	5	4.1E-02

C

Pathway ID	Description	Gene Count	FDR
4014	Ras signaling pathway	4	2.9E-04
4720	Long-term potentiation	3	2.9E-04
5014	Amyotrophic lateral sclerosis (ALS)	3	2.9E-04
5211	Renal cell carcinoma	3	2.9E-04
5218	Melanoma	3	2.9E-04
5220	Chronic myeloid leukemia	3	2.9E-04
4722	Neurotrophin signaling pathway	3	1.2E-03
4015	Rap1 signaling pathway	3	5.1E-03
5219	Bladder cancer	2	5.1E-03
5033	Nicotine addiction	2	5.1E-03

Figure 4.4 Functional Enrichments in CSE Candidate Protein Networks correspond to Cell Communication and Signal Transduction Pathways. The online STRING database was used to identify relevant pathways corresponding to the eighteen candidate proteins identified in Figure 4.2. Curated databases including Biological Processes (A), Molecular Function (B) and KEGG (C) identified significant enrichment in cell communication and signal transduction pathways. Anion binding (B) and Ras signaling pathways (C) also demonstrated elevated enrichment.

4.3.5 Western Blot Validation of CSE Candidate Proteins Identifies Rb, PKCq and MEK2 as Candidate Proteins

In order to further prioritize candidate proteins identified in the CSE analysis, primary microglia cultures were generated for Western blot confirmation. Twelve to fifteen million WT and YAC128 primary microglia were stimulated with CSE for 30min similar to the protein phosphorylation microarray. Stimulated microglia were then lysed and run on the Kinetworks^{TM} Custom KCPS 1.0 Multi-Antibody Protein Screen, which allows one sample to be incubated with 18 antibodies simultaneously (Figure 4.5 D). The antibodies used for the Western blot analysis were the same ones used in the initial microarray screens and correspond to the CSE priority list (Figure 4.2). Three of the eighteen antibodies were identified on the Multi-Antibody Protein Screen in both WT and YAC-CSE, corresponding to retinoblastoma (Rb), protein serine kinase C-theta (PKCq) and MAP kinase 2 (MEK2) (Figure 4.5). Both Rb and MEK2 are pan-specific proteins while PKCq corresponds to a serine (S676) phosphorylation signal. Quantification of these proteins also demonstrated an increase in signal in YAC-CSE as compared to WT-CSE conditions (Figure 4.5 C).

A

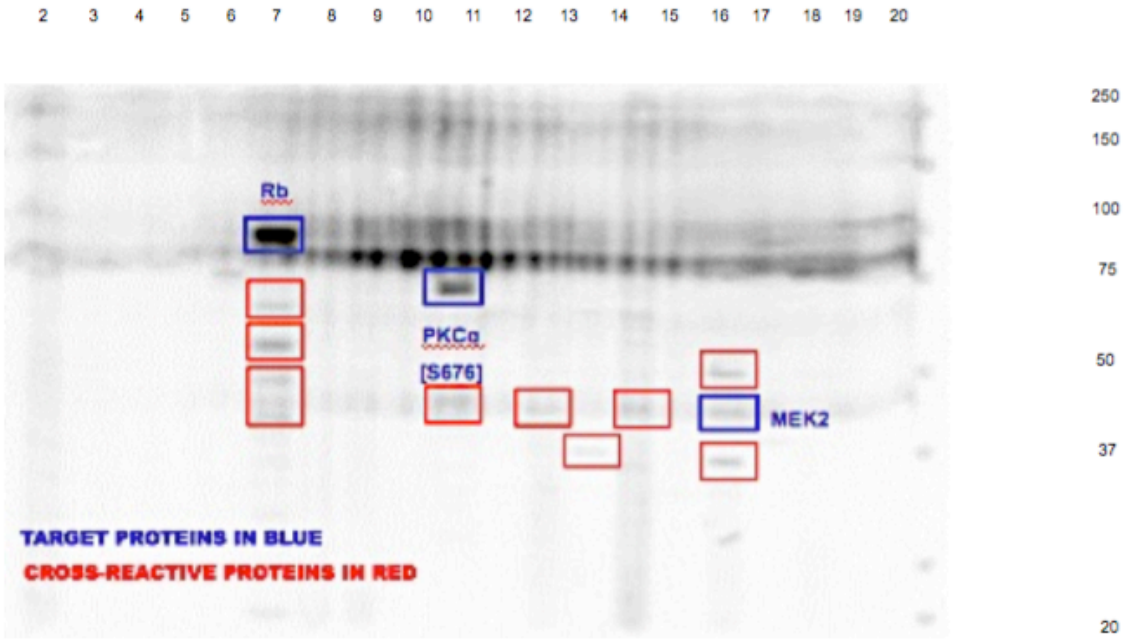
2 3 4 5 6 7 8 9 10 11 12 13 14 15 16 17 18 19 20
Rb
PKCα
[S676]
MEK2
TARGET PROTEINS IN BLUE
CROSS-REACTIVE PROTEINS IN RED
250
150
100
75
50
37
20

B

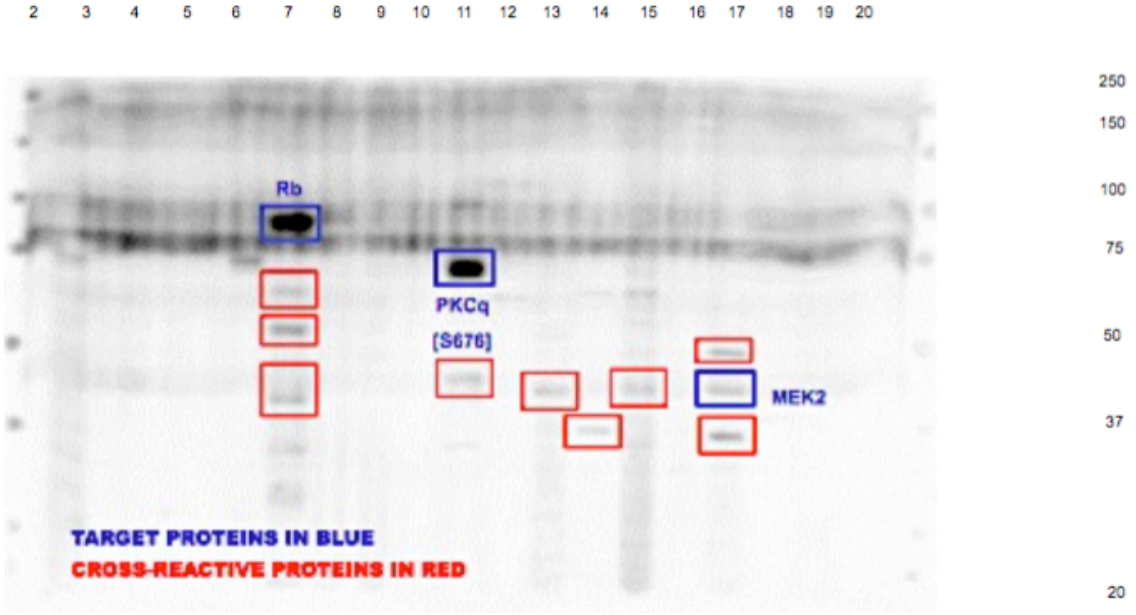
2 3 4 5 6 7 8 9 10 11 12 13 14 15 16 17 18 19 20
Rb
PKCα
[S676]
MEK2
TARGET PROTEINS IN BLUE
CROSS-REACTIVE PROTEINS IN RED
250
150
100
75
50
37
20

C

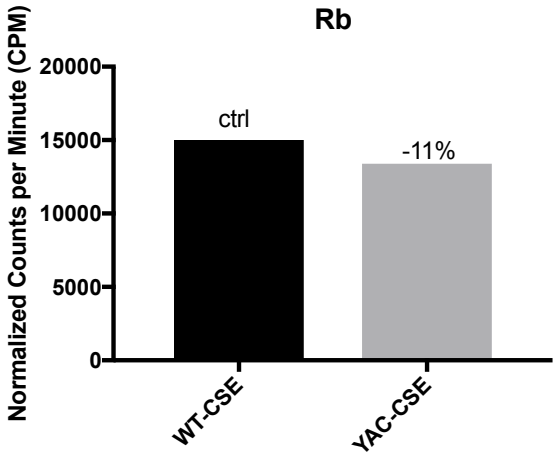
Rb
Normalized Counts per Minute (CPM)
20000
15000
10000
5000
0
ctrl
-11%
WT-CSE
YAC-CSE

D

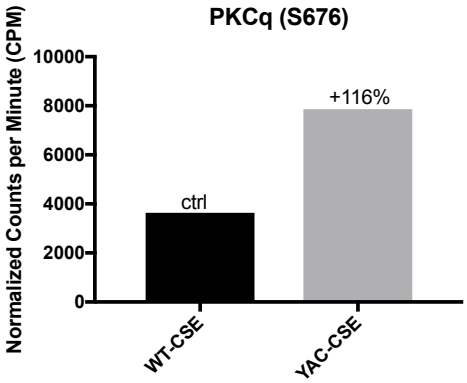
PKCq (S676)
Normalized Counts per Minute (CPM)
10000
8000
6000
4000
2000
0
ctrl
+116%
WT-CSE
YAC-CSE

E

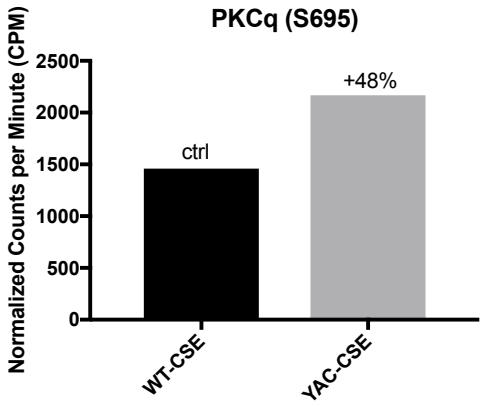
PKCq (S695)
Normalized Counts per Minute (CPM)
2500
2000
1500
1000
500
0
ctrl
+48%
WT-CSE
YAC-CSE

F

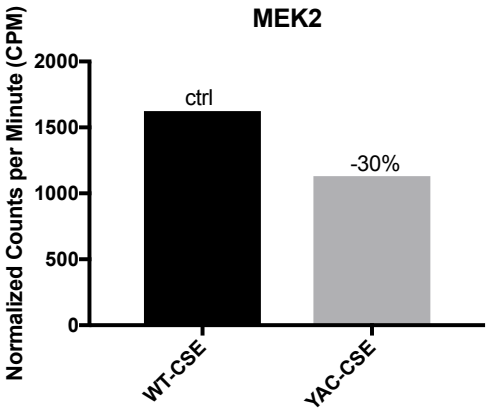
MEK2
Normalized Counts per Minute (CPM)
2000
1500
1000
500
0
ctrl
-30%
WT-CSE
YAC-CSE

G

Lane	Ab Code	Name	Site	MW	Low	High	Detection
2	PK608	Epha3	Y779	110	98	118	No
3	PN525	PGK1	Y196	45	42	50	No
4	NK053	EphA1	Pan	108	98	108	No
5	PK143	ASK1	S1046	155	150	170	No
6	PK0901	PKCq	S695	82	75	85	No
7	NN093	Rb	Pan	106	93	106	**Yes**
8	NK007	ASK1	Pan	155	150	170	No
9	NK104	PKCq	Pan	82	69	77	No
10	PK800	Ron	Y1238	152	147	157	No
11	PK0891	PKCq	S676	82	75	85	**Yes**
12	PN067	Rb	S780	106	115	132	No
13	NK1612	Ron	Pan	40	30	40	No
14	PN187	NBS1	S343	88	80	90	No
15	NK1102	Met	Pan	155	154	178	No
16	PN178	GluR1	S849	102	95	110	No
17	NK1005	MEK2	Pan	44	38	43	**Yes**
18	PN0551	NR1	S896	105	95	105	No
19	PP004	PTPD1	S580	68	65	75	No

Figure 4.5 Western blot Validation of CSE Candidate Proteins Odentifies Rb, PKCq and MEK2 as Priority Leads. WT-CSE and YAC-CSE microglia were probed with 18 antibodies simultaneously (outlined in G), resulting in three priority proteins (A, B). Quantification of Rb protein levels resulted in an 11% reduction in YAC-CSE compared to WT-CSE (C). PKCq phosphorylation levels at serine (S676) increased by 116% in YAC-CSE (D). PKCq phosphorylation levels at serine (S695) also increased in the YAC-CSE sample by 48% as compared to WT-CSE (E). MEK2 protein levels also decreased by 30% in YAC-CSE sample as compared to WT-CSE (F). Normalized counts per minute (CPM) refers to the trace quantity of the band corrected to a scan time of 60seconds. The trace quantity is measured by the area under its intensity profile curve (units corresponding to intensity x mm) and allows for protein levels to be compared between gels.

4.3.6 Validated MEK2 and PKCq Proteins ClusterTtogether following STRING Analysis and Result in Significant Enrichment in Various Cancer-Related Pathways

In order to better understand the potential pathways involved in the three validated proteins, STRING was used to highlight any potential interactions, similar to section 4.3. 3. As mentioned previously, STRING allows for functional associations to be made between proteins allowing for common biological functions to be identified. This is of particular importance in these validated proteins as a means of identifying a potential pathway for subsequent intervention. All three proteins cluster together as demonstrated by the matching colors (Markov cluster analysis 3, Figure 4.6 A). Only MEK2 (corresponding to Map2k2 in STRING figure) and PKCq (indicated as Prkcq in STRING figure), however, demonstrate putative protein-protein interactions as indicated by the joining edges. This implies that MEK2 and PKCq may be involved in single pathway that is relevant to the exaggerated cytokine release demonstrated by mutant-huntingtin expressing microglia in response to CSE stimulation. The STRING database also identified ten KEGG pathways that were significantly enriched in the three validated CSE proteins, including various cancer as well as T-cell receptor signaling pathways (Figure 4.6 B).

A

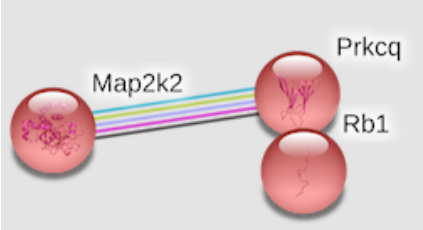

B

Pathway ID	Description	Gene Count	FDR	Proteins Involved
5214	Glioma	2	1.6E-03	Map2k2, Rb1
5218	Melanoma	2	1.6E-03	Map2k2, Rb1
5219	Bladder cancer	2	1.6E-03	Map2k2, Rb1
5220	Chronic myeloid leukemia	2	1.6E-03	Map2k2, Rb1
5223	Non-small cell lung cancer	2	1.6E-03	Map2k2, Rb1
5215	Prostate cancer	2	2.1E-03	Map2k2, Rb1
4660	T-cell receptor signaling pathway	2	2.5E-03	Map2k2, PRKCq
4270	Vascular smooth muscle contraction	2	3.0E-03	Map2k2, PRKCq
5161	Hepatitis B	2	3.7E-03	Map2k2, Rb1
5200	Pathways in cancer	2	1.7E-02	Map2k2, Rb1

Figure 4.6 Functional Enrichments in Validated CSE Candidate Protein Networks correspond to Various Cancer-related Pathways. The online STRING database was used to identify protein-protein interactions (A) and relevant pathways (B) corresponding to the three validated candidate proteins identified in Figure 4.5. A) Matching colors, as identified by Markov Cluster analysis indicate that all three validated candidate proteins cluster as interacting proteins. Figure adapted from http://string-db.org/. Edges (lines) represent protein-protein interactions, which jointly contribute to a shared function but no not necessarily physically bind together. Color of the edges corresponds to different levels of interactions. Blue and magenta correspond to known interactions from curated databases and experimentally determined, respectively. Black corresponds to protein co-expression and purple indicates protein homology. B) STRING database was also used to conduct a preliminary pathway analysis. Only the KEGG curated database identified significant enrichment in various cancer-related pathways.

4.3.7 Additional Protein Enrichments Identified using Three Candidate Proteins Correspond to Metabolism and Cell Cycle Pathways

The online STRING database also allows putative protein-protein interactions to be identified outside of the proteins initially inputted. Using this function, I entered the three validated CSE priority proteins and identified additional protein-protein interactions using the curated databases. With this application, MEK2 and PKCq clustered together in an expanded putative protein-protein network consisting of Braf and Ksr1 (Figure 4.7 A). Both Braf transforming gene (Braf) and Kinase suppressor of ras 1 (Ksr1) are known oncogenes (Sos *et al.* 2014). Braf is involved in cellular growth and proliferation with BRAF inhibitors used for melanoma therapy (Shen *et al.* 2013). Braf interacts with Ksr1 and mediates its proliferative effect through the MEK-ERK signaling cascade (Shen *et al.* 2013). Ksr1, specifically, connects MAP kinase to the RAF pathway and is involved in phosphorylation of both enzymes. RAF is upstream of MEK1/2 and is a strong mediator of anti-apoptotic and pro-survival signaling cascades (Kim *et al.* 2007). Rb1 also forms a putative protein-protein cluster along with Tfdp1, E2f3 and E2f1 (Figure 4.7 A). As discussed in Chapter 2, E2f1 is a cell marker of the cell cycle phase G1 and is elevated in HD post-mortem brain and in HD 3-NP rat models (Pelegri *et al.* 2008). Transcription factor Dp1 (Tfdp1) stimulates E2F-dependent transcription and is involved in cell cycle regulation, DNA replication and apoptosis. Rb also plays a role in cell cycle progression (reviewed in Sachdeva and O'Brien, 2012), suggesting that the cell cycle may be implicated in mutant-huntingtin mediated inflammatory cascades. The STRING database was also used to identify enriched biological pathways implicated in these novel clusters. The Molecular Function database identified five enriched protein pathways, corresponding to various intracellular compound binding and kinase cascades (Figure 4.7 B). Twenty-two enriched protein pathways were identified using the Biological Processes database, corresponding to metabolism, cell proliferation, signal transduction and gene expression functions (Figure 4.7 C). The KEGG database identified thirty-one enriched protein pathways, related to cancer and cell cycle pathways (Figure 4.7 D).

A

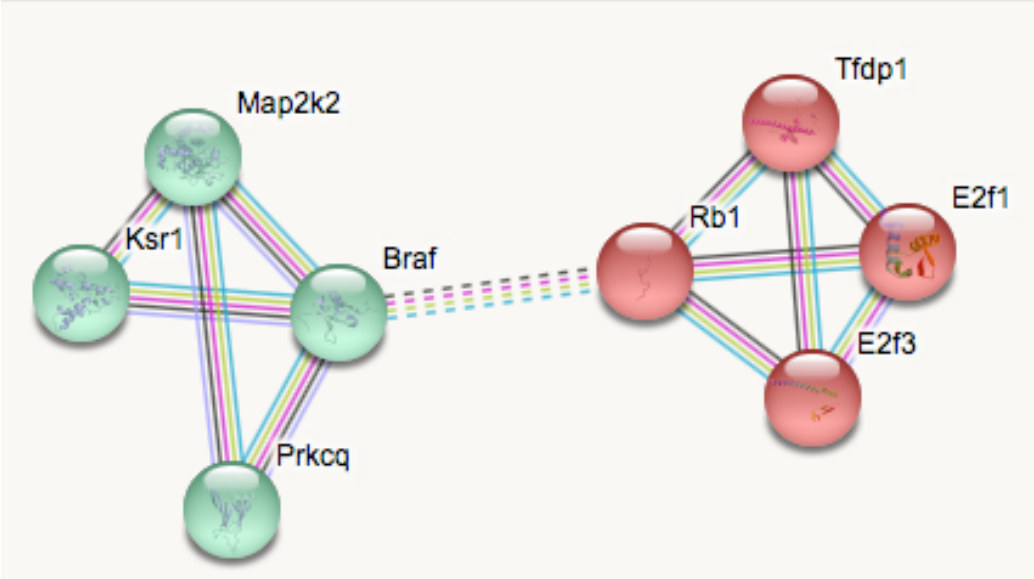

B

Pathway ID	Description	Gene Count	FDR	Proteins Involved
GO.0097159	Organic cyclic compound binding	8	5.4E-03	Braf, E2f1, E2f3, Ksr1, Map2k2, PrkCq, Rb1, Tfdp1
GO.1901363	Heterocyclic compound binding	8	5.4E-03	Braf, E2f1, E2f3, Ksr1, Map2k2, PrkCq, Rb1, Tfdp1
GO.0001047	Core promoter binding	3	1.7E0-2	Ef21, Ef23, Rb
GO.0004672	Protein kinase activity	4	2.2E0-2	Braf, Ksr1, Map2k2, PRKCq
GO.0032947	Protein complex scaffold	2	4.0E-02	Ksr1, Map2k2

C

Pathway ID	Description	Gene Count	FDR	Proteins Involved
GO.0070345	Negative regulation of fat cell proliferation	3	1.3E-05	E2f1, E2f3, Tfdp1
GO.0071930	Negative regulation of transcription factor involved in G1/S transition in mitotic cell cycle	2	1.5E-03	E2f1, Rb1
GO.0035556	Intracellular signal transduction	6	1.6E-03	Braf, E2f1, Ksr1, Map2k2, Prkcq, Rb1
GO.0042127	Regulation of cell proliferation	6	1.7E-03	Braf, E2f1, E2f3, Prkcq, Rb1, Tfdp1
GO.0010604	Positive regulation of macromolecule metabolic process	7	1.8E-03	E2f1, E2f3, Krs1, Map2k2, Prkcq, Rb1, Tfdp1
GO.0031325	Positive regulation of cellular metabolic process	7	2.3E-03	E2f1, E2f3, Krs1, Map2k2, Prkcq, Rb1, Tfdp1
GO.0043276	Anoikis	2	2.8E0-3	E2f1, Tfdp1
GO.0010628	Positive regulation of gene expression	6	3.3E-03	Braf, E2f1, E2f3, Prkc1, Rb1, Tfdp1
GO.0044260	Cellular macromolecule metabolic process	8	6.8E-03	Braf, E2f1, E2f3, Ksr1, Map2k2, Prkcq, Rb1, Tfdp1
GO.0048679	Regulation of axon regeneration	2	9.6E-03	Braf, Map2k2

D

Pathway ID	Description	Gene Count	FDR	Proteins Involved
5219	Bladder cancer	5	1.2E-10	Braf, E2f1, E2f3, Map2k2, Rb1
5223	Non-small cell lung cancer	5	5.0E-10	Braf, E2f1, E2f3, Map2k2, Rb1
5214	Glioma	5	5.3E-10	Braf, E2f1, E2f3, Map2k2, Rb1
5218	Melanoma	5	7.7E-10	Braf, E2f1, E2f3, Map2k2, Rb1
5220	Chronic myeloid leukemia	5	7.7E-10	Braf, E2f1, E2f3, Map2k2, Rb1Tfdp1
5215	Prostate cancer	5	2.1E-09	Braf, E2f1, E2f3, Map2k2, Rb1
5212	Pancreatic cancer	4	1.6E-07	Braf, E2f1, E2f3, Rb1
5200	Pathways in cancer	5	1.0E-06	Braf, E2f1, E2f3, Map2k2, Rb1
4110	Cell cycle	4	1.7E-06	E2f1, E2f3, Rb1, Tfdp1
5161	Hepatitis B	4	3.0E-06	E2f1, E2f3, Map2k2, Rb1

Figure 4.7 Additional STRING analysis of Validated CSE Priority Proteins results in Significant Enrichment of Cell Cycle Related Pathways. The online STRING database was used to identify additional protein-protein interactions (A) and relevant pathways (B) corresponding to the three validated candidate proteins identified in Figure 4.5. A) Matching colors, as identified by Markov Cluster analysis indicate that all three validated candidate proteins cluster as interacting proteins. Figure adapted from http://string-db.org/ Both MEK2 and PKCq cluster together with Braf and Ksr1 while Rb forms a distinct protein cluster with cell cycle related proteins. STRING database was also used to conduct a preliminary pathway analysis. Molecular Function (B), Biological Processes (C), and KEGG (D) curated databases identified significant enrichment in metabolism and cell cycle pathways.

4.3.8 Proteins with Increased Phosphorylation Expression in YAC128 HD microglia compared to WT following MMP3 stimulation

Similar sample generation and bioinformatics analysis was conducted following MMP3 stimulation. Microglia cultures isolated from WT and YAC128 pups were stimulated with MMP3 for 30min and collected for Kinex^{TM} KAM-900P phosphorylation array. Protein lysis was conducted at Kinexus using established chemical cleavage, pre-homogenization and biotin labeling protocols. Two separate arrays were completed as technical replicates with separate microglia cultures generated and stimulated for each (WT MMP3 and YAC MMP3). Kinexus generated analysis reports identified priority proteins in the WT MMP3 vs. YAC MMP3 comparison. These priority proteins demonstrated an increased %CFC (percent change from control) compared to WT meaning that these proteins demonstrated significantly increased phosphorylation in YAC MMP3 microglia versus WT MMP3. Additional analysis was also conducted to identify candidate proteins for future Western blot validation. As discussed in Section 4.2.8, candidate proteins were also assessed for stimulation effect. This refers to increased phosphorylation following MMP3 stimulation but an exaggerated response in HD microglia compared to control. Using the combination of priority leads generated by Kinexus (based entirely on %CFC) and the additional stimulation effect, nine top phosphorylation proteins were identified. The Kinex^{TM} KAM-900P phosphorylation array also evaluates the expression of pan-specific proteins. The corresponding pan-specific proteins for the top nine-phosphorylation candidates were also included in the validation list. Two of the nine-phosphorylation proteins (p70 S6KB and PGK1) did not have corresponding pan-specific proteins available on the array. As a result, two additional proteins with large %CFC differences and stimulation effects were included in the candidate list (MSK1, p38d MAPK) (Figure 4.6).

Protein Name	Phospho-site (human)	Full Target Protein Name	WT Stim effect		YAC Stim Effect	
IRS1	S639	Insulin receptor substrate 1	✔	✔	✔	✔
CHK1	S280	Checkpoint protein-serine kinase 1	✔	✔	✔	✔
EphA3	Y779	Ephrin type-A receptor 3 protein-tyrosine kinase	✔		✔	✔
AurKA (Aurora A)	Pan-specific	Aurora Kinase A (serine/threonine protein kinase 6)	✔	✔	✔	✔
p70 S6K	S447	Ribosomal protein S6 kinase beta-1 (RPS6KB1, p70S6Ka)	✔	✔	✔	✔
FGFR1	Pan-specific	Fibroblast growth factor receptor-tyrosine kinase 1	✔	✔	✔	✔
p70 S6KB	S423	Ribosomal protein S6 kinase beta-2	✔		✔	✔
PGK1	Y196	Phosphoglycerate kinase 1	✔	✔	✔	✔
Ron	Y1238	Macrophage-stimulating protein receptor alpha chain	✔	✔	✔	✔
IRS1	S312	Insulin receptor substrate 1	✔			
CHK1	Pan-specific	Checkpoint protein-serine kinase 1		✔		✔
EphA1	Pan-specific	Ephrin type-A receptor 1 protein-tyrosine kinase		✔		✔
AurKA (Aurora A)	Pan-specific	Aurora Kinase A	✔	✔	✔	✔
p70 S6K	Pan-specific	Ribosomal protein S6 kinase beta-1	✔	✔		✔
FGFR1	Pan-specific	Fibroblast growth factor receptor-tyrosine kinase 1	✔	✔		✔
Ron	Pan-specific	Macrophage-stimulating protein receptor alpha chain	✔		✔	✔
MSK1	S376	Mitogen & stress-activated protein-serine kinase 1			✔	✔
p38d MAPK	Pan-specific	Mitogen-activated protein-serine kinase p38 delta			✔	✔

Figure 4.8 MMP3 Protein Candidate Validation List. Eighteen candidate proteins identified from WT CSE and YAC MMP3 comparison using both arrays. WT Stim and YAC Stim column divided into first and second array. Presence of checkmark corresponds to stimulation effect in the corresponding array.

4.3.9 Candidate Proteins Identified following MMP3 Stimulation Cluster into Three Protein-Protein Interaction Groups

Similar to the CSE candidates identified, I used the online STRING database to evaluate potential protein-protein interactions between the MMP3 candidate proteins. The top-nine phosphorylation proteins identified in Figure 4.6 along with two additional proteins of interest (MSK1, p38 MAPK) were inputted into the database and clustered using a Markov Clustering factor of 3 (corresponding to high associations). Within the eleven candidates, I identified three putative clusters, each highlighted by a different color in Figure 4.7. Three of the candidate proteins overlapped between the CSE and MMP3 analysis (EphA3, PGK1, and Ron) and were included in the separate STRING analyses. Similar to the CSE analysis, PGK1 does not cluster with any of the three protein groups and Ron (also referred to as Mstlr in the STRING interactions) clustered with various proteins. However, in contrast to CSE candidate proteins, EphA3 also did not cluster in the MMP3 candidate list. Each of the clusters contained interactions corresponding to known protein interactions identified from curated databases (blue edges) and experimentally determined (magenta). Putative interactions between two of the three clusters (corresponding to dashed edges) were also identified. Similar to the CSE STRING analysis, the protein-protein interactions identified between the MMP3 candidate proteins will be used to identify potential signaling cascades that differ between mutant-huntingtin expressing microglia and WT microglia in response to MMP3 stimulation.

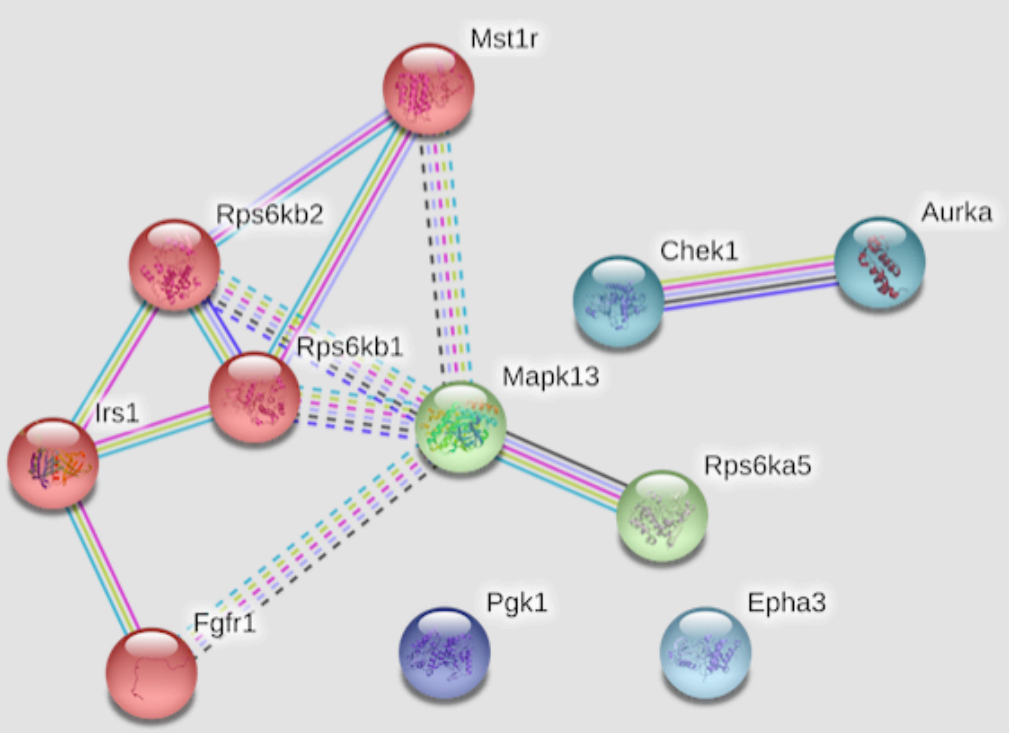

Figure 4.9 STRING Analysis of Candidate MMP3 Proteins. Similar to CSE analysis, STRING online database (http://string-db.org/) was used to identify known protein-protein interactions between the top nine-phosphorylation proteins as well as including two additional proteins (MSK1, p38d MAPK) (n=11 total) (Listed in Figure 4.8). Matching colors, as identified by Markov Cluster analysis, indicates clusters of interacting proteins. Figure adapted from http://string-db.org/. Equivalent names for several candidate proteins used in STRING analysis including (Chek1= CHK1; RPS6KB1= p70 S6K; RPS6KB2= p70 S6KB; Mstlr= Ron; Rps6ka5= MSK1; MAPK13= p38d MAPK). The first protein name is found in the STRING analysis and the corresponding name is identified in Figure 4.8. Edges (lines) represent protein-protein interactions (shared function but not necessarily physical binding). Color of edges corresponds to different levels of interactions. Blue and magenta correspond to known interactions from curated databases and experimentally determined, respectively. Yellow refers to interactions identified using text-mining, black corresponds to protein co-expression and purple indicates protein homology

4.3.10 Pathway Analysis of MMP3 Candidate Proteins Result in Enrichment of Signal Transduction and Protein Kinase Pathways

Similar STRING pathway analysis was conducted with the eleven candidate MMP3 proteins identified in Figure 4.9. The Biological Processes database identified thirty enriched protein networks, corresponding to metabolism, signal transduction and protein phosphorylation (Figure 4.10 A). Nine enriched protein networks were identified in the Molecular Function database, related to various protein kinase-signaling cascades (Figure 4.10 B) as expected. The KEGG database identified sixteen enriched protein networks, corresponding to numerous signaling pathways including P13k-Akt and insulin (Figure 4.10 C).

A

Pathway ID	Description	Gene Count	FDR
GO.0006468	Protein phosphorylation	9	2.2E-08
GO.0018193	Peptidyl-amino acid modification	7	6.1E-05
GO.0016572	Histone phosphorylation	3	1.7E-04
GO.0043491	Protein kinase B signaling	3	6.8E-04
GO.0010604	Positive regulation of marcromolecule metabolic process	8	1.4E-03
GO.0031325	Positive regulation of cellular metabolic process	8	2.1E-03
GO.0019222	Regulation of metabolic process	10	2.5E-03
GO.0032270	Positive regulation of cellular protein metabolic process	6	3.2E-03
GO.0032268	Regulation of cellular protein metabolic process	7	6.1E-03
GO.0007165	Signal transduction	8	7.3E-03

B

Pathway ID	Description	Gene Count	FDR
GO.0004672	Protein kinase activity	9	5.6E-10
GO.0005524	ATP binding	9	3.3E-07
GO.0004674	Protein serine/threonine kinase activity	6	3.1E-06
GO.0035173	Histone kinase activity	3	1.45E-05
GO.0004711	Ribosomal protein S6 kinase activity	2	5.2E-04
GO.0004714	Transmembrane receptor protein tyrosine kinase activity	3	5.7E-04
GO.0035174	Histone serine kinase activity	2	1.2E-03
GO.0004871	Signal transducer activity	5	1.1E-02
GO.0004712	Protein serine/threonine/tyrosine kinase activity	2	2.2E-02

C

Pathway ID	Description	Gene Count	FDR
4150	mTOR signaling pathway	3	4.3E-05
5205	Proteoglycans in cancer	4	4.2E-05
4151	P13k-Akt signaling pathway	4	1.5E-03
4152	AMPK signaling pathway	3	1.5E-03
4722	Neurotrophin signaling pathway	3	1.5E-03
4910	Insulin signaling pathway	3	1.6E-03
4010	MAPK signaling pathway	3	8.3E-03
5221	Acute myeloid leukemia	2	1.2E-02
4012	ErbB signaling pathway	2	1.9E-02
4350	TGF-beta signaling pathway	2	1.9E-02

Figure 4.10 Functional Enrichments in MMP3 Candidate Protein Networks correspond to Various Protein Kinase and Signaling Cascades. STRING database was also used to conduct a preliminary pathway analysis. Biological Processes (A), Molecular Function (B), and KEGG (C) curated databases identified significant enrichment in metabolism and signal transduction pathways. Various biological pathways were also enriched in the eleven candidate MMP3 proteins, corresponding to P13k-Akt, TGF-beta and insulin signaling (C).

4.4 Discussion

In this chapter, I utilized my established *ex vivo* culture system to evaluate signal transduction pathways in microglia expressing mutant huntingtin in response to the proinflammatory activators CSE and MMP3. Using the Kinex^{TM} KAM-900P phosphorylation array, thirty one priority protein leads were identified in the first array and fourteen in the second array following CSE stimulation. Two priority proteins (EphA3 and ASK1) overlapped between the two separate microarrays and were included for Western blot validation. As discussed in section 4.2.7, the priority leads generated by Kinexus were subject to an additional analysis (termed stimulation effect) in order to identify proteins that were significantly phosphorylated following CSE stimulation but demonstrated an exaggerated response in HD microglia.

The use of the recommended leads generated by Kinexus, in combination with the stimulation effect analysis, resulted in nine phosphorylation proteins (EpA3, ASK1, PGK1, PKCq, Ron, Rb, GluR1, NMDAR1, and NBS1). The corresponding pan-specific proteins were also included in the candidate protein list to evaluate phosphorylation/expression ratios. This phosphorylation/expression ratio for a specific protein would provide information on the true phosphorylation state of the protein in question. For example, if a phospho-protein increases and total protein remains constant, then the experimental system, in this case the expression of mHTT in microglia, is suggested to increase the phosphorylation of the protein of interest. If, however, both the phospho-protein and the total protein both increase (or decrease), the ratio of phospho/total protein remains constant and, as a result, the expression of mHTT in microglia, increases (or decreases) the expression of the protein but not its phosphorylation. Although the phosphorylation of the protein would be of great interest in uncovering potential signaling cascades mediated by mHTT expression, potential changes in protein expression could also provide further insight into microglial dysfunction in HD and may serve as potential therapeutic interventions.

Western blot validation of WT-CSE and YAC-CSE treated microglia confirmed the expression of three of the eighteen total candidate proteins. Retinoblastoma (Rb) and MAP kinase 2 (MEK2) expression, along with Protein Serine Kinase (PKCq)

phosphorylation levels at both serine 676 and 695 were validated in the Western blot analysis. Only phosphorylation levels of PKCq were elevated in the YAC-CSE sample (Figure 4.5 D and E) while there were down-regulations in Rb and MEK2 protein levels in the YAC-CSE sample (Figure 4.5 C and F). Additional experiments will need to be conducted in order to compare the levels of Rb, PKCq and MEK2 levels in WT and YAC-CSE stimulated microglia as changes greater than 25% may correspond to real protein level differences. As a result, the lower levels of Rb and MEK2 protein levels in YAC-CSE microglia may be inaccurate and will need to be assessed in additional samples. These proteins, specifically PKCq, will be the focus of future experiments aimed at investigating downstream signaling cascades involved in the exaggerated inflammatory response seen in HD microglia. In the first set of experiments, microglia will be stimulated with CSE or MMP3 and mHTT ASO will be used to reduce mHTT levels. The phospho-proteins of interest will then be evaluated using Western blot to confirm an interaction between mHTT and the protein of interest. If the interaction is present, the levels of the phospho-protein would be expected to be reduced and normalized to WT levels. The second set of experiments will be used to evaluate the role of the phospho-protein in mediating IL-6 release. Pharmacological blockade of the phospho-protein and subsequent investigation of IL-6 cytokine release will be conducted to assess if the phospho-protein of interest normalizes the exaggerated inflammatory response seen in HD microglia. Although only three candidate proteins were confirmed using Western blot analysis, additional blots will be conducted to assess the presence of the other CSE candidate proteins identified in Figure 4.3.

The first Western blot validated protein, Retinoblastoma (Rb), plays a role in the regulation of cell cycle progression, DNA replication and terminal differentiation. The phosphorylation of Rb, termed pRb, is a transcriptional cofactor involved in cell proliferation, apoptosis, and G1 cell cycle arrest (reviewed in Sachdeva and O'Brien, 2012). Previous work in AD has demonstrated the expression of hyperphosphorylated Rb in both cortical neurons and astrocytes surrounding Aβ-containing plaques (Jordan-Sciutto *et al.* 2002). As a cell-cycle regulatory protein, the presence of Rb in the AD brain points to a potential pathogenic cell-cycle re-entry mechanism in the disease. It has been suggested that neurons re-enter the cell cycle during AD, leading to the induction of

apoptotic pathways (Freeman RS *et al.* 1994). pRb knockout mice also demonstrate significant neuronal death in the CNS (Jacks *et al.* 1992), providing further evidence for a the role of Rb in neuronal apoptosis. With respect to HD, Rb and its phosphorylated protein have not been previously implicated but as a disease characterized by neuronal cell death, it would be interesting to evaluate the role of phosphorylated Rb in mutant-huntingtin containing microglia and the potential impact on neuronal viability.

The Rb protein is also a prominent tumor suppressor and plays a major role in cancer-related signaling cascades, along with the p53 transcription factor (reviewed in Sherr and McCormick, 2002). P53 has been previously implicated in HD with elevated levels identified in both cell and mouse models (Grison *et al.* 2011, Sipione *et al.* 2002). Elevated levels of phosphorylated p53 have also been identified in postmortem HD brain leading to activation of apoptosis (Mayo *et al.* 2005). P53 has numerous roles in HD, including mitochondrial dysfunction and cell death. Silencing or inhibition of p53 is neuroprotective *in vitro* as well as *in vivo* (Guo *et al.* 2013). P53 is also implicated in *HTT* gene regulation. Multiple putative p53 responsive elements are present on the *HTT* gene that can be activated to increase huntingtin mRNA and protein expression (Feng *et al.* 2006). More importantly, p53 has been shown to directly interact with mHTT where mHTT may act as an upstream inducer of p53, ultimately leading to the induction of proapoptotic cascades (Grison *et al.* 2011; reviewed in Bowles and Jones, 2014). The connection between mHTT, p53 and Rb point to a potential signaling cascade of interest for further investigation in mutant-huntingtin expressing microglia.

The second Western blot validated protein; MEK2 has been previously implicated in HD. As discussed in the introduction, MAP kinase 2 (MEK2) is a part of the MEK/ERK pathway and plays a role in pro-survival signaling. In the context of HD, both MEK and ERK are involved in the regulation of BDNF transcription and cellular responses in the striatum (Roze *et al.* 2008). Over-expression of active MEK and enhanced ERK activity has also been shown to reduce caspase-3 activation in cell models of HD (26), likely due to reduced numbers of mHTT aggregates. MEK1 over-expression is protective against cell death in PC12 cell models of HD (26), demonstrating the importance of MEK/ERK signaling in various cellular processes involved in HD (reviewed in Bowles and Jones, 2014).

The last Western blot validated protein, Protein Serine Kinase (PKCq) is also potentially linked to HD through the N-methyl-D-aspartate (NMDA) glutamate receptor pathway. N-methyl-D-aspartate (NMDA) glutamate receptor 1 (NMDAR1) is expressed on microglia in the immature and mature murine and human CNS (Kaindl *et al.* 2012) and has been implicated as a mediator of excitotoxicity in the striatum in HD (reviewed in Sepers and Raymond, 2014). Phosphorylation changes in NMDAR1 and GluR1 (Glutamate receptor 1), as a result, may play a role in mediating changes in glutamate release and postsynaptic signaling leading to excitotoxic neuronal cell death in the striatum. Previous work has suggested that the expression of mutant huntingtin influences NMDA receptor currents by increasing the number of functional receptors at the cell surface (Chen *et al.* 1999), which in turn enhances excitotoxic cell death (Zeron *et al.* 2001). Phosphorylation changes have been implicated as regulators of NMDA receptor trafficking (reviewed in Chen and Roche, 2007). The phosphorylation of NMDAR at the S896 residue (identified in Figure 4.2) corresponds to specific phosphorylation of the NR1 receptor subunit of NMDAR1 by protein kinase C (PKC) (Tingley *et al.* 1997). The phosphorylation of the identified S896 residue, along with PKA phosphorylation of an additional S890 residue on the NR1 receptor subunit of NMDAR1, has been shown to increase NMDA receptor surface expression (Scott *et al.* 2001).

Interestingly, PKCq was also identified in the Kinexus screen, implying that the presence of mutant huntingtin in microglia may exacerbate the process of NMDA receptor trafficking to the cell surface and contribute to excitotoxicity. Although NMDA receptor function in the context of HD has been fairly well investigated, the mechanism by which mutant huntingin influences NMDAR-mediated glutamatergic signaling, specifically in microglia is still poorly understood. It would be necessary to evaluate potential phosphorylation changes at baseline in NMDAR in WT and YAC128 microglia to identify potential regulatory mechanisms underlying mutant huntingtin-mediated dysregulation.

Apotosis signaling regulating kinase 1 (ASK1) has also been previously linked to HD in both human patients as well as mouse models. ASK1 is a member of the MAPK family involved in activation of JNK and p38 MAPK signaling cascades. Activated by various stresses including TNF, ER stress and H_2O_2, ASK1 plays a role in apoptosis, cell

survival and differentiation and has been implicated as a potential therapeutic target for Alzheimer's disease (reviewed in Song *et al.* 2014). In the context of HD, variations in genes involved in apoptosis have been investigated in patients as candidates for modulating age of onset. Variations in an ASK1-PEX7 haplotype were responsible for 2.6% of additional variance in age of onset in the HD patient cohort. The sequence variations in ASK1 may lead to changes in the phosphorylation states of downstream MAPK kinases including p38 and p38-regulating proteins and may contribute to alterations in age of onset in HD (Arning *et al.* 2008), although larger patient cohorts would been to be assessed. Mechanistically, ASK is involved in ER-stress induced cell death in cells expressing expanded polyglutamine repeats (Nishitoh *et al.* 2002). ASK1 protein levels are also significantly increased in R6/2 HD mouse cortex and striatum. Inactivation of ASK1 following infusion of anti-Ask1 antibody into the striatum can prevent translocation of mHTT fragments into the nucleus, resulting in improvements of motor deficits and atrophy (Cho *et al.* 2009) Other reductions in ASK1, using peroxisome proliferator-activated receptor gamma (PPARγ) agonist *in vitro* normalized levels of ER stressors, ultimately leading to reductions in mHTT aggregates and increased cell survival (Chiang *et al.* 2015). Peroxisome proliferator-activated receptor gamma (PPARγ) agonist has been previously shown to significantly reduce mHTT aggregates in the cortex and striatum (Chiang *et al.* 2012) and may be mediated by reductions in ASK1. As a result, the increase in phosphorylation of ASK1 identified in Figure 4.2 as a result of mutant huntingtin expression may exacerbate ER-stress and other related HD pathologies including mHTT aggregation.

Phosphoglyerate kinase 1 (PGK1), although not previously linked to HD, is another interesting candidate for further investigation. PGK1 is involved in glycolysis (metabolism of glucose to pyruvate and lactate) and has been primarily implicated in hereditary non-spherocytic haemolytic anaemia (HNSHA) (reviewed in Beutler, 2007). In Alzheimer's disease (AD), increased levels of PGK1 and other enzymes involved in glycolysis have been found in glial cells treated with AD plasma (Jayasena *et al.* 2014). Metabolic abnormalities, manifesting as weight loss despite normal caloric intake, however, are also a feature of HD and may result from disturbances in glycolytic pathways and mitochondrial deficits (reviewed in Krzyszton-Russjan, 2016). In HD

patients, positron emission tomography (PET) studies have demonstrated reduced glucose levels in the basal ganglia and cerebral cortex (Kuhl *et al.* 1985). Although primarily involved in energy production, glucose also plays a role as a signaling molecule (reviewed in Ribeiro *et al.* 2012). Previous work has implicated glucose as a key activator of molecules involved in cell survival and huntingtin clearance. Increased intracellular glucose levels, for example, result in decreased aggregate formation and improved cell survival in cultured cells transfected with a mutant huntingtin construct (Ravikumar *et al.* 2003). In terms of huntingtin clearance, glucose has been shown to reduce phosphorylation of mTOR, which in turn, stimulates autophagy and removal of mHTT (Ravikumar *et al.* 2003). Glucose can also regulate Akt (Clodfelder-Miller *et al.* 2005), the prosurvival protein kinase involved in HTT phosphorylation and subsequent reduction in nuclear mHTT fragments (Warby *et al.* 2009). In microglia, LPS-induced activation has been shown to promote significant metabolic changes by increasing glycolysis *in vitro.* This LPS-induced activation also significantly reduces ATP production and increases lactate levels (end product of glucose metabolism) (Volobouéva *et al.* 2013). Although reactive microglia depend on glucose metabolism to fulfill their diverse functions, increased phosphorylation of PGK1, a key enzyme involved in glycolysis, in mutant-huntingtin expressing cells may contribute to alterations in these mechanisms and contribute to metabolic abnormalities involved in HD.

Macrophage stimulating receptor (Ron), also referred to as Mstlr, has not been previously linked to HD but may be involved in pathogenesis. Ron is a transmembrane tyrosine kinase, and as the name suggests, the specific receptor of MSP (Macrophage-stimulating protein). In macrophages, previous work has implicated activation of Ron by MSP in the induction of various macrophage-specific functions including spreading, migration and phagocytosis. Ron signaling, through MSP, has also been shown to inhibit LPS-induced activation of proinflammatory molecules, including nitric oxide and prostaglandins. This reduction in LPS-dependent inflammation is mediated by alterations in NFκB pathways (reviewed in Wang *et al.* 2002). Inactivation of Ron *in vivo* results in increased LPS-induced inflammatory responses, demonstrating the role of Ron in mitigating the extent of inflammatory responses (Correll *et al.* 1997). In the context of HD, increased phosphorylation of Ron in mutant-huntingtin containing microglia may be

involved in the beneficial role of Ron signaling, namely phagocytosis, or the negative role of increased inflammation. In particular, the phosphorylation of Ron could be inhibitory and may alter the extent of inflammatory response attenuation. In order to better understand the role of Ron in HD, however, future experiments, specifically in microglia and not macrophages, would need to be conducted.

The Nijmegen breakage syndrome protein 1 (NBS1) is another candidate protein identified following CSE stimulation. Nijmegen breaking syndrome (NBS) is a genomic instability disease resulting from mutations in the NBS1 gene. In humans, NBS is characterized by microcephaly, immunodeficiency and increased predisposition to cancer as a result of deficits in cell cycle checkpoints (reviewed in Difilippantonio and Nussenzweig, 2007). In a conditional NBS1 mouse model, one where NBS1 was inactivated in cells of the nestin lineage, namely neurons and astrocytes, cerebellar atrophy and ataxia were identified (Assaf *et al.* 2008). The same Nestin-NBS1 mice also demonstrated altered morphology and organization of glial cells, primarily in the visual system (Baranes *et al.* 2009). This means that NBS1 in microglia is an important contributor to the phenotype of Nijmegen breaking syndrome and may play a role in cerebellar atrophy and ataxia. Since ataxia is also one of the clinical features of HD, it would be interesting to assess the role of NBS1 phosphorylation and downstream signaling in mutant-huntingtin containing microglia.

The two most highly expressed CSE candidate proteins were Retinoblastoma (Rb), and Ephrin A3 (EphA3). EphA3 is a member of the ephrin receptor family and is involved in embryogenesis as well as cancer. Although best characterized in development and cancer, Eph receptors have also been recently implicated as potential targets in Alzheimer's disease pathogenesis as potential receptors for toxic Aβ oligomers (reviewed in Cisse and Checler, 2015). Eph receptors and their ligands may also play a role in inflammation and immune function (reviewed in Coulthard *et al.* 2012). Inflammatory cells in multiple sclerosis lesions express multiple ephrins, including EphA3 (Sobel, 2005) and LPS-administration results in the up-regulation of numerous Eph/ephrin proteins (Ivanov and Romanowsky, 2006). Ephrin-A3 expression has also been identified in astrocytes in adult mouse hippocampus (Jiao *et al.* 2008) and ephrin A3/EphA4 signaling has been shown to regulate hippocampal dendritic spine morphology and

glutamate transport (Carmona *et al.* 2009) as well as LTP (Filosa *et al.* 2009) and hippocampal neuronal damage after transient global ischemia (Yang *et al.* 2014). In terms of microglia specifically, Ephrin-A3 along with ephrin A-4 have been found to contribute to angiogenesis in brain epithelial cells following release of TNF-α (Li *et al.* 2014). In the context of HD, ephrin A3 has not been previously implicated but ephrin A4, its binding partner, shows decreased mRNA levels in HD brain and reductions in protein levels in HD CSF (Fang *et al.* 2009). Additional experiments would need to be conducted to assess the functional importance of EphA3 phosphorylation in mutant-huntingtin containing microglia.

Similar to the CSE condition, eighteen candidate proteins were identified for follow-up validation following MMP3 stimulation using the Kinex^{TM} KAM-900P phosphorylation array and the additional stimulation effect analysis outlined in Section 4.2.8. In the initial Kinexus priority lead reports generated; fifteen proteins were identified in the WT MMP3 vs. YAC MMP3 condition in the first array and ten in the second array. In these priority leads, IRS1, corresponding to insulin receptor 1, overlapped between the two arrays and was included in the final candidate list for subsequent validation by Western blot. For the purposes of this thesis, only candidate proteins identified in the CSE condition were subject to Western blot validation but future experiments will be conducted to confirm the differential expression of the eighteen candidate proteins identified in the MMP3 condition (Figure 4.6). It is interesting to note that three proteins overlap between the CSE condition and the MMP3 analysis (EphA3, Ron, PGK1). It may be important to focus on these three overlapping phosphorylated proteins in future experiments as a way to uncover underlying dysfunction in mutant-huntingtin containing microglia, irrespective of stimulation.

5 Utilizing the Flow Cytometry System to Test Therapeutics

5.1 Introduction

As described in Chapter 1, diverse therapeutic approaches in HD exist. These tactics include, but are not limited to, reducing mutant huntingtin expression through various gene-silencing techniques, enhancement of mutant protein removal via HTT phosphorylation and autophagy, reestablishment of neurotropic support and modulation of glial activity and metabolism deficits (reviewed in Wild and Tabrizi, 2014). Although these approaches do not selectively target neuronal cells, these cells are commonly assessed in therapeutic outcome measures. Dysfunction in the HD brain is thought to be a consequence of mHTT expression in neurons, resulting in selective neurodegeneration of MSNs in the striatum of the brain. As a result, the effects of various therapeutics on neurons is commonly assessed in the HD field. *HTT,* however, is ubiquitously expressed meaning that mechanisms outside of neuronal dysfunction may contribute to disease pathogenesis, namely the immune system. Microglia and astrocytes, together referred to as glial cells, have been previously implicated in HD disease progression and serve as promising candidates target cells for therapeutic intervention. Specifically, astrocytic glutamate uptake and immunomodulation have been identified as targets for future clinical trials in order to modulate excitotoxicity and immune system dysfunction characteristic of HD.

5.1.1 Astrocytic Dysfunction in HD

Astrocytes comprise approximately thirty percent of the cells in the CNS and play a critical role in neuronal development, synapse formation and propagation of action potentials (Liddelow and Barnes, 2017). Because astrocytes have been implicated in the maintenance of the CNS, they have also been hypothesized to play a role in the onset and progression of various neurodegenerative diseases including Parkinson's disease, Alzheimer's disease, amyotrophic lateral sclerosis, and HD. Whether the involvement of

astrocytes in neurodegenerative disease is a result of loss of function or toxic gain of function mechanisms, however, is poorly understood. In instances of toxic insult or injury, astrocytes undergo various changes ranging from hypertrophy to proliferation and migration, commonly referred to as reactive astrogliosis. These reactive astrocytes release a variety or neuroprotective and neurotoxic chemicals, including beneficial neurotropic factors such as transforming growth factor-β (TGF- β) and proinflammatory molecules such as IL-1β and tumor necrosis factor-α (TNF-α) (reviewed in Phatnani and Maniatis, 2015).

In HD, specifically, mutant huntingtin expression in astrocytes has been shown to negatively influence both astrocytic function and neuronal health *in vitro*. In a neuron-glia primary co-culture system, wild-type glial cells protected neurons against mutant-huntingtin-dependent toxicity, while glial cells expressing mutant-huntingtin resulted in increased neuronal death (Shin *et al.* 2005). The mechanism by which mutant-huntingtin expressing astrocytes confer this increased neuronal vulnerability has been attributed to increased excitoxicity. Excitotoxicity is defined as neuronal death caused by excitatory neurotransmitter overstimulation (reviewed in Sepers and Raymond, 2014) and is considered to be a major contributor to the selective neurodegeneration of medium spiny neurons (MSNs) in HD. MSNs receive excitatory glutamatergic signals from the cortex and have been shown to be particularly sensitive to glutamate toxicity (Schwarcz *et al.* 1984).

Previous work in MSN's generated from YAC128 HD mouse brain demonstrated increased vulnerability to cell death following intrastriatal injections of quinolinate, a glutamate analogue (Zeron *et al.* 2002). Glutamate activates NMDA receptors, which transport calcium into the neuron. The overactivation of NMDARs increases calcium permeability and slows deactivation, which results in intracellular calcium overload. This disruption in intracellular calcium levels ultimately leads to mitochondrial energy failure and cell death (reviewed in Sepers and Raymond, 2014). The majority of extracellular glutamate (90%) is removed by excitatory amino acid transporter 2 (EAAT2), which is predominately expressed in astrocytes (Kim *et al.* 2011). In the context of HD, reduced EAAT2 expression has been identified in R6/2 mouse brain (Lievens *et al.* 2001). The human ortholog, GLT, also demonstrates reduced mRNA and protein expression in HD

postmortem brain (Arzberger *et al.* 1997). In HD mouse models, reduced EAAT2 expression results in decreased glutamate uptake and motor dysfunction (Faideau *et al.* 2010, Bradford *et al.* 2009), which is ameliorated following induction of EEAT-2 expression through promoter activation by the antibiotic ceftriaxone (Miller *et al.* 2012, Rothstein *et al*. 2005). Despite the improvement in behavioral phenotypes seen in mouse models, it remains unclear if sustained up-regulation of EAAT2 expression in astrocyte populations will be beneficial for human patients.

Other candidate mechanisms implicated in astrocytic dysfunction in HD, in addition to increased excitotoxicity, have also been identified. These include NFκB signaling, and mitochondrial, cholesterol and brain-derived neurotrophic (BDNF) defects. In the case of NFκB, work completed in two HD mouse models (knock-in Hdh (150Q) and N-terminal fragment R6/2) identified increased susceptibility to LPS-induced inflammation and increased proinflammatory cytokine secretion in the brain of HD mice compared to WT. Similar inflammatory responses were not identified in N171-82Q HD mice that express mHTT in neurons but not glia, suggesting that mHTT expression in glial cells plays a role in the observed inflammation. More importantly, Hsiao and colleagues identified that increased activation of NFκB, specifically in astrocytes, was responsible for up-regulating proinflammatory responses and ultimately resulted in neuronal death. The reversal of NFκB activation, following IKK blockade, reversed the neuronal toxicity, motor deficits and cognitive dysfunction observed in the R6/2 HD mouse model (Hsiao *et al.* 2013). Subsequent work by the same group blocked the upstream activator of NFκB, tumor necrosis factor α (TNF-α) (reviewed in Lawrence, 2009) in R6/2 HD cultured astrocytes and astrocytes derived from human HD induced pluripotent stem cells (iPSCs). Using a dominant-negative inhibitor of soluble TNF-α, referred to as XPro1595 resulted in an amelioration of the exaggerated proinflammatory cytokine profile seen in R6/2 and HD-patient derived astrocytes *in vitro*. Neurons isolated from R6/2 mice and derived from HD iPSCs were also protected against cytokine-induced toxicity following XPro1595 treatment (Hsiao *et al.* 2014). Taken together, both NFκB and upstream signaling in astrocytes may be implicated in astrocytic dysfunction and ultimately in HD pathogenesis.

Other forms of astrocytic dysfunction implicated in HD include mitochondrial,

brain derived neurotropic (BDNF) and cholesterol deficits (reviewed in Phatnani and Maniatis, 2015). In terms of BDNF signaling, HD astrocytes release lower levels of BDNF protein compared to WT (Wang *et al.* 2012). This is thought to be a result of repressed BDNF transcription in astrocytes as well as impaired BDNF exocytosis (Hong *et al.* 2016) as a result of mutant huntingtin expression (Wang *et al.* 2012). Increasing BDNF production in mutant-huntingtin containing astrocytes, through the use adenoviral BDNF cDNA expression in the striatum, was found to delay the onset of motor deficits in R6/2 HD mice (Arregui et al. 2011), implicating BDNF signaling as a potential mediator of astrocytic dysfunction in HD. Multiple transgenic and knock-in HD mouse models demonstrate deficits in brain cholesterol biosynthesis; with reductions in mRNA levels of cholesterol biosynthesis genes identified in primary HD astrocytes (Valenza *et al.* 2010). Subsequent work completed by the same group, identified that the reduction of cholesterol biosynthesis in astrocytes is detrimental to neuronal health. Astrocytes supply neurons with cholesterol through the function of ApoE-containing lipoproteins. Mutant-huntingtin expressing astrocytes secrete less ApoE-lipoprotein bound cholesterol, resulting in reductions in neurite outgrowth and loss of synaptic activity *in vitro.* Increased expression of genes related to cholesterol biosynthesis, SREBP2 and ABCA1, in astrocytes ameliorated this neuronal dysfunction, suggesting that astrocyte-dependent cholesterol biosynthesis is an important contributor to neuronal deficits in HD (Valenza *et al.* 2015). Taken together, mutant huntingtin expression in astrocytes alters various downstream mechanisms including excitotoxicity, and impacts NFκB and BDNF signaling, and mitochondrial, cholesterol function. As a result, amelioration of astrocytic dysfunction in HD may underlie a key therapeutic strategy in the treatment of the disease.

5.1.2 Microglial Dysfunction in HD

Microglial dysfunction is another hallmark of HD pathogenesis and relevant avenue for future therapeutic intervention. As described in greater detail in the introductory chapter, numerous studies have assessed central nervous system inflammation in the context of HD (reviewed in Rocha *et al.* 2016). Postmortem studies in both human HD patients and HD mouse models have identified significant microglial

activation in the brain regions most affected in HD (Sapp *et al.* 2001; Simmons *et al.* 2007). This microglial activation, in turn, results in the increased expression of various proinflammatory molecules, including IL-6, TNF-α, and MMP-9 (Björkqvist *et al.* 2008, Silvestroni *et al.* 2009). Positron Emission Tomography (PET) studies have also found increased microglial activation in the striatum of HD patients *in vivo* (Pavese *et al.* 2006) with activation correlated with disease severity. Cerebrospinal fluid (CSF) analysis in HD patients has also identified various markers of immune system activation including complement factors (C2, C3), apolipoprotein A4 (APOA4) (Fang *et al.* 2009), and metalloproteinases (MMP-3 and MMP-9) (Connolly *et al.* 2016). Microglia and macrophages derived from various HD mouse models also demonstrate altered morphology (Franciosi *et al.* 2012) and increased inflammatory responses to stimulation (Connolly *et al.* 2016).

Numerous signaling pathways underlying microglial dysfunction in HD have also been identified, including kynurenine (KP), and cannabinoid (CB) receptor cascades (reviewed in Connolly *et al.* 2012; Yang *et al.* 2017). The KP pathway is the primary route of tryptophan degradation in mammalian cells, resulting in various metabolites including kynurenic acid (KYNA), quinolinic acid (QUIN), 3-hydroxykynurenine (3-HK) and picolinic acid (PIC) (Tan *et al.* 2012). QUIN is a selective NDMA receptor agonist and may contribute to neurotoxicity (Szalardy *et al.* 2012). More importantly, the enzyme involved in metabolizing tryptophan to 3-HK and QUIN, termed KMO, is predominately expressed in microglia (Heyes *et al.* 1992). The KP pathway has been implicated in HD for various reasons. First, intrastriatal injection of QUIN recapitulates features of HD and has been used as an early mouse model of HD (Coyle and Schwarcz, 1976). Second, 3-HK and QUIN levels have been found to be significantly increased in human HD patient brain (Guidetti *et al.* 2004) and in HD mouse models (Sathyasaikumar *et al.* 2010). As a result, KMO inhibition may underlie a potential therapeutic target in HD. Treatment of R6/2 HD mice with JM6, a KMO inhibitor, for example, prevented striatal neurodegeneration and increased survival in the mice, through the reduction of microglial activation (Zwilling *et al.* 2011). Recent work has used a more selective KMO inhibitor, CHDI-340246, in HD mice leading to restoration of electrophysiological alterations characteristic of HD (Beaumont *et al.* 2016).

Cannabinoid signaling is another potential regulator of microglial dysfunction in HD. Microglia express cannabinoid receptor 2 (CB2) in the brain (Stella *et al.* 2010). Activation of CB2 receptors in microglia, more importantly, lead to reduced secretion of proinflammatory cytokines following stimulation (Correa *et al.* 2011). As a result of their anti-inflammatory effects, CB2 receptors have been identified as potential therapeutic targets in HD. R6/2 HD mice treated with cannabigerol (CBG), an activator of CB1/CB2 receptors, significantly improved motor deficits and increased expression of BDNF and insulin-like growth factor 1 (IGF-1) (Valdeolivas *et al.* 2015). Other CGB derivatives have been assessed in QA and 3-NP induced HD mouse models, leading to reversal of striatal degeneration, motor impairment and microglial activation (Diaz-Alonso *et al.* 2016). Taken together, astrocytic and microglial dysfunction exists in HD and is a potential therapeutic avenue for future disease treatment.

5.1.3 Anti-Inflammatory Drugs for the Treatment of HD

Based on the data implicating immune system dysfunction in HD, various preclinical immunomodulatory therapies have been evaluated in HD (reviewed in Wild and Tabrizi, 2014). In addition to KMO inhibition, modulation of NFκB activity (Träger *et al.* 2014) and CB2 receptor signaling discussed previously, P2X7 antagonism and Semaphorin 4D antibodies have also been developed as potential anti-inflammatory drugs. P2X7 is an adenosine triphosphate (ATP)-gated ion channel receptor is expressed in microglia and astrocytes and overexpressed in synaptic terminals in HD (Diaz-Hernandez *et al.* 2009). ATP-P2X7 binding induces synaptic dysregulation and ultimately results in neuronal death (Jun *et al.* 2007). Treatment of HD mice with P2X7 antagonists leads to a reduction in neuronal loss and restores weight loss and motor deficits (Diaz-Hernandez *et al.* 2009). As a result, P2X7 expression in microglia and neurons is currently under investigation as a potential HD therapeutic.

Anti-Semaphorin immunotherapy is another potential therapeutic avenue for the treatment of HD. Sempahorin 4D (SEMA4D) is a transmembrane signaling molecule involved in microglial activation (Smith *et al.* 2015), neuronal outgrowth and oligodendrocyte maturation. Inhibition of SEMA4D using an anti- SEMA4D monoclonal

antibody in YAC128 HD mice restored striatal, cortical and corpus callosum atrophy and prevented testicular degeneration. Cognitive deficits and anxiety-like behavior were also ameliorated following anti- SEMA4D treatment (Southwell *et al.* 2015). Phase 1 human clinical trials assessing the safety and tolerability of an anti-semaphorin 4D antibody (Vx15/2503) are currently in progress (LaGanke *et al.* 2017).

Laquinimod (LAQ) is another immunomodulatory therapeutic currently investigated in the context of HD. LAQ is a quinoline-3-carboxamide derivative with linomide (roquinimex) as the lead compound. It is an oral compound that is metabolized in the liver by the cytochrome isoenzyme CYP3A4 and eliminated in the urine (Ellrichmann *et al.* 2017). LAQ is able to cross the blood-brain-barrier (Bruck and Wegner, 2011; Thone and Gold, 2011) and may, as a result, exert a neuroprotective effect.

5.1.4 Laquinimod (LAQ) Treatment in HD

Laquinimod (LAQ) is hypothesized to slow disease progression and reduce brain atrophy rate in HD through immune system modulation (Dobson *et al.* 2016). Originally developed to treat Multiple Sclerosis (MS) (Thöne and Linker, 2016) LAQ is currently in human clinical trials to treat both HD and MS. The mechanism by which LAQ produces its neuroprotective effect in HD is currently unknown, but is thought to result from modulation of microglial and/or astrocytic dysfunction present in HD. Previous work has demonstrated that LAQ reduces NFκB activation in astrocytes (Brück *et al.* 2012), restores BDNF levels (Aharoni *et al.* 2012) and is involved in MAPK signaling whereby phosphorylation of downstream kinases p38 and JNK is reduced (Mishra *et al.* 2012). As discussed in Chapter 4.1.2, mutant-huntingtin expression activates MAPK signaling pathways, specifically JNK, resulting in apoptotic cell death (Liu, 1998). LAQ treatment may, as a result, restore normal MAPK signaling and prevent neuronal death. In other disease contexts, including experimental autoimmune encephalomyelitis (EAE), LAQ acts through the aryl hydrocarbon receptor (AhR) pathway. EAE is an autoimmune CNS disease characterized by demyelination and axonal loss as a result of activation of proinflammatory lymphocytes. Transcriptomic analysis of splenocyte samples isolated

from EAE vehicle and LAQ treated mice identified the AhR pathway in LAQ treated samples. Prototypical AhR genes including cytochrome P450 (Cyp1a1) and aryl hydrocarbon receptor demonstrated highest average fold-changes following LAQ treatment in both WT and EAE mice (Kaye *et al.* 2016). Previous work has linked AhR and NFκB signaling (Vogel *et al.* 2014), suggesting that LAQ-dependent of AhR pathways may down-regulate NFκB signaling in astrocytes and other immune cells in various diseases.

In the context of HD, various studies have been initiated in an effort to uncover the effect of LAQ treatment in disease pathogenesis. Proinflammatory cytokine release and NFκB signaling in HD patient peripheral immune cells was assessed following LAQ treatment. In this study, monocytes were isolated from pre-manifest and manifest HD patients along with healthy volunteer and stimulated with LPS. Monocytes cultures were then treated with LAQ prior to cytokine release analysis. LAQ treatment was found to alter the cytokine release of Th-1 activating molecules (IL-β, IL-8, TNF-α), Th-2 activating molecules (IL-5, IL-13) and anti-inflammatory IL-10. No effect of LAQ treatment in NFκB signaling was also determined (Dobson *et al.* 2016). Although this paper investigated the effect of LAQ treatment in human peripheral immune cells, the small sample size and variable cytokine release profiles characteristic of human immune cells make interpreting the results difficult.

Other studies aimed at investigating the role of LAQ in HD examined the effect in white matter pathology and neuronal caspase activity. Although selective degeneration of MSNs has long been considered the major neuropathological hallmark of HD, abnormalities in white matter have also been identified. Loss of myelin and white matter, changes in numbers and turnover rates of oligodendrocytes (Gomez-Tortosa *et al.* 2001), and transcriptional changes in myelin-releated genes in HD brain (Kuhn *et al.* 2011) have been identified. As a therapeutic currently under investigation for MS treatment, a myelin-related disease, Garcia-Miralles and colleagues evaluated the effect of LAQ treatment on myelin abnormalities in HD. Six months of LAQ treatment rescued striatal atrophy and white matter microstructural abnormalities in the corpus callosum of YAC128 HD mice. LAQ treatment also modestly improved motor function and depressive-like behavior in HD mice (Garcia-Miralles *et al.* 2016).

Caspase-6 signaling has also been previously implicated in HD. Caspase-6 (C6) is a member of a family of endopeptidases involved in apoptosis and inflammation. C6 is broadly expressed in the brain and periphery (Albrecht *et al.* 2007), and has been shown to be activated in striatal tissues derived from HD patients (Graham *et al.* 2011) as well as in primary neuronal cultures and tissue derived from YAC128 HD mice (Wong *et al.* 2015). WT primary neuronal cultures were treated with LAQ and C6 activation was measured. LAQ treatment reduced DNA-damage induced activation of C6 in primary neurons but this effect was not mediated by direct inhibition of the C6 endopeptidase. LAQ treatment also reduced the expression of Bax mRNA, a proapopotic molecule implicated in mitochondrial cytochrome c release and caspase activation (Ehrnhoefer *et al.* 2016).

Very recent work has also assessed the effect of LAQ in the R6/2 HD mouse model. LAQ does not affect body weight or survival but has a small effect on motor coordination and balance in older R6/2 mice. Treatment also ameliorated aspects of neurodegeneration, resulting in increased levels of BDNF in striatal neurons and decreased number of mHTT positive cells in both the striatum and cortex (Ellrichmann *et al.* 2017). The effect of LAQ on the immune system in R6/2 HD mouse model was not assessed, however, and is an important area for further investigation.

Previous work completed in the lab measured the effect of LAQ treatment on primary HD microglia. Mutant-huntingtin expressing microglia demonstrate exaggerated proinflammatory IL-6 release in response to stimulation compared to WT (Connolly *et al.* 2016). LAQ treatment did not modulate this exaggerated cytokine release *in vitro* (Figure 1), although there is data to suggest that LAQ may have a neuroprotective effect *in vivo* (Ellrichmann *et al.* 2017). Although the exact reason for this disparity is unknown, there is strong evidence to suggest that LAQ needs to be converted to an active metabolite in order to exert its neuroprotective effect and this only occurs *in vivo* and not *in vitro*. In order to better understand the *in vivo* effect of LAQ in the brain, microglia and astrocyte populations were isolated from WT and YAC128 adult mice treated with LAQ and vehicle (water) using the flow cytometry system outlined in Chapter 2 (Figure 2). Differentially expressed genes in sorted microglia and astrocyte populations have been evaluated using RNA-Seq and will be functionally validated in the future using

quantitative PCR. The identified genes and pathways will then be used to focus future *in vitro* work aimed at understanding both the role of mutant huntingtin in glial populations as well as the effect of LAQ treatment on the innate immune system.

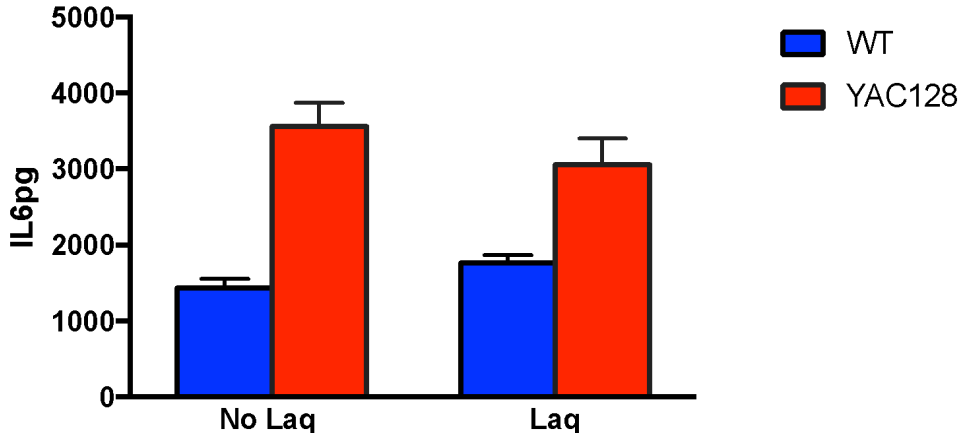

Figure 5: Laquinimod has Minimal Effect on Microglial Immune Response to CSE *in vitro*. Pure primary microglia cultures from both WT and YAC128 pups were treated with 5μM Laquinimod or PBS for 24hr prior to stimulation with IFN-γ and CSE. Media was collected for IL-6 cytokine detection and cells were collected and lysed for quantification of total protein analysis. (n=4 per condition) (Connolly *et al. unpublished*)

Genotype	Microglia		Astrocytes	
WT	Vehicle	LAQ	Vehicle	LAQ
YAC128	Vehicle	LAQ	Vehicle	LAQ

Figure 5: Conditions for LAQ RNA-Seq Trial. Microglia and astrocyte populations will be isolated from adult WT and YAC128 murine brain treated with vehicle (water) or LAQ for RNA-seq analysis and functional validation (n=4-6 per condition).

5.2 Methods

5.2.1 Isolation of Adult Microglia and Astrocytes from WT and YAC128 Brain following LAQ treatment

Three to four-month old male WT and YAC128 (FVB/N background) mice were singly-housed and treated with 10mg/kg of Laquinimod (LAQ) or vehicle (water) for four weeks (5 days per week) using oral gavage. Three cohorts were scheduled based on age and genotype with animals randomly assigned to control or LAQ treatment groups. Cohort I consisted of 20 mice (numbered M1-M20) (WT: n=11 and YAC128: n=9). Cohort II consisted of 12 mice (numbered M21-M32) (WT: n= 7 and YAC128: n=5). Cohort III consisted of two mice (numbered M33 and M34; both WT). The treatment and cohort assignment for separate microglia and astrocyte RNA-Seq analysis and subsequent validation is outlined in Tables 5.1-5.2. Two mice were processed per sorting day with microglia and astrocyte populations isolated from whole brain tissue according to methods outlined in Chapter 2 with one modification. Following myelin removal, CD11b and ACSA-2 positive selection was completed using the QuadroMACS^{TM} separator and not the automated AutoMACS ^{TM} separator.

CD11b selection was completed first in cohort I and ACSA-2 selection was first in cohort II to obtain suitable samples from both populations for RNA-Seq analysis. CD11b selection was described in detail in Chapter 4 (BACCre primary microglia isolation) with the same protocol used in the first enrichment step of cohort I. In contrast to the methods outlined in Chapter 4, the CD11b-negative fraction obtained following QuadroMACS^{TM} separation was spun down at 1000rpm for 5min at 4°C and re-suspended in 270uL of FACS buffer and 30uL of Miltenyi® ACSA-2 Microbeads for 15min 4°C. The samples were washed with 2mL of FACS buffer and re-suspended in 500uL of FACS buffer to be applied to primed MACS® LS columns (similar priming step as outlined in Chapter 4).

Following column selection, the ACSA-2 positive samples were stained with Anti-GLAST-APC antibody (1:11, Miltenyi® Biotec) in 100uL of FACS buffer. An additional 150uL of FACS buffer was added to the sample along with Ebioscience® 7AAD Viability Dye at a dilution of 1:250. The sample was then subject to flow

cytometry sorting as detailed in Chapter 2. The ACSA-2 negative samples (brain cell populations remaining following microglia and astrocyte isolation) were also collected as negative control samples for subsequent validation experiments. These samples were spun down at 1000rpm for 5min at 4°C and re-suspended in 100uL of FACS buffer prior to antibody labeling. The samples were stained with CD11b-PE (1:100, Ebioscience®) and GLAST-APC (1:11, Miltenyi®) and were gated as CD11b-negative and GLAST-negative. Sorted microglia and astrocyte samples were collected into empty Eppendorf tubes, spun down at 1000rpm for 5min at 4°C and re-suspended in 500uL of Trizol reagent to stabilize RNA for subsequent RNA-Seq analysis.

Table 5.1 Microglia RNA-Seq Samples

WT Vehicle	WT LAQ	YAC128 Vehicle	YAC128 LAQ
M13 Mic	M6 Mic	M5 Mic	M2 Mic
M17 Mic	M14 Mic	M7 Mic	M8 Mic
M25 Mic	M18 Mic	M9 Mic	M10 Mic
M33 Mic	M20 Mic	M15 Mic	M16 Mic
		M27 Mic	

Table 5.2 Astrocyte RNA-Seq Samples

WT Vehicle	WT LAQ	YAC128 Vehicle	YAC128 LAQ
M19 Astro	M4 Astro	M5 Astro	M8 Astro
M25 Astro	M6 Astro	M7 Astro	M10 Astro
M33 Astro	M18 Astro	M9 Astro	M16 Astro
M34 Astro	M32 Astro	M15 Astro	M24 Astro
		M27 Astro	M28 Astro
		M31 Astro	

5.2.2 Library Preparation and RNA-Sequencing

RNA was isolated from microglia and astrocyte samples from each condition (WT Vehicle, WT LAQ, YAC128 Vehicle, YAC128 LAQ; n=4-6 per condition) using

the RNeasy Mini kit according to manufacturers instructions (QIAGEN). RNA samples were run on the Agilent Bioanalyzer Pico-Chip to ensure RNA is of sufficient quality and quantity for library preparation. RNA libraries were prepared with an mRNA kit (Truseq Stranded mRNA Library Prep kit; Illumina) on an Illumina Neoprep instrument and sequenced on a NextSeq paired-end run (42 x 42; v3; Illumina).

5.2.3 RNA-Seq Bioinformatic Analysis

RNA-Seq data was generated using the Illumina platform and short reads were aligned to the mouse genome using the STAR aligner. Raw read counts were tabulated for each gene using Cufflinks. Low expressed genes, defined as those with an average of counts per million (CPM) less than or equal to 2, were removed from the analysis, resulting in approximately 13,000 analyzed expressed genes. The statistical modeling package, EdgeR, was used to build a linear model that captures the effect of genotype (WT vs. YAC128), treatment (Vehicle vs. LAQ) genotype-specific treatment effects (genes that respond differently to LAQ depending on genotype; WT LAQ vs. YAC LAQ). Using this linear model, differentially expressed genes (FDR <0.05) were identified in the microglia and astrocyte conditions. In microglia and astrocyte samples, date of RNA collection (batch) was significantly correlated with gene expression, and was therefore included as a covariate in the linear model. As a result, the covariates used for the linear model were genotype, treatment and batch.

Pathway analysis was also conducted on both microglia and astrocyte samples using GSEA (Gene Set Enrichment Analysis). The pathway analysis output consisted of four different databases: Gene Ontology (GO), Curated databases (including Reactome, KEGG), Hallmark (curated signatures) and Immunologic. The pathways with FWER <0.05 (family-wise error rate) were used to generate Figures 5.4, 5.7, 5.10, 5.13 5.16 and 5.19 using Cytoscape.

5.3 Results

5.3.1. RNA-seq analysis Identifies Significantly Differentially Expressed Genes in Isolated Microglia and Astrocyte Samples from Both Treatment Conditions

Young adult-aged WT and YAC128 (FVB/N background) male mice were singly housed and randomly assigned to vehicle and Laquinimod (LAQ) treatment conditions. Four to six mice for each genotype were administered water or 10mg/kg LAQ for four weeks (5 days per week) using oral gavage. The LAQ dose and route of administration was chosen based on work previously published (Garcia-Miralles *et al.* 2016). Microglia and astrocyte populations were sequentially isolated from whole brain from two mice per sorting day according to the methods outlined in Chapter 2.2. RNA from the isolated glial populations was extracted using a modified Trizol protocol by the BRC-RNA-seq core (UBC). Following confirmation of sufficient RNA quality using a Bioanalyzer, RNA-seq data was generated using the Illumina platform and short reads were aligned to the mouse genome using the STAR aligner. Raw read counts were tabulated for each gene using Cufflinks and lowly expressed genes (defined as those with an average of counts per million, CPM, less than or equal to 2) were removed from the analysis, resulting in approximately 13,000 analyzed genes.

Differentially expressed genes, corresponding to FDR <0.05 (false-discovery rate; proportion of false positives among the identified differentially expressed genes; measure of sensitivity; Gusnanto *et al.* 2007), were identified based on genotype (WT vs. YAC128) and treatment (Vehicle vs. LAQ). 1106 differentially expressed genes were identified based on genotype differences in isolated microglia (WT vehicle vs. YAC128 vehicle) compared to 2 identified in astrocytes. In terms of LAQ treatment, a greater number of differentially expressed genes were identified in WT-treated microglia and astrocyte as compared to YAC128 (Figure 5.1). Seven differentially expressed genes were identified in HD microglia versus only 2 in HD astrocytes treated with LAQ (Figure 5.1).

Microglia

Condition	Differentially Expressed Genes
WT Vehicle vs. YAC Vehicle	1106 genes
WT Vehicle vs. WT LAQ	31 genes
YAC Vehicle vs. YAC LAQ	7 genes

Astrocytes

Condition	Differentially Expressed Genes
WT Vehicle vs. YAC Untreated	2 genes
WT Vehicle vs. WT LAQ	138 gene
YAC Vehicle vs. YAC LAQ	2 gene

Figure 5.1 Summary of Differentially Expressed Genes (DEGs) in Isolated Microglia Populations from WT and YAC128 mice following Vehicle and LAQ Treatment. Bioinformatic analysis of sequenced samples (WT Vehicle, WT LAQ, YAC Vehicle, YAC LAQ) identified differentially expressed genes in each condition. A larger effect of Laquinimod treatment was seen in the microglia samples as compared to astrocytes and a larger baseline differences in WT versus HD microglia was also identified.

5.3.2. Isolated Microglia from Adult Vehicle-Treated WT and YAC128 Whole Brain Express Significantly Differentially Expressed Genes related to Prolactin and Transcriptional Processes

Following the RNA-seq analysis detailed in Section 5.2.2-5.2.3, the top ten differentially expressed genes (DEGs) between WT and YAC128 vehicle treated mice were identified. Significant differential expression, corresponding to a FDR <0.05 (false-discovery rate; proportion of false positives among the identified differentially expressed genes; measure of sensitivity; Gusnanto *et al.* 2007) was identified in all of the top ten genes (Figure 5.2). Most of the genes identified demonstrated fairly small log-fold changes, while prolactin (Prl) corresponded to an eighteen-fold down-regulation in YAC128 microglia. These log fold changes refer to the mean differences in gene expression between control and experimental samples (Gusnanto *et al.* 2007) and may point to gene expression changes of biological relevance. The majority of DEGs identified in Figure 5.2 correspond to transcriptional-related functions (Ppig, Top1, Nufip2, Pnisr). Other differentially expressed genes were also related to immune function (Prl), excitatory signalling (Filip1), and angiogenesis (Krit1). The top hit, prolactin (Prl) is a positive regulator of JAK/STAT signaling, a pathway introduced in Chapter 4.1.1 as altered in HD (Träger *et al.* 2013a). All top ten differentially expressed genes were down-regulated in the HD microglia. The identification of differentially expressed genes based on genotype will focus future experimental work aimed at uncovering the mechanisms underlying dysfunction in mutant-huntingtin expressing microglia.

Gene Name	Log2 Fold Change	P-value	FDR	Protein Function
Prl	-18.48354	6.04E-43	8.81E-39	TNF/IL-17/immune signaling
Filip1	-2.1731776	1.82E-20	1.33E-16	Dendritic spine morphology & excitatory signaling
Ppig	-1.8987998	1.44E-14	7.01E-11	Protein folding & RNA splicing
Top1	-1.592994	3.31E-12	1.21E-08	Cell proliferation & DNA replication
Nufip2	-1.6022946	2.12E-11	6.19E-08	RNA binding
Zpf950	-2.0054824	6.44E-11	1.49E-07	Undefined
2810474O19Rik	-2.0103171	7.14E-11	1.47E-07	Undefined
Chic1	-2.7684202	8.38E-11	1.53E-07	Vesicular transport
Krit1	-1.6667508	2.71E-10	4.39E-07	Angiogenesis & endothelial cell migration
Pnisr	-1.6900211	8.34E-10	1.22E-06	RNA binding

Figure 5.2 Differentially Expressed Genes at Baseline in Isolated Microglia Populations from Vehicle treated WT and YAC128 Mice. Top ten differentially expressed genes in vehicle WT and YAC128 microglia (n=4-5 per genotype). All differentially expressed genes demonstrate a significant FDR <0.05.

5.3.3 Isolated Microglia from Vehicle- treated WT and YAC128 Whole Brain Express Additional Differentially Expressed Genes Related to Growth Hormone Signaling and Immune Cell Function following Adjusted Analysis

Another way to prioritize potential significant differentially expressed genes is to evaluate the log-fold changes present between the two conditions being compared. Statistically, p-value and FDR provide a measure of the likelihood that the gene of interest is significantly different between two comparisons but this mathematical analysis may shield relevant biological mechanisms that lack the statistical power. With these caveats in mind, I completed an additional adjusted analysis in each of the comparisons completed to ensure that important genes of interest were not overlooked using statistical methods. In this adjusted analysis, I looked at the top differentially expressed genes identified comparing WT and YAC128 vehicle-treated microglia with a log-fold change of greater than or equal to two. The logFC≥2 criteria was used in order to focus on genes with robust differences in WT vs. YAC128 microglia for future validation. The inclusion of the logFC≥2 criteria resulted in nine additional differentially expressed genes not identified in the previous analysis (Figure 5.2). The genes, highlighted in red, correspond to growth hormone signaling (Gh), immune function (T2, Nkx-6), potassium ion transport (Kcnk4), cellular movement (1700101E01Rik) and glycolytic processes (Aldob). All additional genes identified also have a significant FDR<0.05.

Gene Name	Log2 Fold Change	P-value	FDR	Protein Function
Prl	-18.48354038	6.04E-43	8.81E-39	Prolactin; positive regulation of STAT/JAK signalling/STAT import into nucleus
Gh	-9.664533454	4.73E-07	7.58E-05	Negative regulation of neuronal death
Sftpc	-8.006700956	2.32E-05	0.001222274	Lung fibrosis & protein binding
Aldob	7.13314661	4.28E-04	0.011275742	Glycolytic process
T2	5.976475928	1.17E-03	0.023227278	Adaptive immunity
Lrriq1	-5.635754888	3.26E-03	0.04568077	Undefined
Gm10863	5.631676338	2.47E-03	0.037877593	Undefined
1700101E01Rik	-5.575077983	3.57E-03	0.048167683	Cilia and flagella processes
Nkx6-1	-5.330775501	4.41E-03	0.054926962	Glial cell differentiation
Kcnk4	5.173680707	5.27E-04	0.013075682	Potassium ion transport

Figure 5.3 Differentially Expressed Genes at Baseline in Isolated Microglia Populations from Vehicle-treated WT and YAC128 Mice following Adjusted Analysis. Top ten differentially expressed genes in untreated WT and YAC128 microglia (n=4-5 per genotype) with minimum log FC>2. Genes highlighted in red correspond to novel differentially expressed genes not identified in previous analysis outlined in Figure 5.2.

5.3.4 Mitochondrial and Proteosome Functional Gene Sets are Enriched in HD Microglia

Next, we sought to assign biological relevance to the identified gene expression changes by carrying out a Gene Set Enrichment Analysis (GSEA) of the WT vs. YAC128 vehicle-treated microglia. GSEA allows for the identification of relevant biological pathways without relying on each gene in the cluster to be statistically significant (Miller *et al.* 2016) GSEA gene clusters were identified with significant FWER <0.05 (family-wise error rate) corresponding to mitochondrial (Figure 5.4 A and D) and ribosomal functions (Figure 5.4 B and C).

A

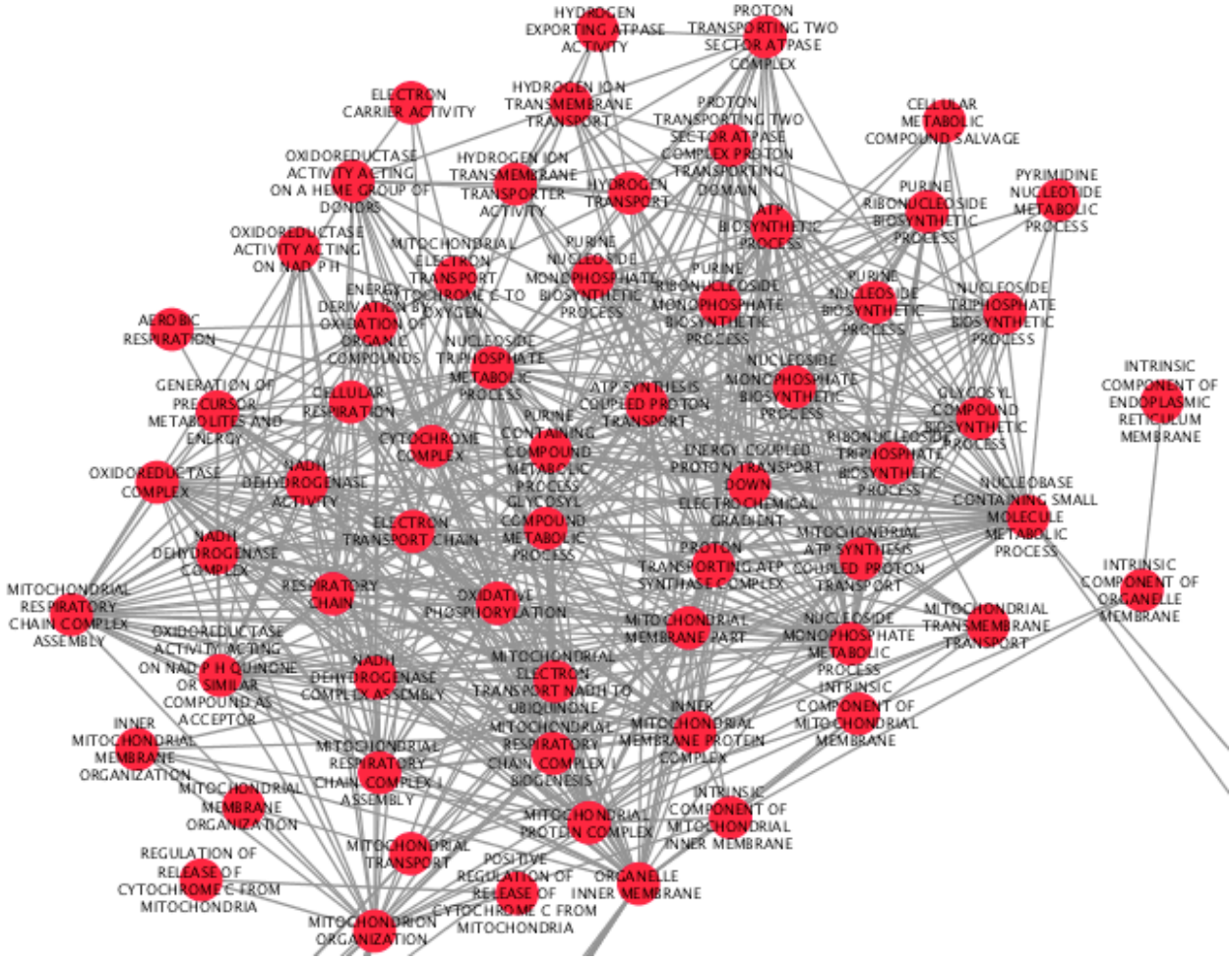
HYDROGEN EXPORTING ATPASE ACTIVITY
PROTON TRANSPORTING TWO SECTOR ATPASE COMPLEX
ELECTRON CARRIER ACTIVITY
HYDROGEN ION TRANSMEMBRANE TRANSPORT
PROTON TRANSPORTING TWO SECTOR ATPASE COMPLEX PROTON TRANSPORTING DOMAIN
CELLULAR METABOLIC COMPOUND SALVAGE
OXIDOREDUCTASE ACTIVITY ACTING ON A HEME GROUP OF DONORS
HYDROGEN ION TRANSMEMBRANE TRANSPORTER ACTIVITY
HYDROGEN TRANSPORT
PURINE RIBONUCLEOSIDE BIOSYNTHETIC PROCESS
PYRIMIDINE NUCLEOTIDE METABOLIC PROCESS
ATP BIOSYNTHETIC PROCESS
OXIDOREDUCTASE ACTIVITY ACTING ON NAD P H
MITOCHONDRIAL ELECTRON TRANSPORT
PURINE NUCLEOSIDE MONOPHOSPHATE BIOSYNTHETIC PROCESS
PURINE RIBONUCLEOSIDE MONOPHOSPHATE BIOSYNTHETIC PROCESS
PURINE NUCLEOSIDE BIOSYNTHETIC PROCESS
NUCLEOSIDE TRIPHOSPHATE BIOSYNTHETIC PROCESS
ENERGY DERIVATION BY OXIDATION OF ORGANIC COMPOUNDS
CYTOCHROME C TO OXYGEN
AEROBIC RESPIRATION
NUCLEOSIDE TRIPHOSPHATE METABOLIC PROCESS
NUCLEOSIDE MONOPHOSPHATE BIOSYNTHETIC PROCESS
INTRINSIC COMPONENT OF ENDOPLASMIC RETICULUM MEMBRANE
GENERATION OF PRECURSOR METABOLITES AND ENERGY
CELLULAR RESPIRATION
ATP SYNTHESIS COUPLED PROTON TRANSPORT
GLYCOSYL COMPOUND BIOSYNTHETIC PROCESS
PURINE CONTAINING COMPOUND METABOLIC PROCESS
CYTOCHROME COMPLEX
ENERGY COUPLED PROTON TRANSPORT DOWN ELECTROCHEMICAL GRADIENT
RIBONUCLEOSIDE TRIPHOSPHATE BIOSYNTHETIC PROCESS
OXIDOREDUCTASE COMPLEX
NADH DEHYDROGENASE ACTIVITY
NUCLEOBASE CONTAINING SMALL MOLECULE METABOLIC PROCESS
ELECTRON TRANSPORT CHAIN
GLYCOSYL COMPOUND METABOLIC PROCESS
MITOCHONDRIAL ATP SYNTHESIS COUPLED PROTON TRANSPORT
NADH DEHYDROGENASE COMPLEX
PROTON TRANSPORTING ATP SYNTHASE COMPLEX
INTRINSIC COMPONENT OF ORGANELLE MEMBRANE
MITOCHONDRIAL RESPIRATORY CHAIN COMPLEX ASSEMBLY
RESPIRATORY CHAIN
OXIDATIVE PHOSPHORYLATION
MITOCHONDRIAL MEMBRANE PART
NUCLEOSIDE MONOPHOSPHATE METABOLIC PROCESS
MITOCHONDRIAL TRANSMEMBRANE TRANSPORT
OXIDOREDUCTASE ACTIVITY ACTING ON NAD P H QUINONE OR SIMILAR COMPOUND AS ACCEPTOR
NADH DEHYDROGENASE COMPLEX ASSEMBLY
MITOCHONDRIAL ELECTRON TRANSPORT NADH TO UBIQUINONE
INTRINSIC COMPONENT OF MITOCHONDRIAL MEMBRANE
INNER MITOCHONDRIAL MEMBRANE ORGANIZATION
MITOCHONDRIAL RESPIRATORY CHAIN COMPLEX I BIOGENESIS
INNER MITOCHONDRIAL MEMBRANE PROTEIN COMPLEX
MITOCHONDRIAL RESPIRATORY CHAIN COMPLEX I ASSEMBLY
MITOCHONDRIAL MEMBRANE ORGANIZATION
INTRINSIC COMPONENT OF MITOCHONDRIAL INNER MEMBRANE
MITOCHONDRIAL PROTEIN COMPLEX
MITOCHONDRIAL TRANSPORT
REGULATION OF RELEASE OF CYTOCHROME C FROM MITOCHONDRIA
POSITIVE REGULATION OF RELEASE OF CYTOCHROME C FROM MITOCHONDRIA
ORGANELLE INNER MEMBRANE
MITOCHONDRION ORGANIZATION

B

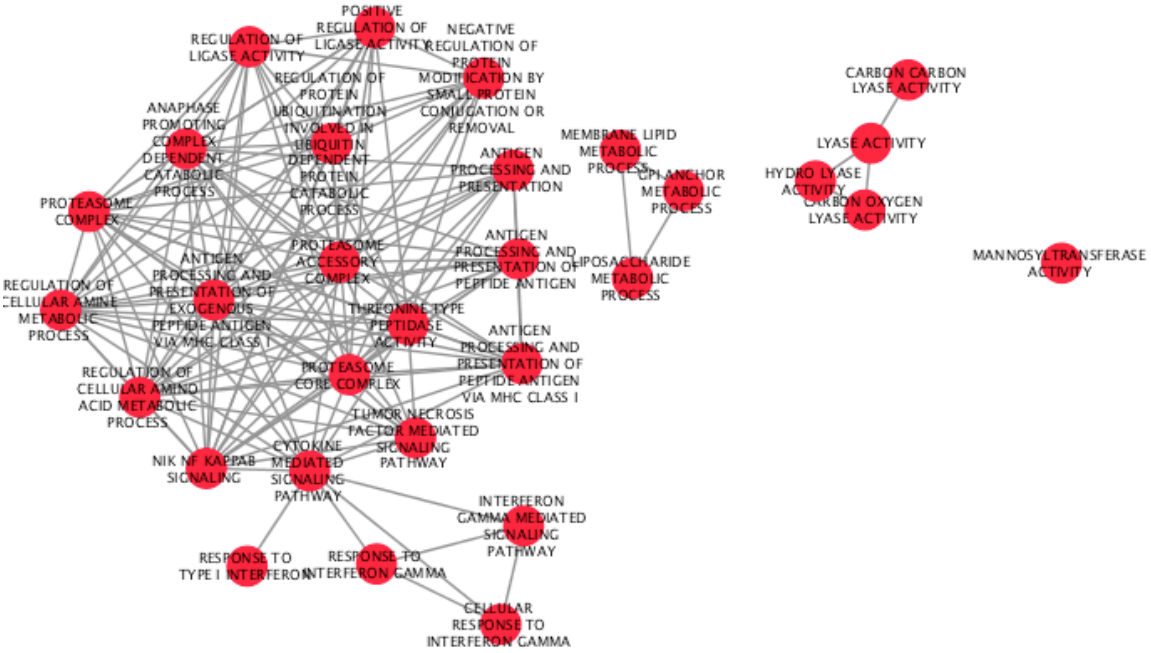
POSITIVE REGULATION OF LIGASE ACTIVITY
REGULATION OF LIGASE ACTIVITY
NEGATIVE REGULATION OF PROTEIN MODIFICATION BY SMALL PROTEIN CONJUGATION OR REMOVAL
REGULATION OF PROTEIN UBIQUITINATION INVOLVED IN UBIQUITIN DEPENDENT PROTEIN CATABOLIC PROCESS
ANAPHASE PROMOTING COMPLEX DEPENDENT CATABOLIC PROCESS
ANTIGEN PROCESSING AND PRESENTATION
MEMBRANE LIPID METABOLIC PROCESS
GPI ANCHOR METABOLIC PROCESS
PROTEASOME COMPLEX
PROTEASOME ACCESSORY COMPLEX
ANTIGEN PROCESSING AND PRESENTATION OF PEPTIDE ANTIGEN
LIPOSACCHARIDE METABOLIC PROCESS
ANTIGEN PROCESSING AND PRESENTATION OF EXOGENOUS PEPTIDE ANTIGEN VIA MHC CLASS I
REGULATION OF CELLULAR AMINE METABOLIC PROCESS
THREONINE TYPE PEPTIDASE ACTIVITY
ANTIGEN PROCESSING AND PRESENTATION OF PEPTIDE ANTIGEN VIA MHC CLASS I
PROTEASOME CORE COMPLEX
REGULATION OF CELLULAR AMINO ACID METABOLIC PROCESS
TUMOR NECROSIS FACTOR MEDIATED SIGNALING PATHWAY
CYTOKINE MEDIATED SIGNALING PATHWAY
NIK NF KAPPAB SIGNALING
INTERFERON GAMMA MEDIATED SIGNALING PATHWAY
RESPONSE TO TYPE I INTERFERON
RESPONSE TO INTERFERON GAMMA
CELLULAR RESPONSE TO INTERFERON GAMMA
CARBON CARBON LYASE ACTIVITY
LYASE ACTIVITY
HYDRO LYASE ACTIVITY
CARBON OXYGEN LYASE ACTIVITY
MANNOSYLTRANSFERASE ACTIVITY

C

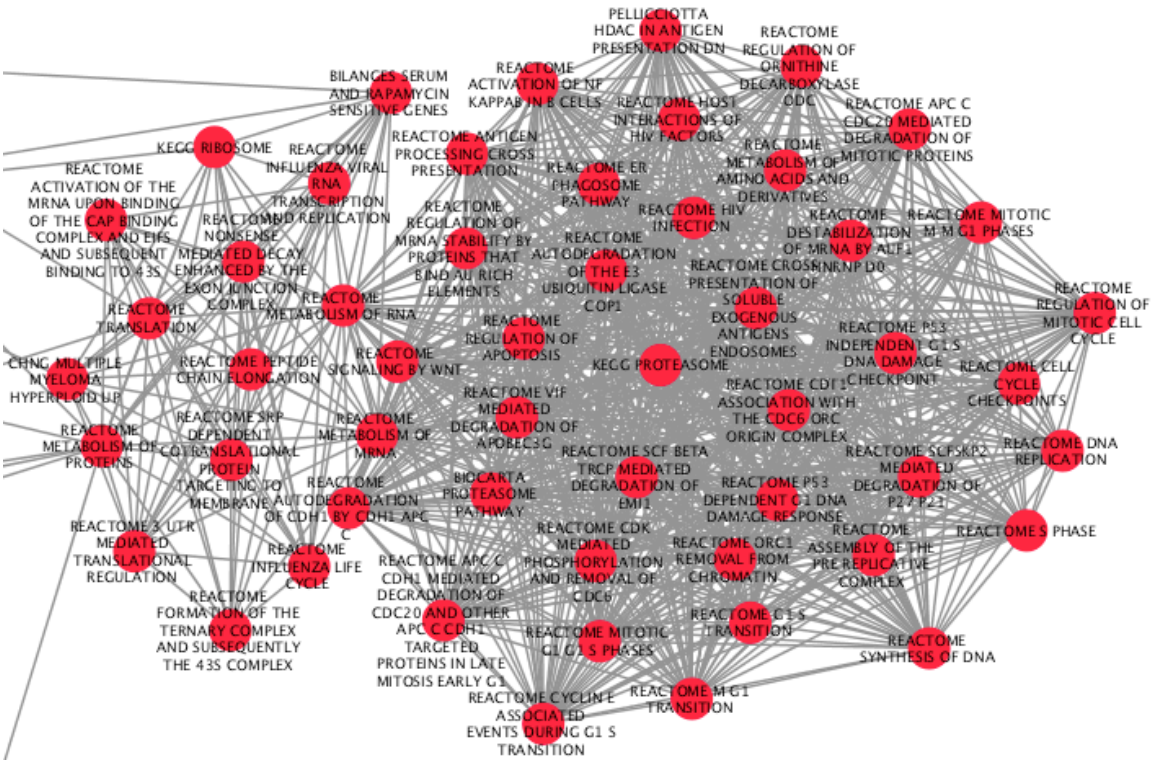
PELLICCIOTTA HDAC IN ANTIGEN PRESENTATION DN
REACTOME REGULATION OF ORNITHINE DECARBOXYLASE ODC
BILANCES SERUM AND RAPAMYCIN SENSITIVE GENES
REACTOME ACTIVATION OF NF KAPPAB IN B CELLS
REACTOME HOST INTERACTIONS OF HIV FACTORS
REACTOME APC C CDC20 MEDIATED DEGRADATION OF MITOTIC PROTEINS
KEGG RIBOSOME
REACTOME INFLUENZA VIRAL RNA TRANSCRIPTION AND REPLICATION
REACTOME ANTIGEN PROCESSING CROSS PRESENTATION
REACTOME ER PHAGOSOME PATHWAY
REACTOME METABOLISM OF AMINO ACIDS AND DERIVATIVES
REACTOME ACTIVATION OF THE MRNA UPON BINDING OF THE CAP BINDING COMPLEX AND EIFS AND SUBSEQUENT BINDING TO 43S
REACTOME NONSENSE MEDIATED DECAY ENHANCED BY THE EXON JUNCTION COMPLEX
REACTOME REGULATION OF MRNA STABILITY BY PROTEINS THAT BIND AU RICH ELEMENTS
REACTOME HIV INFECTION
REACTOME DESTABILIZATION OF MRNA BY ALF1
REACTOME MITOTIC M M G1 PHASES
REACTOME AUTODEGRADATION OF THE E3 UBIQUITIN LIGASE COP1
REACTOME CROSS PRESENTATION OF SOLUBLE EXOGENOUS ANTIGENS ENDOSOMES
REACTOME TRANSLATION
REACTOME METABOLISM OF RNA
REACTOME REGULATION OF APOPTOSIS
REACTOME REGULATION OF MITOTIC CELL CYCLE
REACTOME P53 INDEPENDENT G1 S DNA DAMAGE CHECKPOINT
CHNC MULTIPLE MYELOMA HYPERPLOID UP
REACTOME PEPTIDE CHAIN ELONGATION
REACTOME SIGNALING BY WNT
KEGG PROTEASOME
REACTOME CELL CYCLE CHECKPOINTS
REACTOME VIF MEDIATED DEGRADATION OF APOBEC3G
REACTOME CDT1 ASSOCIATION WITH THE CDC6 ORC ORIGIN COMPLEX
REACTOME METABOLISM OF PROTEINS
REACTOME SRP DEPENDENT CO TRANSLATIONAL PROTEIN TARGETING TO MEMBRANE
REACTOME METABOLISM OF MRNA
REACTOME SCF BETA TRCP MEDIATED DEGRADATION OF EMI1
REACTOME SCFSKP2 MEDIATED DEGRADATION OF P27 P21
REACTOME DNA REPLICATION
BIOCARTA PROTEASOME PATHWAY
REACTOME P53 DEPENDENT G1 DNA DAMAGE RESPONSE
REACTOME AUTODEGRADATION OF CDH1 BY CDH1 APC C
REACTOME CDK MEDIATED PHOSPHORYLATION AND REMOVAL OF CDC6
REACTOME ORC1 REMOVAL FROM CHROMATIN
REACTOME S PHASE
REACTOME 3 UTR MEDIATED TRANSLATIONAL REGULATION
REACTOME INFLUENZA LIFE CYCLE
REACTOME ASSEMBLY OF THE PRE REPLICATIVE COMPLEX
REACTOME APC C CDH1 MEDIATED DEGRADATION OF CDC20 AND OTHER APC C CDH1 TARGETED PROTEINS IN LATE MITOSIS EARLY G1
REACTOME FORMATION OF THE TERNARY COMPLEX AND SUBSEQUENTLY THE 43S COMPLEX
REACTOME G1 S TRANSITION
REACTOME MITOTIC G1 G1 S PHASES
REACTOME SYNTHESIS OF DNA
REACTOME CYCLIN E ASSOCIATED EVENTS DURING G1 S TRANSITION
REACTOME M G1 TRANSITION

D

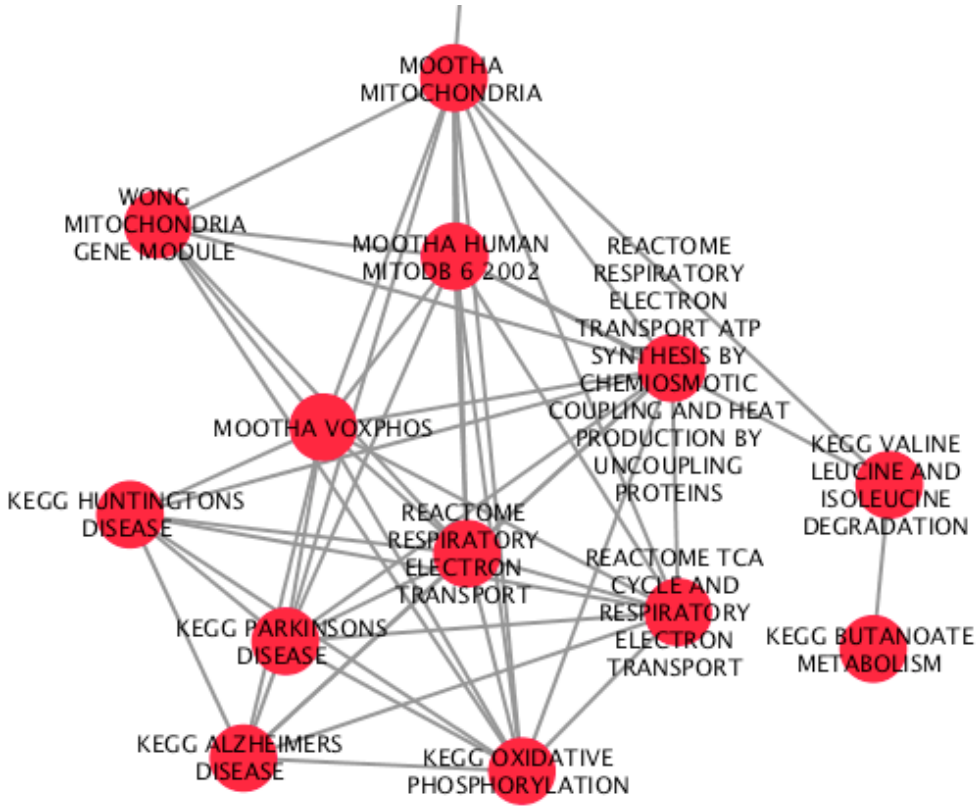

5.4 GSEA Pathway Analysis of Differentially Expressed Genes at Baseline in Isolated Microglia Populations from Vehicle-treated WT and YAC128 Mice correspond to Mitochondrial and Proteosome Gene Sets. Gene sets enriched in GSEA pathway analysis in vehicle-treated WT and HD microglia corresponds to mitochondrial (A, D) and proteasome (B, C) gene sets. The size and color of the node is correlated with the size of the gene set category and significance (red indicates very significant and white indicates lower significance). The gene nodes were similar across all gene sets. Similar categories cluster together with the thickness of the edge (line) correlated with how similar the categories are. Figure generated using Cytoscape.

5.3.5 WT Microglia Isolated from LAQ-treated Mice Express Significant Up-regulation of Genes Related to Immune Cell Function and Hormone Signaling

Differential gene expression between WT vehicle and LAQ-treated microglia was observed following RNA-seq analysis. Significant up-regulation in eight of the top ten genes, corresponding to an FDR <0.05, was identified (Figure 5.5). The rest of the top ten genes identified were up-regulated following LAQ treatment and related to immune cell mechanisms, including interferon (H2-D1) and complement (Cfb) signaling as well as leukocyte migration (Amica1). Interestingly, prolactin, identified previously as down-regulated in vehicle-treated HD microglia (Figure 5.2), was down-regulated following LAQ treatment in WT microglia. Growth hormone, Gh, was also down-regulated in vehicle HD microglia (Figure 5.3) and was also down-regulated in WT-LAQ treated microglia. Further work will need to be conducted in order to assess the effect of LAQ on WT microglia, specifically in terms of Prl and Gh levels.

Gene Name	Log2 Fold Change	P-value	FDR	Protein Function
Prl	-10.271341	4.48E-38	7.12E-34	Positive regulation of STAT/JAK signaling/STAT import into nucleus
Cfb	3.67708596	9.50E-12	6.93E-08	Complement activation/cell proliferation
H2-D1	1.29773194	8.30E-09	4.04E-05	Antigen presentation & Interferon-gamma signaling
Gh	-5.2712553	1.18E-08	4.29E-05	Negative regulation of neuronal death
Ifi27l2a	1.88795553	1.72E-08	5.01E-05	Aging & response to virus
H2-K1	1.27382108	4.52E-08	1.10E-04	Antigen presentation & immune response
Irf7	2.06793947	6.65E-08	1.22E-04	Regulation of interferon production
Ccl2	1.26679436	6.71E-08	1.22E-04	TNF/IL-17/immune signaling
Amica1	2.58572516	9.99E-08	1.62E-04	Leukocyte migration
H2-DMa	1.10059019	1.51E-07	2.2E-04	MHC class II protein binding

Figure 5.5 Differentially Expressed Genes following LAQ Treatment in Isolated Microglia Populations from WT Mice. Top ten differentially expressed genes in LAQ-treated WT microglia (n=4). All genes have significant FDR <0.05.

5.3.6 Microglia Isolated from WT-LAQ treated Mice Express Additional Differentially Expressed Genes related to Autophagy and the Innate Immune System following Adjusted Analysis

Similar to section 5.3.3, an adjusted analysis was conducted comparing WT vehicle and LAQ-treated microglia. The top ten differentially expressed genes with a logFC≥2 resulted in five additional genes, Usp18, Cxcl10, Gipc3, Napsa and Tgtp2 (outlined in red; Figure 5.6). All additional hits demonstrated a significant FDR <0.05. Several of these additional genes are implicated in various immune responses including leukocyte chemotaxis (Cxcl10), interferon-gamma response (Tgtp2) as well as proteolysis (Usp18, Napsa) and Wnt receptor signaling (Gipc3). The significant up-regulation of these additional genes in WT-LAQ treated microglia may underlie a potential immunomodulatory and proteolytic LAQ function in the brain.

Gene Name	Log2 Fold Change	P-value	FDR	Protein Function
Prl	-10.27134142	4.88E-38	7.12E-34	Prolactin; positive regulation of STAT/JAK signaling/STAT import into nucleus
Cfb	3.677085965	9.50E-12	6.93E-08	Complement activation/cell proliferation
Gh	-5.271253341	1.18E-08	4.29E-05	Negative regulation of neuronal death
Irf7	2.067939468	6.65E-08	1.22E-04	Regulation of interferon production
Amica1	2.585725159	9.99E-08	1.62E-04	Leukocyte migration
Usp18	1.988734952	2.70E-06	3.29E-03	Inflammatory response & proteolysis
Cxcl10	2.11376065	1.02E-05	8.28E-03	Regulation of leukocyte chemotaxis
Gipc3	7.095503399	3.59E-05	0.022782723	Wnt receptor signaling
Napsa	3.063273587	6.25E-05	0.032581834	Autophagy & proteolysis
Tgtp2	2.203570643	7.17E-05	0.036093911	Cellular response to interferon-gamma

Figure 5.6 Differentially Expressed Genes following LAQ Treatment in Isolated Microglia Populations from WT Mice following Adjusted Analysis. Top ten differentially expressed genes in WT microglia (n=4) with minimum log FC>2. Genes highlighted in red correspond to novel differentially expressed genes not identified in previous analysis outlined in Figure 5.5. All genes have a significant FDR <0.05.

5.3.7 Morphogenesis Gene Sets Identified in GSEA Pathway Analysis of WT-LAQ treated Microglia

Gene Set Enrichment Analysis (GSEA) of differentially expressed genes identified in WT vehicle vs. LAQ-treated microglia was also conducted. GSEA gene clusters were identified with significant FWER <0.05 (family-wise error rate) corresponding to morphogenesis gene sets (Figure 5.7), although more specific enrichment in nervous system development was also identified.

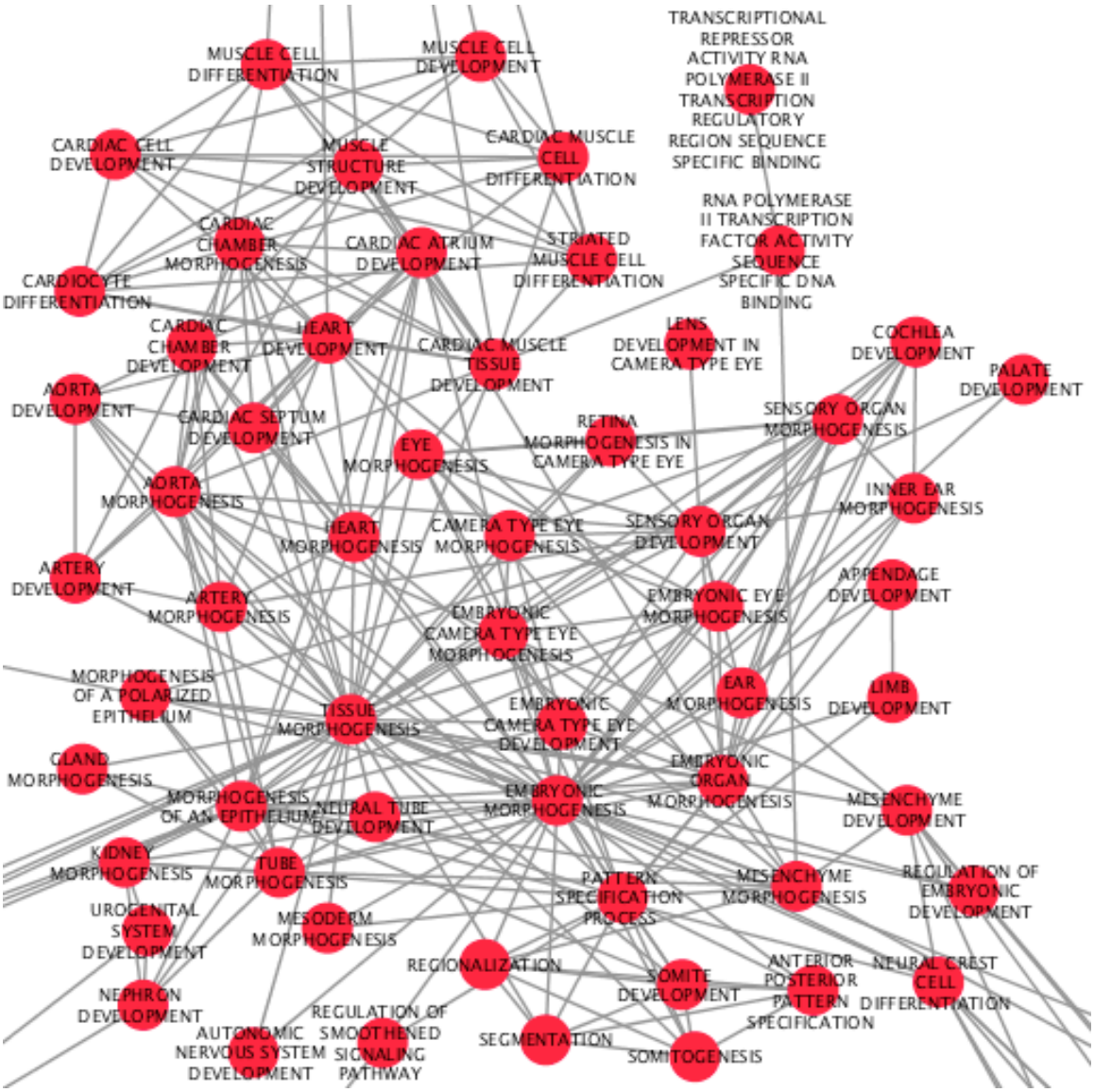

5.7 GSEA Pathway Analysis of Differentially Expressed Genes in Isolated Microglia Populations from WT Mice following LAQ Treatment Identifies Morphogenesis Gene Sets. Gene sets enriched in GSEA pathway analysis in WT vehicle and LAQ-treated microglia corresponds to morphogenesis gene sets. The size and color of the node is correlated with the size of the gene set category and significance (red indicates very significant and white indicates lower significance). All gene sets were of similar size. Similar categories cluster together with the thickness of the edge (line) correlated with how similar the categories are. Figure generated using Cytoscape

5.3.8 Microglia Isolated from YAC128-LAQ treated Mice Express Significant Differentially Expressed Genes Related to Immune Function and Growth Hormone Signaling

Four significant differentially expressed genes related to immune function (Mmp13, Amica1, Oas1) and growth hormone signaling (Gh) were identified in YAC-LAQ treated microglia (outlined in red; Figure 5.8). Four significant differentially expressed genes related to hormone signaling (Prl, Gh) and immune function (Pomc, Amica1) were identified in YAC-LAQ treated microglia (outlined in red; Figure 5.8). All of the top ten differentially expressed genes observed in YAC-LAQ treated microglia were up-regulated when compared to YAC-vehicle treated microglia and were also related to various immune system functions including leukocyte migration (Epcam), chemotaxis and response to cytokine stimuli (Cxcl16), and interferon production (Irf7). Significant up regulation of a gene involved in cellular responses to hormone stimuli (Cga) was also identified and may be involved in the effects of Gh and Prl signaling following LAQ treatment.

The last significantly up-regulated gene following LAQ treatment in HD microglia is a member of the cytochrome P450 (Cyp1a1) family. As discussed in Section 5.1.4, Cyp1a1 is a member of the aryl hydrocarbon receptor-signaling cascade. Similar up regulation of Cyp1a1 gene expression was also identified following LAQ treatment in EAE splenocytes (Kaye *et al.* 2016), suggesting that LAQ may exert its effect through a common AhR-dependent mechanism. LAQ is also hypothesized to exert its neuroprotective effect *in vivo* following conversion to an active metabolite. Cyp1a1 may be responsible for converting LAQ into its necessary active metabolite in the brain. Together these signaling cascades may provide potential mechanisms by which LAQ exerts its immunomodulatory affect in HD microglia, however, additional experimental work will need to be conducted in order to evaluate the role of mutant huntingtin expression in these immune cell cascades.

Gene Name	Log2 Fold Change	P-value	FDR	Protein Function
Prl	8.86125088	1.35E-59	8.72E-06	Prolactin; positive regulation of STAT/JAK signaling/STAT import into nucleus
Gh	8.52718835	8.51E-29	0.00673278	Negative regulation of neuronal death
Pomc	3.54744606	2.64E-09	0.030860352	Negative regulation of TNF-alpha
Amica1	2.36287194	2.66E-09	0.030860352	Leukocyte migration
Cyp1a1	5.71606114	1.30E-07	0.456088148	Cytochrome P45; drug metabolic process
Cga	3.44155574	2.38E-06	0.490591994	Cellular response to hormone stimulus
Ly6a	1.47885498	1.43E-05	0.490591994	Lymphocyte antigen
Epcam	3.25326823	5.73E-05	0.490591994	Leukocyte migration
Cxcl16	0.73807116	6.95E-05	0.490591994	Chemotaxis, cell growth & response to cytokine stimulus
Irf7	1.24963389	2.19E-04	0.519131126	Regulation of interferon production

Figure 5.8 Differentially Expressed Genes following LAQ Treatment in Isolated Microglia Populations from YAC128 Mice. Top ten differentially expressed genes in LAQ-treated YAC128 microglia (n=4). Top four genes have significant FDR <0.05

5.3.9 YAC128-LAQ treated Microglia Express Additional Differentially Expressed Genes related to Lipid Metabolism, Phagocytosis and Drug Metabolism following Adjusted Analysis

Adjusted analysis of LAQ-treated microglia resulted in three additional differentially expressed genes related to lipid metabolism (Alox12e), phagocytosis (CD109) and drug metabolism (Cyp2e1) (outlined in red; Figure 5.9). Similar to WT-LAQ treated microglia, several of the differentially expressed genes identified in YAC-LAQ treated microglia were also previously identified in microglia genotype comparisons (Figure 5.2 and Figure 5.3). In particular, prolactin (Prl) expression is significantly down-regulated in YAC-vehicle treated microglia (Figure 5.2) and up-regulated in YAC microglia following LAQ treatment (Figure 5.8). Growth hormone (Gh) is also significantly down-regulated in HD-vehicle treated microglia, following the adjusted analysis (Figure 5.3) with LAQ treatment resulting in increased expression of Gh in YAC microglia (Figure 5.8). The reversal of prolactin and growth hormone gene expression following LAQ treatment provides a potential mechanism by which LAQ exerts its neuroprotective effect, specifically in microglia. Further work aimed at assessing the involvement of growth hormone and prolactin signaling in specific brain regions, including the striatum and cortex, will provide insight into the effect of LAQ specifically in the context of HD.

Gene Name	Log2 Fold Change	P-value	FDR	Protein Function
Prl	8.861250881	1.35E-59	1.97E-55	Positive regulation of STAT/JAK signalling
Gh	8.537188346	8.51E-29	6.21E-25	Negative regulation of neuronal death
Pomc	3.547446064	2.64E-09	9.72E-06	Negative regulation of TNF-alpha
Amica1	2.36287194	2.66E-09	9.72E-06	Leukocyte migration
Cyp1a1	5.716061145	1.30E-07	3.80E-04	Cytochrome P450; drug metabolic process
Cga	3.441555741	2.38E-06	5.78E-03	Cellular response to hormone stimulus
Epcam	3.253268227	5.73E-05	0.104505888	Leukocyte migration
Alox12e	4.14377127	0.000293788	0.389829361	Lipid metabolism
Cd109	2.208461749	0.000592218	0.532428123	Phagocytosis
Cyp2e1	-3.204431114	0.001330178	0.858739379	Cytochrome P450; drug metabolic process

Figure 5.9 Differentially Expressed Genes following LAQ Treatment in Isolated Microglia Populations from YAC128 Mice following Adjusted Analysis. Top ten differentially expressed genes in WT microglia (n=4) with minimum log FC>2. Genes highlighted in red correspond to novel differentially expressed genes not identified in previous analysis outlined in Figure 5.8. The top six genes have a significant FDR <0.05.

5.3.10 Ribosomal and Mitochondrial Functional Gene Sets are Identified in YAC128-LAQ treated Microglia

Gene Set Enrichment Analysis (GSEA) of differentially expressed genes identified in YAC vehicle versus LAQ-treated microglia was also conducted. The majority of functional gene sets correspond to ribosome and mitochondrial gene sets (Figure 5.10 A and B). Interestingly, significant enrichment of genes previously implicated in Parkinson's disease was also identified following GSEA analysis (Figure 5.10 B).

A

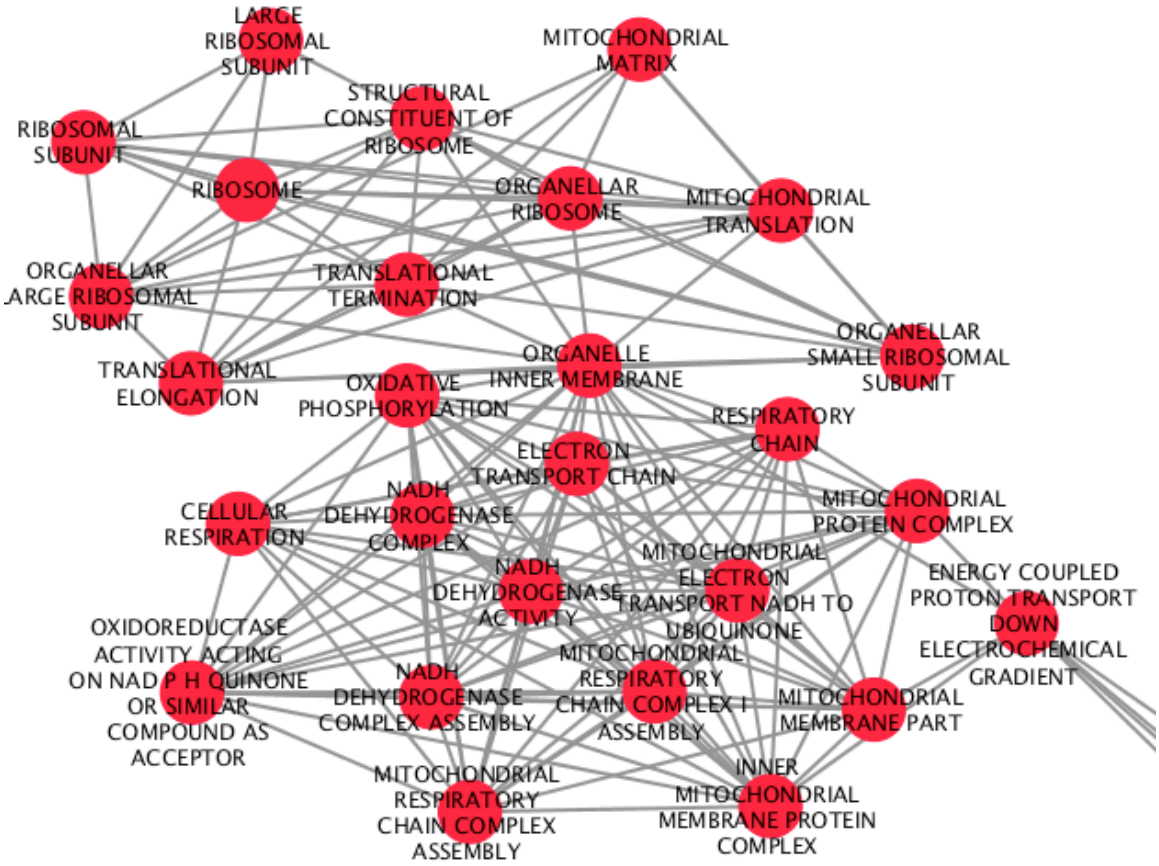
LARGE RIBOSOMAL SUBUNIT
MITOCHONDRIAL MATRIX
STRUCTURAL CONSTITUENT OF RIBOSOME
RIBOSOMAL SUBUNIT
RIBOSOME
ORGANELLAR RIBOSOME
MITOCHONDRIAL TRANSLATION
ORGANELLAR LARGE RIBOSOMAL SUBUNIT
TRANSLATIONAL TERMINATION
ORGANELLAR SMALL RIBOSOMAL SUBUNIT
TRANSLATIONAL ELONGATION
ORGANELLE INNER MEMBRANE
OXIDATIVE PHOSPHORYLATION
RESPIRATORY CHAIN
ELECTRON TRANSPORT CHAIN
NADH DEHYDROGENASE COMPLEX
CELLULAR RESPIRATION
MITOCHONDRIAL PROTEIN COMPLEX
MITOCHONDRIAL ELECTRON TRANSPORT NADH TO UBIQUINONE
NADH DEHYDROGENASE ACTIVITY
ENERGY COUPLED PROTON TRANSPORT DOWN ELECTROCHEMICAL GRADIENT
OXIDOREDUCTASE ACTIVITY ACTING ON NADP H QUINONE OR SIMILAR COMPOUND AS ACCEPTOR
MITOCHONDRIAL RESPIRATORY CHAIN COMPLEX I ASSEMBLY
NADH DEHYDROGENASE COMPLEX ASSEMBLY
MITOCHONDRIAL MEMBRANE PART
MITOCHONDRIAL RESPIRATORY CHAIN COMPLEX ASSEMBLY
INNER MITOCHONDRIAL MEMBRANE PROTEIN COMPLEX

B

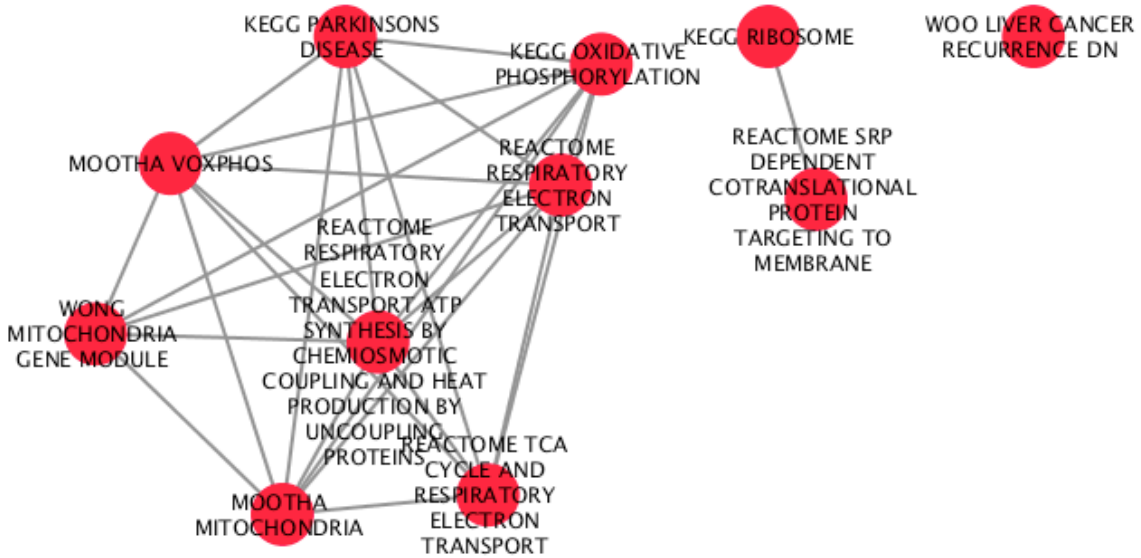

Figure 5.10 GSEA Pathway Analysis of Differentially Expressed Genes in Isolated Microglia Populations from YAC128 Mice following LAQ Treatment Identifies Ribosomal and Mitochondrial Functional Gene Sets. Gene sets enriched in GSEA pathway analysis in YAC128 LAQ-treated microglia corresponds to ribosomal and mitochondrial gene sets. The size and color of the node is correlated with the size of the gene set category and significance (red indicates very significant and white indicates lower significance). Similar categories cluster together with the thickness of the edge (line) correlated with how similar the categories are. Figure generated using Cytoscape.

5.3.11 Isolated Astrocytes from Vehicle-treated WT and YAC128 Whole Brain Express Numerous Significant Differentially Expressed Genes related to Immune Function and Cellular Transport

Significant differential gene expression was identified following RNA-seq analysis in vehicle-treated WT and YAC128 astrocytes. The majority of the top-ten differentially expressed genes are significantly down-regulated in YAC128-vehicle treated astrocytes compared to WT. The differentially expressed genes identified in HD astrocytes encompass a variety of cellular processes. These processes include immune function (Cc12, Cfh, Bmp5, Ccl24), cellular transport (Slcla5, Slc39a2), autophagy and proteolysis (Ctsc) and insulin receptor signaling (Irs3) (Figure 5.11). The differences in various cellular differences in HD astrocytes demonstrate the significant role of mutant-huntingtin expression in altering astrocytic function and provide further evidence for the relevance of glial cells in HD.

Gene Name	Log2 Fold Change	P-value	FDR	Protein Function
Ccl2	-6.5216652	5.69E-08	0.000830659	TNF/IL-17/immune signaling
Cfh	-3.1555872	8.50E-06	0.052607145	Regulation of complement activation
Slc1a5	-2.7251869	1.25E-05	0.052607145	Glutamine secretion & import across plasma membrane
Cdr1	-10.064545	1.70E-05	0.052607145	Cerebellar degeneration related antigen
Fam46a	-3.381673977	1.80E-05	0.052607145	Regulation of blood coagulation
Bmp5	-2.908795552	5.12E-05	0.121534725	TGF-beta signaling
Slc39a2	7.804441061	6.64E-05	0.121534725	Zinc ion transporter
Ctsc	-2.087322917	6.70E-05	0.121534725	Regulation of proteolysis & apoptosis
Ccl24	-8.614934245	7.49E-05	0.121534725	Cellular response to interferon-gamma
Irs3	-4.347899582	1.05E-04	0.134346233	Insulin receptor signaling

Figure 5.11 Differentially Expressed Genes at Baseline in Isolated Astrocyte Populations from Vehicle-treated WT and YAC128 Mice. Top ten differentially expressed genes in untreated WT and YAC128 astrocytes (n=4-6 per genotype). Top five differentially expressed genes demonstrate a significant FDR <0.05.

5.3.12 Astrocytes Isolated from YAC128-vehicle treated Mice Express Additional Differentially Expressed Genes Related to Various Cellular Processes following Adjusted Analysis

Adjusted analysis of vehicle-treated YAC128 astrocytes resulted in five additional differentially expressed genes related to various cellular processes including adrenal gland development (Fstl3), cell adhesion (Lgals4), growth factor response (Fbn2), vesicular (Cilp2) and actin cytoskeleton (Nuak2) (outlined in red; Figure 5.12). Similar to the previous top ten differentially expressed gene lists, the majority of significant differences between WT and YAC128-vehicle treated astrocytes are a result of down-regulation of gene expression.

Gene Name	Log2 Fold Change	P-value	FDR	Protein Function
Ccl2	-6.521665158	5.69E-08	0.000830659	TNF/IL-17/immune signaling
Cdr1	-10.06454531	1.70E-05	0.052607145	Cerebellar degeneration protein
Slc39a2	7.804441061	6.64E-05	0.121534725	Zinc ion transport
Ccl24	-8.614934245	7.49E-05	0.121534725	Chemokine-mediated signaling pathway
Irs3	-4.347899582	1.05E-04	0.134346233	Insulin receptor signaling
Fstl3	-5.381059287	1.05E-04	0.134346233	Adrenal gland development
Lgals4	5.393191825	1.19E-04	0.134346233	Cell adhesion
Fbn2	-3.90095322	1.2E-04	0.134346233	Regulation of cellular response to growth factor
Cilp2	-5.159701332	1.44E-04	0.149665782	Vesicular exosome
Nuak2	-4.644138365	1.55E-04	0.150802442	Actin cytoskeleton & apoptotic processes

Figure 5.12 Differentially Expressed Genes in Isolated Astrocyte Populations from Vehicle-treated WT and YAC128 Mice following Adjusted Analysis. Top ten differentially expressed genes in WT and YAC128 astrocytes (n=4 per genotype) with minimum log FC>2. Genes highlighted in red correspond to novel differentially expressed genes not identified in previous analysis outlined in Figure 5.11. Top two genes have a significant FDR <0.05.

5.3.13 Ribosomal and Mitochondrial Functional Gene Sets enriched in HD Astrocytes

Gene Set Enrichment Analysis (GSEA) of differentially expressed genes identified in WT versus YAC128 vehicle-treated astrocytes was also conducted. The majority of highly enriched gene sets correspond to mitochondrial and ribosomal (Figure 5.13 A and B). Immune activation signaling was also significantly upregulated in HD astrocytes (Figure 5.13 B).

A

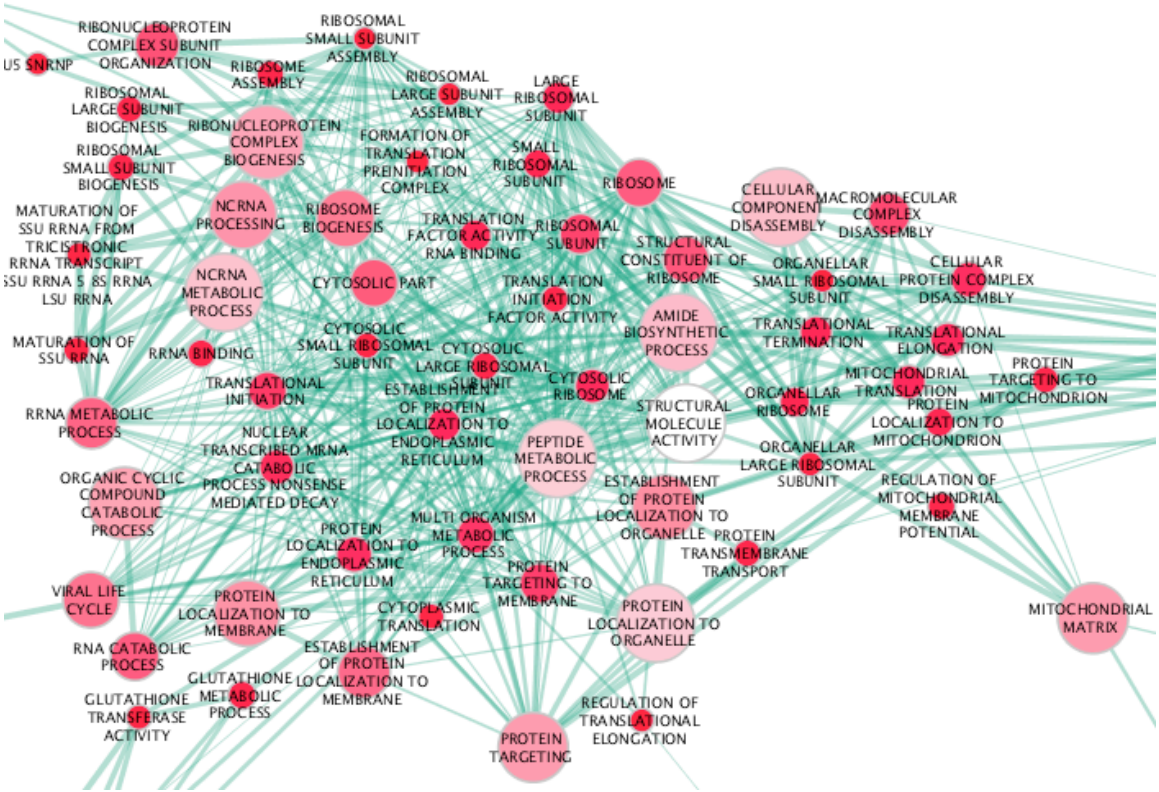
RIBONUCLEOPROTEIN COMPLEX SUBUNIT ORGANIZATION
RIBOSOMAL SMALL SUBUNIT ASSEMBLY
U5 SNRNP
RIBOSOME ASSEMBLY
RIBOSOMAL LARGE SUBUNIT ASSEMBLY
LARGE RIBOSOMAL SUBUNIT
RIBOSOMAL LARGE SUBUNIT BIOGENESIS
RIBONUCLEOPROTEIN COMPLEX BIOGENESIS
FORMATION OF TRANSLATION PREINITIATION COMPLEX
SMALL RIBOSOMAL SUBUNIT
RIBOSOMAL SMALL SUBUNIT BIOGENESIS
RIBOSOME
CELLULAR COMPONENT DISASSEMBLY
MACROMOLECULAR COMPLEX DISASSEMBLY
MATURATION OF SSU RRNA FROM TRICISTRONIC RRNA TRANSCRIPT
NCRNA PROCESSING
RIBOSOME BIOGENESIS
TRANSLATION FACTOR ACTIVITY RNA BINDING
RIBOSOMAL SUBUNIT
STRUCTURAL CONSTITUENT OF RIBOSOME
ORGANELLAR SMALL RIBOSOMAL SUBUNIT
CELLULAR PROTEIN COMPLEX DISASSEMBLY
SSU RRNA 5 8S RRNA LSU RRNA
NCRNA METABOLIC PROCESS
CYTOSOLIC PART
TRANSLATION INITIATION FACTOR ACTIVITY
AMIDE BIOSYNTHETIC PROCESS
TRANSLATIONAL TERMINATION
TRANSLATIONAL ELONGATION
MATURATION OF SSU RRNA
RRNA BINDING
CYTOSOLIC SMALL RIBOSOMAL SUBUNIT
CYTOSOLIC LARGE RIBOSOMAL SUBUNIT
MITOCHONDRIAL TRANSLATION
PROTEIN TARGETING TO MITOCHONDRION
TRANSLATIONAL INITIATION
ESTABLISHMENT OF PROTEIN LOCALIZATION TO ENDOPLASMIC RETICULUM
CYTOSOLIC RIBOSOME
STRUCTURAL MOLECULE ACTIVITY
ORGANELLAR RIBOSOME
RRNA METABOLIC PROCESS
NUCLEAR TRANSCRIBED MRNA CATABOLIC PROCESS NONSENSE MEDIATED DECAY
PEPTIDE METABOLIC PROCESS
PROTEIN LOCALIZATION TO MITOCHONDRION
ORGANELLAR LARGE RIBOSOMAL SUBUNIT
ORGANIC CYCLIC COMPOUND CATABOLIC PROCESS
REGULATION OF MITOCHONDRIAL MEMBRANE POTENTIAL
ESTABLISHMENT OF PROTEIN LOCALIZATION TO ORGANELLE
PROTEIN LOCALIZATION TO ENDOPLASMIC RETICULUM
MULTI ORGANISM METABOLIC PROCESS
PROTEIN TRANSMEMBRANE TRANSPORT
PROTEIN TARGETING TO MEMBRANE
VIRAL LIFE CYCLE
PROTEIN LOCALIZATION TO MEMBRANE
CYTOPLASMIC TRANSLATION
PROTEIN LOCALIZATION TO ORGANELLE
MITOCHONDRIAL MATRIX
RNA CATABOLIC PROCESS
ESTABLISHMENT OF PROTEIN LOCALIZATION TO MEMBRANE
GLUTATHIONE METABOLIC PROCESS
GLUTATHIONE TRANSFERASE ACTIVITY
REGULATION OF TRANSLATIONAL ELONGATION
PROTEIN TARGETING

B

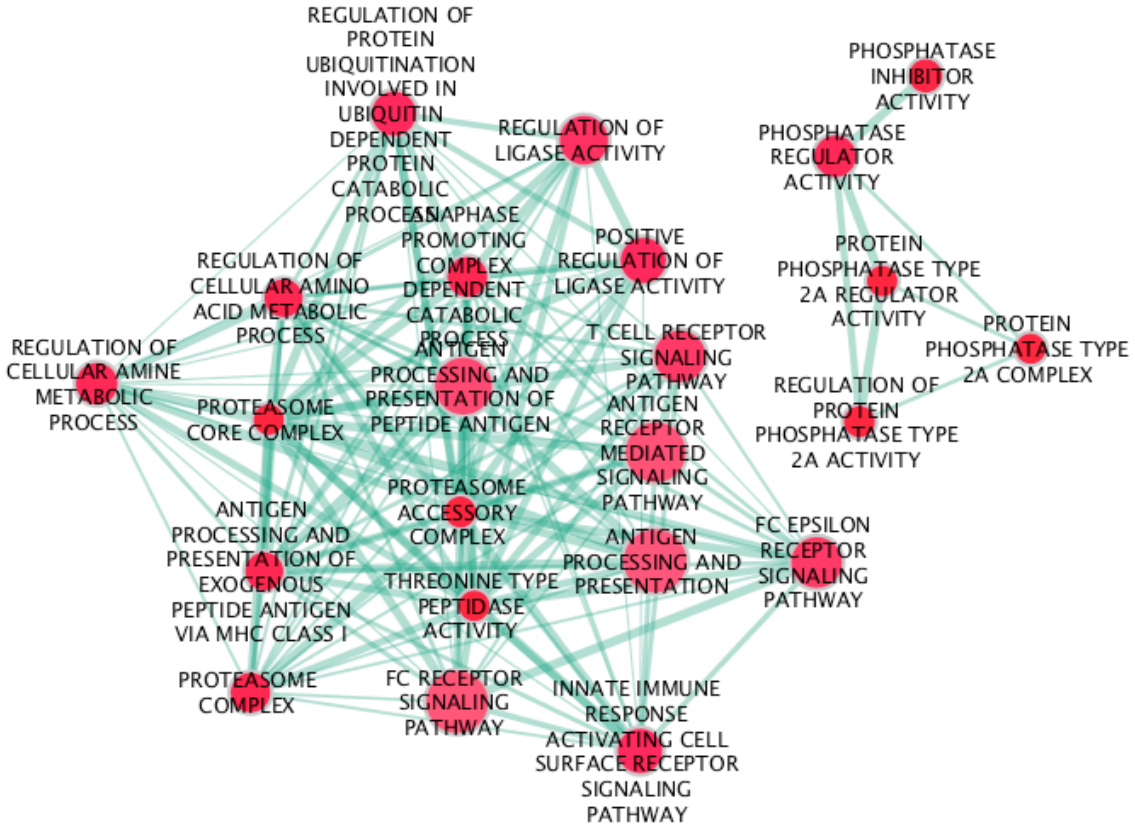

Figure 5.13 GSEA Pathway Analysis of Differentially Expressed Genes at Baseline in Isolated Astrocyte Populations from Vehicle-treated WT and YAC128 Mice Correspond to Ribosomal and Mitochondrial Gene Sets. Gene sets enriched in GSEA pathway analysis in vehicle-treated WT and HD astrocytes corresponds to ribosomal and mitochondrial gene sets (A and B). The size and color of the node is correlated with the size of the gene set category and significance (red indicates very significant and white indicates lower significance). Similar categories cluster together with the thickness of the edge (line) correlated with how similar the categories are. Figure generated using Cytoscape.

5.3.14 Astrocytes Isolated from WT-LAQ treated Mice Express Differentially Expressed Genes related to Immune Cell Function, Cellular Transport, and Signaling

Significantly differentially expressed genes were identified in WT-LAQ treated astrocytes related to immune function (Ccl2, Postn, Coch), cellular transport (Slc1a5, Slc5a5, Slc16a12), cellular signaling (Adra2a, Fzd2), and hemostasis (Serpind1) (Figure 5.14). Similar to baseline differences in vehicle-treated WT and YAC128 astrocytes, the majority of differentially expressed genes identified in WT-LAQ treated astrocytes are down-regulated. As a result, LAQ may down-regulate inflammatory signaling cascades and cellular transport and signaling processes.

Gene Name	Log2 Fold Change	P-value	FDR	Protein Function
Slc1a5	-2.773624262	1.05E-09	1.53E-05	Glutamine secretion & import across plasma membrane
Serpind1	-3.510194212	3.10E-08	0.000226493	Hemostasis
Ccl2	-5.11188913	5.54E-08	0.000269525	TNF/IL-17/immune signaling
Gm14169	2.530635212	1.04E-06	0.003330292	Undefined
Adra2a	-1.470204905	1.14E-06	0.003330292	Activation of MAPK activity by adrenergic receptor signaling
Fzd2	-1.596943482	1.83E-06	0.004444412	Wnt signaling
Slc16a12	-2.543585028	2.34E-06	0.00487661	Monocarboxylic acid transport
Slc5a5	-2.262120635	4.16E-06	0.00624851	Sodium glucose transporter
Postn	-2.728222881	4.32E-06	0.00624851	Wound healing
Coch	-2.519004896	4.56E-06	0.00624851	Regulation of innate immune response

Figure 5.14 Differentially Expressed Genes following LAQ Treatment in Isolated Astrocyte Populations from WT Mice. Top ten differentially expressed genes in LAQ-treated WT astrocytes (n=4). All top ten genes have a significant FDR <0.05.

5.3.15 Adjusted Analysis of WT-LAQ treated Astrocytes Results in Additional Differentially Expressed Genes Related to Cellular Responses to Growth Factors and Ion Transport

Two additional differentially expressed genes were identified in WT-LAQ treated astrocytes following adjusted analysis (logFC≥2) (outlined in red; Figure 5.15). These additional differentially expressed genes are involved in cellular responses to various growth factors (Fbn2) and ion transport (Calhm2).

Gene Name	Log2 Fold Change	P-value	FDR	Protein Function
Slc1a5	-2.773624262	1.05E-09	1.53E-05	Glutamine transport
Serpind1	-3.510194212	3.10E-08	0.000226493	Chemotaxis & hemostasis
Ccl2	-5.11188913	5.54E-08	0.000269525	TNF/IL-17/immune signaling
Gm14169	2.530635212	1.04E-06	0.003330292	Undefined
Slc16a12	-2.543585028	2.34E-06	0.00487661	Transmembrane transport
Slc5a5	-2.262120635	4.16E-06	0.00624851	Sodium ion transport
Postn	-2.728222881	4.32E-06	0.00624851	Cellular response to TNF
Coch	-2.519004896	4.56E-06	0.00624851	Regulation of innate immune response
Fbn2	-3.393824831	4.71E-06	0.00624851	Regulation of cellular response to growth factor
Calhm2	-2.955923098	7.88E-06	0.008852661	Ion transport

Figure 5.15 Differentially Expressed Genes in Isolated Astrocyte Populations following LAQ Treatment from WT Mice following Adjusted Analysis. Top ten differentially expressed genes in WT astrocytes following LAQ treatment (n=4) with minimum log FC>2. Genes highlighted in red correspond to novel differentially expressed genes not identified in previous analysis outlined in Figure 5.3. All top genes have a significant FDR <0.05.

5.3.16 Inflammatory Functional Gene Sets Enriched in WT-LAQ Treated Astrocytes

Similar to section 5.3.13, functional gene sets related to inflammatory processes were identified in WT-LAQ treated astrocytes (Figure 5.16). Cytokine signaling and production (Figure 5.16 A) and interferon signaling (Figure 5.16 B) are examples of the inflammatory processes identified following GSEA analysis, although additional enriched gene sets related to toll-like receptor signaling and leukocyte activation were also identified (Figure 5.16 A). As a result, LAQ treatment in WT astrocytes may modulate inflammatory pathways.

A

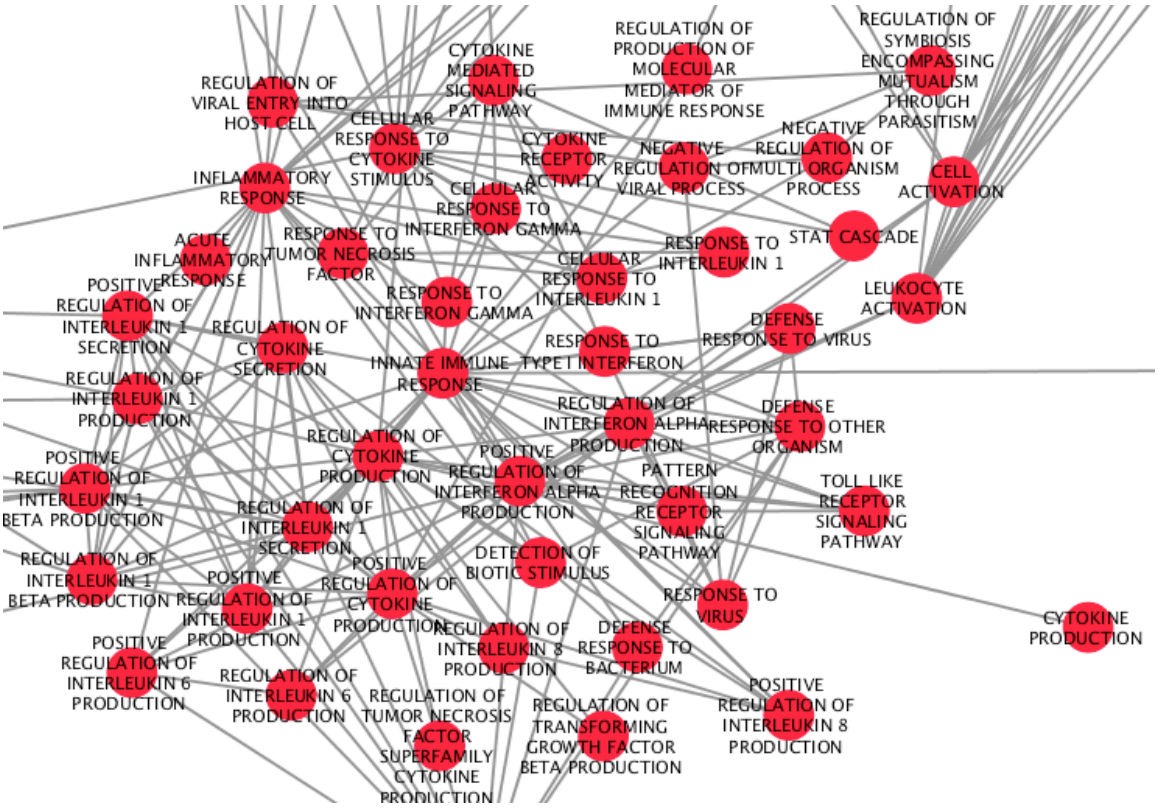
REGULATION OF SYMBIOSIS ENCOMPASSING MUTUALISM THROUGH PARASITISM
REGULATION OF PRODUCTION OF MOLECULAR MEDIATOR OF IMMUNE RESPONSE
CYTOKINE MEDIATED SIGNALING PATHWAY
REGULATION OF VIRAL ENTRY INTO HOST CELL
CELLULAR RESPONSE TO CYTOKINE STIMULUS
CYTOKINE RECEPTOR ACTIVITY
NEGATIVE REGULATION OF VIRAL PROCESS
NEGATIVE REGULATION OF MULTI-ORGANISM PROCESS
CELL ACTIVATION
INFLAMMATORY RESPONSE
CELLULAR RESPONSE TO INTERFERON GAMMA
STAT CASCADE
RESPONSE TO INTERLEUKIN 1
ACUTE INFLAMMATORY RESPONSE
RESPONSE TO TUMOR NECROSIS FACTOR
CELLULAR RESPONSE TO INTERLEUKIN 1
LEUKOCYTE ACTIVATION
POSITIVE REGULATION OF INTERLEUKIN 1 SECRETION
RESPONSE TO INTERFERON GAMMA
DEFENSE RESPONSE TO VIRUS
REGULATION OF CYTOKINE SECRETION
RESPONSE TO TYPE I INTERFERON
INNATE IMMUNE RESPONSE
REGULATION OF INTERLEUKIN 1 PRODUCTION
REGULATION OF INTERFERON ALPHA PRODUCTION
DEFENSE RESPONSE TO OTHER ORGANISM
REGULATION OF CYTOKINE PRODUCTION
POSITIVE REGULATION OF INTERFERON ALPHA PRODUCTION
PATTERN RECOGNITION RECEPTOR SIGNALING PATHWAY
TOLL LIKE RECEPTOR SIGNALING PATHWAY
POSITIVE REGULATION OF INTERLEUKIN 1 BETA PRODUCTION
REGULATION OF INTERLEUKIN 1 SECRETION
DETECTION OF BIOTIC STIMULUS
REGULATION OF INTERLEUKIN 1 BETA PRODUCTION
POSITIVE REGULATION OF CYTOKINE PRODUCTION
RESPONSE TO VIRUS
REGULATION OF INTERLEUKIN 1 PRODUCTION
CYTOKINE PRODUCTION
REGULATION OF INTERLEUKIN 8 PRODUCTION
DEFENSE RESPONSE TO BACTERIUM
POSITIVE REGULATION OF INTERLEUKIN 6 PRODUCTION
REGULATION OF INTERLEUKIN 6 PRODUCTION
REGULATION OF TUMOR NECROSIS FACTOR SUPERFAMILY CYTOKINE PRODUCTION
REGULATION OF TRANSFORMING GROWTH FACTOR BETA PRODUCTION
POSITIVE REGULATION OF INTERLEUKIN 8 PRODUCTION

B

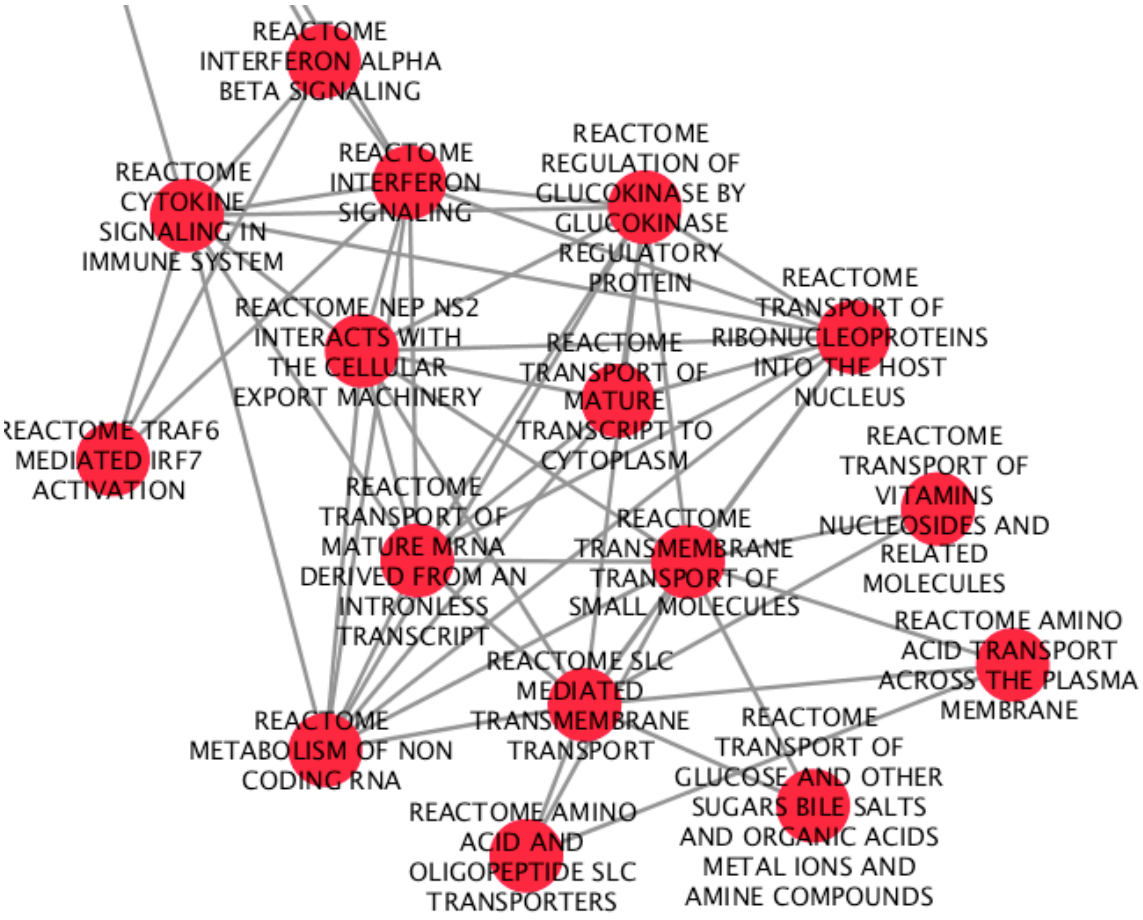

Figure 5.16 GSEA Pathway Analysis of Differentially Expressed Genes in Isolated Astrocyte Populations from WT Mice following LAQ Treatment Identifies Mitochondrial, Ribosomal and Protease Gene Sets. Gene sets enriched in GSEA pathway analysis in WT vehicle and LAQ-treated astrocytes corresponds to mitochondrial, ribsosomal (A) and inflammatory (B) gene sets. The size and color of the node is correlated with the size of the gene set category and significance (red indicates very significant and white indicates lower significance). NcRNA processing and mitochondrial function (A) and protease metabolism (B) are highly enriched in terms of size and significance of genes present. Similar categories cluster together with the thickness of the edge (line) correlated with how similar the categories are. Figure generated using Cytoscape.

5.3.17 Isolated Astrocytes from YAC128-LAQ treated Mice Express Differentially Expressed Genes Related to Various Cellular Processes including Drug Metabolism, Neuronal Maintenance, and Immune Cell Function

Two significant differentially expressed genes were identified in YAC128-LAQ treated astrocytes following RNA-seq analysis (Prl and Cyp1a1). Three of the genes identified were significantly up-regulated following LAQ treatment in both HD microglia and HD astrocytes. Prl, Cyp1a1 and Gh were significantly up-regulated following LAQ treatment in HD microglia (Figure 5.8) and HD astrocytes (Figure 5.17). The up-regulation of these three genes was more robust in HD astrocytes as compared to controls, suggesting that LAQ may exert a greater effect in astrocytes as compared to microglia. Other differentially expressed genes identified in YAC128-LAQ treated astrocytes include various cellular processes including immune signaling (Pomc), ion transport (Atp2a3), ubiquitin-protein activity (Wsb1), steroid metabolism (Akr1c14), and transcriptional regulation (Neat1). Overall, LAQ treatment in HD astrocytes resulted in up-regulation of several genes, which contrasts the significant down-regulation of gene expression identified in WT-LAQ treated astrocytes (Figure 5.14 and 5.15).

Gene Name	Log2 Fold Change	P-value	FDR	Protein Function
Prl	11.81727893	3.95E-32	5.77E-28	Positive regulation of STAT/JAK signaling/ STAT import into nucleus
Cyp1a1	6.265103769	7.94E-07	0.0057964	Cytochrome P450; drug metabolic process
Pomc	3.014541239	1.10E-04	0.474823774	Negative regulation of TNF-alpha
Atp2a3	-0.938937798	1.30E-04	0.474823774	Calcium ion transport
Gh	10.98559399	1.82E-04	0.530069309	Negative regulation of neuronal death
Wsb1	-0.869354688	2.23E-04	0.542911848	Ubiquitin-protein transferase activity
Kcp	-2.433448188	3.88E-04	0.730650931	Hemopoietic progenitor cell differentiation
Neat1	-1.101605932	4.24E-04	0.730650931	Transcriptional regulation
Fzd6	-0.905601894	4.50E-04	0.730650931	Platelet activation
Akr1c14	-1.392727891	9.30E-04	0.985998701	Hippocampus development & steroid metabolic process

Figure 5.17 Differentially Expressed Genes in Isolated Astrocyte Populations from LAQ-treated YAC128 Mice. Top ten differentially expressed genes in isolated YAC128 astrocytes following LAQ treatment (n=5-6). Top two differentially expressed genes demonstrate a significant FDR <0.05.

5.3.18 HD Astrocytes Isolated from LAQ-treated Mice Express Additional Differentially Expressed Genes related to Apoptosis and Lipid Metabolism along with other Basic Cellular Processes

Adjusted analysis of YAC128-LAQ treated astrocytes resulted in the differential expression of five additional genes (outlined in red; Figure 5.18). These differentially expressed genes were primarily down-regulated in HD astrocytes following LAQ treatment and correspond to proteolysis (Adam5) and membrane components (Hrct1). The other additional genes are up-regulated following LAQ treatment and correspond to apoptosis (Alox15) and lipid metabolism (Alox12e). The inclusion of these differentially expressed genes will allow for additional biological mechanisms underlying LAQ treatment in astrocytes to be uncovered.

Gene Name	Log2 Fold Change	P-value	FDR	Protein Function
Prl	11.81727893	3.95E-32	5.77E-28	Positive regulation of STAT/JAK signaling/ STAT import into nucleus
Cyp1a1	6.265103769	7.94E-07	0.0057964	Cytochrome P450; drug metabolic process
Pomc	3.014541239	0.00011032	0.474823774	Negative regulation of TNF-alpha
Gh	10.98559399	0.00018158	0.530069309	Negative regulation of neuronal death
Kcp	-2.433448188	0.000387712	0.730650931	Hemopoietic progenitor cell differentiation
540416O09Rik	-2.158347116	0.00101329	0.985998701	Undefined
Hrct1	-1.846436944	0.001535897	0.998044597	Membrane component
Alox15	3.637988761	0.001679255	0.998044597	Regulation of engulfment of apoptotic cell; wound healing
Adam5	-2.267738579	0.002397303	0.998044597	Proteolysis
Alox12e	4.739608052	0.002487329	0.998044597	Lipid metabolism

Figure 5.18 Differentially Expressed Genes in Isolated Astrocyte Populations following LAQ Treatment from YAC128 Mice following Adjusted Analysis. Top ten differentially expressed genes in YAC 128 astrocytes following LAQ treatment (n=4) with minimum log FC>2. Genes highlighted in red correspond to novel differentially expressed genes not identified in previous analysis outlined in Figure 5.17. Top two genes have a significant FDR <0.05.

5.3.19 Mitochondrial Functional Gene Sets are Enriched in YAC128-LAQ Treated Astrocytes

Gene sets related to mitochondrial function were significantly enriched in YAC128-LAQ treated astrocytes. Mitochondrial dysfunction is a hallmark of HD pathogenesis and may be modulated by LAQ treatment in astrocytes. As a result, mitochondrial function may be an important therapeutic avenue for treatment of HD.

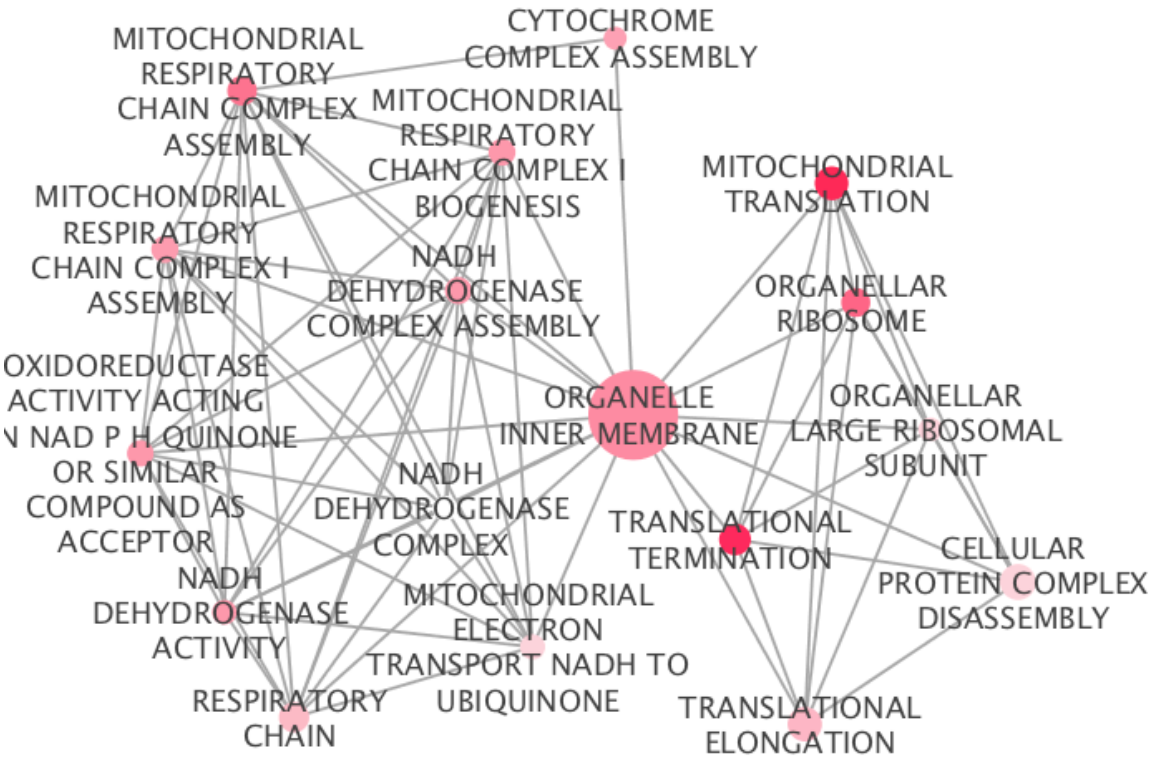

Figure 5.19 GSEA Pathway Analysis of Differentially Expressed Genes in Isolated Astrocyte Populations from YAC128 Mice following LAQ Treatment Identifies Mitochondrial Gene Sets. Gene sets enriched in GSEA pathway analysis in YAC128 LAQ-treated astrocytes corresponds to mitochondrial gene sets. The size and color of the node is correlated with the size of the gene set category and significance (red indicates very significant and white indicates lower significance). Organelle inner membrane genes are highly enriched in terms of size and significance of genes present. Similar categories cluster together with the thickness of the edge (line) correlated with how similar the categories are. Figure generated using Cytoscape.

5.4 Discussion

In this chapter I used my established flow cytometry system to evaluate the effect of LAQ, a current HD therapeutic, on the glial transcriptome. Using this technique, I was able to isolate microglia and astrocyte populations from the brains of adult WT and YAC128 vehicle and LAQ-treated mice of sufficient quality for RNA-seq analysis. The design of the experiment allowed for genotype, cell-type and treatment effects to be assessed, along with relevant biological pathways underlying potential differences in these comparisons. At baseline (vehicle-treated), a greater number of differentially expressed genes were identified in HD microglia compared to astrocytes, suggesting that mutant-huntingtin expression in microglia may play a more important role in HD pathogenesis.

An additional independent cohort of vehicle and LAQ-treated mice were included in the RNA-seq experimental design for subsequent validation of differentially expressed genes. I was unable to validate the differentially expressed genes identified using both standard RT-quantitative PCR (qPCR) and Taq-man probe RT-quantitative PCR methods. Because RNA-seq may identify splice variants of genes, I designed qPCR primers using the highest read aligned identified for each gene. This would ensure that the primers are specific for the splice variant and genetic sequence identified in the RNA-seq analysis. Designing specific primers, and assessing their efficiency in previously generated microglia and astrocyte samples, however, did not result in successful validation.

There are several technical considerations that may influence the lack of validation identified. First, RNA-seq has a large dynamic range and high sensitivity thus allowing quantification of lowly expressed genes (Bhargava *et al.* 2014). Although direct comparison between the sensitivity of RNA-seq and qPCR is not easily found in the literature, RNA-seq may be a more sensitive measure of gene expression compared to qPCR. Second, the differentially expressed genes identified may demonstrate low expression that can only be identified using RNA-seq. Third, the number of technical replicates (n=4-6 per condition) used for the RNA-seq analysis may not be sufficient for estimating and decreasing experimental error (Fang and Cui, 2011). Although the

biological samples used were not pooled, an n of four to six may not be sufficient in accurately identifying differentially expressed genes with low expression. Increasing the number of biological replicates would prevent variation between samples from masking true biological effects.

Additional steps may be taken to improve validation of identified differentially expressed genes. In addition to isolating glial populations from additional animals for technical qPCR validation, a separate and comparable RNA-seq analysis can be conducted to confirm the differentially expressed genes identified. Isolation of glial population from adult brain is not an overtly rapid process. The entire protocol takes three hours and in this time it is safe to assume that RNA expression may change. Although RNA-quality, as measured by the 260/280 ratio on a Nanodrop spectrometer, was sufficient in isolated samples for both RNA-seq and qPCR, a different tissue may be better equipped at identifying lowly expressed genes.

Previous work completed in HD patient peripheral immune cells also evaluated potential transcriptional changes at the basal, unstimulated level. No significant differences in gene expression were identified in LPS-stimulated HD monocytes compared to controls, suggesting that mutant-huntingtin expression has a priming effect at the basal level. This priming effect, in turn, is responsible for the exaggerated cytokine release seen in HD monocytes following stimulation. The majority of differentially expressed genes in unstimulated HD monocytes were up-regulated and related to proinflammatory cytokine and chemokine genes. Proinflammatory functional gene sets were significantly enriched in HD monocytes following GSEA analysis. Of these gene sets, 85 were up-regulated gene sets related to innate immunity, the inflammatory response in addition to NFκB and JAK/STAT signaling. Six functional gene sets were down-regulated and involved vacuole, lysosome and catabolic functions. Interestingly, both growth factor binding and chemokine receptor binding were also significantly up-regulated in HD monocytes (Miller *et al.* 2016). Transcriptomic analysis of HD microglia identified growth hormone signaling and immune cell function alterations (Figure 5.3), suggesting that altered immune function may underlie HD-dependent pathology in both the peripheral and central immune system.

Cytochrome P450 was also identified in the transcriptomic analysis and is

significantly up-regulated following LAQ treatment in both HD microglia and HD astrocytes. As discussed in the introduction, cytochrome P450 (Cyp1a1) is a member of the prototypical AhR pathway and has been previously shown to be up-regulated following LAQ treatment in EAE mice (Kaye *et al.* 206). The AhR pathway has been linked to NFκB signaling (Vogel *et al.* 2014) suggesting that LAQ treatment may down-regulate NFκB signaling in various diseases including EAE and HD.

Growth hormone (GH) and Prolactin (PRL) are two potential genes of interest for future LAQ studies. Both growth hormone and prolactin are down-regulated in HD microglia at baseline and up-regulated following LAQ treatment. In the case of astrocytes, GH and PRL are up-regulated in HD astrocytes (not significant enough to make top ten gene lists) and up-regulated further following LAQ treatment, similar to HD microglia. Growth hormone (GH) is released into circulation from the anterior pituitary gland in the brain to exert its effect on appetite, cognitive function, energy, memory, mood, neuroprotection and sleep. Specific binding sites for GH are present in the choroid plexus, hippocampus, hypothalamus and spinal cord (Lai *et al.* 1991, Nyberg and Burman, 1996), suggesting that the CNS is a target for GH. GH has also been identified in the putamen, the region most affected by HD, suggesting that GH expression may be involved in disease pathogenesis. The regulation of GH receptors and its transcript in the CNS is poorly understood but the density of GH binding the human and rat brain have been shown to decrease with age, in various regions including the caudate putamen (Lai *et al.* 1993, Nyberg, 1997). GH has been shown to have a neuroprotective effect in experimental rat models of spinal cord injury (Hanci *et al.* 1994) and hypoxic ischemia (Gustafson *et al.* 1999) (reviewed in Nyberg, 2000). The neuroprotective effect of GH has also been demonstrated in *in vitro* and *in vivo* models of amyotrophic lateral sclerosis. GH signaling occurs through the JAK-STAT, MAPK and PI3K pathways (reviewed in Chung *et al.* 2015), which have been previously implicated in immune cell function as discussed in the introductory section of Chapter 4. As a result, GH signaling may be neuroprotective in other neurodegenerative diseases, including HD, through modulation of immune cell pathways.

In the context of HD, a lack of consensus with respect to the levels of GH is present. In some cases, plasma GH levels are significantly decreased in manifest HD

subjects (Wang *et al.* 2014) and increased in others (Saleh *et al.* 2009). Other studies have suggested that GH secretion becomes more irregular with worsening motor and functional impairment in human patients (Aziz *et al.* 2010). The lack of agreement between these studies, however, may be due to low patient sample sizes and inherent differences in baseline hormone measures in human patients. In the case of HD mouse models, hypothalamic alterations have been assessed (reviewed in van Wamelen DJ *et al.* 2014) but little work has focused on GH specifically. In one study, intraperiotneal administration of GH in a 3-NP rat model of HD accelerated behavioral deterioration and did not restore weight loss (Park *et al.* 2013). This mouse model does not express mutant huntingtin and it may be mHTT that is affected by GH treatment. As a result, additional work will need to be completed to assess the potential neuroprotective effect of GH administration in mHTT-expressing HD mouse models. Another study focused on the growth hormone-insulin like growth factor-1 (GH-IGF-1) axis and found that full-length huntingtin levels modulate body weight by influencing IGF-1 expression, irrespective of CAG size (Pouladi *et al.* 2010). Both these studies, however, provide limited insight into the role of growth hormone in the HD brain. As a result, additional mechanistic studies assessing the link between mutant-huntingtin expression and GH function, as well as the effect of LAQ treatment on this interaction, will need to be conduced.

The other candidate gene identified in the RNA-seq analysis, prolactin, has also been previously implicated in HD. Plasma prolactin levels are significantly decreased in HD patients compared to controls (Wang *et al.* 2014) and impaired prolactin responses have also been previously reported in HD patients (Hayden et al. 1977) as a potential consequence of abnormal hypothalamic activity. Similar to GH, little work has been completed in HD mouse models with respect to prolactin function. As GH and prolactin develop from common progenitor cells (Laron, 2011), they may work together to affect energy metabolism and immune responses (reviewed in Redelman et al. 2008). As immune activation is a feature of HD, future work aimed at evaluating GH and prolactin expression in HD microglia and astrocytes may focus future therapeutic interventions and provide a potential mechanism by which LAQ exerts its neuroprotective effect.

6 Discussion

6.1 Study Objectives

At the start of this thesis, I established four objectives based on the development of a flow cytometry system to isolate specific cell populations from culture and whole mouse brain: 1) application of this system to evaluate *HTT* expression in the cell cycle, 2) to verify the efficacy of various microglia-specific conditional knockout mouse models, 3) to investigate signaling transduction cascades in mutant-huntingtin expressing microglia, 4) to evaluate the glial transcriptome in response to LAQ treatment. The ultimate goal of this thesis was to provide a technical means of investigating the cell-intrinsic effects of mutant huntingtin expression in different cell types. By doing so, different biological questions ranging from potential mechanisms of HTT regulation to the mechanisms underlying glial dysfunction in HD can be investigated. Ultimately, this work will inform both future technical experiments as well as advance our understanding of the role of mHTT expression in glial cells. Here I further discuss the findings of my work as well as potential future directions.

6.2 Establishment of a Flow Cytometry System and Application to *HTT* Expression in the Cell Cycle

Using a combination of previously published protocols and technical optimization, I established a flow cytometry system to isolate specific cell populations of interest from both cultured cells as well as intact adult murine brain. The isolation of pure, viable cell populations of interest resulted in RNA and protein of excellent quality for use in downstream applications. In one application, this flow cytometry system was used to evaluate the cell cycle as a novel *HTT* regulatory mechanism. As discussed in the introductory section of Chapter 2, *HTT* regulation at the transcriptional level is currently poorly understood. Although several transcriptional factors able to modify *HTT* expression have been identified (Becanovic *et al*. 2015, Ryan *et al*. 2006, Tanaka *et al.* 2004, R. Wang *et al.* 2012), how the gene is regulated is still largely unknown. One hypothesis was that gene expression at the transcript level might vary through the

progression of the cell cycle. In order to answer this simple question, I isolated various cell types into the different phases of the cell cycle and measured *HTT* transcript and protein expression. Using cell lines derived from both the periphery (kidney and cervix) and CNS (neurons), I concluded that *HTT* transcript expression does not significantly vary across the cell cycle. The reason for this is that *HTT* gene expression may be fairly stable over time and may exhibit a long half-life.

Another aspect of regulation assessed was the subcellular localization of HTT protein. HeLa FUCCI cells were employed as means of investigating a potential cell-cycle dependent mechanism of HTT localization. Although HTT is predominately cytoplasmic in the various cell cycle phases, the use of a C-terminal HTT antibody identified nuclear puncta in G1 cells. These results, however, may be influenced by the antibody, fixation and permeabilization used. As a result, future experiments with additional antibodies would need to be conducted to confirm the potential nuclear localization of HTT in G1 cells. Additional experiments may also be undertaken to evaluate potential mutant and wild-type huntingtin localization differences in the cell cycle. With this in mind, HeLa FUCCI cells can be transfected with mutant and wild-type huntingtin constructs expressing an HA tag. The presence HA tag can then be visualized using an anti-HA antibody, allowing for the localization of wild-type and mutant huntingtin to be visualized simultaneously using immunofluorescence. Any potential localization differences between wild-type and mutant huntingtin, more importantly, would provide further insight into differences in protein function and would focus future therapeutic interventions aimed at reducing mutant huntingtin expression.

The flow cytometry system was also used to isolate glial populations from the adult murine brain. Through technical optimization, pure microglia and astrocyte populations from whole brain, as well as specific brain regions, were isolated. More importantly, these populations expressed cell-type specific transcripts, providing further evidence of sorting purity. Although my thesis focused primarily on the isolation of microglial and astrocyte populations, it is possible to isolate other brain cell populations as well, including oligodendrocytes and, potentially, neurons.

In the case of oligodendrocytes, an O4-Miltenyi^{TM} microbead kit may be used for enrichment (using either automated AutoMACS^{TM} separation or QuadroMACS^{TM} manual

column separation), along with an O4-conjugated antibody. The isolation of oligodendrocytes from HD mouse brain is an area of interest for several reasons. First, white matter abnormalities have been identified in both human HD patients (Gregory *et al.* 2015; Phillips *et al.* 2016) as well as mouse models (Teo *et al.* 2016). As the cell population responsible for producing myelin, oligodendrocytes play an important role in white matter pathology (reviewed in Bradl and Lassman, 2010). A similar RNA-seq experiment to the one conducted in Chapter 5 could be designed to investigate the potential mechanisms underlying mutant-huntingtin expression in oligodendrocytes. Since LAQ treatment may ameliorate white matter structural abnormalities in YAC128 HD mice (Garcia-Miralles *et al.* 2016), the isolation of oligodendrocytes from WT and YAC128 brain may provide further mechanistic insight into the effect of LAQ on oligodendrocyte function. A similar experiment can also be conducted to other therapeutics, included SEMA45 (Sempahorin 4D antibody). As discussed in the introduction of Chapter 5, SEMA4D is involved in oligodendrocyte maturation and has been shown to have a beneficial effect on corpus callosum atrophy in YAC128 mice (Southwell *et al.* 2015). RNA-seq analysis of isolated oligodendrocytes from WT and HD-treated mice would provide further insight into the mechanism by which anti-SEMA4D treatment may exert its neuroprotective effect.

The isolation of neuronal cells from adult murine brain is also theoretically possible, although technically difficult. In a neurodegenerative disease such as HD, characterized by neuronal cell loss, a technique able to isolate adult neurons from brain tissue would be of particular interest. The company, Miltenyi^{TM} has introduced a Neuron Isolation Kit for use in isolation of neurons from adult mouse brain. Similar to the magnetic bead enrichments used for isolating microglia and astrocyte populations (Chapter 2.2.4 and 2.2.6), the Neuron Isolation Kit uses magnetic beads along with a column separator to enrich for neuronal populations prior to flow cytometry sorting. However, in contrast to CD11b and ACSA-2 Microbeads^{TM} used in microglia and astrocyte enrichments, the Neuron Isolation Kit uses a negative selection principle. This means that the cells of interest (neurons) are not retained in the column but are collected as flow-through. The flow-through is then stained with microglia and astrocyte-specific antibodies and the negatively stained population is identified as neuronal. This process, as

a result, is not as pure as the positive selection used in enriching for microglia and astrocyte populations.

I have previously attempted to use the Neuron Isolation Kit for isolation of neurons from adult mouse brain. Although I was able to attain viable cells using the protocol, I found that transcript expression of prototypical neuronal transcripts such as β-tubulin III, MAP-2, and Neurofilament, were not highly expressed in the sorted neuronal populations (data not included in thesis). Although this result may be due to the fact that diverse neuronal populations are isolated as a result of the negative selection technique used, it is likely that these neurons are significantly altered as a result of the technical process. Arguably, the best way to isolate neurons from adult mouse brain would be through the use of an extracellular neuronal specific antibody. The conjugated antibodies used for microglia and astrocyte populations are extracellular, meaning that fixation and permeabilization are not required for visualization of antibody binding and subsequent isolation.

To my knowledge, there are no commercially available, extracellular neuronal flurochrome conjugated antibodies available. Instead, various studies have used intracellular NeuN-labeling to identify neurons using flow cytometry. In instances where gene expression is evaluated, the use of fixed and permeabilized cells, however, is not ideal. As a result, currently available extracellular antibodies (i.e. synaptophysin) may be conjugated with chosen flurochromes to circumvent these potential limitations. There is, however, the possibility that flurochrome conjugation is not successful. And even if an extracellular neuronal flurochrome-conjugated antibody is generated, it is unclear if the flow cytometry processing would be gentle enough to keep neuronal processes and other morphological characteristics intact for antibody labeling. Thus, neuronal isolation from adult mouse brain, while biologically relevant to various areas of neuroscience research, still requires technical optimization.

6.3 Verification of Efficacy of Microglia-Specific Conditional Knockout Models

One way to evaluate the cell-intrinsic effect of a gene of interest is through the use of conditional knockout models. Through the use of *Cre-loxP* technology, genes can be removed from specific cell types as well as during specific times (i.e. development). As discussed in the introductory chapter, immune activation plays a prominent role in various neurodegenerative diseases including Frontotemporal dementia and Alzheimer's disease, as well as HD. Crossing mice expressing Cre under the myeloid lineage cell promoter (Lysozyme) with a transgenic mouse of choice (i.e. BACHD) allows for the gene of interest to be specifically removed from monocytic cells, including microglia. In this way, the effect of specific gene expression in microglia and the consequence of this expression in behavioral and neuropathological phenotypes can be accurately assessed.

BACCre and GLyz mice were previously generated in the lab, as discussed in the introductory section of Chapter 3. Both are microglia-specific conditional knockout models meaning that the specific gene of interest (mutant huntingtin and progranulin, respectively) is removed from microglia in the brain. Significant reductions of gene expression were seen in microglia cultures derived from BACCre (Figure 3.6) and GLyz mice (data included in manuscript in preparation, Petkau *et al.*). The next step was to assess if significant knockdown was also present in microglia isolated from BACCre and GLyz adult brain. Using the established flow cytometry system, I isolated microglia from both mouse models and measured the efficacy of genetic knockout. In the GLyz mouse model, a 75% reduction in *Grn* transcript expression was identified in microglia sorted from GLyz mice as compared to WT.

A similar experiment was also conducted in the BACCre mouse model whereby mutant HTT protein expression was measured in microglia sorted from BACCre brain. There was an approximately 50% reduction in 1C2 protein expression in BACCre microglia compared to WT (Figure 3.7). Approximately 150-300,000 microglia can be isolated from a single adult brain (Figure 3.2). In the case of Western blots, it is generally prudent to use approximately one million cells to attain sufficient protein concentration. As a result, microglia samples were pooled (n=4 per genotype) to achieve sufficient

protein concentration. In the future, additional microglia sorts may be conducted to increase the number of technical replicates needed for statistical analysis.

The lack of absolute knockdown identified in sorted GLyz and BACCre microglia may be a consequence of various mechanisms. As discussed in chapter 3, a Cre toxicity effect has been identified in BACCre primary microglia, leading to alterations in morphology (manuscript in preparation; Connolly *et al.*). A similar up-regulation of Cre expression was also seen in microglia isolated from BACCre mice as compared to WT-Cre (Figure 3.3 D). The presence of a toxic Cre effect may reduce microglial survival (Figure 3.2) and ultimately impact the extent of genetic knock down. Additional studies will need to be conducted in order to identify the precise mechanism involved in Lysozyme-mediated deletion in BACCre and GLyz microglia. These can include 1) evaluating the knock down in peripheral monocytes to identify potential efficiency differences in Lyz expression in central and peripheral immune cells 2) assessing genetic knock down using a different myeloid-lineage promoter (Cx3Cr1) and 3) investigate the extent of genetic knock down in other cell-type specific conditional knock out models (i.e. astrocytes or neurons) to identify if the efficiency of Cre-mediated deletion is dependent on cell type. The conclusion of this study has generated various questions about microglia-specific conditional knockout models and the efficacy of the *Cre/loxP* system. Understanding the effect of Cre toxicity, particularly, will be important in interpreting the behavioral and neuropathological results of Lyz-mediated deletion of mutant huntingtin and progranulin expression in microglia.

In the context of HD, the lack of robust phenotypic reversal seen in BACCre mice may imply that mutant-huntingtin expression in microglia does not have a significant effect on HD pathogenesis. In order to accurately answer this question, the converse experiment would also need to be conducted. This means that mutant-huntingtin would need to be removed from neurons and astrocytes (BACHD mouse crossed to a Nestin-Cre mouse; promoter specific for neurons and astrocytes) and retained in microglia. If this also does not ameliorate BACHD-related phenotypes then the interpretation may be that HD pathogenesis is a consequence of ubiquitous mHTT expression and that removal in a specific cell type is not sufficient to reverse HD features.

6.4 Signaling Transduction Cascades in Mutant-Huntingtin expressing Microglia

I conducted a protein microarray study aimed at assessing phosphorylation changes in HD microglia at baseline and following stimulation with LPS and MMP3. Although several pathways have been implicated in microglial dysfunction in HD, including cannabinoid and kynurenine signaling cascades, the impact of these pathways in mediating exaggerated cytokine release has not been investigated. Commercially available protein phosphorylation arrays allow for the unbiased evaluation of additional signaling cascades involved in the experimental system being assessed. In this case, the upstream signaling pathways involved in LPS and MMP3-mediated cytokine release in HD microglia can be better understood.

Although several of the candidate proteins identified in the CSE phosphorylation array have been previously implicated in HD immune cell function (NMDAR1, GluR1, and ASK1), the majority are novel findings. These novel proteins, however, are linked to different mechanisms previously implicated in HD pathogenesis including metabolic deficits (PGK1), neuronal death (Rb), as well as exaggerated inflammatory responses following stimulation (Ron, EphA3). As a result, future studies aimed at evaluating the mechanism by which mutant-huntingin expression in microglia mediates increased inflammatory responses may focus on Rb and EpA3 phosphorylation signaling cascades. Although these two proteins did not cluster together following STRING analysis (Figure 4.3), the analysis is rudimentary and does not preclude these proteins from acting together in a signal cascade. The addition of pan-specific proteins in the candidate lists is important in ensuring that the phosphorylation increases identified in HD microglia following stimulation are real but also provides additional mechanistic information.

The role of mutant huntingtin in these signaling cascades, however, is also an important avenue for further research. As a result, preliminary experiments aimed at investigating the function of mutant huntingtin expression in protein phosphorylation pathways have been designed. As discussed in more detail in the chapter 4 discussion, future experiments will be conducted to evaluate the potential link between mutant huntingtin and the phospho-protein of interest as well as the impact of pharmacological

blockade of protein phosphorylation on ameliorating increased cytokine release. The combination of both approaches will highlight how mutant huntingtin is involved in microglial dysfunction and if this dysfunction can be reversed with protein kinase inhibitors as a therapeutic strategy. Another possible analysis could also look at the correlation between gene expression and protein expression/phosphorylation changes in HD microglia. RNA-seq analysis generated in chapter 5 identified differentially expressed genes in HD microglia compared to control. Although the primary comparison in chapter 4 was WT CSE vs. YAC CSE, analysis reports were also generated for baseline WT vs. HD microglia phosphorylation/protein expression differences. A combination of both methods may provide further information on the mechanisms underlying mutant-huntingtin expression in microglia.

6.5 Evaluation of the Glial Transcriptome at Baseline and in Response to LAQ

Transcriptomic analyses allow for the rapid identification of differentially expressed genes in various biological conditions. In the context of HD, transcriptional dysregulation is has been previously identified, where greater than 80% of striatal-enriched genes are down regulated in both HD mouse models as well as in human caudate brain tissue (Desplats *et al.* 2006). With the advent of computational and microarray processing, an increasing number of transcriptomic analyses in HD have been conducted. One of the first gene expression profiling studies was conducted in YAC128 HD mouse brain of various ages, resulting in the identification of thirteen differentially expressed genes (Becanovic *et al.* 2010). Subsequent work has moved to HD patients in two main cell types, brain and peripheral blood. Transcriptomic analysis in peripheral blood has focused on basal dysfunction (Miller *et al.* 2016), and the identification of potential relevant biomarkers (Runne *et al.* 2007; Mastrokolias *et al.* 2015). HD patient brain tissue has also been used to identify areas of transcriptional dysregulation (Labadorf *et al.* 2016) as well as alternative splicing (Lin *et al.* 2016). A recent study also assessed the correlation of HD signatures identified in peripheral blood and caudate brain tissue and found significant similarity (Mina *et al.* 2016).

Interestingly, differentially expressed genes identified in human HD prefrontal cortex were enriched for immune response, neuroinflammation and developmental genes (Labadorf *et al.* 2016), highlighting the significance of glial involvement in HD pathogenesis. As a result, transcriptomic analysis in immune cells is a relevant avenue for future HD research. Although peripheral immune system dysfunction present in HD, the disease is still a disorder of the central nervous system, and as a result, the innate immune system is of particular importance. Transcriptomic analyses of whole brain from HD mouse models use a heterogeneous population of cells. Although bioinformatic analyses are able to distinguish between different cell types, these computational approaches may be limited.

With these ideas in mind, I used the established flow cytometry system to isolate pure populations of microglial and astrocytic cells from WT and HD mouse brain and evaluated both intrinsic transcriptional dysregulation as well as potential effects of LAQ treatment. I anticipated issues with RNA quality and amount due to the relative severity of the flow cytometry protocol, but a minimum of four useful samples was attained for each outlined condition. The RNA-seq analysis identified 1106 differentially expressed genes in HD microglia and 2 in HD astrocytes, when compared to matched controls. As a result, innate dysfunction in HD microglia may be a more relevant disease phenotype as compared to astrocytes, although additional work would need to be conducted. The majority of differentially expressed genes identified in HD astrocytes corresponded to immune cell function and cellular transport. Since astrocytes are involved in synaptic transmission, it is expected that a large proportion of differentially expressed genes would be involved in cellular ion transport. On the other hand, mitochondrial and proteosomal functional gene sets were enriched in HD microglia. This implies that mitochondrial and protein related functions might be altered in mutant-huntingtin expressing microglia.

As is the case in large-scale transcriptomic studies, a major obstacle is centered on interpreting the vast amounts of data. Although the statistical measures of FDR, p-value and log-fold change may identify potential genes of interest; there is the possibility that genes of biological significance are not identified using these approaches. Additional methods including GSEA pathway analysis may focus biologically important pathways in

an effort to interpret innate glial cell dysfunction in HD. In terms of LAQ treatment, the working mechanism may be that astrocytes convert LAQ into an active metabolite through the up regulation of Cyp1a1 expression and that this metabolite then exerts its effect in microglia. The comparison of baseline genotype differences and subsequent improvement following LAQ treatment implicate growth hormone and prolactin signaling as relevant pathways for additional experimental validation and investigation.

6.6 Concluding Remarks

I have successfully accomplished the objectives set out at the beginning of my thesis. This work has expanded knowledge of potential *HTT* regulatory mechanisms as well as increased our understanding of glial cell dysfunction in the context of HD. Following the establishment of a flow cytometry system; I found that *HTT* expression does not vary across the cell cycle. Using an adapted technique, I identified robust but not absolute genetic knock down in two microglia-specific conditional knock out mouse models. Building upon the neuroinflammation focus, I identified mutant-huntingtin specific changes in protein phosphorylation expression in microglia as a means of identifying potential signaling cascades involved in exaggerated cytokine release. Finally, I examined transcriptional dysfunction in HD microglia and astrocyte populations and the effect of LAQ treatment on gene expression in these cell types. The methodologies established in this study, as well as the results generated, create a basis upon which future studies aimed at assessing the cell-intrinsic effect of mutant huntingtin expression and the role of inflammation in HD can be based.

References:

Abada,YS., Schreiber R., Ellebroek B. (2013) Motor, emotional and cognitive deficits in adult BACHD mice: a model for Huntington's disease. Behav Brain Res. 238: 243-51.

Abram CL., Roberge GL., Hu Y., Lowell CA. (2014) Comparative analysis of the efficiency and specificity of myeloid-Cre deleting strains using ROSA-EYFP reporter mice. J Immunol Methods. 408: 89-100.

Aguzzi A., Barres BA., Bennett ML (2013) Microglia: Scapegoat, Saboteur or Something Else? Science. 339(6116): 156-61.

Aharoni R., Saada R., Eilam R *et al.* (2012) Oral treatment with laquinimod augments regulatory T-cells and brain-derived neurotrophic factor expression and reduces injury in the CNS of mice with experimental autoimmune encephalomy-elitis. J Neuroimmunol. 251: 14-24.

Aharony I., Ehrnhoefer DE., Shruster A *et al.* (2015) A Huntingtin-based peptide inhibitor of caspase-6 provides protection from mutant huntingtin-induced motor and behavioral deficits. Hum Mol Genet. 24(9): 2604-14.

Ahmed Z., Sheng H., Xu YF *et al.* (2010) Accelerated lipofuscinosis and ubiquitination in granulin knockout mice suggest a role for progranulin in successful aging. Am. J. Pathol. 177(1): 311-24.

Aidt FH., Nielsen SM., Kanters J *et al.* (2013) Dysfunctional mitochondrial respiration in the striatum of the Huntington's disease transgenic R6/2 mouse model. PLoS Curr. 5.

Akiyama H., McGeer PL (1990) Brain microglia consitutively express beta-2 integrins. J Neuroimmunol. 30(1): 81-93.

Albrecht S., Bourdeau M., Bennett D. *et al.* (2007) Activation of caspase-6 in aging and mild cognitive impairment. Am J Pathol. 170(4): 1200-9.

Almeida S., Sarmento-Ribeiro AB., Januario C (2008) Evidence of apoptosis and mitochondrial abnormalities in peripheral blood cells of Huntington's disease patients. Biochem Biophys Res Commun. 374(4): 599-603.

Anderson, KE., Marder, KS. (2001) An overview of psychiatric symptoms in Huntington's disease. Curr Psychiatry Rep. 3(5):379-88.

Andrew SE., Goldberg YP., Kremer B *et al.* (1993) The relationship between trinucleotide (CAG) repeat length and clinical features of Huntington's disease. Nature Genetics. 4(4): 398-403.

Anon, *et al* . (1993) A novel gene containing a trinucleotide repeat that is expanded and unstable on Huntington's disease chromosomes. The Huntington's Disease Collaborative Research Group. Cell. 72(6): 971-83.

Apostol BL., Illes K., Pallos J, Bodai L *et al.* (2006) Mutant huntingtin alters MAPK signaling pathways in PC12 and striatal cells: ERK1/2 protects against mutant huntingtin-associated toxicity. Hum Mol Genet. 15: 273-85.

Arning L., Monte D., Hansen W., Wieczorek S *et al.* (2008) ASK1 and MAP2K6 as modifiers of age of onset in Huntington's disease. J Mol Med (Berl). 86(4): 485-90.

Arrasate M., Finkbeiner S (2012) Protein aggregates in Huntington's disease. Exp Neurol. 238(1): 1-11.

Arregui L., Benitez JA., Razgado LF *et al.* (2011) Adenoviral astrocyte-specific expression of BDNF in the striat of mice transgenic for Huntington's disease delays the onset of the motor phenotype. Cell Mol Neurobiol. 31(8): 1229-43.

Arteaga-Bracho EE, Gulinello M., Winchester ML. *et al.* (2016) Postnatal and adult consequences of loss of huntingtin during development: implications for Huntington's disease. Neurobiol Dis. 96: 144-155.

Assaf Y., Galron R., Shapira I *et al* (2008) MRI evidence of white matter damage in a mouse model of Nijmegen breakage syndrome. Exp Neurol. 209(1): 181-91.

Azberger T., Krampfl K., Leimgruber S., Weindl A (1997) Changes in NMDA receptor subunit (NR1, NR2B) and glutamate transporer (GLT1) mRNA expression in Huntington's disease—an in situ hybridization study. J Neuropathol Exp Neurol. 56: 440-54.

Aziz NA., Pijl H., Folich M *et al.* (2010) Growth hormone and ghrenlin secretion are associated with clinical severity in Huntington's disease. Eur J Neurol. 17(2): 280-8.

Augood SJ., Faull RL., Emson PC (1996) Reduction in encephalin and substance P messenger RNA in the striatum of early grade Huntington's disease. Brain Res Bull. 72: 152-8.

Baldo, B., Paganetti P., Grueninger S. *et al* (2012) TR-FRET-based duplex immunoassay reveals an inverse correlation of soluble and aggregated mutant huntingtin in huntington's disease. Chem Biol. 19: 264-75.

Battista N., Bari M., Tarditi A *et al.* (2007) Severe deficiency of the fatty acid amide hydrolase (FAAH) activity segregates with the Huntington's disease mutation in peripheral lymphocytes. Neurobiol Dis. 27(1): 108-16.

Baranes K., Raz-Prag D., Nitzan A *et al.* (2009) Conditional inactivation of the NBS1 gene in the mouse central nervous system leads to neurodegeneration and disorganization of the visual system. Exp Neurol. 218(1): 34-32.

Bartzokis G *et al.* (1994) In vivo MRI evaluation of age related increases in iron. AJNR AM J Neuroradiol. 15: 1129-38.

Bayram-Weston, Z., Jones L., Dunnet SB., Brooks SP (2016) Comparison of mHTT Antibodies in Huntington's Disease Mouse Models Reveal Specific Binding Profiles and Steady State Ubiquitin Levels with Disease Development. PLoS ONE., 11(15): e0155834.

Beaumont V., Mrzljak L., Dijkman U *et al.* (2016) The novel KMO inhibitor CHDI-340246 leads to a restoration of electrophysiological alterations in mouse models of Huntington's disease. Exp Neurol. 282: 99-118.

Becanovic K., Pouladi MA., Lim RS *et al.* (2010) Transcriptional changes in Huntington's disease identified using genome-wide expression profiling and cross-platform analysis. Hum Mol Genet. 19(8): 1438-52.

Becanovic K., Norremolle A., Neal SJ *et al.* (2015) A SNP in the HTT promoter alters NF-kB binding and is a bidirectional genetic modifier of Huntington's disease. Nat Neurosci. 18(6): 807-16.

Benraiss A., Wang S., Herrlinger S *et al.* (2016) Human glia can both induce and rescue aspects of disease phenotype in Huntington's disease. 7: 11758.

Berggren K., Agrawal S., Fox JA *et al.* (2017) Amyloid precursor protein haploinsufficiency preferentially mediates brain iron accumulation in mice

transgenic for the Huntington's disease mutation. J Huntingtons Dis. Epub ahead of print.
Beutler E (2007) PGK deficiency. Br J Haemotol. 136(1): 3-11.
Bhargava V., Head SR., Ordoukhanian P *et al.* (2014) Technical variations in low-input RNA-seq methodologies. Sci Rep. 4: 3678.
Björkqvist M., Wilde EJ., Thiele J *et al.* (2008) A novel pathogenic pathway of immune activation detectable before clinical onset in Huntington's disease. J Exp Med. 205(8): 1869-77.
Block F., Kunkel M., Schwarz M. (1993) Quinolinic acid lesion of the striatum induces impairment in spatial learning and motor performance in rats. Neurosci Lett. 149(2):126-8.
Bodai L., Marsh JL. (2012) A novel target for Huntington's disease: ERK at the crossroads of signaling. The ERK signaling pathway is implicated in Huntington's disease and its upregulation ameliorates pathology. Bioessays. 34(2): 142-8.
Bonifati DM., Kishore U. (2007) Role of complement in neurodegeneration and neuroinflammation. Mol Imm. 44: 999-1010.
Bouchard J., Truong J., Bouchard K *et al.* (2012) Cannabinoid receptor 2 signaling in peripheral immune cells modulates disease onset and severity in mouse models of Huntington's disease. J Neurosci. 32(50): 18259-68.
Bowles KR., Jones L (2014) Kinase signaling in Huntington's Disease. J Huntin Dis. 3: 89-123.
Bradford, J., Shin JY., Roberts M *et al.* (2009) Expression of mutant huntingtin in mouse brain astrocytes causes age-dependent neurological symptoms. PNAS. 106 (52): 22480–22485. Available from: doi:10.1073/pnas.0911503106.
Bradford, J., Shin JY., Roberts M *et al.* (2010) Mutant huntingtin in glial cells exacerbates neurological symptoms of Huntington disease mice. J Biol Chem. 285 (14): 10653–10661.
Bradl M., Lassmann H (2010) Oligodendrocytes: biology and pathology. Acta Neuropathol. 119(1): 37-53.
Braubach P., Orynbayev M., Adnronache Z *et al.* (2014) Altered Ca(2+) signaling in skeletal muscle fibers of R6/2 mouse, a model of Huntington's disease. J Gen Physiol. 144(5): 393-413.
Brown SE., Bowling AC., MacGarvey U *et al.* (1997) Oxidative damage and metabolic dysfunction in Huntington's disease: selective vulnerability of the basal ganglia. Ann Neurol. 41(5): 646-53.
Brück W., Pförtner R., Pham T *et al.* (2012) Reduced astrocytic NFκB activation by laquinimod protects from cuprizone-induced demyelination. Acta Neuropathol (Berl). 124: 411-24.
Bryne LM., Rodrigues FB., Blennow K *et al.* (2017) Neurofilament light protein in blood as a potential biomarker of neurodegeneration in Huntington's disease: a retrospective cohort analysis. Lancet Neurol. pii: S1474-4422(17) 30124-2.
Butters N., Wolfe J., Martone M *et al.* (1985) Memory disorders associated with Huntington's disease: verbal recall, verbal recognition and procedural memory. Neuropsychologia. 23(6): 729-43.
Carmona MA., Murai KK., Wang L *et al.* (2009) Glial ephrin A3 regulates hippocampal

dendritic morphology and glutamate transport. PNAS. 106(30): 12524-9.
Carroll, JB., Lerch JP., Franicosi S. *et al* (2011) Natural history of disease in the YAC128 mouse reveals a discrete signature of pathology in Huntington disease. Neurobiol Dis . 43, 257-65.
Cartier *et al.* (2005) Chemokine receptors in the central nervous system: role in brain inflammation and neurodegenerative diseases. Brain Res Rev. 48:16-42.
Cartier *et al.* (2014) The role of microglia in human disease: therapeutic tool or target? Acta Neuropathol. 128: 363-80.
Cassano T., Calcagnini S., Pace L *et al.* (2017) Cannabinoid receptor 2 signaling in neurodegenerative disorders: from pathogenesis to a promising therapeutic target. Front Aging Neurosci. 11(30): 1-10.
Cattaneo E., Rigamonti D., Goffredo D *et al.* (2001) Loss of normal huntingtin function: new developments in Huntington's disease research. Trends Neurosci. 24(3): 182-8.
Cha JH., Frey AS., Alsdorf SA *et al.* (1999) Altered neurotransmitter receptor expression in transgenic mouse models of Huntington's disease. Philos Trans R Sco Lond B Biol Sci. 354: 981-89.
Cha JH (2007) Transcriptional signatures in Huntington's disease. Prog Neurobiol. 83: 228-48.
Chan EY., Luthi-Carter R., Strand A *et al.* (2002) Increased huntingtin protein length reduces the number of polyglutamine-induced gene expression changes in mouse models of Huntington's disease. Hum Mol Genet. 11: 1939-51.
Chander KJ., Chandler RL., Broeckelmann EM *et al.* (2007) Relevance of BAC transgene copy number in mice: transgene copy number variation across multiple transgenic lines and correlations with transgene integrity and expression. Mamm Genome. 18(10): 693-708.
Chandra A., Sharma A., Calingasan NY *et al.* (2016) Enhanced mitochondrial biogenesis ameliorates disease phenotype in a full-length mouse model of Huntington's disease. Hum Mol Genet. 25(11): 2269-82.
Chang KH., Chen YC., Wu YR *et al.* (2012) Downregulation of genes involved in metabolism and oxidative stress in the peripheral leukocytes of Huntington's disease patients. PLoS One. 7(9): e46492.
Chang KH., Wu YR., Chen YC., Chen CM (2015) Plasma inflammatory biomarkers for Huntington's disease patients and mouse model. Brain Behav Immun. 44: 121-7.
Cheadle, C., Vawter MP., Freed WJ., Becker KG (2003) Analysis of microarray data using Z score transformation. J Mol Diagn. 5(2): 73-81.
Chen N., Luo T., Wellington C *et al.* (1999) Subtype-specific enhancement of NDMA receptor currents by mutant huntingtin. J Neurochem. 72(5): 1890-8.
Chen BS., Roche KW (2007) Regulation of NMDA receptors by phosphorylation. Neuropharmacology. 53(3): 362-8.
Chen J., Marks E., Lai B *et al.* (2013) Iron accumulates in Huntington's disease neurons: protection by deferoxamine. PLoS One. 8(10): e77023.
Chiang MC., Chern Y., Huang RN *et al.* (2012) PPARgamma rescue of the mitochondrial dysfunction in Huntington's disease. Neurobiol Dis. 45(1): 322-8.
Chiang MC., Cheng YC., Nicol CJ *et al.* (2015) Rosiglitazone activation of PPARγ-dependent signaling is neuroprotective in mutant hunting expressing cells. Exp

Cell Res. 338(2): 183-93.
Chung JY., Sunwoo JS., Kim MW., Kim M (2015) The neuroprotective effects of human growth hormone as a potential treatment for amyotrophic lateral sclerosis. Neural Regen Res. 10(8): 1201-3.
Cho KJ., Lee BI., Cheon SY *et al.* (2009) Inhibition of apoptosis signal-regulating kinase 1 reduces endoplasmic reticulum stress and nuclear huntingtin fragments in a mouse model of Huntington disease. Neuroscience. 163(4): 1128-34.
Choo YS., Johnson GV., MacDonald M *et al.* (2004) Mutant huntingtin directly increases susceptibility of mitochondria to the calcium-induced permeability transition and cytochrome c release. Hum Mol Genet. 13: 1407-20.
Cisse M., Checler F (2015) Eph receptors: new players in Alzheimer's disease pathogenesis. Neurobiol Dis. 73: 137-49.
Clausen BE., Burkhardt C., Reith W., Renkawitz R., Forster I (1999) Conditional gene targeting in macrophages and granulocytes using LysMcre mice. Transgenic Res. 8(4): 265-77.
Clodfelder-Miller B., De Sarno P., Zmijewska AA *et al.* (2005) Physiological and pathological changes in glucose regulate brain Akt and glycogen synthase kinase-3. J Biol Chem. 280: 39723-31.
Connolly C., Hill A., Leavitt BR (2012) Microglia in Huntington Disease. Microglia: Biology, Functions and Roles in Disease. 253-71.
Connolly C., Magnusson-Lind A., Lu G *et al.* (2016) Enhanced immune response to MMP3 stimulation in microglia expressing mutant huntingtin. Neuroscience. 14(325): 74-88.
Correa F., Hernangomez-Herrero M., Mestre L *et al.* (2011) The endocannabinoid anandamide downregulates IL-23 and IL-12 subunits in a viral model of multiple sclerosis: evidence for a cross-talk between IL-12p70/IL-23 axis and IL-10 in microglial cells. Brain Behav Immun. 25(4): 736-49.
Correll PH., Iwama A., Tondat S *et al.* (1997) Deregulated inflammatory response in mice lacking the STK/RON receptor tyrosine kinase. Genes Funct. 1:69-83.
Coulthard MG., Morgan M., Woodruff TM *et al.* (2012) Eph/Ephrin Signaling in Injury and Inflammation. Am J Pathol. 181: 1493-1503.
Coyle JT., Schwarcz R (1976) Lesions of striatal neurons with kainic acid privides a model for Huntington's chorea. Nature. 263 (5574): 244-6.
Craufurd D., Snowden J. (2002) Neuropsychological and neuropsychiatric aspects of Huntington's disease. In: Bates G, Harper PS, Jones L, editors. Huntington's Disease. 3rd ed. Oxford: Oxford University Press; 2002. p. 62-94.
Crotti A., Benner C., Kerman BE *et al.* (2014) Mutant huntingtin promotes autonomous microglia activation via myeloid lineage-determining factors. Nat Neurosci. 17(4): 513-21.
Crotti, A. and Glass, CK. (2015) The choreography of neuroinflammation in Huntington's disease. Trends Immunol. 36(6): 364-73
Cui L., Jeong H., Borovecki F *et al.* (2006) Transcriptional repression of PGC-1α by mutant huntingtin leads to mitochondrial dysfunction and neurodegeneration. Cell. 127(1): 59-69.
Dalrymple A., Wild EJ., Joubert R *et al.* (2007) Proteomic profiling of plasma in Huntington's disease reveals neuroinflammatory activation and biomarker

candidates. J Proteome Res. 6: 2833-40.
Davies, SW., Turmaine, M., Cozens BA *et al.* (1997) Formation of neuronal intranuclear inclusions underlies the neurological dysfunction in mice transgenic for the HD mutation. Cell. 90 (3):537-48.
De Mario A., Scarlatti C., Costiniti V *et al.* (2016) Calcium handling by endoplasmic reticulum and mitochondria in a cell model of Huntington's disease. PLoS Curr. 8: pii: ecurrents.hd.37fcb1c9a27503dc845594ee4a7316c3.
Desplats PA., Kass KE., Gilmartin T *et al.* (2006) Selective deficits in the expression of striatal-enriched mRNAs in Huntington's disease. 96(3): 743-57.
Devane WA., Axelrod J (1994) Enzymatic synthesis of anadamide, an endogenous ligand for the cannabinoid receptor, by brain membranes. PNAS. 91: 6698-701.
Diaz-Alonso J., Paraiso-Luna K., Navarrete C *et al.* (2016) VCE-003.2, a novel cannabigerol derivative, enhances neuronal progenitor cell survival and alleviates symptomatology in murine models of Huntington's disease. Sci Rep. 6: 29789.
Diaz-Hernandez M., Diez-Zaera M., Sanchez-Nogueiro J *et al.* (2009) Altered P2X7-receptor level and function in mouse models of Huntington's disease and therapeutic efficacy of antagonist administration. FASEB. 23(6): 1893-906.
Difilippantonio S., Nussenzweig A (2007) The NBS1-ATM connection revisited. Cell cycle. 6(19): 2366-70.
DiFiglia M., Sapp E., Chase KO *et al.* (1997) Aggregation of huntingtin in neuronal intranuclear inclusions and dystrophic neuritis in brain. Science. 277 (5334): 1990-3.
Dobson L., Träger U., Farmer R. *et al.* (2016) Laquinimod dampens hyperactive cytokine production in Huntington's disease patient myeloid cells. J Neurochem. 137(5): 782-94.
Dragatsis I., Levine MS., Zeitlin S (2000) Inactivation of Hdh in the brain and testis results in progressive neurodegeneration and sterility in mice. Nat Genet. 26(3): 300-6.
Dunkelberger JR., Song WC (2010) Complement and its role in innate and adaptive immune responses. Cell Res. 20(1): 34-50.
Duran-Vilaregut J., del Valle J., Manich G *et al.* (2011) Role of matrix metalloproteinase-9 (MMP-9) in striatal blood-brain barrier disruption in a 3-nitropropionic acid model of Huntington's disease. Neuropathol Appl Neurobiol. 37(5): 525-37.
Ehrnhoefer DE., Caron NS., Deng Y. *et al.* (2016) Laquinimod decreases Bax expression and reduces caspase-6 activation in neurons. Exp Neurol. 293(Pt A): 121-8.
Ehrnhoefer DE., Skotte NH., Ladha S *et al.* (2014) p53 increases caspase-6 expression and activation in muscle tissue expressing mutant huntingtin. Hum Mol Genet. 23: 717-29.
Ellrichmann G., Blusch A., Fatoba O *et al.* (2017) Laquinimod treatment in the R6/2 mouse model. Sci Rep. 7(1): 4947.
Faideau, M., Kim J., Cormier K *et al*. (2010) In vivo expression of polyglutamine-expanded huntingtin by mouse striatal astrocytes impairs glutamate transport: a correlation with Huntington's disease subjects. Hum Mol Genet. 19 (15): 3053–3067.
Fang Q., Strand A., Law W *et al.* (2009) Brain specific proteins decline in the cerebrospinal fluid of humans with Huntington disease. Mol Cell Proteom. 8(3):

451-66.
Fang Z., Cui X (2011) Design and validation issues in RNA-seq experiments. Brief Bioinform. 12(3): 280-7.
Farley SJ., McKay BM., Disterhoft JF., Weiss C. (2011) Reevaluating hippocampus dependent learning in FVB/N mice. BehavNeurosci.125(6):871-8.
Feng Z., Jin S., Zupnick A *et al.* (2006) p53 tumor suppressor protein regulates the levels of huntingtin gene expression. Oncogene. 25(1): 1-7.
File SE., Mahal A., Mangiarini L., Bates GP. (1998) Striking changes in anxiety in Huntington's disease transgenic mice. BrainRes.805:234-40.
Filiano AJ., Martens LH., Young AH. *et al.* (2013) Dissociation of frontemporal dementia-related deficits and neuroinflammation in progranulin haploinsufficient mice. J Neurosci. 33(12): 5352-61.
Fisher, ER and Hayden, MR. (2014) Multisource ascertainment of Huntington's Disease in Canada: prevalence and population at risk. Mov Disord. 29(1): 105-14.
Fliosa A., Paixao S., Honsek SD *et al.* (2009) Neuron-glia communication via EphA4/ephrin A3 modulates LTP through glial glutamate transport. Nat Neurosci. 12(10): 1285-92.
Franciosi S, Ryu JK, Shim Y, Hill AM, Connolly C, Hayden MR, McLarnon JG, Leavitt BR (2012) Age-dependent neurovascular abnormalities and altered microglial morphology in the YAC128 mouse model of Huntington Disease. Neurobiology of Disease. 45(1):438-49.
Freeman RS., Estus S., Johnson EM Jr. (1994) Analysis of cell cycle-related gene expression in post-mitotic neurons: selective induction of Cyclin D1 during programmed cell death. Neuron. 12(2): 343-55.
Gafni J., Ellerby LM (2002) Calpain activation in Huntington's disease. J Neurosci. 22: 4842-49.
Gama Sosa MA., De Gasperi R., Elder GA (2012) Modeling human neurodegenerative diseases in transgenic systems. Hum Genet., 131(4): 535-63.
Garcia-Miralles M., Hong X., Tan LJ *et al.* (2016) Laquinimod rescues striatal, cortical and white matter pathology and results in modest behavioral improvements in the YAC128 model of Huntington's disease. Sci Rep. 6: 31652.
Gasset-Rosa F., Chillion-Marinas C., Goginashvili A *et al.* (2017) Polyglutamine-expanded huntingtin exacerbates age-related disruption of nuclear integrity and nucleocytoplasmic transport. Neuron. 94(1): 48-57.
Gaveriaux Ruff,C., Kieffer,B (2007) Conditional gene targeting in the mouse nervous system: insights into brain function and diseases. Pharmand Therap. 113: 619-34.
Genetic Modifiers of Huntington's Disease (GeM-HD) Consortium (2015). Identification of Genetic Factors that Modify Clinical Onset of Huntington's Disease. Cell. 162(3): 516-26.
Ghosal N., Dearborn JT., Wozniak DF., Cairns NJ. (2012) Core features of frontotemporal dementia recapitulated in progranulin knockout mice. Neurobiol Dis. 45(1): 395-408.
Gines S., Paoletti P., Alberch J (2010) Impaired TrkB-mediated ERK1/2 activation in Huntington disease knock-in striatal cells involves reduced p52/p46 Shc expression. J Biol Chem. 285(28): 21537-48.
Goldberg YP., Nicholson DW., Rasper DM *et al.* (1996) Cleavage of huntingtin by

apopain, a proapoptotic cysteine protease, is modulated by the polyglutamine tract. Nat Genet. 13(4): 442-9.
Goldmann T., Jordao MJC., Wieghofer P *et al.* (2016) Origin, fate and dynamics of macrophages at CNS interfaces. Nat Immunol. 17(7): 797-805.
Gollin SM., Leary JF., Sjoulson I., Doherty RA (1985) Flow cytometric detection of lymphocyte alterations in Huntington's disease. Life Sci. 36(7): 619-26.
Gomez-Tortosa E., MacDonald ME., Friend JC *et al.* (2001) Quantitative neuropatholgical changes in presymptomatic Huntington's disease. Ann Neurol. 49(1): 29-34.
Graham RK., Deng Y., Slow EJ *et al.* (2006) Cleavage of caspase-6 site is required for neuronal dysfunction and degeneration due to mutant huntingtin. Cell. 125: 1179-91.
Graham RK., Ehrnhoefer DE., Hayden MR. *et al.* (2011) Caspase-6 and neurodegeneration. Trends Neurosci. 34(12): 646-56.
Gray, M., Shirasaki DI., Cepeda C *et al.* (2008) Full-length human mutant huntingtin with a stable polyglutamine repeat can elicit progressive and selective neuropathogenesis in BACHD mice. J Neurosci. 28 (24): 6182–6195.
Gregory S., Cole JH., Farmer RE *et al.* (2015) Longitudinal diffusion tensor imaging shows progressive changes in white matter in Huntington's disease. J Huntingtons Dis. 4(4): 333-46.
Grison A., Mantovani F., Comel A *et al.* (2011) Ser46 phosphorylation and prolyl-isomerase Pin1-mediated isomerization of p53 are key events in p53-dependent apoptosis induced by mutant huntingtin. Proc Natl Acad Sci U S A. 108(44): 17979-84.
Guidetti P., Luthi-Carter RE., Augood SJ., Schwarcz R (2004) Neostriatal and cortical quinolinate levels are increased in early grade Huntington's disease. Neurobiol Dis. 17(3): 455-61.
Guo X., Disatnik M., Monbureau M *et al.* (2013) Inhibition of mitochondrial fragmentation diminishes Huntington's disease-associated neurodegeneration. J Clin Invest. 123(12): 5371-88.
Gusella, JF., Wexler NS., Conneally PM *et al.* (1983) A Polymorphic DNA Marker Genetically linked to Huntington's disease. Nature., 306(5940):234-8.
Gusnanto A., Calza S., Pawitan Y *et al.* (2007) Identification of differentially expressed genes and false discovery rate in microarray studies. Curr Opin Lipidol. 18(2): 187-93.
Gustafson K., Hagberg H., Bengtsson BA *et al.* (1999) Possible protective role of growth hormone in hypoxia-ischemia in neonatal rats. Pediatr Res. 45: 318-23.
Hamm RJ., Pike BR., O'Dell DM., Lyeth BG., Jenkins LW., (1994) The rotarod test: an evaluation of its effectiveness in assessing motor deficits following traumatic brain injury. J Neurotrauma. 11(2):187-96.
Hanci N., Kudy C., Oguzoglu SA (1994) The effects of synthetic growth hormone on spinal cord injury. J Neurosurg Sci. 38: 43-9.
Hare D., Ayton S., Bush A., Lei P (2013) A delicate balance: Iron metabolism and diseases of the brain. Front Aging Neurosci. 5(34).
Harper, B. (2005) Huntington Disease. [Online]. Available from:

doi.10.1258/jrsm.98.12.550.
Hayashi Y., Ishibashi H., Hashimoto K., Nakanishi H (2006) Potentiation of the NMDA receptor-mediated responses through the activation of the glycine site by microglia secreting soluble factors. Glia. 53(6): 660-8.
Hayden MR., Vinik AI., Paul M., Beighton P (1977) Impaired prolactin release in Huntington's chorea. Evidence for dopaminergic excess. Lancet. 2(8035): 423-6.
Heikkinen, T., Lehtimaki K., Vartiainen N. *et al*. (2012) Characterization of neurophysiological and behavioral changes, MRI brain volumetry and 1H MRS in zQ175 knock-in mouse model of Huntington's disease. PLoS One . 7: e50717.
Heinrich PC., Behrmann I., Muller-Newen G *et al.* (1998) Interleukin-6 type cytokine signaling through the gp130/Jak/STAT pathway. Biochem J. 334 (Pt 2): 297-314.
Heinrich PC., Behrmann I., Haan S *et al.* (2003) Principles of interleukin (IL)-6 type cytokine signaling and its regulation. Biochem J. 374: 1-20.
Heinz S *et al.* (2010) Simple combinations of lineage-determining transcription factors prime cis-regulatory elements from macrophage and B cell identities. Mol Cell. 38: 576-89.
Hensely K (2010) Neuroinflammation in Alzheimer's disease: mechanisms, pathologic consequences, and potential for therapeutic manipulation. J Alzheimers Dis. 21: 1-14.
Hensman Moss DJ., Flower MD., Lo KK *et al.* (2017) Huntington's disease blood and brain show a common gene expression pattern and share an immune signature with Alzheimer's disease. Sci Rep. 7: 44849.
Herndon ES., Hladik CL., Shang P *et al.* (2009) Neuroanatomical profile of polyglutamine immunoreactivity in Huntington disease brains. J Neuropathol Exp Neurol. 68(3): 250-61.
Heyes MP., Saito K., Crowley JS *et al.* (1992) Quinolinic acid and kynurenine pathway metabolism in inflammatory and non-inflammatory neurological disease. Brain. 115(5): 1249-73.
Hickey MA., Gallant K., Gross GG., Levine MS., Chesselet MF (2005) Early behavioral deficits in R6/2 mice suitable for use in preclinical drug testing. Neurobiol Dis. 20(1):1-11.
Hickey, MA., Kosmalska A., Enayati J. *et al.* (2008) Extensive early motor and non-motor behavioral deficits are followed by striatal neuronal loss in knock-in Huntington's disease mice. Neuroscience. 157:280-95.
Hines DJ., Choi HB., Hines RM *et al.* (2013) Prevention of LPS-induced microglia activation, cytokine production and sickness behavior with TLR4 receptor interfering peptides. PLoS One. 8(3):e603888.
Ho LW., Brown R., Maxwell M *et al.* (2001) Wild type huntingtin reduces the cellular toxicity of mutant huntingtin in mammalian cell models of Huntington's disease. J Med Genet. 38(7): 450-2.
Hockly E., (2003). Standardization and statistical approaches to therapeutic trials in the R6/2 mouse. Brain Res Bull.61: 469-79.
Hong Y., Zhao T., Li XJ., Li S (2016) Mutant huntingtin impairs BDNF release from astrocytes by disrupting conversion of Rab3a-GTP into Rab3a-GDP. J Neurosci. 36(34): 8790-801.
Hsiao HY., Chen YC., Chen HM., Tu PH., Chern Y (2013) A critical role of astrocyte-

mediated nuclear factor-κB-dependent inflammation in Huntington's disease. Hum Mol Genet. 22(9): 1826-42.
Hsiao HY., Chiu FL., Chen CM *et al.* (2014) Inhibition of soluble tumor necrosis factor is therapeutic in Huntington's disease. Hum Mol Genet. 23(16): 4328-44.
Huck JH., Freyer D., Bottcher C *et al.* (2-15) De novo expression of dopamine D2 receptors on microglia after stroke. J Cereb Blood Flow. 35(11): 1804-11.
Humbert S., Bryson EA., Cordelieres FP *et al.* (2002) The IGF-1/Akt pathway is neuroprotective in Huntington's disease and involves huntingtin phosphorylation by Akt. Dev Cell. 2(6): 831-7.
Ivanov AI., Romanovsky AA (2006) Putative dual role of ephrin-Eph receptor interactions in inflammation. IUBMB Life. 58: 389-94.
Jacks T., Fazeli A., Schmidt E *et al.* (1992) Effects of an Rb mutation in the mouse. Nature. 359: 295-300.
Jayasena T., Polijak A., Braidy N *et al.* (2014) Upregulation of glycolytic enzymes, mitochondrial dysfunction and increased cytotoxicity in glial cells treated with Alzheimer's diease plasma. PLoS ONE. 10(3): e0116092.
Jeon J., Kim W., Jang J *et al.* (2016) Gene therapy by proteasome activator, PA28γ, improves motor coordination and proteasome function in Huntington's disease YAC128 mice. Neuroscience. 324: 20-8.
Jiao JW., Feldheim DA., Chen DF (2008) Ephrins as negative regulators of adult neurogenesis in diverse regions of the central nervous system. PNAS. 105(25): 8778-83.
Jin J., Albertz J., Guo Z *et al.* (2013) Neuroprotective effects of PPARγ agonist rosiglitazone in N171-82Q mouse model of Huntington's disease. J Neurochem. 125(3): 410-9.
Johnson GL., Lapadat R (2002) Mitogen-activated protein kinase pathways mediated by ERK, JNK, and p38 protein kinases. Science. 298(5600): 1911-2.
Johri A., Beal MF (2010) Hungting-ton for new proteases: MMPs as the new target? Neuron. 67(2): 171-3.
Jordan-Sciutto K., Malaiyandi LM., Bowser R (2002) Altered distribution of cell cycle transcriptional regulators during Alzheimer's disease. J Neuropathol Exp Neurol. 61(4): 358-67.
Jun DJ., Kim J., Jung SY *et al.* (2007) Extracellular ATP mediates necrotic cell swelling in SN4741 dopaminergic neurons through P2X7 receptors. J Biol Chem. 282(52): 37350-8.
Jung S., Aliberti J., Graemmel P *et al.* (2000) Analysis of fractalkine receptor CX3CR1 function by targeted deletion and green fluorescent protein reporter gene insertion. Mol Cell Biol. 20(11): 4106-4114.
Kaindl AM., Degos V., Peineau S *et al.* (2012) Activation of microglia N-methyl-D-aspartate receptors triggers inflammation and neuronal cell death in the developing and mature brain. Ann Neurol. 72(4): 536-49.
Kato G., Inada H., Wake H *et al.* (2016) Microglial contact prevents excess depolarization and rescues neurons from excitotoxicity. eNeuro. 3(3): ENEURO. 0004-16.
Kaur, C. *et al.* (2007) From blood to brain: amoeboid microglial cell, a nascent macrophage and its functions in the developing brain. Acta Pharmacol Sin. 28:

1087-96.
Kaye J., Piryatinsky V., Birnberg T *et al.* (2016) Laquinimod arrests experimental autoimmune encephalomyelitis by activating the aryl hydrocarbon receptor. PLoS. 113(41): E6145-E6152.
Kawashima T., Murata K., Akira S *et al.* (2001) STAT5 induces macrophage differentiation of M1 leukemia cells through activation of IL-6 production mediated by NF-kappaB p65. J Immunol. 167: 3652-60.
Khoshnan A., Ko J., Watkin EE *et al.* (2004) Activation of IkappaB kinase complex and nuclear factor-kappaB contributes to huntingtin neurotoxicity. J Neurosci. 24(37): 79999-8008.
Kim YS, Kim SS, Cho JJ *et al.* (2005) Matrix metalloproteinase-3: a novel signaling proteinase from apoptotic neuronal cells that activates microglia. J Neurosci 25(14):3701–3711.
Kim JY., Kim YJ,, Lee S., Park JH (2009) The critical role of ERK in death resistance and invasiveness of hypoxia-selected glioblastoma cells. BMC. 9:27.
Krabbe G., Miniami SS., Etchegaray JI *et al.* (2017) Microglial NFκB-TNFα hyperactivation induces obsessive-compulsive behavior in mouse models of progranulin-deficient frontotemporal dementia. PNAS. Pii: 201700477. doi: 10.1073/pnas. 1700477114. [Epub ahead of print].
Kraft *et al.* (2012) Activated microglia proliferate at neuritis of mutant huntingtin-expressing neurons. Neurobiol Aging. 33(3): 621.e 17-33.
Kratter, I., Zahed H., Lau A *et al.* (2016) Serine 421 regulates mutant huntingtin toxicity and clearance in mice. J of Clin Invest. 126(9): 3585-97.
Krzyszton-Russjan J. (2016) Pathophysiology and molecular basis of selected metabolic abnormalities in Huntington's disease. Postepy Hig Med Dosw (Online). 70(0): 1331-42.
Kuhl DE., Metter EJ., Riege WH., Markham CH (1984) Patterns of cerebral glucose utilization in Parkinson's disease and Huntington's disease. Ann Neurol. 15 Suppl: S119-25.
Kuhl DE., Markham CH., Metter EJ *et al.* (1985) Local cerebral glucose utilization in symptomatic and presymptomatic Huntington's disease. Res Publ Assoc Res Nerv Ment Dis. 63: 199-209.
Kuhn SA., van Landeghem FK., Zacharias R *et al.* (2004) Microglia express GABA(B) receptors to modulate interleukin release. Mol Cell Neurosci. 25(2): 312-22.
Kuhn A., Thu D., Waldvogel HJ *et al.* (2011) Population-specific expression analysis (PSEA) reveals molecular changes in diseased brain. Nat Methods. 8(11): 945-7.
Kumar A., Ratan RR (2016) Oxidative stress and Huntington's disease: the good, the bad and the ugly. J Huntington's dis. 5(3): 217-37.
Kwan JY., Jeong SY., van Gelderen P *et al.* (2012) Iron accumulation in deep cortical layers accounts for MRI signal abnormalities in ALS: correlating 7 Teslsa MRI and Pathology. PLoS ONE. 7(4): e35241.
Kwan *et al.* (2012) Mutant huntingtin impairs immune cell migration in Huntington's disease. J Clin Invest. 122(12): 4737-47.
Labadorf A., Hoss, AG., Lagomarsino V. *et al.* (2016) RNA Sequence Analysis of Human Huntington Disease Brain Reveals an Extensive Increase in Inflammatory and Developmental Gene Expression. PLoS ONE. 11(7): e0160295.

LaGanke C., Samkoff L., Edwards K *et al.* (2017) Safety/tolerability of the anti-semaphorin 4D antibody VX15/2503 in a randomized phase 1 trial. Neurol Neuroimmunol Neuroinflamm. 4(4): e367.
Lai Z., Emtner M., Roos P., Nyberg F (1991) Characterization of putative growth hormone receptors in human choroid plexus. Brain Res. 546: 222-6.
Lai Z., Roos P., Zhai Q *et al.* (1993) Age-related reduction of growth hormone-binding sites in the human brain. Brain Res. 621: 250-66.
Laron Z (2011) The growth hormone-prolactin relationship: a neglected issue. Pediatr Endocrinol Rev. 9(2): 546-8.
Lawrence T. (2009) The Nuclear Factor NF κB Pathway in Inflammation. Col Spring Harb Perspect Biol. 1(6): a001651.
Lawson LJ, *et al.* (1990) Heterogeneity in the distribution and morphology of microglia in the normal adult mouse brain. Neuroscience. 39:151–170.
Leavitt BR., van Raamsdonk JM., Shehadeh J *et al.* (2006) Wild-type huntingtin protects neurons from excitotoxicity. J Neurochem. 96(4): 1121-9.
Levy DE., Darnell JE (2002) Stats: transcriptional control and biological impact. Nat Rev Mol Cell Biol. 3: 651-62.
Li H., Li SH., Yu ZX *et al.* (2001) Huntingtin aggregate-associated axonal degneneration is an early pathological event in Huntington's disease mice. J Neurosci. 21(21): 8473-81.
Li Y., Liu DX., Li MY *et al.* (2014) Ephrin-A3 and ephrin-A4 contribute to microglia-induced angiogenesis in brain endothelial cells. Anat Rec (Hoboken). 297(10): 1908-18.
Lin L., Park JW., Ramachandran S *et al.* (2016) Transcriptome sequencing reveals aberrant alternative splicing in Huntington's disease. Hum Mol Genet. 25(16): 3454-66.
Liddelow SA., Barres BA (2017) Reactive Astrocytes: Production, Function and Therapeutic Potential. Immunity. 46(6): 957-67.
Lievens JC., Rival T., Iche M *et al.* (2005) Expanded polyglutamine peptides disrupt EFG receptor signaling and glutamate transporter expression in Drosophilia. Hum Mol Genet. 14:713-24.
Liu YF (1998) Expression of polyglutamine-expanded Huntingtin activates the SEK1-JNK pathway and induces apoptosis in a hippocampal neuronal cell line. J Biol Chem. 273(44): 28873-7.
Liu YF., Dorow D., Marshall J (2000) Activation of MLK2-mediated signaling cascades by polyglutamine-expanded huntingtin. J Biol Chem. 275(25): 19035-40.
Loonstra A., Vooijs M., Beverloo HB., *et al.* (2001) Growth inhibition and DNA damage induced by Cre recombinase in mammalian cells. Proc. Natl. Acad. Sci. U.S.A. 98: 9209-14.
Lopez-Sendon Moreno JL., Garcia Caldentey J., Trigo Cubillo P *et al.* (2016) A double-blind, randomized, cross-over, placebo-controlled, pilot trial with Sativex in Huntington's disease. J Neurol. 263(7): 1390-400.
Lovestone S., Hodgson S., Sham P *et al.* (1996) Familial psychiatric presentation of Huntington's disease. J Med Genet. 33(2):128-31.
Lu B., Nagappan G., Guan X *et al.* (2013) BDNF-based synaptic repair as a disease modifying strategy for neurodegenerative disease. Nat Rev Neurosci. 14(6): 401-

6.
Mahadevan M., Tsilfidis C., Sabourin L *et al.* (1992) Mytonic dystrophy mutation: an unstable CTG repeat in the 3' untranslated region of the gene. Science. 225 (5049): 1235-55.
Maher P., Dargusch R., Bodai L *et al.* (2011) ERK activation by the polyphenols fisten and resveratrol provides neuroprotection in multiple models of Huntington's disease. Hum Mol Genet. 20:261-70.
Mailleux P., Vanderhaeghen JJ (1992) Distribution of neuronal cannabinoid receptor in the adult rat brain: a comparative receptor binding radioautography and in situ hybridization histochemistry. Neurosceince. 48: 655-668.
Mangiarini, L., Sathasivam K., Seller M *et al.* (1996) Exon 1 of the HD gene with an expanded CAG repeat is sufficient to cause a progressive neurological phenotype in transgenic mice. Cell. 87 (3): 493–506.
Martin L., Latypova X., Wilson CM *et al.* (2013) Tau protein kinases: involvement in Alzheimer's disease. Ageing Res Rev 12:289–309.
Martin-Aparicio E., Yamamoto A., Hernandez F *et al.* (2001) Proteasomal-dependent aggregate reversal and absence of cell death in a conditional mouse model of Huntington's disease. J Neurosci. 21(22): 8772-81.
Mastrokolias A., Ariyurek Y., Goeman JJ *et al.* (2015) Huntington's disease biomarker progression profile identified by transcriptomic sequencing of peripheral blood. Eur J Hum Genet. 23(10): 1349-56.
Mayo LD., Seo YR., Jackson MW *et al.* (2005) Phosphorylation of human p53 at serine 46 determines promoter selection and whether apoptosis is attenuated or amplified. J Biol Chem. 280(25): 2593-9.
Mazarei, G., Leavitt, B.R (2014) Murine Models of HD. Movement Disorders (Second Edition): Genetics and Models. Elsevier: 533-546.
Menalled L., El-Khodor BF., Patry M *et al.* (2009) Systemic behavioral evaluation of Huntington's disease transgenic and knock-in mouse models. Neurobiol Dis. 35(3):319-36.
Menalled L., Lutz C., Ramboz S *et al.* (2014) A Field Guide to Working with Mouse Models of Huntington's Disease. http://chdifoundation.org/a-field-guide-to-working-with-mouse-models-of-huntingtons-disease/.
Metlzer M., Gan L., Mazarei G *et al.* (2010) Phosphorylation of huntingtin at Ser421 in YAC128 neurons is associated with protection of YAC128 neurons from NMDA-mediated excitotoxicity and is muated by PP1 and PP2A. J Neurosci. 30(43): 14318-29.
Miller JP, Holcomb J, Al-Ramahi I *et al.* (2010) Matrix metalloproteinases are modifiers of huntingtin proteolysis and toxicity in Huntington's disease. Neuron 29(67 (2)):199–212.
Miller JR., Lo KK., Andre R *et al.* (2016) RNA-seq of Huntington's disease patient myeloid cells reveals innate transcriptional dysregulation associated with proinflammatory pathway activation. 25(14): 2893-2904.
Miller JRC., Pfister EL., Liu W *et al.* (2017) Allele-selective suppression of mutant huntingtin in primary human blood cells. Sci Rep. 7: 46740.
Mina E., van Roon-Mom W., Hettne K *et al.* (2016) Common disease signatures from gene expression analysis in Huntington's disease human blood and brain.

Orphanet Journal of Rare Disease. 11:97.
Mishra MK., Wang J., Silva C *et al.* (2012) Kinetics of proinflammatory monocytes in a model of multiple sclerosis and its perturbation by laquinimod. Am J Pathol. 181: 642-51.
Moffitt H., McPhail GD., Woodman B *et al.* (2009) Formation of polyglutamine inclusions in a wide range of non-CNS tissues in the HdhQ150 knock-in mouse model of Huntington's disease. PLoS One. 4(11): e8025.
Molero AE., Arteaga-Bracho EE., Chen CH *et al.* (2016) Selective expression of mutant huntingtin during development recapitulates characteristic features of Huntington's disease. PNAS. 113(20): 5736-41.
Moller, T. (2010) Neuroinflammation in Huntington's Disease. J Neural Transm. DOI 10.1007/s00702-010-0430-7.
Monif M., Reid CA., Powell KL *et al.* (2009) The P2X7 receptor drives microglial activation and proliferation: a trophic role for P2X7R pore. 29(12): 3781-91.
Moriguchi S., Mizoguchi Y., Tomimatsu Y *et al.* (2003) Potentiation of NMDA receptor-mediated synaptic responses by microglia. Brain Res Mol Brain Res. 119(2): 160-9.
Morris R. (1984) Developments of a water-maze procedure for studying spatial learning in the rat. J Neurosci Methods.11(1):47-60.
Morton AJ., Wood NI., Hastings MH *et al*. (2005) Disintegration of the sleep-wake cycle and circadian timing in Huntington's disease. J of Neurosci. 25(1): 157-63.
Nakamura Y., Si QS., Kataoka K. (1999) Lipopolysaccharide-induced microglial activation in culture: temporal change and release of cytokines and nitric oxide. Neurosci Res. 35(2): 95-100.
Nance,MA., Myers,RH. (2001) Juvenile onset Huntington's disease: clinical and research perspectives. Ment Retard Dev Disabil Res Rev.7(3): 153-7.
Nayak *et al.* (2011) Huntington's Disease: An Immune Perspective. Neurol Research Intern. 2011: 1-7.
Nestler EJ, Greengard P. Protein Phosphorylation is of Fundamental Importance in Biological Regulation. In: Siegel GJ, Agranoff BW, Albers RW, et al., editors. Basic Neurochemistry: Molecular, Cellular and Medical Aspects. 6th edition. Philadelphia: Lippincott-Raven; 1999. Available from: https://www.ncbi.nlm.nih.gov/books/NBK28063/
Niemelä V., Landtblom AM., Blennow K., Sundblom J (2017) Tau or neurofilament light- Which is the more suitable biomarker for Huntington's disease. 12(2): e0172762.
Nimmerjahn A, *et al.* (2005) Resting microglial cells are highly dynamic surveillants of brain parenchyma in vivo. Science. 308:1314–1318.
Nishitoh H., Matsuzawa A., Tobiume K *et al.* (2002) ASK1 is essential for endoplasmic reticulum stress-induced neuronal cell death triggered by expanded polyglutamine repeats. Genes Dev. 16(11): 1345-55.
Nuñez E., Benito C., Pazos MR *et al.* (2004) Cannabinoid CB2 receptors are expressed by perivascular microglial cells in the human brain: an immunohistochemical study. Synapse. 53: 208-13.
Nyberg F., Burman P (1996) Growth hormone and its receptors in the central nervous system—Location and functional significance. Horm Res. 45: 18-22.

Nyberg F (1997) Aging effects on growth hormone receptors binding in the brain. Exp Gerontol. 32: 521-28.
Nyberg F (2000) Growth hormone in the brain: characteristics of specific brain targets for the hormone and their functional significance. Front Neuroendocrinol. 21(4): 330-48.
Olmos, G. and Llado, J. (2014) Tumor Necrosis Factor Alpha: A link between neuroinflammation and excitotoxicity. Mediators of Inflammation. 2014: 1-12.
Oliveira JM (2010) Mitochondrial bioenergetics and dynamics in Huntington's disease: tripartite synapses and selective striatal degeneration. J Bioenerg Biomembr. 42(3): 227-34.
Ortega Z., Lucas JJ (2014) Ubiquitin –proteosome system involvement in Huntington's disease. Front Mol Neurosci. 7:77.
Palazuelos J., Aguado T., Pazos MR *et al.* (2009) Microglial CB2 cannabinoid receptors are neuroprotective in Huntington's disease excitotoxicity. Brain. 132: 3152-64.
Pallier PN., Drew CK., Morton AJ. (2009) The detection and measurement of locomotor deficits in a transgenic mouse model of Huntington's disease are task-and-protocol dependent: influence of non-motor factors on locomotor function. Brain Res Bull. 78:347-55.
Paolicelli RC., Bolasco G., Pagani F *et al.* (2011) Synaptic pruning by microglia is necessary for normal brain development. Science. 333(6048): 1458-8.
Pardo R., Colin E., Regulier E *et al.* (2006) Inhibition of calcineurin by FK506 protects against polyglutamine-huntingtin toxicity through an increase of huntingtin phosphorylation at S421. J Neurosci. 26(5): 1635-45.
Park JE., Lee ST., Im WS., Kim M (2013) Growth hormone deteroriates the functional outcome in an experimental model of Huntington's disease induced by 3-nitropionic acid. J Mov Disord.
Pavese N., Gerhard A., Tai YF *et al.* (2006) Microglial activation correlates with severity in Huntington disease: a clinical and PET study. Neurology. 66(11): 1638-43.
Petaku, TL., Neal SJ., Orban PC. *et al.* (2010) Progranulin expression in the developing and adult murine brain. J Comp Neurol. 518(19): 393-47.
Petkau, TL., Leavitt B.R (2014) Progranulin in neurodegenerative disease. Trends in Neurosciences. 37(7): 388-398.
Phatnani H., Maniatis T (2015) Astrocytes in neurodegenerative disease. Cold Spring Harb Perspect Biol. 7(6). pii. A020628.
Phillips OR., Joshi SH., Squitieri F *et al.* (2016) Major superficial white matter abnormalities in Huntington's disease. Front Neurosci. 10: 197.
Pocock JM., Kettenmann H (2007) Neurotransmitter receptors on microglia. Trends Neurosci. 30(10): 527-35.
Politis M., Pavese N., Tai YF *et al.* (2008) Hypothalamic involvement in Huntington's disease: an in vivo PET study. Brain. 131 (Pt 11): 2860-9.
Pouladi MA., Xie Y., Skotte NH *et al.* (2010) Full-length huntingtin levels modulate body weight by influencing insulin-like growth factor 1 expression. Hum Mol Genet. 19(8): 1528-38.
Pouladi MA., Stanek LM., Xie Y. *et al.* (2012) Marked differences in neurochemistry and aggregates despite similar neuropathological features of Huntington disease in the full length BACHD and YAC128 mice. Hum Mol Genet. 21(10): 2219-32.

Politis M., Lahiri N., Niccolini F *et al.* (2015) Increased central microglial activation associated with peripheral cytokine levels in premanifest Huntington's disease gene carriers. Neurobiol Dis. 83: 115-21.

Pringsheim T., Wiltshire K., Day L *et al.* (2012) The incidence and prevalence of Huntington's disease: a systematic review and meta-analysis. Mov. Disord., 27, 1083–1091.

Qin H., Wilson CA., Lee SJ *et al.* (2005) LPS induces CD40 gene expression through the activation of NF-kappa B and STAT-1alpha in macrophages and microglia. Blood. 106(9): 3114-22.

Quintanilla RA., Jin YA., von Bernhardi R., Johnson GV (2013) Mitochondrial permeability transition pore induces mitochondria injury in Huntington disease. Mol Neurodegener. 8: 45.

Quinti L., Dayalan Naidu S., Träger U *et al.* (2017) KEAP-1 modifying small molecule reveals muted NFR2 signaling responses in neural stem cells from Huntington's disease patients. PNAS. 114(23): E4676-E4685.

Ransohoff RM., Perry VH (2009) Microglia Physiology: Unique stimuli, specialized responses. Ann Rev Immunol. 27: 119-45.

Ravikumar B., Stewart A., Kita H *et al.* (2003) Raised intracellular glucose concentrations reduce aggregate and cell death caused by mutant huntingtin exon 1 by decreasing mTOR phosphorylation and inducing autophagy. Hum Mol Genet. 12(9): 885-94.

Rawlins, MD., Wexler NS., Wexler AR *et al*. (2016) The Prevalence of Huntington's disease. Neuroepidemiology., 46(2): 144-53.

Redelman D., Welnia LA., Taub D., Murphy WJ (2008) Neuroendocrine hormones such as growth hormone and prolactin are integral members of the immunological cytokine network. Cell Immunol. 252:111-21.

Ribeiro FM., Dobransky T., Carvalho EA., *et al.* (2012) Energy Metabolism in Huntington's Disease. INTECH Open Access Publisher.

Rocha NP., Ribeiro FM., Furr-Stimming E., Teixeira AL (2016) Neuroimmunology of Huntington's disease: Revisiting Evidence from Human Studies. Mediators Inflamm. 2016: 8653132.

Rodrigues FB., Byrne LM., McColgan P *et al.* (2016) Cerebrospinal fluid inflammatory biomarkers reflect clinical severity in Huntington's disease. PLoS One. 11(9): e0163479.

Rodrigues FB., Byrne L., McColgan P *et al.* (2016) Cerebrospinal fluid tau concentration predicts clinical phenotype in Huntington's disease. J Neurochem. 139 (1): 22-5.

Roze E., Betuing S., Deyts C. *et al.* (2008) Mitogen-and stress activated protein kinase 1 deficiency is involved in expanded huntingtin induced transcriptional dysregulation and striatal death. FASEB. 22(4): 1083-94.

Runne H., Kuhn A., Wild E *et al.* (2007) Analysis of potential transcriptomic biomarkers for Huntington's disease in peripheral blood. PNAS. 104(36): 14424-9.

Sachdeva UM., O'Brien JM (2012) Understanding pRb: toward necessary development of targeted treatments for retinoblastoma. J Clin Invest. 122(2): 425-34.

Sagredo O., Gonzalez S., Aroyo I *et al.* (2009) Cannabinoid CB2 receptor agonists protect the striatum against malonate toxicity: relevance for Huntington's disease. Glia. 57: 1154-67.

Saleh N., Moutereau S, Durr A (2009) Neuroendocrine disturbances in Huntington's disease. PLoS One. 4(3): e4962.
Saleppico S *et al.* (1996) Iron regulates microglial cell mediated secretory and effector functions. Cell Immunol. 170(2): 251-9.
Samii A *et al.* (2004) Parkinson's disease. Lancet. 363: 1783-93.
Sanberg PR., Fibiger HC., Mark RF *et al.* (1981) Body weight and dietary factors in Huntington's disease patients compared with matched controls. Med J of Aust. 1(8): 407-9.
Sapp E., Kegel B., Aronin N *et al.* (2001) Early and progressive accumulation of reactive microglia in the Huntington disease brain. J Neuropathol Exp Neurol. 60(2): 161-72.
Sathasivam K., Hobbs C., Turmaine M *et al.* (1999) Formation of polyglutamine inclusions in non-CNS tissue. Hum Mol Genet. 8(5): 813-22.
Sathasivam K., Lane A., Legleiter J *et al.* (2010) Identical oligomeric and fibrillar structures captured from the brains of R6/2 and knock-in mouse models of Huntington's disease. Hum Mol Genet. 19: 65-78.
Sathyasaikumar KV., Stachowski EK., Amori L (2010) Dysfunctional kynureine pathway metabolism in the R6/2 mouse model of Huntington's disease. J Neurochem. 113(6): 1416-25.
Sato, K (2015) Effects of Microglia on Neurogenesis. Glia. 63(8): 1394-1405.
Saudou F., Humbert S (2016) The Biology of Huntingtin. Neuron. 89(5): 910-26.
Saura J., Tusell JM., Serratosa J (2003) High-yield isolation of murine microglia by mild trypsinization. Glia. 44(3): 183-9.
Schafer DP., Lehrman EK., Kautzman AG *et al.* (2012) Microglia sculpt postnatal neural circuits in an activity and complement-dependent manner. Neuron. 74(4): 691-705.
Schauwecker PE. (2005) Susceptibility to excitotoxic and metabolic striatal neurodegeneration in the mouse is genotype dependent.BrainRes. 1040:112-20.
Scott DB., Blanpied TA., Swanson GT *et al.* (2001) An NMDA receptor ER retention signal regulated by phosphorylation and alternative splicing. J Neurosci. 21: 3063-72.
Semaka A., Creighton S., Warby S., Hayden MR *et al.* (2006) Predictive testing for Huntingon's disease: interpretation and significance of intermediate alleles. Clin Genet. 70(4): 283-94.
Seo H., Sonntag KC., Kim W *et al.* (2007) Proteosome activator enhances survival of Huntington's disease neuronal model cells. PLoS one. 2(2): e238.
Sharp AH., Love SJ., Schilling G *et al.* (1995) Widespread expression of Huntington's disease gene (IT15) protein product. Neuron. 14(5):1065-74.
Shen CH., Yuan P., Lorenzo-Perez R *et al.* (2013) Phosphorylation of BRAF by AMPK impairs BRAF-KSR1 association and cell proliferation. Mol Cell. 52(2): 161-72.
Sheridan GK., Murphy KJ (2013) Neuron-glia crosstalk in health and disease: fractalkine and CX3CR1 take center stage. Open Biol. 3(12): 130181.
Shin JY., Fang ZH., Yu ZX *et al.* (2005) Expression of mutant huntingtin in glial cells contributes to neuronal excitotoxicity. J Cell Biol. 171(6): 1001-12.
Shuai K., Liu B (2003) Regulation of JAK-STAT signaling in the immune system. Nat Rev Immunol. 3: 900-11.

Silvestroni A. *et al.* (2009) Distinct neuroinflammatory profile in postmortem human Huntington's disease. Neuroreport. 20: 1098-1103.
Simmons D *et al.* (2007) Ferritin Accumulation in Dystrohic Microglia is an early event in the development of Huntington's disease. Neuroreport. 20(12): 1098-1103.
Sipione S., Rigamonti D, Valenza M (2002) Early transcriptional profiles in huntingtin-inducible striatal cells by microarray analyses. Hum Mol Genet. 11(17): 1953-65.
Slow, E.J., van Raamsdonk J., Rogers D *et al.* (2003) Selective striatal neuronal loss in a YAC128 mouse model of Huntington disease. Hum Mol Gen. 12 (13): 1555–1567.
Slow EJ., Graham RK., Osmand AP *et al.* (2005) Absence of behavioral abnormalities and neurodegeneration in vivo despite widespread neuronal huntingtin inclusions. PNAS. 102(32): 1140-7.
Smith ES., Jonason A., Reilly C *et al.* (2015) SEMA4D compromises blood-brain barrier, activates microglia, and inhibits remyelination in neurodegenerative disease. Neurobiol Dis. 73: 254-68.
Sobel RA (2005) Ephrin A receptors and ligands in lesions and normal appearing white matter in multiple sclerosis. Brain Pathol. 15: 35-45.
Sofic E., Riederer P., Heinsen H *et al.* (1988) Increased iron (III) and total iron content in post mortem substantia nigra of parkinsonian brain. J Neural Transm. 74(3): 199-205.
Song C., Perides G., Liu YF (2002) Expression of full-length polyglutamine-expanded Huntingtin disrupts growth factor receptor signaling in rat phenpchromocytoma (PC12) cells. J Biol Chem. 277(8): 6703-7.
Song, J., Park KA., Lee WT., Lee JE (2014) Apoptosis signal regulating kinase 1 (ASK1): potential as a therapeutic target for Alzheimer's disease. Int J Mol Sci. 15(2): 2119-29.
Sos ML., Levin RS., Gordan JD *et al.* (2014) Oncogene Mimicry as a mechanism of primary resistance to BRAF inhibitors. Cell Rep. 8(4): 1037-48.
Southwell, A.L., Warby SC., Carroll JB *et al.* (2013) A fully humanized transgenic mouse model of Huntington disease. Hum Mol Genet.22(1):18-34.
Southwell AL., Francisosi S., Villanueva EB *et al.* (2015) Anti-semaphorin 4D immunotherapy ameliorates neuropathology and some cognitive impairment in the YAC128 mouse model of Huntington's disease. Neurobiol Dis. 76: 46-56.
Southwell, AL., Smith-Dijak A.,Kay C *et al.* (2016) An enhanced Q175 knock-in mouse model of Huntington disease with higher mutant huntingtin levels and accelerated disease phenotypes. Hum Mol Genet. Jul 4. pii: ddw212. [Epub ahead of print]
Squitieri F., Maglione V., Orobello S., Fornai F (2011) Genotype, aging-dependent abnormal caspase activity in Huntington disease blood cells. 118(11): 1599-607.
Stella N (2010) Cannabinoid and cannabinoid-like receptors in microglia, astrocytes and astrocytomas. Glia. 58: 1017-1030.
Stellwagen D., Malenka RC (2007) Synaptic scaling mediated by glial TNF-alpha. Nature. 440(7087): 1054-9.
Stephan AH., Barres BA., Stevens B (2012) The complement system: an unexpected role in synaptic pruning during development and disease. Ann Rev Neurosci. 35: 369-89.
Stevens B., Allen NK., Vazquez LE *et al.* (2007) The classical complement cascade

mediates CNS synapse elimination. Cell. 131(6): 1164-78.
Streit WJ. (2002) Microglia as neuroprotective, immunocompetent cells of the CNS. Glia. 40(2): 133-139.
Szklarczyk D., Franceschini A., Wyder S *et al.* (2015) STRING v10: protein-protein interaction networks, integrated over the tree of life. Nucleic Acids Research. 43: D447-52.
Szlardy I., Klivenyi P., Zadori D *et al.* (2012) Mitochondrial disturbances, tryptophan metabolites and neurodegeneration: medical chemistry aspects. Curr Med Chem. 19: 1899-1920.
Tai YF., Pavese N., Gerhard A *et al.* (2007) Microglial activation in presymptomatic Huntington's disease gene carriers. Brain. 130(Pt 7): 1759-66.
Tan L., Yu J., Tan L (2012) The kynurenine pathway in neurodegenerative diseases: mechanistic and therapeutic considerations. J Neurol Sci. 323(1-2): 1-8.
Telenius H., Kremer HP., Theilmann J *et al.* (1993) Molecular analysis of juvenile Huntington's disease: the major influence on (CAG)n repeat length is the sex of the affected parent. Hum Mol Genet. 2(10): 1535-40.
Tellez-Nagel I., Johnson AB., Terry RD (1974) Studies on brain biopsies of patients with Huntington's chorea. J Neuropathol Exp Neurol. 33(2): 308-32.
Teo RT., Hong X., Yu-Taeger L *et al.* (2016) Structural and molecular myelination deficits occur prior to neuronal loss in the YAC128 and BACHD models of Huntington disease. Hum Mol Genet. 25(13): 2621-32.
Thöne J., Linker RA (2016) Laquinimod in the treatment of multiple sclerosis: a review of the data so far. Drug Des Devel Ther. 10: 1111-8.
Tingley WG., Ehlers MD., Kameyama K *et al.* (1997) Characterization of protein kinase A and protein kinase C phosphorylation of N-methyl-D-aspartate receptor NR1 subunit using phosphorylation site-specific antibodies. J Biol Chem. 272: 5157-66.
Träger U., Magnusson A., Lahiri Swales N *et al.* (2013) JAK/STAT signaling in Huntington's Disease Immune Cells. PLoS Curr. 5: ecurrents.hd
Träger U., Andre R., Lahiri N *et al.* (2013) HTT-lowering reverses Huntington's disease immune dysfunction caused by NFκB-pathway dysregulation. Brain. 137 (Pt 3): 819-33
Träger U., Andre R., Lahiri N *et al.* (2014) HTT-lowering reverses Huntington's disease immune dysfunction caused by NFκB pathway dysregulation. Brain. 137 (Pt 3): 819-33.
Träger U., Andre R., Magnusson-Lind A *et al.* (2015) Characterization of immune cell function in fragment and full-length Huntington's disease mouse models. Neurobiol Dis. 73: 388-98.
Tremblay ME., Majewska AK (2011) A role for microglia in synaptic plasticity? Commun Integr Biol. 4(2): 220-222.
Tsunemi T., Ashe TD., Morrison BE *et al.* (2012) PGC-1α rescues Huntington's disease proteotoxicity by preventing oxidative stress and promoting TFEB function. Sci Transl Med. 4(142): 142ra97.
Turnbull AV, Rivier CL (1999) Regulation of the hypothalamic- pituitary-adrenal axis by cytokines: actions and mechanisms of action. Physiol Rev 79:1–77.
Tydlacka S., Wang CE., Wang X *et al.* (2008) Differential activities of the ubiquitin-

proteosome system in neurons versus glia may account for preferential accumulation of misfolded proteins in neurons. J Neurosci. 28: 13285-95.
Valdeolivas S., Navarrete C., Cantarero I *et al.* (2015) Neuroprotective properties of cannabigerol in Huntington's disease: studies in R6/2 mice and 3-nitropropionate-lesioned mice.
Valekova, I., Karkovska L., Kotrcova E *et al.* (2016) Revelation of the INFα, IL-10, IL-8 and IL-1β as promising biomarkers reflecting immuno-pathological mechanisms in porcine Huntington's disease model. J Neuroimmunol. 293: 71-81.
Valenza M., Leoni V., Karasinkska JM *et al.* (2010) Cholestrol defect is marked across multiple rodent models of Huntington's disease. J Neurosci. 30(32): 10844-50.
Valenza M., Marullo M., Di Paolo E *et al.* (2015) Disruption of astrocyte-neuron cholesterol cross talk affects neuronal function in Huntington's disease. Cell Death Differ. 22(4): 690-702.
Van der Burg JM., Björkqvist M., Brundin P (2009) Beyond the brain: widespread pathology in Huntington's disease. Lancet Neurol. 8(8): 765-74.
Van Raamsdonk JM., Pearson J., Rogers DA *et al.* (2005) Loss of wild-type huntingtin influences motor dysfunction and survival in the YAC128 mouse model of Huntington disease. Hum Mol Genet. 14(10): 1379-92.
Van Raamsdonk JM., Pearson J., Murphy Z *et al.* (2006) Wild-type huntingtin ameliorates striatal neuronal atrophy but does not prevent other abnormalities in the YAC128 mouse model of Huntington disease. BMC Neurosci. 7: 80.
Van Raamsdonk, JM., Murphy Z, Selva DM *et al.* (2007) Testicular degeneration in Huntington disease. Neurobiology of Disease. 26(3):512–520.
Van Wamelen DJ., Aziz NA., Roos RA., Swaab DF (2014) Hypothalamic alterations in Huntington's disease patients: comparison with genetic rodent models. J Neuroendocrinol. 26(11): 761-75.
Vescei L., Szalardy L., Fulop F., Toldi J (2013) Kynurenines in the CNS: recent advances and new questions. Nat Rev Drug Discov. 12(1): 64-82.
Vezzani A., Viviani B (2015) Neuromodulatory properties of inflammatory cytokines and their impact on neuronal excitability. Neuropharm. 96: 70-82.
Vinther-Jensen T., Börnsen L., Budtz-Jørgensen E *et al.* (2016) Selected CSF biomarkers indicate no evidence of early neuroinflammation in Huntington disease. Neurol Neuroimmunol Neuroinflamm. 3(6): e287.
Vogel CF., Khan EM., Leung PS *et al.* (2014) Cross-talk between aryl hydrocarbon receptor and the inflammatory response: a role for nuclear factor-κB. J Biol Chem. 289(3): 1866-75.
Voloboueva LA., Emery JF., Sun X., Giffard RG (2013) Inflammatory response of microglial BV-2 cells includes a glycolytic shift and is modulated by mitochondrial glucose-regulated protein 75/mortalin. FEBS Lett. 587(6): 756-62.
Vonsattel JP., Myers RH., Stevens TJ *et al.* (1985) Neuropathological classification of Huntington's disease. J of Neuropath and Experim Neurol. 44(6): 559-77.
Vonsattel, JP., DiFiglia, M. (1998) Huntington's disease. J of Neuropath and Exp Neurol. 57(5):369-84.
Wagner, LA., Menalled L., Goumeniouk A et al. (2008) Chapter 6- Huntington's Disease. Animal and Translational Models for CNS Drug Discovery. Pg 207-66.
Wang MH., Zhou YQ., Chen YQ (2002) Macrophage-stimulating protein and RON

receptor tyrosine kinase: potential regulators of macrophage inflammatory activities. Scand J Immunol. 56: 545-53.

Wang L., Lin F., Wang J *et al.* (2012) Truncated N-terminal huntingtin fragment with expanded polyglutamine (htt552-100Q) suppresses brain-derived neurotrophic factor transcription in astrocytes. Acta Biochim Biophys Sin (Shanghai). 44(3): 249-58.

Wang JQ., Chen Q., Wang X *et al.* (2013) Dysregulation of mitochondrial calcium signaling and superoxide flashes causes mitochondrial genomic DNA damage in Huntington disease. J Biol Chem. 288(5): 3070-84.

Wang R., Ross CA., Cai H *et al.* (2014) Metabolic and hormonal signatures in pre-manifest Huntington's disease patients. Front Physiol. 5: 231.

Wang, N., Gray M., Lu XH *et al.* (2014) Neuronal targets for reducing mutant huntingtin expression to ameliorate disease in a mouse model of Huntington's disease. Nat Med. 20(5): 536-41.

Warby SC., Chan EY., Metlzer M *et al.* (2005) Huntingtin phosphorylation on serine 421 is significantly reduced in the striatum and by polyglutamine expansion in vivo. Hum Mol Genet. 14(11): 1569-77.

Warby SC., Doty CN., Graham RK *et al.* (2009) Phosphorylation of huntingtin reduces the accumulation of its nuclear fragments. Mol Cell Neurosci. 40(2): 121-7.

Weiss, WF., Hodgdon TK., Kaler EW., Lenhoff AM., Roberts CJ. *et al*. (2007). Nonnative protein polymers: structure, morphology, and relation to nucleation and growth. Biophys J . 93: 4392-403.

Weiss A., Träger U., Wild EJ *et al.* (2012) Mutant huntingtin fragmentation in immune cells tracks Huntington's disease progression. J Clin Invest. 122(10): 3731-6.

Weller, A., Leguisamo AC., Towns L *et al.* (2003) Maternal effects in infant and adult phenotypes of 5HT1A and 5HT1B receptor knockout mice. Dev Psychobiol. 42: 194-205.

Wellington CL., Ellerby LM., Hackam AS *et al.* (1998) Casapase cleavage of gene products associated with triplet expansion disorders generates truncated fragments containing the polyglutamine tract. J Biol Chem. 273(15): 9158-67.

Wild E., Tabrizi SJ. (2014) Targets for future clinical trials in Huntington's disease: what's in the pipeline? Mov Disord. 29(11): 1434-45.

Wild EJ., Boggio R., Langbehn D *et al.* (2015) Quanification of mutant huntingtin protein in cerebrospinal fluid from Huntington's disease patients. J Clin Invest. 125(5): 1979-86.

Wong BK., Ehrnhoefer DE., Graham RK. *et al.* (2015) Partial rescue of some features of Huntington Disease in the genetic absence of caspase-6 in YAC128 mice. Neurobiol Dis. 76: 24-36.

Wu Y., Olesen-Dissing L., MacVicar BA., Stevens B (2015) Microglia: Dynamic Mediators of Synapse development and plasticity. Trends Immunol. 36(10): 605-13.

Yamamoto A., Lucas JJ., Hen R (2000) Reversal of neuropathology and motor dysfunction in a conditional model of Huntington's disease. Cell. 101(1): 57-66.

Yang J., Luo X., Huang X *et al.* (2014) Ephrin A3 reverse signaling regulates hippocampal neuronal damage and astrocytic glutamate transport after transient global ischemia. J Neurochem. 131(3): 383-94.

Yang HM., Yang S., Huang SS *et al.* (2017) Microglial activation in the pathogenesis of Huntington's disease. Front Aging Neurosci. 9(193): 1-9.

Yano H., Baranov SV., Baranova OV *et al.* (2014) Inhibition of mitochondrial protein import by mutant huntingtin. Nat Neurosci. 17(6): 822-31.

Yin F., Banerjee R., Thomas B *et al.* (2010) Exaggerated inflammation, impaired host defense and neuropathology in progranulin-deficient mice. J. Exp. Med. 207(1): 117-28.

Yong VW., Power C., Forsyth P., Edwards DR (2001) Metalloproteinases in biology and pathology of the nervous system. Nat Rev Neurosci. 2(7): 502-11.

Yoon S Kim, Sung S Kium, Joeng J Cho, *et al.* (2006) Matrix Metalloproteinase-3: A Novel Signaling proteinase from apoptotic neuronal cells that activates microglia. FASEB J. 20 Nov.

Young AB., Shoulson I., Penney JB et al. (1986) Huntington's disease in Venezuela: neurologic features and functional decline. Neurology. 36(2): 244-9.

Zakzanis KK.(1998) The subcortical dementia of Huntington's disease. J Clin Exp Neuropsychol. 20(4):565-78.

Zeron MM., Chen N., Moshaver A *et al.* (2001) Mutant huntingtin enhances excitotoxic cell death. Mol Cell Neurosci. 17(1): 41-53.

Zhang H., Pelech S (2012) Using protein microarrays to study phosphorylation mediated-signal transduction. Semin Cell Dev Biol. 23(8): 872-82.

Zhang H., Shi X., Pelech S. (2016) Monitoring protein kinase expression and phosphorylation in cell lysates with antibody microarrays. Methods Mol Biol. 1360: 107-22.

Zheng X., Zhang Z., Kang A *et al.* (2015) Thinking outside the brain for cognitive impairment: is peripheral immunomodulation on the way? Neuropharmacology. 96(Pt A): 94-104.

Zuccato C., Ciammola A., Rigamonti D., Leavitt BR *et al.* (2001) Loss of huntingtin-mediated BDNF gene transcription in Huntington's disease. Science. 293(5529): 493-8.

Zuccato C., Marullo M., Conforti P *et al.* (2008) Systemic assessment of BDNF and its receptor levels in human cortices affected by Huntington's disease. Brain Pathol. 18: 255-38.

Zuccato C., Valenza M., Cattaneo E (2010) Molecular Mechanisms and Potential Therapeutical Targets in Huntington's disease. Physiol Rev. 90: 905-81.

Zwilling D., Huang SY., Sathyasaikumar KV *et al.* (2011) Kyneurein 3-monooxygenase inhibition in blood ameliorates neurodegeneration. Cell. 145(6): 863-74.